Molecular Insights Into the Adaptability of the Gut

Nadya Morrow

Thesis submitted to the University of Ottawa
in partial Fulfillment of the requirements for the
Doctorate in Philosophy in Biochemistry

Department of Biochemistry, Microbiology and Immunology
Faculty of Medicine
University of Ottawa

Abstract

The small intestine delivers dietary fat in the form of triglyceride (TG)-rich lipoproteins to fuel the body. The production and clearance of TG-rich lipoproteins become dysregulated in people living with type 2 diabetes resulting in more dietary fat in circulation than healthy individuals following the same meal, contributing to cardiovascular risk. The response of the intestine to obesity through adaptive or maladaptive changes is not well understood. This thesis characterizes the intestinal response to diet-induced obesity and dyslipidemia, as well as extreme models of physiology including the ketogenic diet and chronic cold stress. **I hypothesized that hormonal signalling regulates absorptive surface area which in turn modulates intestinal lipid metabolism in response to increases in energy intake.** The second chapter evaluates the intestinal changes to chronic high-fat, high-cholesterol (HFHC) diet feeding in *Ldlr*$^{-/-}$ mice with or without the addition of dietary nobiletin, a flavonoid previously shown to improve insulin sensitivity and attenuate atherosclerosis progression. Adding nobiletin to a HFHC diet normalized jejunal lipid storage and jejunal *de novo* synthesis of intestinal lipids. Lower fasting and post-prandial intestinal lipid levels achieved by nobiletin were associated with a more efficient handling of an acute dietary fat challenge, namely, greater intestinal TG secretion and clearance rates compared to mice fed the HFHC diet alone. The third chapter demonstrates that short-term ketogenic, but not HFHC diet feeding increases fasting intestinal lipid stores and intestinal surface area compared to controls. In response to an acute dietary fat challenge, mice previously fed the ketogenic diet had elevated plasma TG levels. The fourth chapter evaluates the requirement of glucagon-like peptide 1 receptor (GLP-1R), GLP-2R, and glucose-dependent insulinotropic polypeptide (GIPR) signalling in the expansion of intestinal surface area that occurs in response to the increased food intake that accompanies chronic cold stress in mice. Using *Glp1r*$^{-/-}$*Gipr*$^{-/-}$ and *Glp1r*$^{-/-}$*Glp2r*$^{-/-}$ mice, we found that cold stress-induced increases in jejunal villi length and crypt depth, but not small intestinal length, require GLP-2R signalling. Acute dietary fat challenges

revealed no impact of cold stress on lipid handling in male mice, but in female mice, greater intestinal-TG secretion was observed in a GLP-1R/2R-dependent manner. Overall, these studies provide molecular insights into early and chronic changes in the intestinal response to increases in dietary fat or food intake. Furthermore, this thesis expands the intestinotrophic actions of endogenous gut hormone action and highlights sex differences in the intestinal response to these metabolic challenges.

Keywords

Small intestine, Lipids, Lipoproteins, Cytosolic lipid droplets, Glucagon-like peptide 1, Glucagon-like peptide 2, Nobiletin, Dyslipidemia, Insulin resistance.

Acknowledgments

I would like to express my deepest gratitude to my thesis supervisor, Dr. Erin Mulvihill. Over the years, you have taught me how to carefully and creatively design experiments, troubleshoot, and craft a compelling scientific narrative. You have provided me with numerous opportunities to develop my writing skills and have engaged me in enriching scientific discussions, creating a supportive space to articulate my ideas, expand my knowledge, and grow as a scientist. You have also instilled in me the values of service, collaboration, leadership, humility, kindness, and the importance of showing up. I am incredibly fortunate that my path led me to do graduate studies in your lab. Thank you for being a mentor and a champion.

I would like to thank the Canadian Institutes of Health Research and the National Science and Engineering Research Council of Canada for supporting the work in this thesis. I am also grateful to have received doctoral research awards from the Canadian Institutes of Health Research, Queen Elizabeth II Graduate Scholarship in Science and Technology, and the UOHI Graduate Endowment Fund.

I have been privileged to work alongside many wonderful colleagues in the Mulvihill lab. I am grateful to Dr. Natasha Trzaskalski, Evgenia Fadzeyeva, and Dr. My-Anh Nguyen, who warmly welcomed and trained me when I joined the lab. Thank you to Cassandra Locatelli, my co-first author for Chapter 3 and islet biology translator, for your dedication and team spirit to achieve our goals. To Antonio Hanson, my co-first author for Chapter 4, thank you for your attention to detail and unwavering positivity. Thank you, Serena Pulente for your team spirit and unbelievable ability to plan and be efficient. I appreciate the time and support from Ali Abdalbari and Andrew Clément. Special thanks to Dr. Ilka Lorenzen-Schmidt and Dr. Arianne Morissette for their patience and dedication to my projects. I have also had the pleasure of training exceptional undergraduate students—Chelsea Klein, Mélodie Bellefleur, Hoda Osman, Sebastian Cino, Ethel

Messika-Zeitoun, Hadeel Alhadi, Mariam Mahran, Ishika Tripathi, and Sara Imran—whose curiosity and work ethic have taught me invaluable lessons. Thank you all for making the lab a fun place to work. This work would not have been possible without the support, time, and skills of these remarkable individuals.

I am sincerely grateful to my thesis advisory committee members, Dr. Mireille Ouimet, Dr. Morgan Fullerton, and Dr. Subash Sad, for their time, thoughtful comments, and insightful questions throughout the years. I also extend my gratitude to Dr. Kyoung-Han Kim and Dr. Murray Huff for their continuous support, encouragement, and guidance. Thank you to Dr. Jacqueline Dron and Dr. Amy Burke for your advice, encouragement, and meticulous proofreading over the years. The Heart Institute has been an incredible training environment. Xiaoling Zhao, our amazing histopathologist – thank you for your expertise and ability to adapt to our always growing needs, and of course the life chats along the way. Thank you to Vivian Franklin, Kelsey Bolger, Alison Conley, Ann Nguyen, and the ACVS staff for their support. I also appreciate the friendship and encouragement from Cameron Stotts, Termeh Aslani, Claire Fong-McMaster, Yena Oh, Alex Ross, and Ramis Ileri— even a wave from down the hall always brightened my day (or evening).

Outside of the lab, I am grateful to Melissa, Brit, Celina, Maddy, Tori, Em, Ben, Natan, and Hanna for their friendship and support over the years. I am incredibly fortunate to have so many amazing people in my life. My mother, Myriam, is the MVP in the pursuit of my dreams—thank you for stocking my freezer with homemade meals, organizing my life every time you visit, and for your boundless excitement for my future. You taught me independence and resilience. My father, Al, also keeps my freezer full and reminds me to exercise, watch basketball, and to not “sweat the small stuff”. My brother, Cory, wiser beyond his years, keeps me grounded and teaches me how to enjoy life. Thank you to my aunt Badia who always makes me laugh and teaches me recipes, even though there is always way too much food.

I am so lucky to have so many amazing memories from the last six years.

Co-authorship statement

Portions of this thesis have been prepared for publication. I wrote the initial draft of each manuscript and revised with recommendations from Dr. Erin Mulvihill and co-authors. I participated in the design, execution, and analysis of all experiments presented in this thesis with the following exceptions:

Chapter 2: Nadya M. Morrow, Natasha A. Trzaskalski, Antonio A. Hanson, Evgenia Fadzeyeva, Dawn E. Telford, Sanjiv S. Chhoker, Brian G. Sutherland, Jane Y. Edwards, Murray W. Huff, Erin E. Mulvihill

Dr. Erin Mulvihill and Dr. Murray Huff provided intellectual input and scientific expertise into the hypothesis, design, and experimental details. Natasha Trzaskalski assisted with animal studies and plasma GLP-1 measurements. Antonio Hanson assisted with animal studies and plasma immunoblotting. Evgenia Fadzeyeva assisted with animal studies. Dawn Telford assisted with animal studies, gene expression analyses, fast protein liquid chromatography, and plasma analyses. Sanjiv Chhoker assisted with tissue immunoblotting. Brian Sutherland assisted with animal studies and tissue lipid analyses. Jane Edwards assisted with gene expression analyses and tissue immunoblotting.

Chapter 3: Nadya M. Morrow*, Cassandra A. A. Locatelli*, Natasha A. Trzaskalski, Chelsea T. Klein, Antonio A. Hanson, Hadeel Alhadi, Ishika Tripathi, Andrew C. Clément, Sara Imran, Ilka Lorenzen-Schmidt, and Erin E. Mulvihill

*Co-first authors

Dr. Erin Mulvihill and Cassandra Locatelli provided intellectual input and scientific expertise into the hypothesis, design, and experimental details. Cassandra Locatelli also assisted with animal studies, gene expression analyses, plasma analyses, data analysis, and

figure generation. Natasha Trzaskalski assisted with tissue lipid analyses. Chelsea Klein assisted with lipid droplet and intestinal morphology analyses. Antonio Hanson assisted with plasma immunoblotting. Hadeel Alhadi assisted with adipocyte analyses. Andrew Clément assisted with tissue lipid analyses. Ishika Tripathi assisted with intestinal morphology analyses. Sara Imran assisted with intestinal morphology analyses. Ilka Lorenzen-Schmidt performed all mouse breeding and assisted with histological image acquisition.

Chapter 4: Nadya M. Morrow*, Antonio A. Hanson*, Claire Fong-McMaster, Dawson B.H. Livingston, Hoda Osman, Lauren Hamilton, Natasha A. Trzaskalski, Cassandra A. A. Locatelli, Mélodie Bellefleur, Ethel Messika-Zeitoun , Sebastian Cino , Serena M. Pulente, Iryna Abramchuk, Xiaoling Zhao, Ilka Lorenzen-Schmidt, Arianne Morissette, Krista A. Power, Mary-Ellen Harper, Erin E Mulvihill

*Co-first authors

Dr. Erin Mulvihill and Antonio Hason provided intellectual input and scientific expertise into the hypothesis, design, and experimental details. Antonio Hanson also assisted with animal studies, plasma analyses, intestinal morphology analyses, and data analysis. Claire Fong-McMaster performed tissue respirometry analyses and Dr. Mary-Ellen Harper provided the resources for these experiments. Dawson Livingston performed fecal short chain fatty acid analyses and Dr. Krista Power provided the resources for these experiments. Hoda Osman assisted with intestinal morphology analyses and Ki67 data analyses. Lauren Hamilton performed the tissue mitochondrial mass analyses and Dr. Mary-Ellen Harper provided the resources for these experiments. Serena Pulente assisted with animal experiments and gene expression analyses. Natasha Trzaskalski assisted with animal experiments and plasma analyses. Cassanda Locatelli assisted with animal experiments and plasma analyses. Mélodie Bellefleur assisted with animal experiments, histology, and intestinal morphology analyses. Ethel Messika-Zeitoun assisted with histology. Sebastian Cino assisted with animal experiments

and molecular analyses. Iryna Abramchuk assisted with intestinal morphology analyses. Xiaoling Zhao optimized the Ki67 immunostaining. Ilka Lorenzen-Schmidt performed all mouse breeding, colony management, genotyping, and assisted with histological image acquisition. Arianne Morissette assisted with animal experiments and manuscript preparation.

Table of Contents

List of figures

List of abbreviations

ABCA1	ATP-Binding Cassette Transporter A1
ABCG1	ATP-Binding Cassette Transporter G1
ABCG5	ATP-Binding Cassette Transporter G5
ABCG8	ATP-Binding Cassette Transporter G8
ACC	Acetyl-CoA Carboxylase
ACACA	Acetyl-CoA Carboxylase Alpha
ACAT	Acyl-CoA:Cholesterol Acyltransferase
ACAT1	Acetyl-CoA Acetyltransferase 1
ACLY	ATP Citrate Lyase
ACP	Acyl Carrier Protein
ACS	Acyl-CoA Synthetase
Actb	Beta-actin
ADP	Adenosine Diphosphate
AGPAT	1-Acylglycerol-3-Phosphate O-Acyltransferase
AGPAT1	1-Acylglycerol-3-Phosphate O-Acyltransferase 1
ApoAI	Apolipoprotein AI

ApoAIII	Apolipoprotein AIII
AKT	Protein Kinase B
AMP	Adenosine Monophosphate
AMPK	AMP-Activated Protein Kinase
ANGPTL	Angiopoietin-Like Protein
ANGPTL4	Angiopoietin-Like Protein 4
ANGTL3	Angiopoietin-Like Protein 3
ANOVA	Analysis of Variance
APOBEC	Apolipoprotein B mRNA Editing Catalytic Polypeptide-like
Apoc3	Apolipoprotein C3
ApoB48	Apolipoprotein B48
APP/PS1	Amyloid Precursor Protein/Presenilin 1
ASBT	Apical Sodium Bile Acid Transporter
ATGL	Adipose Triglyceride Lipase
ATP	Adenosine Triphosphate
AUC	Area Under the Curve
BAT	Brown Adipose Tissue
BHB	Beta-hydroxybutyrate

BDH1	Beta-Hydroxybutyrate Dehydrogenase 1
C57BL/6J	Mouse Strain
CD1	Cluster of Differentiation 1
CD36	Cluster of Differentiation 36 (Fatty Acid Translocase)
CD146	Melanoma Cell Adhesion Molecule
CE	Cholesterol Ester
CETP	Cholesteryl Ester Transfer Protein
CGI-58	Comparative Gene Identification-58 (ABHD5)
CLD	Cytosolic Lipid Droplet
CLD	Cytoplasmic Lipid Droplet
CLOCK	Circadian Locomotor Output Cycles Kaput
CO_2	Carbon Dioxide
COPII	Coat Protein Complex II
CPT1	Carnitine Palmitoyltransferase I
CRE	cAMP Response Element
CREB	cAMP Response Element-Binding Protein
CVD	Cardiovascular Disease
DAG	Diacylglycerol

DAPI	4',6-diamidino-2-phenylindole
DGAT1	Diacylglycerol acyltransferase 1
DGAT2	Diacylglycerol acyltransferase 2
DIRKO	Double incretin receptor knockout
DPP4	Dipeptidyl peptidase-4
E2	Estradiol
EGF	Epidermal Growth Factor
eNOS	Endothelial Nitric Oxide Synthase
ER	Endoplasmic Reticulum
FA	Fatty acid
FABP	Fatty Acid-Binding Protein
FABP5	Fatty Acid-Binding Protein 5
FABPpm	Fatty Acid-Binding Protein, Plasma Membrane
FADS2	Fatty Acid Desaturase 2
FASN	Fatty Acid Synthase
FATP	Fatty Acid Transport Protein
FGF7	Fibroblast Growth Factor 7
FITC-	Fluorescein Isothiocyanate

FPLC	Fast Protein Liquid Chromatography
FoxO1	Forkhead box protein O1
G6Pase	Glucose-6-Phosphatase
GBD	Grain-Based Diet
GCGR	Glucagon Receptor
GCG	Preproglucagon Gene
GIP	Glucose-dependent Insulinotropic Polypeptide
GIPR	Glucose-dependent Insulinotropic Polypeptide Receptor
GLP-1	Glucagon-like peptide-1
GLP-1R	Glucagon-like peptide-1 Receptor
GLP-2	Glucagon-like Peptide-2
GLP-2R	Glucagon-like Peptide-2 Receptor
GLPDRKO	Glucagon-like peptide double receptor knockout
GPAT	Glycerol-3-Phosphate Acyltransferase
GPAT3	Glycerol-3-Phosphate Acyltransferase 3
GPAT4	Glycerol-3-Phosphate Acyltransferase 4
GPCR	G Protein-Coupled Receptor
HDL	High-Density Lipoprotein

HFD	High-Fat Diet
HFHC	High-Fat, High-Cholesterol
HMGCR	3-Hydroxy-3-Methylglutaryl-CoA Reductase
HMGCS2	3-Hydroxy-3-Methylglutaryl-CoA Synthase 2
HTGL	Hepatic Triglyceride Lipase
i.p.	Intraperitoneal
i.v.	Intravenous
IDL	Intermediate-Density Lipoprotein
IGF	Insulin-like growth factor-1
IGF-1	Insulin-Like Growth Factor 1
IGF-1R	Insulin-like growth factor-1 receptor
IGF-2	Insulin-Like Growth Factor 2
INSIG	Insulin-Induced Gene
IRS	Insulin Receptor Substrate
KATP	ATP-Sensitive Potassium Channel
KD	Ketogenic diet
KGF	Keratinocyte Growth Factor
LDL	Low-Density Lipoprotein

LDLR	Low-Density Lipoprotein Receptor
LPL	Lipoprotein Lipase
LTT	Lipid tolerance test
MASLD	Metabolic dysfunction-associated steatotic liver disease
MAG	Monoacylglycerol
MAGL	Monoacylglycerol Lipase
MAPK	Mitogen-Activated Protein Kinase
MGAT	Monoacylglycerol Acyltransferase
Mogat2	Monoacylglycerol O-acyltransferase 2
mTORC1	Mammalian target of rapamycin complex 1
MTP	Microsomal Triglyceride Transfer Protein
NEFA	Non-esterified Fatty Acid
NPC1L1	Niemann-Pick C1-Like 1 Protein
NPC2	Niemann-Pick C2 Protein
OCT	Optimal cutting temperature
PBS	Phosphate-buffered saline
PC1/3	Prohormone convertase 1/3
PDK	Phosphoinositide-Dependent Kinase

PFK-1	Phosphofructokinase-1
PHLPP	Pleckstrin Homology Domain Leucine-Rich Repeat Protein Phosphatase
PI3K	Phosphoinositide 3-Kinase
PLIN1	Perilipin 1
PLIN2	Perilipin 2
PP2A	Protein Phosphatase 2A
PPARα	Peroxisome proliferator-activated receptor alpha
PPARγ	Peroxisome Proliferator-Activated Receptor Gamma
Rps9	Ribosomal protein S9
SCAP	SREBP Cleavage-Activating Protein
SCFA	Short-chain Fatty Acid
SCD1	Stearoyl-CoA Desaturase 1
SDS-PAGE	Sodium dodecyl sulfate–polyacrylamide gel electrophoresis
SEM	Standard error of the mean
SGLT-1	Sodium-Glucose Linked Transporter 1
SLD	Standard Laboratory Diet
SREBP1c	Sterol Regulatory Element-Binding Protein 1c
SREBP2	Sterol Regulatory Element-Binding Protein 2

SR-B1	Scavenger Receptor Class B Type 1
TAG	Triacylglycerol
T2DM	Type 2 Diabetes Mellitus
TCA	Tricarboxylic Acid (Cycle)
TEM	Transmission electron microscopy
TG	Triglyceride
TN	Thermoneutral
TRL	Triglyceride-rich lipoproteins
UCP-1	Uncoupling Protein 1
VLDL	Very Low-Density Lipoprotein
WD	Western-style diet
WT	Wild-type
ZO-1	Zonula Occludens-1

List of tables

Chapter 1 : Introduction

A version of this chapter has been published:

Morrow, N.M., Morissette A., Mulvihill, E.E. (2024). Immunomodulation and inflammation: Role of GLP-1R and GIPR expressing cells within the gut. Peptides. *176,* 171200.

Morrow, N.M., Hanson, A.A. & Mulvihill, E.E. (2021). Distinct Identity of GLP-1R, GLP-2R, and GIPR Expressing Cells and Signaling Circuits Within the Gastrointestinal Tract. Front Cell Dev Biol. *9*,703996.

1.1 The small intestine

The small intestine, which extends between the stomach and the colon, is primarily responsible for nutrient absorption. It also integrates nutrient use with the presence of various hormone-producing specialized enteroendocrine cells (Gribble and Reimann 2019). Within the small intestine lumen, the surface area is ideally maximized to enhance nutrient absorption through villi and microvilli, which increase intestinal surface area by 30-600-fold (Kiela and Ghishan 2016). A single layer of epithelial cells lines the surface of each villus to serve as the gateway for controlled nutrient absorption and a barrier to dietary antigens and diverse microorganisms (Turner 2009). Absorptive enterocytes populate the villus tip and account for >80% of intestinal epithelial cells. The remaining mature cell types include mucin-producing goblet cells, antimicrobial defensins-producing Paneth cells, and cytokine-producing tuft cells which reside throughout the epithelium (Figure 1.1) (Ensari and Marsh 2018). Shallow invaginations surrounding each villus are intestinal crypts, which house highly mitotic stem cells that give rise to progenitor cells, which in turn proliferate and become mature epithelial cells (Gehart and Clevers 2019). The continuous supply of progenitor and epithelial cells physically promotes the

transit of the latter from the crypts up to the villus tip, where they replace the previously shed apoptotic epithelial cells (Gehart and Clevers 2019). Therefore, in addition to the maximized absorptive surface area, the constantly renewing barrier protects the internal environment from the harsh conditions of the intestinal lumen. This single epithelial layer sits on a basement membrane surrounding a connective tissue core called the lamina propria, which contains lymphocytes and innate immune cells (Ensari and Marsh 2018). Each villus is supplied by an arteriole that forms a capillary network, a venule that drains into larger vessels at the crypts, and one to two terminal lymphatic vessels of the mesenteric network called lacteals (Ensari and Marsh 2018). Pericytes coat villus blood vessels while smooth muscle cells coat lacteals. The lamina propria also contains connective tissue scaffolds, enteric nerves, fibroblasts and smooth muscle cells (Bernier-Latmani and Petrova 2017). The lamina propria is encapsulated by a myofibroblast shell that directly contacts the vascular network. From the villus tip to the muscularis mucosa, onto which villi are anchored, spans the mucosal layer. The submucosal layer contains blood and lymphatic vessels and a plexus of parasympathetic nerves (Bernier-Latmani and Petrova 2017), while the smooth muscle cell-rich muscularis propria allows for contractile peristalsis (Collins, Nguyen et al. 2021). The final outer layer of the intestine is the serosa, composed of loose connective tissue and squamous epithelial cells (Collins, Nguyen et al. 2021), and is continuous with the mesentery. The mesentery supports the intestine in the peritoneum and also contains blood vessels, nerves, and lymphatics (Argikar and Argikar 2018). A complex integration of signals, including local enteroendocrine production of peptide hormones, coordinate barrier function with nutrient absorption and transit, impacting both the dynamic and highly efficient process of nutrient assimilation. The extremely precise and beautiful design of the gut highlights that the energy used to maintain it serves beyond what is often assumed to solely be a passive conduit for nutrients.

Figure 1.1 Small intestinal architecture and cell types. Villus architecture is organized as fibroblast-like cells (left), blood, lymph, and immune cells (middle), and enteric cells (right). Reproduced from: Morrow, N.M., Hanson, A.A. & Mulvihill, E.E. (2021). Distinct Identity of GLP-1R, GLP-2R, and GIPR Expressing Cells and Signaling Circuits Within the Gastrointestinal Tract. Front Cell Dev Biol. 9,703996.

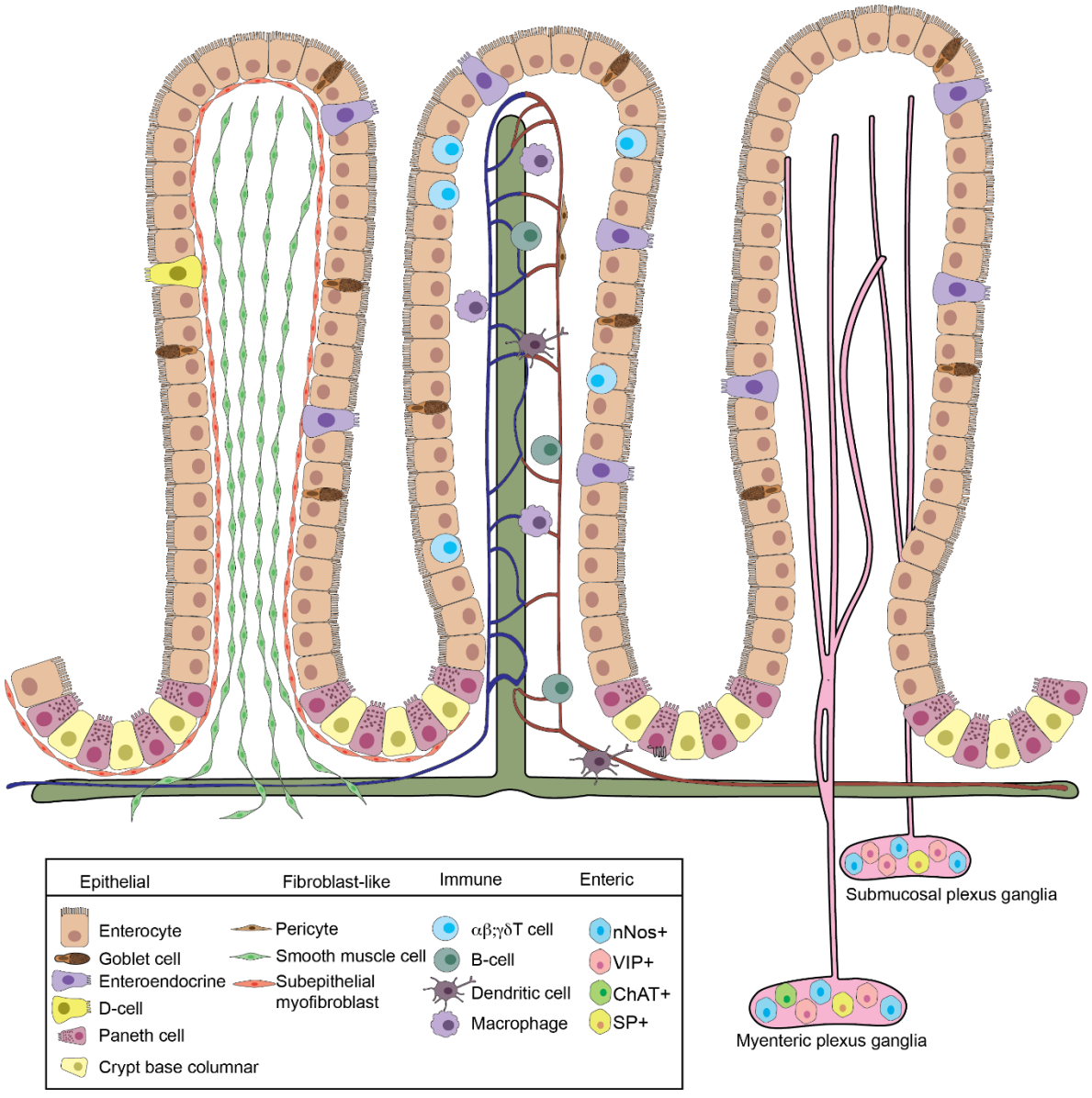
Epithelial
Enterocyte
Goblet cell
Enteroendocrine
D-cell
Paneth cell
Crypt base columnar
Fibroblast-like
Pericyte
Smooth muscle cell
Subepithelial myofibroblast
Immune
αβ;γδT cell
B-cell
Dendritic cell
Macrophage
Enteric
nNos+
VIP+
ChAT+
SP+
Submucosal plexus ganglia
Myenteric plexus ganglia

1.2 Macronutrient absorption

Once mechanically digested food encounters enzymes from salivary glands, pancreas, and the intestinal brush border, chemical digestion takes place. Nutrient absorption, in this section, will refer to the transport of macronutrients from the intestinal lumen to the blood circulation.

1.2.1 Dietary Glucose absorption

Pancreatic and brush-border enzymes in the proximal small intestine, including lactase and sucrase-isomaltase hydrolyze dietary carbohydrates. Mature enterocytes residing on the upper one-third of intestinal villi absorb the resulting monosaccharides (Hediger and Rhoads 1994). These monosaccharides include D-glucose, D-galactose, and D-fructose, however, they cannot simply diffuse through the plasma membrane of enterocytes from the lumen of the small intestine. To circumvent this, the sodium-potassium ATPase on the basolateral membrane of enterocytes pumps sodium ions out of the cell, creating an electrochemical gradient across the cell membrane (Hediger and Rhoads 1994). This electrochemical gradient allows the sodium-dependent glucose transporter-1 (SGLT-1), spanning the apical plasma membrane of enterocytes, to couple the transport of two sodium ions with one D-glucose or one D-galactose molecule into the cell (Hediger and Rhoads 1994). While glucose serves as a major energy source for most mammalian cells (Hediger and Rhoads 1994), enterocytes use amino acids such as glutamine, glutamate, and aspartate as a primary fuel source (Alpers 2000). Therefore, as enterocytes accumulate these monosaccharides, glucose can passively move down its concentration gradient out of the cell via a transporter. This passive transport was thought to be primarily facilitated by glucose transporter GLUT2 (Hediger and Rhoads 1994). The exclusive use of GLUT2 in enterocytes is challenged by the post-prandial hyperglycemia observed in individuals

living with Fanconi-Bickel syndrome, where a single base deletion causes a truncated GLUT2 protein (Santer, Schneppenheim et al. 1997). Additionally, studies in global *Glut2*$^{-/-}$ mice with a transgenic re-expression of GLUT2 in β-cells (RIPGLUT1xGLUT2$^{-/-}$) display normal post-prandial glycemia (Thorens, Guillam et al. 2000). Studies investigating compensatory mechanisms using isolated intestinal perfusions in RIPGLUT1xGLUT2$^{-/-}$ mice reveal a requirement for a glucose-phosphorylation event and the action of glucose-6-phosphate translocase for basolateral glucose transport (Stumpel, Burcelin et al. 2001). Apical GLUT5 transports fructose into enterocytes (Burant, Takeda et al. 1992, Davidson, Hausman et al. 1992). Undigested carbohydrates, like cellulose, remain in the colon where they are fermented by the gut microbiota.

1.2.2 Dietary Fat absorption

Greater than 95% of dietary fat is absorbed (Pan and Hussain 2012). Fats provide a more efficient form of energy storage compared to carbohydrates and proteins. The hydrophobicity of dietary fat, however, dictates that it must first be hydrolyzed and emulsified. In the stomach, dietary phospholipids stabilize the emulsion of dietary fats with stomach acid. The exocrine pancreas secretes pancreatic lipases and phospholipase A into the duodenum to hydrolyze dietary fats. Pancreatic lipase hydrolyzes triacylglycerol molecules into 1,2-diacyglycerol (DAG), 2-monoacylglycerol (MAG), glycerol, and free fatty acids, as well as cholesterol esters into free cholesterol (Pan and Hussain 2012). Pancreatic phospholipase A2 hydrolyzes phospholipids to lisophospholipids and free fatty acids. Concomitantly, the gall bladder secretes bile acids previously synthesized in hepatocytes into the duodenum via the bile duct. Bile acids combine with phospholipids to form an outer later around insoluble free fatty acids, MAG, DAG, lisophospholipids, cholesterol, plant sterols, and fat-soluble vitamins. The resulting amphipathic vesicle-like structures are called a mixed micelle (Bernier-Latmani and Petrova 2017).

Micelles facilitate passive diffusion and active transport of MAG, DAG, free fatty acids, and free cholesterol into enterocytes (Figure 1.2). MAG can enter enterocytes by passive diffusion

(Schulthess, Lipka et al. 1994), down their concentration gradient, although there is evidence for protein-mediated uptake as well (Ho and Storch 2001). Most dietary fatty acids diffuse through the apical plasma membrane of enterocytes while the remainder enter through peripheral plasma membrane fatty acid-binding protein (FABPpm), fatty acid transport proteins (FATPs), and fatty acid translocase/cluster of differentiation 36 (FAT/CD36) by active transport (Pan and Hussain 2012). Niemann-Pick C1-like 1 protein (NPC1L1) transports dietary cholesterol and plant sterols into enterocytes, whose activity is inhibited by the drug ezetimibe as a cholesterol-lowering therapy (Phan, Dayspring et al. 2012). While the entire small intestine is biologically capable of absorbing dietary fat, the jejunum performs the bulk of this process (D'Aquila, Hung et al. 2016).

Following the entry of dietary fat in the cytoplasm, enterocytes must efficiently coordinate their transport to prevent lipotoxicity (Bernier-Latmani and Petrova 2017). Enzymes of the smooth endoplasmic reticulum activate fatty acids and resynthesize them into triacylglycerol molecules (Figure 1.2). Specifically, the acyl-CoA synthetase enzyme activates fatty acids to fatty acyl-CoA (Iqbal and Hussain 2009, D'Aquila, Hung et al. 2016). Triglyceride synthesis occurs through one of two pathways. The predominant pathway in the small intestine is the MAG pathway, where acyl coenzyme A:monoacylglycerol acyltransferase (MGAT) catalyzes the covalent linkage of one fatty acyl-CoA to MAG yielding DAG, which is then acetylated to form one triacylglycerol molecule by the enzymes acyl coenzyme A:diacylglycerol acyltransferase 1 and 2 (DGAT 1 and 2). The minor pathway of triacylglycerol synthesis is using glucose for the synthesis of DAG. Glycerol-3-phosphate acyltransferases 3 and 4 (GPAT3/GPAT4) catalyze the acetylation of glycerol-3-phosphate, yielding lysophosphatidic acid. The enzyme 1-acyl-sn-glycerol-3-phosphate acyltransferases (AGPAT1-5) catalyzes the esterification of lysophosphatidic acid into phosphatidic acid. Phosphatidic acid phosphohydrolase catalyzes the hydrolysis of the phosphate group on phosphatidic acid to yield DAG, which is converted to a triacylglycerol molecule by DGAT 1 and/or 2 as in the MGAT pathway (Pan and Hussain 2012). Short chain fatty acids, classified

as 6 carbons or less, are not resynthesized into triglycerides. Rather, they directly enter the blood circulation and bind to albumin for transport into the portal circulation (Schonfeld and Wojtczak 2016).

Figure 1.2 Dietary fatty acid absorption and triglyceride synthesis in an enterocyte. Micelles in the lumen of the small intestine facilitate the passive diffusion and active transport of monoacylglycerol (MAG), diacylglycerol (DAG), and free fatty acids at the apical membrane. Active transport of fatty acids is performed by fatty acid binding protein (FABPpm), fatty acid transport proteins (FATP), and fatty acid translocase/cluster determinant 36 (CD36). Enzymes of the smooth endoplasmic reticulum (ER) activate fatty acids and resynthesize them into triglycerides. The predominant pathway begins with Acyl coenzyme A:monoacylglycerole acyltransferase (MGAT) catalyzing the linkage of one fatty acyl-CoA to monoacylglycerol yielding DAG. Acyl coenzyme A:diacylglycerol acyltransferase 1 and 2 (DGAT) catalyzes the linkage of one fatty acyl-CoA to DAG, yielding a triacylglycerol molecule. The secondary pathway begins with glycerol-3-phosphate acyltransferase 3 and 4 (GPAT3/4) to catalyze the linkage of a fatty acyl-CoA to glycerol-3-phosphate yielding lysophosphatidic acid. The enzyme 1-acyl-sn-glycerol-3-phosphate acyltransferases (AGPAT1-5) catalyze the esterification of lysophosphatidic acid into phosphatidic acid. Phosphatidic acid phosphohydrolase catalyse the hydrolysis of the phosphate group on phosphatidic acid to yield DAG, which is converted to a triacylglycerol through the action of DGAT 1 and/or 2. Triacylglycerol molecules are temporarily stored in cytosolic lipid droplets (CLD) or are incorporated into chylomicrons for transport into circulation. Created with Biorender.

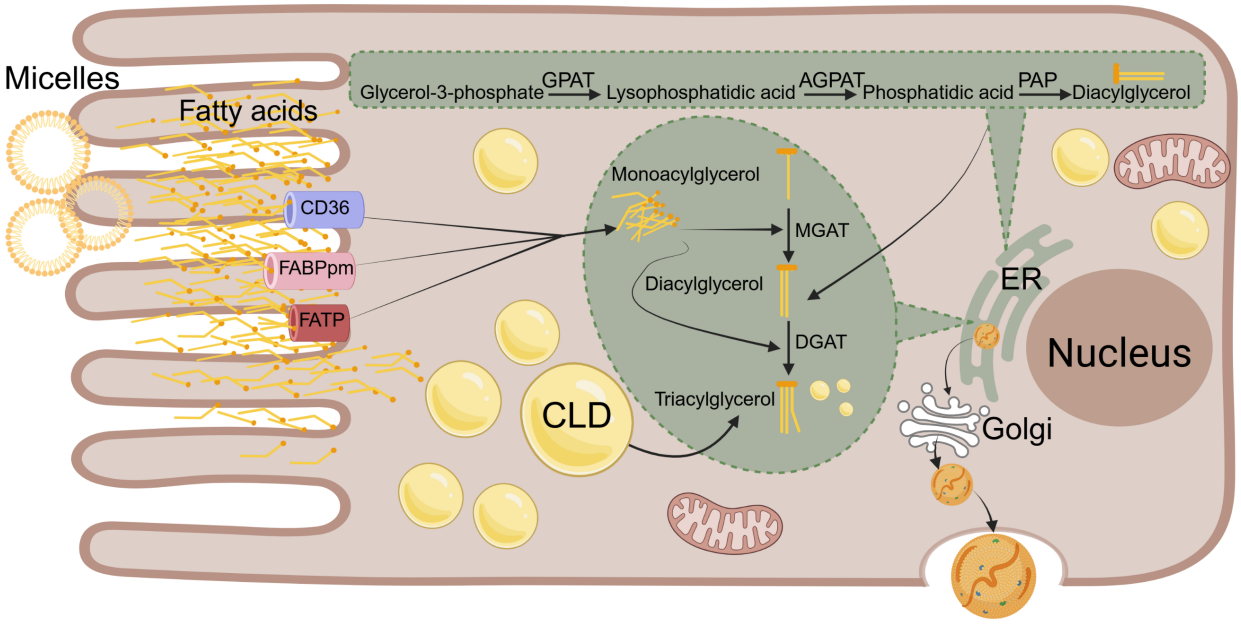
Micelles
Fatty acids
Glycerol-3-phosphate
GPAT
Lysophosphatidic acid
AGPAT
Phosphatidic acid
PAP
Diacylglycerol
CD36
FABPpm
FATP
Monoacylglycerol
MGAT
Diacylglycerol
DGAT
Triacylglycerol
CLD
ER
Nucleus
Golgi

Enzymes of the smooth endoplasmic reticulum also convert free cholesterol into cholesterol ester, primarily with the addition of an oleoyl-CoA group. The enzyme cholesterol acyl transferase (ACAT) catalyzes this esterification (Iqbal and Hussain 2009, D'Aquila, Hung et al. 2016). ABCG5 and ABCG8 heterodimer sterol transporters actively export approximately 95% of plant sterols and 50% of dietary cholesterol from enterocytes back into the lumen for excretion into the feces (Mulvihill 2018). The apical sodium bile acid transporter (ASBT) reabsorbs over 90% of bile acids for circulation back to the liver while the remainder are excreted with the feces. At this point, triacylglycerol molecules along with cholesterol esters are temporarily stored in cytoplasmic lipid droplets (CLD) or are incorporated into lipoproteins for transport into circulation (Iqbal and Hussain 2009, Hung, Carreiro et al. 2017, Mulvihill 2018). Enterocyte CLD will be further described in section 1.5.3.

1.3 Regulators of post-prandial metabolism

Hormone, originating from the Greek word *hormon,* meaning “set in motion” was proposed by Bayliss and Starling through their discovery of a secretin, a gut-derived hormone that stimulates the pancreas to secrete digestive juices (Bayliss and Starling 1902). Beyond their role in facilitating digestion, hormones coordinate the cellular metabolic response to macronutrients.

1.3.1 Gut hormones GLP-1, GLP-2, and GIP

Glucose-dependent insulinotropic polypeptide (GIP) was initially discovered for its role in inhibiting gastric acid secretion and motility in excised canine stomach pouches when administered at high doses (Brown and Pederson 1970) and was called “gastric inhibitory polypeptide” (Brown, Dryburgh et al. 1975). Later, however, it was shown to not have this effect in humans (Meier, Goetze et al. 2004). Earlier studies demonstrated that intravenous infusion of intestinal mucosal extracts lowered blood glucose in rabbits and dogs, pointing to the existence of an intestinal hormone that stimulates endocrine pancreatic secretion, termed “incretin” (Moore

1906, BARRE 1932). In line with this, glucose tolerance tests in humans revealed a greater insulin response to oral versus intravenous (Elrick, Stimmler et al. 1964, McIntyre, Holdsworth et al. 1964). Studies administering purified GIP and glucose intravenously in healthy individuals identified GIP as the first incretin hormone (Dupre, Ross et al. 1973). Activation of the β-cell GIP receptor (GIPR) enhances insulin secretion in response to elevated blood glucose and, to a lesser extent, amplifies glucagon secretion from α-cells in both healthy individuals and those living with type 2 diabetes mellitus (T2DM) (Baggio and Drucker 2007, Christensen, Vedtofte et al. 2011, El and Campbell 2020). While the incretin effect of GIP occurred at physiological doses, GIP could only inhibit gastric acid secretion at extremely high doses. As such, GIP was renamed glucose-dependent insulinotropic polypeptide (Muller, Adriaenssens et al. 2025).

GIP is produced from enteroendocrine K cells in the small intestine. GIP is derived from a 144 amino acid (rodent) (Higashimoto, Simchock et al. 1992, Higashimoto and Liddle 1993, Tseng, Jarboe et al. 1993) or 153 amino acid (human) (Takeda, Seino et al. 1987) precursor, proGIP, and is active in its 1-42 amino acid form. Most K cells express prohormone convertase 1/3 (PC1/3), which cleaves proGIP at arginine 65, resulting in the biologically active GIP(1-42) (Ugleholdt, Poulsen et al. 2006) that is stored in secretory granules (~450 nm) (Buchan, Polak et al. 1978). A small population of K cells express PC2 instead of PC1/3, resulting in GIP(1-31), which is amidated by peptidyl-glycine α-amidating monooxygenase, resulting in GIP(1-30) (Fujita, Asadi et al. 2010). GIP is also produced by α-cells in the pancreatic islet as well as neurons (Muller, Adriaenssens et al. 2025). Studies using antibodies to neutralize GIP demonstrate significantly blunted insulin release upon oral glucose in rats (Lauritsen, Holst et al. 1981). Upon intraduodenal delivery of glucose, GIP antiserum blunts the incretin effect in anesthetized rats but does not completely abolish it (Ebert and Creutzfeldt 1982). Additionally, in non-anesthetized rats, 14 days GIP antiserum treatment did not significantly impact oral glucose tolerance, pointing to the existence of another hormone contributing to the “incretin effect” (Ebert and Creutzfeldt 1982).

The generation of the first glucagon-detecting antibody (Unger, Eisentraut et al. 1959) enabled the development of the radioimmunoassay to detect glucagon in blood and tissue samples other than the pancreas, including the intestine (Unger, Ketterer et al. 1966, Moody, Markussen et al. 1970, Murphy, Elmore et al. 1971). Furthermore, glucagon-like immunoreactivity in the blood was observed upon intraduodenal, but not intravenous, infusion of glucose in dogs with pancreatic resection (Unger, Ohneda et al. 1968). Not only did this confirm extra-pancreatic release, but specific rise in glucagon-like immunoreactivity was observed in the mesenteric vein, highlighting the gut as a likely source. Moreover, jejunal glucagon-like immunoreactivity was shown to stimulate insulin release (Unger, Ohneda et al. 1968). Immunostaining and electron microscopy studies revealed distinct morphology of glucagon immunoreactive pancreatic α-cells compared to intestinal cells, inspiring the name of “L-cells” (Grimelius, Capella et al. 1976). Further studies identified that glucagon originates from a larger precursor molecule, called proglucagon, that undergoes tissue-selective processing (Muller, Finan et al. 2019).

Using anglerfish islet preproglucagon cDNA, the predicted protein sequence revealed the presence of two peptides with striking homology to glucagon and GIP (Lund, Goodman et al. 1981, Lund, Goodman et al. 1982, Lund, Goodman et al. 1983). The identification of these two glucagon-related peptides in rats, hamster, bovine, and human proglucagon sequence led to their identification as glucagon-like peptide 1 (GLP-1) and glucagon-like peptide 2 (GLP-2) (Bell, Sanchez-Pescador et al. 1983, Bell, Santerre et al. 1983, Lopez, Frazier et al. 1983, Heinrich, Gros et al. 1984, Heinrich, Gros et al. 1984). In the gut, posttranslational processing of the 160 amino acid proglucagon by prohormone convertase 1/3 (PC1/3) yields active peptides glicentin, GLP-1, intervening peptide 2 (IP2), and GLP-2 (Mojsov, Heinrich et al. 1986, Orskov, Holst et al. 1986). In addition to the L cell, there is evidence of GLP-1 production in pancreatic α-cells and neurons. GLP-1, first identified from amino acids 1-37 and 1-33 (Drucker, Mojsov et al. 1986), is active upon N-terminal truncation yielding GLP-1(7-37) and GLP-1(7-36)amide (Drucker, Philippe

et al. 1987, Holst, Orskov et al. 1987). The activation of β-cell GLP-1 receptor (GLP-1R) promotes glucose-stimulated insulin secretion and inhibits glucagon secretion (Orskov, Holst et al. 1988, Nauck, Kleine et al. 1993, Baggio and Drucker 2007). The active form of GLP-2 in tissue and circulation is the complete 1-33 amino acid (Brubaker, Crivici et al. 1997) upon C-terminal truncation of 2 amino acids (Orskov, Buhl et al. 1989). The intestinotrophic effects of GLP-2 were first demonstrated in mice and accelerated clinical trials testing the effectiveness of this action in individuals living with intestinal failure because of surgical resection, known as short bowel syndrome (Brubaker 2018) to improve nutrient absorption and reduce parenteral nutrition requirements.

GLP-1, GLP-2, and GIP initiate signalling in their target cells through their respective class B, G-protein coupled receptor (GPCR). GCPRs have 7 transmembrane helices, and in the cases of GIPR, GLP-1R and GLP-2R, signal via Gs-mediated cAMP production and downstream signaling cascades. They are all class B1 GPCRs and share significant sequence similarity (Usdin, Mezey et al. 1993). Enterocytes, hepatocytes, and adipocytes do not express GLP-1R, GLP-2R, or GIPR. Therefore, their impact on metabolism is indirect. The physiological secretion of the peptide hormones GIP, GLP-1, and GLP-2 are tightly controlled by the nutrient-sensing abilities of their respective enteroendocrine cells. Additionally, the serine protease dipeptidyl peptidase 4 (DPP4) limits the bioavailability of GIP, GLP-1, and GLP-2 by cleaving the first two amino acids rendering them inactive to initiate receptor signalling (Deacon, Johnsen et al. 1995, Knudsen and Pridal 1996, Hansen, Deacon et al. 1999). In healthy humans, GIP has a circulating half-life of 7 min (Meier, Nauck et al. 2004), GLP-1 has a circulating half-life of 1-2 min (Deacon, Johnsen et al. 1995), and GLP-2 has a circulating half-life of 7 min (Drucker, Shi et al. 1997, Hartmann, Harr et al. 2000). GIP concentrations are much greater than GLP-1 in the post-prandial state (Meek, Lewis et al. 2021). Prolonged activation of GLP-1, GLP-2, and GIP receptors is achieved through

receptor agonists resistant to DPP4 cleavage or through compounds that inhibit DPP4 activity (Jeppesen, Sanguinetti et al. 2005, Baggio and Drucker 2007).

1.3.2 Enteroendocrine cells

Enteroendocrine cells are highly sensitized to nutrient intake due to their polarized shape, direct contact with the lumen, and proximity to the vasculature for peptide hormone secretion. Enteroendocrine cells are equipped with GPCRs and transporters to sense the macronutrients and release the appropriate hormones (Spreckley and Murphy 2015). These include: G-protein coupled receptor family C group 6 subtype A (GPRC6A), taste receptors, G-protein coupled receptor 93 (GPR93) (peptones), free-fatty acid receptor 2 (FFAR2), free-fatty acid receptor 3 (FFAR3), short-chain fatty acid (SCFA) receptors, free-fatty acid receptor 1 (FFAR1), free-fatty acid receptor 4 (FFAR4), long-chain fatty acid (LCFA), and G-protein coupled receptor 119 (GPR119) (Spreckley and Murphy 2015). Upon ligand binding to a cell surface receptor and subsequent cell depolarization, hormone-containing granules fuse with the lateral and basal membrane for discharge into the villus capillaries (Paternoster and Falasca 2018). This idealistic design favours rapid and precise peptide delivery in circulation to initiate signaling through their respective receptors to control metabolism.

1.3.2.1 L cells produce GLP-1 and GLP-2

GLP-1+ cells reside in crypts and the villus epithelium; their density along the gut increases distally with the highest abundance in the ileum in rodents and the colon in humans (Eissele, Goke et al. 1992). Within L-cells, GLP-1 is stored in granules in its active form (7-36 amide) (Eissele, Goke et al. 1992) in the small (Orskov, Bersani et al. 1989) and large intestine (Deacon, Johnsen et al. 1995). GLP-1+ cells are also found in the stomach fundus (Ribeiro-Parenti, Jarry et al. 2021). GLP-1 and GLP-2 are co-secreted in equimolar ratios. In rodents, upon PKA activation, cAMP binds its response element in the promoter of *Gcg* (Drucker and Brubaker

1989, Drucker, Jin et al. 1994). Insulin activates *Gcg* expression in the intestinal L cell via a PI3-K-dependent, Akt-independent nuclear translocation of β-catenin, which heterodimerizes with transcription factor-4/lymphoid enhancer binding factor (TCF-4/LEF) (Brubaker 2018). Additionally, the transcription factor paired box 6 (PAX6) increases the transcription of *Gcg* (Hill, Asa et al. 1999). Colonic L-cells contain twice as much GLP-1 peptide than proximal intestine L-cells (Reimann, Habib et al. 2008). Forty-eight hours of fasting in rats significantly reduces ileal *Gcg* mRNA (25-50%), which was associated with a 41-60% decrease in plasma bioactive GLP-2 levels (Nelson, Murali et al. 2008). Both plasma GLP-2 and ileal *Gcg* mRNA levels were found to be restored upon 2 days of refeeding or 4 days of continuous intragastric, but not intravenous, refeeding with total parenteral nutrition solution (32% energy from fat 68% energy from dextrose) (Nelson, Murali et al. 2008), highlighting the critical importance of luminal nutrient exposure for gut hormone release.

Figure 1.3 Nutrient stimulation for L cells. The transcription factor PAX6 promotes the expression of preproglucagon (*GCG*). Microvilli protrude from the apical side of the cell into the lumen. Incoming macronutrients from the lumen are detected and sensed by apical receptors. Long-chain fatty acids are sensed by G-protein coupled receptors GPR119, GPR43/FFAR2, and GPR41/FFAR3. GPR119 is also a receptor for oleoylethanolamide (OEA). Bile acids are detected by Takeda G-protein coupled receptor 5 (TGR5). Amino acids are sensed by GPRC6A. Sweet taste receptors (T1R2/T1R3) sense the presence of glucose. Microbial fermentation leads to the production of short chain fatty acids (SCFA), which are sensed by GPR40/FFAR1 and GPR120/FFAR4. On the basolateral side, somatostatin receptors 2 and 5 (SSTR2/5) sense somatostatin from D cells, and the interleukin-6 and leptin receptors are expressed. Chylomicrons also stimulate GLP-1 secretion independent of lipoprotein lipase (LPL) activity. Created with Biorender.

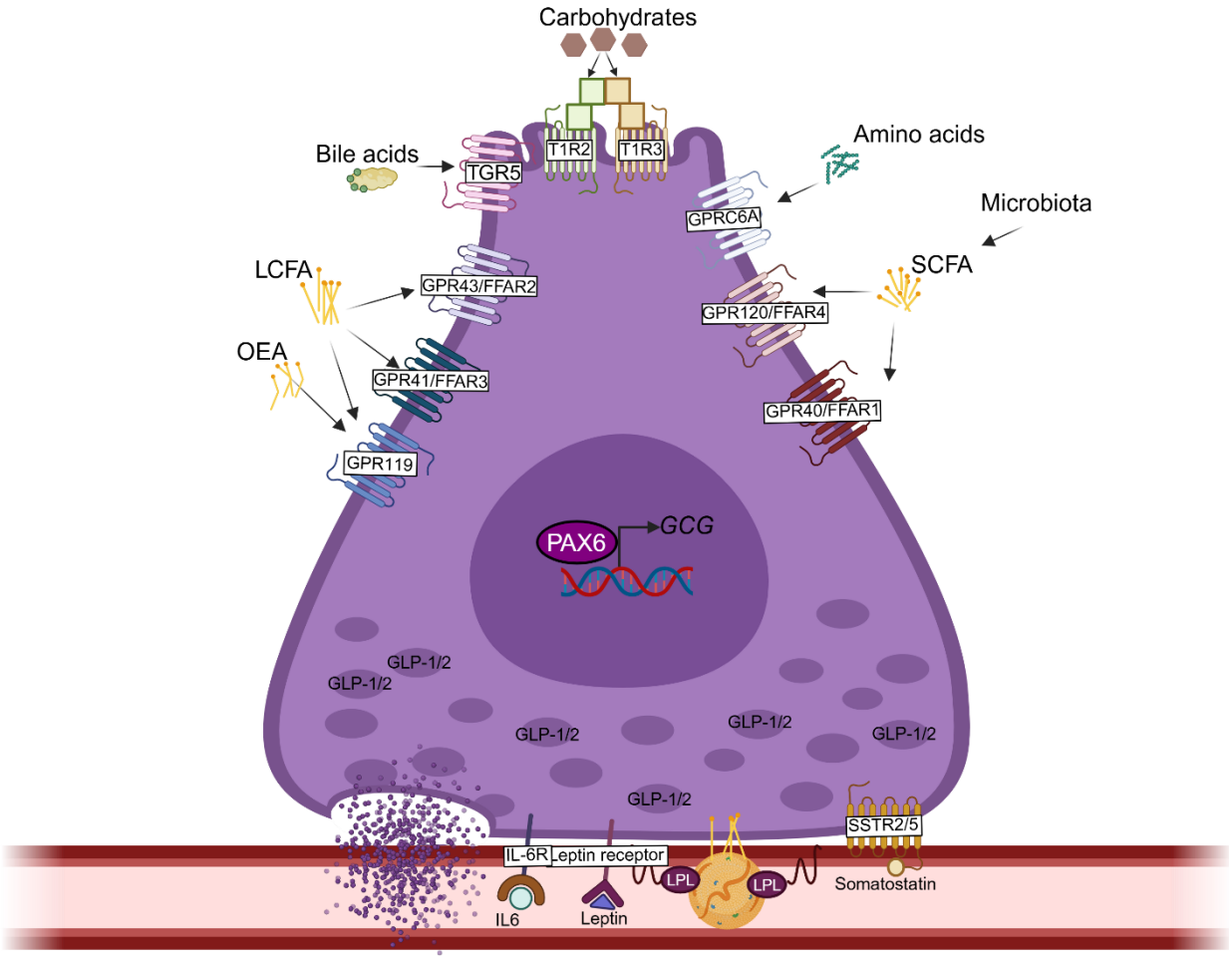
Carbohydrates
T1R2
T1R3
Bile acids
TGR5
Amino acids
GPRC6A
Microbiota
LCFA
GPR43/FFAR2
SCFA
GPR120/FFAR4
OEA
GPR41/FFAR3
GPR40/FFAR1
GPR119
PAX6
GCG
GLP-1/2
GLP-1/2
GLP-1/2
GLP-1/2
GLP-1/2
GLP-1/2
SSTR2/5
IL-6R
Leptin receptor
LPL
LPL
Somatostatin
IL6
Leptin

1.3.2.2 Carbohydrate secretagogues

In healthy men, oral glucose has been shown to significantly increase plasma total GLP-1 (GLP-1(1-36) and GLP-1(7-36)) levels after 30 minutes (Herrmann, Goke et al. 1995). The same study revealed that intraduodenal infusion of glucose induces a rapid 200% increase in GLP-1 that returns to baseline by 30 min (Herrmann, Goke et al. 1995). In rats, ileal luminal perfusion of a 5% glucose solution induces a rapid rise (~2-fold) in portal plasma GLP-1 in 30 minutes (Herrmann, Goke et al. 1995). The GLP-1/GLP-2 ratio (detecting C-terminal of GLP-1 and N-terminal of GLP-2) has been shown to significantly increase at 120 and 250 min during an oral glucose tolerance test in obese men (Matikainen, Bjornson et al. 2016). Intraduodenal administration of sucrose, sucralose, and the artificial sweetener PALSWEET in rats have each been shown to significantly increase lymph GLP-2 output compared to saline control (Sato, Hokari et al. 2013), indicating that GLP-2 can be stimulated by non-caloric cues from the gut lumen.

1.3.2.3 Fatty acid secretagogues

In healthy men, oral ingestion of corn oil has been shown to induce a 1000% increase in the early phase of GLP-1 secretion, which did not return to baseline even after 120 min (Herrmann, Goke et al. 1995). A 20% infusion of Intralipid, an emulsion of essential fatty acids, in the perfused rat ileum, however, does not significantly increase portal plasma GLP-1 from baseline (Herrmann, Goke et al. 1995). This suggests that since orally ingested fatty acids do not typically reach the ileum, a direct sensing mechanism for this lipid composition does not exist in the ileum, or that GLP-1 in this experiment bypassed portal circulation. Consistent with the latter option, experiments directly administering corn oil into either duodenal or ileal luminal compartments in anesthetized rats demonstrate significantly increased plasma GLP-1 obtained from the carotid artery to the same extent from baseline (Roberge and Brubaker 1993). Taken together, these experiments highlight the complexity of GLP-1 secretion as it relates to time, location of nutrient exposure and circulatory compartment.

The GLP-1/GLP-2 ratio remains consistent throughout an oral fat tolerance test performed in obese men, where this ratio is significantly higher at 120 and 250 min during an oral glucose tolerance test due to a drop in GLP-2 at these time points (Matikainen, Bjornson et al. 2016). This finding is in line with a more predominant role for GLP-2 in lipid metabolism compared to glucose absorption. Lymph fistula experiments in rats reveal post-prandial levels in intestinal lymph are 5-6 times higher for GLP-1 compared to portal venous plasma (D'Alessio, Lu et al. 2007, Lu, Yang et al. 2007). Similarly, GLP-2 concentrations in the lymph are significantly higher (~2-fold) than in blood at fasting and 2 hours after (~3-fold) duodenal infusion of perilla oil (Sato, Hokari et al. 2013). The physiological advantage for lymph versus blood secretion is not clear; however, DPP4 activity during fasting or post-meal is 20-fold higher in plasma than in lymph (D'Alessio, Lu et al. 2007), suggesting a route to bypass the degradation by DPP4.

Studies *in vitro* or *ex vivo* have shown that in the presence of glucose, chylomicrons significantly increase GLP-1 secretion from murine immortalized enteroendocrine cells (GLUTag), murine duodenal cultures, and human duodenal cultures (Psichas, Larraufie et al. 2017). Experiments in GLUTag cells reveal that chylomicron-induced release of GLP-1 requires lipoprotein lipase, which is highly expressed in duodenal L cells and GLUTag cells (Psichas, Larraufie et al. 2017). However, lipoprotein lipase is dispensable in chylomicron-stimulated GLP-1 secretion in duodenal cultures, which may be related to the lack of basolateral access to chylomicrons (Psichas, Larraufie et al. 2017). The relationship between chylomicrons and GLP-1 secretion is interesting given the control GLP-1R action has on systemic post-prandial chylomicron levels, which will be further discussed in section 1.6.

1.3.2.4 Mixed meal

Oral galactose and amino acids rapidly increase plasma GLP-1 levels in healthy humans (Herrmann, Goke et al. 1995). Oral ingestion of a mixed meal containing soybean oil, casein, and glucose induces a rapid ~6-fold increase in GLP-1 levels by 15 and 30 minutes, which returns to

baseline by 120 minutes (Herrmann, Goke et al. 1995). Ileal luminal perfusion of a mixed meal in rats induces a rapid rise (2-fold) in portal plasma GLP-1 in 30 minutes (Herrmann, Goke et al. 1995). Additionally, in response to a meal, in patients living with short bowel syndrome with a preserved colon (jejuno-colonic anastomosis), both baseline and meal-stimulated GLP-1 and GLP-2 are elevated, with GLP-2 levels threefold greater than control patients (average concentration of 72 pmol/L), which persists throughout the post-prandial period (Jeppesen, Hartmann et al. 2000), indicating that colonic L cells can compensate for the loss of ileal L cells when all or large parts of the ileum are surgically removed .

1.3.2.5 Hormonal control of GLP-1 release

Plasma GLP-1 levels peak within 5-15 minutes of food ingestion, where certainly these nutrients do not reach the ileum to directly stimulate L cells (Borgstrom, Dahlqvist et al. 1957). Plasma GIP secretion in response to duodenal luminal administration of corn oil occurs earlier than GLP-1 secretion (Roberge and Brubaker 1993, Rocca and Brubaker 1999), and administration of corn oil to duodenal luminal compartments elicits the same plasma GLP-1 response compared to corn oil administration to ileal luminal compartments (Roberge and Brubaker 1993). Despite the presence of L cells in the duodenum, they are not responsible for the GLP-1 release as removing the jejunum-ileum before infusing the duodenal compartment with fat prevents the observed increase of plasma GLP-1 (Roberge, Gronau et al. 1996). Importantly, intravenous infusion of post-prandial levels of GIP increases plasma GLP-1 levels 2-fold, independent of blood glucose levels (Roberge and Brubaker 1993), suggesting that GIP stimulates early GLP-1 secretion in response to duodenal luminal nutrients. Indeed, GLP-1 secretion is abolished upon corn oil infusion to the proximal duodenal compartment in vagotomised rats (Rocca and Brubaker 1999). Electrical stimulation of the vagus nerve stimulates GLP-1 secretion, even in the absence of nutrients (Rocca and Brubaker 1999). GIP can stimulate the first phase of GLP-1 secretion independent of the vagus nerve, but only when infused at

suprapharmacological levels, as evidenced by the rapid rise and fall in plasma GLP-1 upon supraphysiological infusion of GIP in sham and vagotomised rats (Rocca and Brubaker 1999). Additionally, L cells express leptin receptors. Leptin stimulates GLP-1 secretion from rodent (GLUTag) and human L cells (NCI-H716) *in vitro* in a dose-dependent manner, as well as in *ob/ob* mice (Anini and Brubaker 2003). Overall, these studies unveil the existence of a neuroendocrine loop that in the proximal and distal intestine to stimulate ileal L cells when dietary fat enters the duodenum.

1.3.2.6 Enteroendocrine K cells produce GIP

GIP mRNA (Tseng, Jarboe et al. 1993) and peptide concentrations (Bryant, Bloom et al. 1983) are enriched in duodenal and jejunal mucosal tissues in rodents and humans compared to the distal ileum. Correspondingly, K-cells in the proximal small intestine contain more GIP protein and secrete more GIP in response to intestinal lard oil perfusion than distal K cells (Iwasaki, Harada et al. 2015). In K cells, transcription factor X6 (RFX6) binds the *Gip* promoter to increase mRNA expression (Suzuki, Harada et al. 2013) (Figure 1.4). Pancreatic and duodenal homeobox-1 (PDX1) is a transcription factor that maintains K-cell number, intestinal GIP protein and mRNA expression (Ikeguchi, Harada et al. 2018). The number of K cells and their *Gip* mRNA content increases with age, which corresponds to the GIP hypersecretion observed in 1 year old mice compared to 3–4-month-old mice (Ikeguchi, Harada et al. 2018). Moreover, the mRNA expression of transcription factor *Pdx1*, but not *Rfx6* increases with age in K cells (Ikeguchi, Harada et al. 2018). High-fat feeding does not increase K-cell number in mice, instead, it increases GIP protein and mRNA expression, which correlates to increased *Rfx6* and *Pdx1* mRNA expression (Suzuki, Harada et al. 2013). Both glucose (4-fold) and fat (2.5-fold) ingestion increase *Gip* mRNA expression compared to chow-diet feeding (Higashimoto, Opara et al. 1995). Therefore, through different mechanisms, both diet-induced obesity and aging lead to increased GIP reserves for secretion into circulation.

Figure 1.4 Nutrient stimulation of K cells. Regulatory factor x6 (RFX6) and insulin promoter factor 1 (PDX1) enhance the expression of GIP. Long-chain fatty acids are sensed by G-protein coupled receptors GPR119, GPR43/FFAR2, and GPR41/FFAR3. GPR119 is also a receptor for oleoylethanolamide (OEA). Luminal glucose is transported through the sodium-glucose linked transporter-1 (SGLT1). GLUT5 transports luminal fructose. Amino acids are sensed by GPRC6A. Microbial fermentation leads to the production of short chain fatty acids (SCFA), which are sensed by GPR120/FFAR4 and GPR40/FFAR1. On the basolateral side, lipoprotein lipase (LPL) action on chylomicrons stimulate GIP secretion. Created with Biorender.

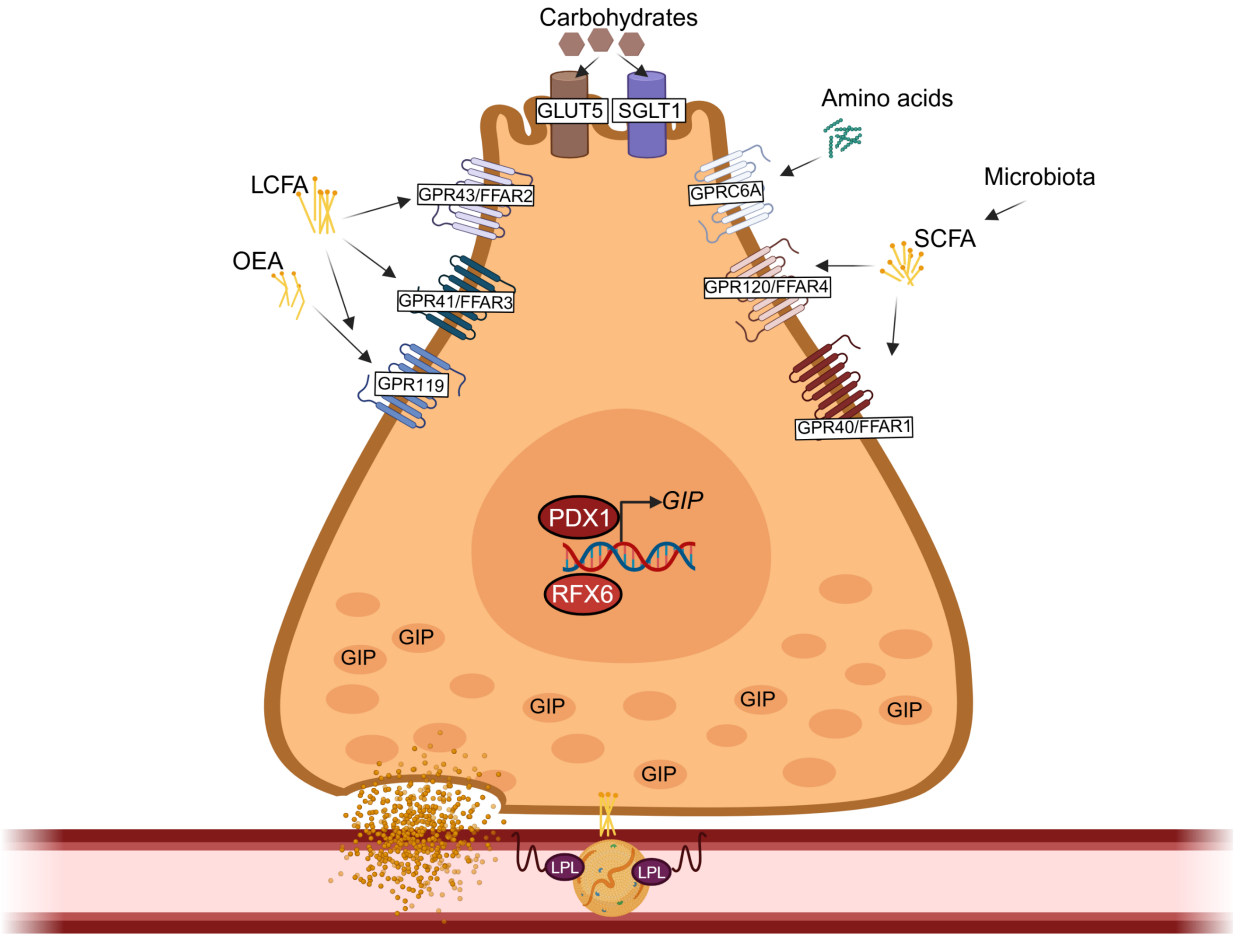
Carbohydrates
GLUT5
SGLT1
Amino acids
LCFA
GPR43/FFAR2
GPRC6A
Microbiota
SCFA
OEA
GPR41/FFAR3
GPR120/FFAR4
GPR119
GPR40/FFAR1
PDX1
GIP
RFX6
GIP
GIP
GIP
GIP
GIP
GIP
LPL
LPL

1.3.2.7 Carbohydrate secretagogues

Carbohydrates stimulate GIP secretion into circulation (Figure 1.4) (Pederson, Schubert et al. 1975, Brown and Otte 1979, McCullough, Miller et al. 1983). Consistent with K cell location, glucose delivery in the upper intestine significantly increases circulating levels while glucose injection in the colon does not (Moriya, Shirakura et al. 2009, Wang, Khan et al. 2025). GIP secretion increases more rapidly in response to simple, fast-absorbing carbohydrates compared to complex, slow-absorbing carbohydrates (Collier, McLean et al. 1984). K and L cells express the SGLT-1 glucose transporter on the apical membrane. Therefore, as glucose is being absorbed by neighbouring enterocytes, the coupled uptake of two sodium ions with each molecule of glucose triggers cell membrane depolarization and voltage-gated entry of calcium ions, thereby releasing the peptide hormones (Gribble and Reimann 2019). Genetic elimination of ATP-sensitive potassium (K_{ATP}) channels (*Kir6.2*$^{-/-}$mice) significantly increases glucose absorption and glucose-stimulated GIP secretion, associated with an increase in duodenal *Sglt1* mRNA expression (Ogata, Seino et al. 2014). Indeed, *Sglt1* knockout mice display impaired plasma insulin, GIP, and GLP-1 in response to an oral gavage of glucose (Gorboulev, Schurmann et al. 2012). Preventing glucose absorption with SGLT1 inhibitor phloridizin abolishes glucose-stimulated GIP secretion in healthy wild-type (Sykes, Morgan et al. 1980) and *Kir6.2*$^{-/-}$ mice (Ogata, Seino et al. 2014). Interestingly, glucose metabolism is not required for the stimulation of GIP secretion, as shown by the administration of nonmetabolizable sugar α-methyl-D-glucopyranoside, however, SGLT1 inhibitor phloridizin significantly blunts this action (Moriya, Shirakura et al. 2009).

1.3.2.8 Fatty acid secretagogues

Many studies have identified dietary fat as a strong stimulus for GIP secretion (Pederson, Schubert et al. 1975, Brown and Otte 1979, McCullough, Miller et al. 1983). Plasma GIP levels rise significantly upon oral fat consumption compared to glucose in mice (Shibue, Yamane et al.

2015) and in humans (Yamane, Harada et al. 2012). Ingestion of a mixed carbohydrate and fat meal significantly increases plasma GIP levels compared to carbohydrates alone in healthy humans (Collier, McLean et al. 1984) but this increase is not as great as ingestion of fat alone in healthy humans (Creutzfeldt, Ebert et al. 1978). GIP secretion in response to oral fat is greater in patients with obesity and glucose intolerance and does not change with the addition of glucose to the meal (Creutzfeldt, Ebert et al. 1978).

Chylomicrons, intestinally produced triglyceride rich lipoproteins, promote GIP secretion from K cells (Figure 1.4). Earlier work demonstrates that blocking chylomicron transit from the endoplasmic reticulum to the Golgi by Pluronic L-81 in rats robustly reduces (~4.5 fold) lymph GIP levels and secretion rates in response to fat delivery by Liposyn to levels similar to saline controls (Lu, Yang et al. 2012). Therefore, GIP secretion from K cells in response to Liposyn requires post-Golgi chylomicron transit, not lipid absorption alone (Lu, Yang et al. 2012). This work is supported by experiments preventing micelle formation via common bile duct ligation; this abolishes GIP secretion upon a lard gavage compared to sham controls, independent of meal transit (Shibue, Yamane et al. 2015). GIP secretion increases in response to chylomicrons alone or in the presence of glucose in both murine and human duodenal cultures in a dose-dependent fashion (Psichas, Larraufie et al. 2017). Glucose stimulation of chylomicron secretion is well documented (Robertson, Parkes et al. 2003, Stahel, Xiao et al. 2019, Xiao, Stahel et al. 2019) where glucose promotes chylomicron secretion from lipid stores in enterocytes, which may in turn provide additional stimulus for GIP secretion.

The free fatty acid receptor GPR120 is enriched in proximal K cells while GPR40, GPR41, and GPR43 are significantly enriched in distal K cells (Iwasaki, Harada et al. 2015). *Gpr120*$^{-/-}$ mice display a 75% reduction in plasma GIP concentration upon lard oil gavage compared to wild-type mice (Iwasaki, Harada et al. 2015). Similarly, oral pretreatment with a GPR120 partial antagonist, grifolic acid methyl ether, reduces GIP secretion by 80% in response to lard oil gavage (Iwasaki,

Harada et al. 2015). All GIP+ cells express fatty acid-binding protein 5 (FABP5) (Shibue, Yamane et al. 2015). While whole-body elimination of FABP5 in mice does not impact GIP content or K cell number, these mice secrete significantly less GIP into plasma 60 minutes after a lard gavage compared to wild-type controls (Shibue, Yamane et al. 2015).

GIP concentrations in the bloodstream are the highest in hepatic portal plasma, however, lymph GIP concentrations are ~3-fold higher upon the same stimulus (D'Alessio, Lu et al. 2007, Lu, Yang et al. 2008), indicating peptide transit from K cells to villus lacteals. Co-intraduodenal infusion of mixed nutrients (carbohydrate, dextrose) and lipid (20% Liposyn) in rats significantly increase GIP secretion in lymph to a greater extent than either nutrient at the same meal caloric value alone, suggesting a synergistic effect (Lu, Yang et al. 2008). As discussed for the case of GLP-1 and GLP-2 in the lymph, the role of lymphatic GIP levels is unclear. Further characterization of the lymph GLP-1R+, GLP-2R+, and GIPR+ cells in fasted and postprandial state are required.

1.3.3 Endocrine hormones

In addition to the role of the exocrine pancreas in nutrient digestion described above, the endocrine pancreas comprises specialized cells that release hormones to maintain metabolic balance. Islet cell populations are distinguished by the hormone they predominantly produce: α-cells with glucagon, β-cells with insulin, δ-cells with somatostatin, γ-cells with pancreatic polypeptide, and ε-cells with ghrelin (Campbell and Newgard 2021). These hormones play important roles in metabolic homeostasis. Since glucose serves as the major fuel source for the brain, pancreatic islets are charged with maintaining blood glucose levels. Hormones secreted from the pancreas have great influence on the metabolism of glucose, amino acids, and lipids (Campbell and Newgard 2021).

1.3.3.1 Insulin

The year 2021 marked the 100 year anniversary of Banting and Best's description of the discovery of insulin at the University of Toronto (Lewis and Brubaker 2021). Insulin promotes metabolic fuel storage, thereby activating anabolic pathways. Post-prandial rises in blood glucose levels trigger insulin secretion, which can be amplified by amino acids, fatty acids, and other hormones that rise in concert (Campbell and Newgard 2021).

β-cells store insulin in granules in preparation for increases in blood glucose levels in the post-prandial state. As post-prandial glucose is metabolized in the β-cell by glycolysis, the cellular ATP/ADP ratio increases. β-cells express K_{ATP} channels; and as ATP produced from glycolysis increases, these channels close leading to the accumulation of intracellular potassium. This increase in intracellular potassium triggers the cell membrane to depolarize, leading to the opening of voltage-gated calcium channels. The influx of calcium ions activates the exocytosis of the readily releasable pool of insulin granules, known as the first phase of insulin secretion. The first phase of insulin secretion covers the first 10-20 minutes of the post-prandial period. The second phase of insulin secretion consists of a lower but sustained secretion rate, driven by the readily releasable pool as well as granules from a storage pool, lasting the remainder of the post-prandial period (Campbell and Newgard 2021).

1.3.3.2 Insulin receptor signalling

Virtually all mammalian cells express the insulin receptor and are therefore responsive to insulin (Haeusler, McGraw et al. 2018). Upon ligand binding, the insulin receptor internalizes and is either degraded in the lysosome or recycled back to the cell surface. Therefore, as plasma insulin levels rise, the receptor cell surface levels decrease, leading to termination of insulin signalling. Correspondingly, as plasma insulin levels fall, the receptor repopulates the cell surface (Haeusler, McGraw et al. 2018).

The insulin receptor is a tyrosine kinase, meaning it phosphorylates tyrosine residues on target proteins (Figure 1.5). Upon insulin binding, the insulin receptor autophosphorylates its own tyrosine residue as well as the insulin receptor substrate proteins (Haeusler, McGraw et al. 2018). The availability of these “phosphotyrosine sites” allows for lipid kinase PI3K to bind insulin receptor substrate proteins, which synthesize the triphosphorylated inositol, PtdIns(3,4,5)P_3 (PIP_3) at the plasma membrane. This converts the initial tyrosine phosphorylation signal into a lipid kinase signal. PIP_3 availability at the plasma membrane recruits phosphoinositide-dependent kinase (PDK), which can then phosphorylate the threonine 308 residue of AKT (Haeusler, McGraw et al. 2018). Concomitantly, mTOR2 phosphorylates serine 473 of AKT, leading to its activation. Activated AKT can now phosphorylate target proteins at serine or threonine residues, including the gluconeogenic transcription factor forkhead family box O (FOXO). AKT also leads to the activation of mTORC1 by phosphorylating and inhibiting TSC. The active mTORC1 leads to the increased expression and phosphorylation of transcription factor sterol regulatory element binding protein 1c (SREBP1c) (Haeusler, McGraw et al. 2018). Through AKT-mediated phosphorylation, insulin impacts glucose production, glucose uptake, as well as the synthesis of glycogen, proteins, and lipids.

Termination of the insulin signalling cascade is mediated by a series of dephosphorylation events catalyzed by phosphatases. Protein tyrosine phosphatase 1B (PTP1B) dephosphorylates tyrosine residues on the insulin receptor and the insulin receptor substrate proteins (Haeusler, McGraw et al. 2018). Lipid phosphatases PTEN and SHIP2 convert PIP_3 into PIP_2, (Haeusler, McGraw et al. 2018). Phosphatases pleckstrin homology domain and leucine-rich repeat protein phosphatase 1α (PHLPP1α), PHLPP1β, and PHLPP2 dephosphorylate AKT at serine 473. Protein phosphatase 3A (PP2A) also dephosphorylates AKT (Haeusler, McGraw et al. 2018).

Figure 1.5 Overview of the insulin receptor signalling pathway upstream of de novo lipogenesis in hepatocytes. Upon insulin binding, the insulin receptor autophosphorylates itself and the insulin receptor substrate (IRS) proteins. The lipid kinase PI3K can now bind insulin receptor substrate proteins, where it synthesizes the triphosphorylated inositol, PtdIns(3,4,5)P3 (PIP3) at the plasma membrane. PIP3 recruits phosphoinositide-dependent kinase (PDK) to phosphorylate AKT at threonine 308 while mTOR2 phosphorylates AKT at serine 473. AKT can now phosphorylate target proteins including transcription factors such as forkhead family box O (FOXO), leading to its nuclear exclusion, and TSC, leading to MTORC1-dependent upregulation of sterol regulatory element binding protein 1c (SREBP-1C). In the phosphorylated state, SREBP-1C enters the nucleus to turn on the expression of genes involved in de novo lipogenesis such as fatty acid synthase (*Fasn*), acetyl-CoA carboxylase *(Acaca*), and stearoyl-CoA desaturase 1 (*Scd1*). Adapted from Morrow, N.M., and Mulvihill E.E. (2023). Complexity in Hepatic Insulin Resistance – Unraveling the Role of Ubiquitin-Specific Protease 14 in Protein Homeostasis of Metabolic Transcription Factors. J Pharmacol Exp Ther. 1; 1-4.

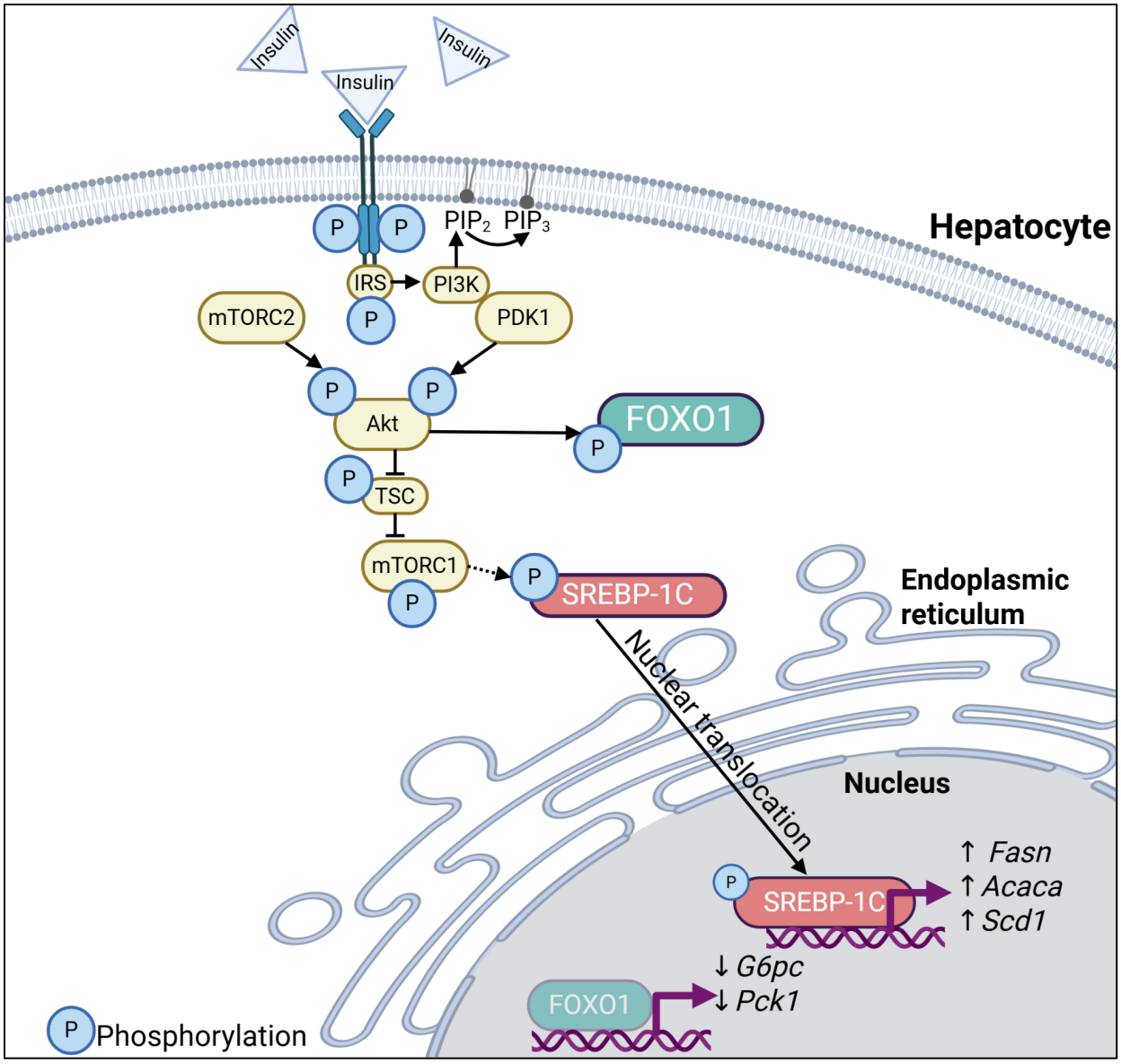
Insulin
Insulin
Insulin
Hepatocyte
P
P
PIP2
PIP3
IRS
PI3K
P
mTORC2
PDK1
P
P
Akt
FOXO1
P
P
TSC
mTORC1
P
P
SREBP-1C
Endoplasmic reticulum
Nuclear translocation
Nucleus
P
SREBP-1C
↑ Fasn
↑ Acaca
↑ Scd1
↓ G6pc
↓ Pck1
FOXO1
P Phosphorylation

1.3.3.3 Glucagon

In 1923, Kimball and Murlin discovered the pancreatic "glucose agonist" that opposed the role of insulin in glucose homeostasis, named glucagon (Kimball and Murlin 1923). Pancreatic α-cells produce glucagon (Vuylsteke, Cornelis et al. 1952, Fodden and Read 1954). Post-prandial glucose and insulin levels suppress glucagon secretion, whereas fasting rises in amino acid and fatty acid levels stimulate it (Campbell and Newgard 2021). Transcription factors PAX6, cMAF, and MAFB within α-cells induce transcription of the *GCG* gene and translation to the proglucagon 160-amino acid precursor peptide (Zeigerer, Sekar et al. 2021). The *GCG* gene also contains a cAMP-response element. Therefore, when cellular cAMP levels rise, the cAMP-response element binding protein (CREB) promotes *GCG* transcription (Zeigerer, Sekar et al. 2021). By contrast, insulin inhibits α-cell *GCG* expression (Zeigerer, Sekar et al. 2021). Proglucagon processing in the α-cell by prohormone convertase 2 (PC2/PCSK2) also yields major proglucagon fragment and glicentin-related pancreatic polypeptide (Zeigerer, Sekar et al. 2021).

Glucagon promotes the mobilization and oxidation of metabolic stores, thereby activating catabolic pathways. Glucagon binds to its GPCR, GCGR, from the class B family of GPCR. While liver hepatocytes express the greatest levels of *Gcgr*, cells in the kidney, adipose, pancreas, spleen, intestine, and adrenal glands (rats) also express a functional GCGR (Zeigerer, Sekar et al. 2021). The GCGR exists as a heterotrimer, α/β/γ, and in the inactive state is bound to the $G_{s\alpha}$ subunit. In hepatocytes, glucagon bindings to its receptor and activates its canonical pathway via G protein G_s (Zeigerer, Sekar et al. 2021). When glucagon activates G_s, the $G_{s\alpha}$ subunit disassociates from the G protein α/β/γ heterotrimer, thereby allowing it to interact with adenylate cyclase (Zeigerer, Sekar et al. 2021). Upon this interaction, adenylate cyclase becomes active, enhancing its production of cAMP. As cellular levels of cAMP rise, protein kinase A becomes active. Protein kinase A translocates to the nucleus, phosphorylating cAMP response element binding protein (CREB)-regulated transcription coactivator 2 (CRTC2), allowing it to bind to CRE

elements in the promoters of target genes, inducing their transcription (Zeigerer, Sekar et al. 2021). These gene expression programs include the *de novo* glucose production, gluconeogenesis, and breakdown of glycogen, glycogenolysis (Zeigerer, Sekar et al. 2021). Glucagon also stimulates the catabolism of amino acids, leading to the production of urea (Wewer Albrechtsen, Holst et al. 2023). Glucagon inhibits *de novo* lipogenesis and enhances the activity of adipocyte hormone-sensitive lipase (ATGL) to hydrolyze stored triglycerides (Wewer Albrechtsen, Holst et al. 2023). The glucagon signal terminates when GCGR is phosphorylated by GPCR kinase, liberating it from Gs. This liberation enables the recruitment of β-arrestins to the GCGR, where this new complex is directed to the clathrin coated pits of the cell membrane, leading to the internalization of the ligand-receptor complex (Luttrell and Lefkowitz 2002, Zeigerer, Sekar et al. 2021). Here, GCGR can either be recycled back to the plasma membrane or degraded by the lysosome.

1.3.3.4 Leptin

In 1949, the V stock of Jackson Laboratory mice had 43 obese mice out of 212, where this 3:1 ratio is indicative of a recessive gene which was named “obese” with the symbol “*ob*”. These mice rapidly gained weight, to about four times that of littermate controls, and homozygotes were found to be sterile (Ingalls, Dickie et al. 1950). Cloning and sequencing of the mouse and human *ob* gene uncovered a 4.5 kb adipose tissue mRNA encoding a 167-amino acid sequence with 84% conservation from mouse to human (Zhang, Proenca et al. 1994). Characterization of the *ob* gene in C57BL/6J *ob/ob* mice revealed a nonsense mutation and a 20-fold increase in the *ob* mRNA levels (Zhang, Proenca et al. 1994).

The discovery of the adipocyte-secreted protein, leptin, named after the Greek word “leptos” for thin (Kelesidis, Kelesidis et al. 2010), expanded the role of adipocytes in energy metabolism beyond energy storage. Adipocytes secrete the majority of leptin, however, the placenta, stomach, and skeletal muscle also contribute to this pool. Leptin secretion follows

diurnal variation with higher levels in the evening and early morning, where levels correlate with the amount of energy stored in fat (Kelesidis, Kelesidis et al. 2010). Leptin levels significantly decrease upon fasting (Boden, Chen et al. 1996). The leptin receptor is produced from the diabetes (*db*) gene (Tartaglia, Dembski et al. 1995). The leptin receptor is expressed in brain, particularly in the hypothalamus, where leptin activates neural circuits that modulate appetite. In the mesolimbic dopamine system, leptin modulates the motivation and reward circuits of feeding. In the nucleus of the solitary tract of the brainstem, leptin contributes to satiety (Kelesidis, Kelesidis et al. 2010).

1.4 Lipoprotein metabolism

Triacylglycerol and cholesterol ester molecules are hydrophobic. These molecules, however, must be transported from the cells that absorb or synthesize them to other tissues for energy use or storage, steroid synthesis, or cell membrane formation. Blood and lymphatic vasculature are aqueous mediums, where highly polar molecules, such as proteins, circulate. As such, several enzymes catalyze the formation of lipid-protein complexes, called lipoproteins, to tightly package these hydrophobic triacylglycerol and cholesterol ester molecules within their cores (Griel and McCarthy 1969). Specifically, the monolayer of phospholipids and apolipoproteins that surround their hydrophobic cores increase the solubility of lipoproteins in blood and lymph. Lipoproteins in the systemic circulation are broadly divided into 4 classes: Chylomicron, very low-density lipoprotein (VLDL), low density lipoprotein (LDL), and high-density lipoprotein (HDL) (Figure 1.6). Plasma lipoproteins are classically defined by the densities at which they float upon ultracentrifugation: chylomicrons above 1.006 g/mL, VLDL above 1.019 g/mL, LDL above 1.063 g/mL, and HDL above 1.21 g/mL (Griel and McCarthy 1969). The brain synthesizes its own class of lipoproteins to transport lipids in the aqueous cerebrospinal fluid within the central nervous system, however, this will not be the focus of the thesis and I direct the

reader to excellent reviews on this topic (Merrill, Davidson et al. 2023, Tsujita, Melchior et al. 2024).

1.4.1 Chylomicrons

As absorbed fatty acids and partial glycerol lipids are resynthesized into triacylglycerol and cholesterol ester molecules within the endoplasmic reticulum, the scaffold protein for chylomicrons is being transcribed from the *APOB* gene. During translation in the rough endoplasmic reticulum, a large multiprotein complex, including APOBEC-1, converts codon 2153 (CAA) in the mRNA transcript to a premature stop codon (UAA), yielding a product that is 48% of the primary sequence, hence the name apoB48 (Chen, Habib et al. 1987, Hospattankar, Higuchi et al. 1987, Powell, Wallis et al. 1987, Higuchi, Hospattankar et al. 1988). In mice, ~88% of enterocyte apoB mRNA is apoB48 (Higuchi, Kitagawa et al. 1992). Microsomal triglyceride transfer protein (MTP) not only assists in apoB48 protein folding, but also transfers triacylglycerol, cholesterol ester and phospholipid molecules onto apoB48 as it is being translated into the endoplasmic reticulum lumen, forming primordial chylomicrons (Julve, Martin-Campos et al. 2016). Primordial chylomicrons detach from the endoplasmic reticulum membrane and expand their lipid cores by MTP or by fusing with cytosolic lipid droplets. Chylomicrons also acquire apolipoprotein A-IV (apoAIV), resulting in a pre-chylomicron particle (Pan and Hussain 2012). Next, pre-chylomicron transport vesicles shuttle these particles for fusion to the cis-Golgi, where they acquire Apo-AI and Apo-AIII (Mulvihill 2018). Secretory vesicles containing these mature chylomicrons bud off from the trans-Golgi and fuse with the enterocyte basolateral membrane to release mature chylomicrons into the lamina propria of the villus (Pan and Hussain 2012). The core of chylomicrons consists of 80-90% triacylglycerol, 10% cholesterol ester, and trace fat soluble vitamins (A, D, E, K) while the surface is 2% free cholesterol, 7% phospholipid, and 2% apolipoproteins.

Figure 1.6 Lipoprotein classes and their associated apolipoproteins. Chylomicrons, very-low density lipoproteins (VLDL), low-density lipoproteins (LDL), and high-density lipoproteins (HDL). Free cholesterol (FC), triglyceride (TG), cholesterol ester (CE), phospholipid (PL). Created with Biorender.

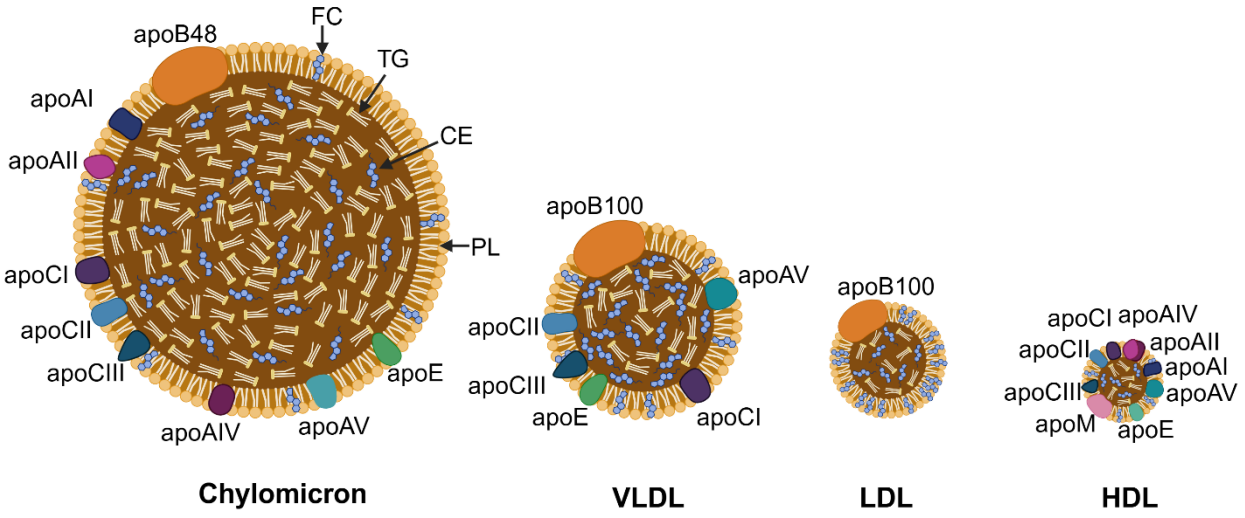
apoB48
FC
TG
apoAI
CE
apoAII
PL
apoCI
apoCII
apoCIII
apoE
apoAIV
apoAV
Chylomicron
apoB100
apoAV
apoCII
apoCIII
apoE
apoCI
VLDL
apoB100
LDL
apoCI
apoAIV
apoCII
apoAII
apoAI
apoCIII
apoAV
apoM
apoE
HDL

Chylomicrons enter the lymphatic lacteal where evidence for both transcellular and paracellular transport in lymphatic endothelial cells exists and is debated (Dixon 2010). Once in the lymph, chylomicrons acquire apoC-II, C-III and E from HDL (Julve, Martin-Campos et al. 2016). Chylomicrons enter the blood circulation at the left subclavian vein via the thoracic duct, thereby bypassing the liver and transporting dietary fat to the heart, muscle, and adipose tissue (D'Aquila, Hung et al. 2016, Mulvihill 2018). Chylomicrons are too large to cross endothelial cell junctions of the vasculature to reach their target organs. The heart, muscle, mammary, and adipose tissue express lipoprotein lipase (LPL) as an inactive enzyme and secrete it into the interstitial space. Here, glycosylphosphatidylinositol anchored high density lipoprotein binding protein 1 (GPIHBP1) binds to LPL and transports it across endothelial cells of the vasculature to the lumen. Here, LPL is also anchored by heparan sulfate proteoglycans (Feingold 2000, Julve, Martin-Campos et al. 2016, Chait, Ginsberg et al. 2020). LPL dimerizes, noncovalently, leading to its active form (Osborne, Bengtsson-Olivecrona et al. 1985). In the capillary lumen, several active LPL enzymes bind one chylomicron, where chylomicron apoC-II stimulates the hydrolytic activity of LPL, converting liberated fatty acids from triacylglycerol molecules within the chylomicron core. LPL activity is limited by chylomicron apoC-III, which inactivates it (Julve, Martin-Campos et al. 2016). The liberated fatty acids are either taken up into target tissue by CD36 and FABPs or are captured by circulating albumin for transport to the liver (Feingold 2000).

The hydrolysis of fatty acids via LPL shrinks the chylomicron core size, leaving the phospholipid surface in excess. These excess phospholipids are transferred to HDL, along with apoC-II, apoC-III, and apoE down their concentration gradients (Chait, Ginsberg et al. 2020). The resulting chylomicron particle, called the chylomicron remnant, is too small to remain attached to the LPL-GPIHBP1 complex. The released chylomicron remnant, now enriched in cholesterol ester relative to the original chylomicron, interacts with hepatic triglyceride lipase (HTGL) at the hepatocyte cell surface. Here, HTGL bound by GPIHBP1 hydrolyzes phospholipids and any

remaining triacylglycerol molecules. Hepatocyte LDL receptor (*LDLR*) and LDL-receptor related protein (LRP) use apoE on the chylomicron remnant as a ligand to endocytose the particle (Julve, Martin-Campos et al. 2016). Upon internalization, dietary cholesterol esters are delivered to the lysosome and apoB48 is directed to proteasomal degradation. Additionally, apoE is released by the *LDLR* or LRP receptors into the circulation, where it binds to HDL (Chait, Ginsberg et al. 2020).

1.4.2 VLDL, IDL, and LDL

VLDL particles deliver their lipids in the fasted state (Chait, Ginsberg et al. 2020). Substrates for very-low density lipoprotein (VLDL) synthesis include cholesterol from chylomicron remnants, dietary fatty acids, as well as fatty acids, phospholipids, and cholesterol synthesized *de novo* (Nielsen and Karpe 2012). ApoB100, transcribed from the *APOB* gene, serves as the scaffold protein for VLDL particle formation and is synthesized in the rough endoplasmic reticulum (van Zwol, van de Sluis et al. 2024). Similar to enterocytes, MTP transfers triacylglycerol, phospholipids, and cholesterol ester molecules to apoB100 while it is being translated into the endoplasmic reticulum lumen. ApoB100 must be sufficiently lipidated, otherwise it is ubiquitinated and sent for proteasomal degradation (van Zwol, van de Sluis et al. 2024). In mice, but not humans, rabbits, or hamsters, only 30% of hepatic apoB mRNA by adulthood encodes apoB100, whereby the remaining 70% actually encodes apoB48 due to the presence of the premature stop codon (Higuchi, Kitagawa et al. 1992), leading to the production of VLDL particles containing apoB48. Within the smooth endoplasmic reticulum, lipid droplets offer more triacylglycerol substrate to the growing VLDL particle. Next, VLDL particles bud off from the endoplasmic reticulum membrane and travel to the Golgi via the COPII trafficking machinery. Within the Golgi, VLDL particles undergo posttranslational modifications and final lipidations (van Zwol, van de Sluis et al. 2024). Mature VLDL particles destined for secretion then fuse with the plasma membrane of hepatocytes, releasing VLDL particles into liver sinusoids and circulation. Proteins

involved in the additional lipidation and VLDL transport within the endoplasmic reticulum to the Golgi continue to be identified (van Zwol, van de Sluis et al. 2024).

The apoE and apoC apolipoproteins carried on plasma HDL are rapidly transferred to new VLDL particles to which they have greater affinity. In humans, VLDL particles also become enriched in cholesterol esters from HDL, via the cholesterol ester transfer protein (CETP) (Burks, Stitziel et al. 2025). Mice, however, do not express CETP and therefore carry most of their cholesterol on HDL (Agellon, Walsh et al. 1991, Guyard-Dangremont, Desrumaux et al. 1998). Reaching their target tissues, VLDL, like chylomicrons, bind to several LPL molecules, where apoC-II activates LPL-mediate triacylglycerol hydrolysis. High levels of chylomicrons, however, outcompete VLDL particles for LPL access (Chait, Ginsberg et al. 2020). Additionally, due to their smaller size, less LPL molecules are required to bind to VLDL particles than chylomicrons to complete hydrolysis. As such, the hydrolysis rate for VLDL particles is much slower than that for chylomicrons. Additional enzymes that encounter VLDL particles include hepatic lipase and endothelial lipase, which also hydrolyze the lipid cores of these particles (Burks, Stitziel et al. 2025). Lipolytic activity is limited by angiopoietin-like proteins (ANGPTL) 3, 4, and 8, as well as apoC-III (Burks, Stitziel et al. 2025), where ANGTL3 inhibition is a therapeutic target under current investigation to lower LDL cholesterol levels (Adam, Mintah et al. 2020). The ~80% depletion of the VLDL triacylglycerol core triggers the release of remnant particles and the transfer of excess phospholipids, free cholesterol, apoE, and most of its apoC-II and apoC-III molecules to neighboring HDL particles (Chait, Ginsberg et al. 2020).

VLDL remnants are classified as intermediate-density lipoproteins (IDL) and are composed of apoB100, apoE, and a phospholipid monolayer surrounding its original cholesterol ester core. In humans, IDL particles receive additional cholesterol ester from HDL via CETP, further enriching their core (Feingold 2000). Eventually, the apoE ligand on IDL binds to the hepatic HTGL-GPIHBP1 complex for hydrolysis of the remaining triacylglycerol and some surface

phospholipids. The smaller, denser particle then lives one of two metabolic fates: receptor-mediated endocytosis into hepatocytes via the LDLR or conversion into an LDL particle (Feingold 2000). In both cases, IDL loses it apoE to neighbouring HDL particles. In the second case, the HTGL-GPIHBP1 releases LDL into circulation. LDL circulates throughout the body to deliver cholesterol ester to cells. Since the only apolipoprotein remaining on LDL is apoB100, this serves as the ligand for receptor mediated endocytosis by the LDL (Brown and Goldstein 1986). In healthy humans, LDL receptors clear 70% of LDL particles predominantly from hepatocytes. Bulk phase endocytosis and scavenger receptors, which are not regulated by intracellular cholesterol levels, clear the remainder of circulating LDL particles.

1.4.3 HDL

Both the liver and the ileum of the small intestine secrete apoAI, which is considered a lipid poor, nascent HDL particle (Rader 2006). Nascent HDL particles contain some apoAII and very little apoC and apoE. In this form, nascent HDL accepts free cholesterol and phospholipids that are being effluxed from the plasma membranes of cells via ABCA1 (Rader 2006). Nascent HDL also accepts free cholesterol, phospholipid, some apoC, and some apoE from triglyceride rich lipoproteins that are being hydrolyzed by LPL (Rader 2006). As free cholesterol accumulates on the nascent HDL surface, LCAT esterifies free cholesterol with a fatty acid from phospholipids, resulting in the movement of hydrophobic cholesterol esters into the core of the HDL particle (Rader 2006). As such, once the disc-like nascent HDL particle fills out into a spherical HDL particle, classified as HDL_3, who is now available to accept more free cholesterol. As HDL_3 continues to accept free cholesterol, including from ABCG1, LCAT continues to expand the cholesterol ester core, leading to the classification of HDL_2 (Francis 2016). CETP on HDL_2 can transfer one mole of cholesterol ester to VLDL, IDL, and LDL for one mol of triglyceride, which is the primary pathway in humans. Otherwise, HDL_2 can be taken up by the hepatocyte for degradation in the lysosomes via the LDLR with apoE as the ligand, or HDL_2 can transfer

cholesterol ester to hepatocytes via the scavenger receptor B1 (SR-B1), yielding the smaller, HDL_3 particle (Francis 2016). The cholesterol ester obtained from HDL_2 via SR-B1 is hydrolyzed to free cholesterol and becomes part of the ER free cholesterol pool, which can be used for membrane biosynthesis, bile acid synthesis, excretion into bile as free cholesterol or the formation of new VLDL particles (Francis 2016). HDL_3 can return to the circulation to accept more free cholesterol or it can be cleared by the kidneys (Rader 2006). The half-life of HDL is 4-6 days, where it can perform this reverse cholesterol transport pathway many times.

1.4.4 Cholesterol control in hepatocytes

Hepatocytes maintain strict control over cellular free cholesterol levels to maintain cell health in part through the transcriptional regulation of HMG CoA reductase, the rate-limiting step in *de novo* cholesterol synthesis, and the LDLR for LDL particle binding and uptake (Scott Kiss and Sniderman 2017). Sterol regulatory element binding protein-2 (SREBP2) transcriptionally regulates both HMG CoA reductase and LDL receptor expression when it can enter the nucleus and bind the sterol response elements within their promoters to turn on their transcription. When the free cholesterol pool in the endoplasmic reticulum is high, however, the SREBP cleavage-activating protein (SCAP) and insulin-induced gene 1 (INSIG 1) trap SREBP2 in the endoplasmic reticulum (Horton, Goldstein et al. 2002). Specifically, cholesterol binds to SCAP and oxysterols bind to INSIG, tightening their bind. When the endoplasmic reticulum pool of free cholesterol is low, and therefore less oxysterols are present, INSIG releases the SCAP/SREBP2 complex, which allows a specific sequence of SCAP to bind to CopII coat proteins. The CopII-SCAP-SREBP-2 complex moves to the Golgi, where site 1 protease (S1P) and S2P cleave SREBP-2, removing the domains that SCAP binds to and releasing the soluble, mature transcription factor nSREBP2 (Scott Kiss and Sniderman 2017). Now, nSREBP2 enters the nucleus and binds to the sterol response element within the promoters of *HMGCR* and *LDLR,* turning on their transcription (Horton, Goldstein et al. 2002). This leads to increased HMG CoA reductase and LDLR protein

levels, in the ER membrane and cell surface, respectively, leading to increased synthesis and uptake of cholesterol.

The cholesterol obtained from LDL cholesterol is used for membrane biosynthesis in all cells and bile acid synthesis in hepatocytes. In adrenals, ovaries, and testes, however, cholesterol is used for hormone synthesis. Free cholesterol is transported to the endoplasmic reticulum via NPC1 and NPC2, where it can be re-esterified by ACAT2 for VLDL production, by ACAT1 lipid droplet storage, or used for bile acid synthesis (Feingold 2000, Scott Kiss and Sniderman 2017). As excess cholesterol ester accumulates in cells, oxysterols are produced. Oxysterols serve as ligands that activate the transcription factor liver X receptor (LXR), which then turns on the transcription of many genes including ABCA1 via their LXR response element in their promoter (Scott Kiss and Sniderman 2017). ABCA1 promotes the efflux of excess cholesterol to circulating apoA-I, beginning HDL formation.

1.4.4.1 Ldlr$^{-/-}$ mouse

Initiation of lipid accumulation within the arterial wall occurs very early in life and atherosclerosis progresses with time. To capture these changes and identify contributing factors, preclinical experiments are required. Generation of the *Ldlr*$^{-/-}$ mouse by Herz, Brown, and Goldstein on the C57BL/6 genetic background (Ishibashi, Brown et al. 1993) has led to an expansion in the study of atherogenesis. Generation of heterozygous and *Ldlr*$^{-/-}$ mice revealed a 35% and 50% elevation, respectively, in plasma total cholesterol levels compared to wild-type controls (Ishibashi, Brown et al. 1993). Interestingly, while female wild-type and heterozygous mice had significantly lower total plasma cholesterol than in male mice, this difference was lost in *Ldlr*$^{-/-}$ mice. FPLC tracings revealed a 2-fold increase in cholesterol in the IDL/LDL fraction in heterozygous mice, where the increase was similar in male and female mice. *Ldlr*$^{-/-}$ mice displayed a massive increase in cholesterol in the IDL/LDL fraction, 7.4-fold for male and 9-fold for female (Ishibashi, Brown et al. 1993). Additionally, a small increase in cholesterol in the VLDL fraction

was observed. Interestingly, cholesterol in the HDL fraction was higher in the male compared to female mice, independent of genotype. While feeding a 0.2% cholesterol/10% coconut diet did not significantly impact the FPLC tracings for cholesterol in wild-type mice, cholesterol content increased 3-fold in these fractions in *Ldlr*$^{-/-}$ mice (Ishibashi, Brown et al. 1993). *Ldlr*$^{-/-}$ mice display a 30-fold decrease in the clearance rate (10 min to 300 min) of ^{125}I-labeled VLDL from plasma, indicating that LDLR clears VLDL remnants and IDL from plasma. The caveat being that these VLDL particles were generated in *Ldlr*$^{-/-}$ mice thereby being particles with extended half-lives themselves (Ishibashi, Brown et al. 1993). This increase in time that these particles circulate leads to more conversion to LDL particles, explaining the rise in LDL levels observed in these mice. Together, these data indicate that the LDL receptor is essential for apoE particle clearance. Importantly, this study also shows that restoring LDLR activity by injecting *Ldlr*$^{-/-}$ mice with a recombinant adenovirus expressing the human LDL receptor cDNA restores the IDL/LDL peak in cholesterol (Ishibashi, Brown et al. 1993).

Despite the increase in LDL-cholesterol observed in chow-fed *Ldlr*$^{-/-}$ mice, atherosclerosis does not manifest. Therefore, a diet high in cholesterol is required. On a chow diet (0.01% cholesterol, 4.4% fat) for 28 weeks, *Ldlr*$^{-/-}$ mice have elevated LDL cholesterol (20.7 mmol/L) and develop atherosclerosis with normal triglycerides, body weight gain, fasting glucose, free fatty acids, and insulin (Hartvigsen, Binder et al. 2007). On a Western diet (0.06% cholesterol, 21% milk fat) for 28 weeks, *Ldlr*$^{-/-}$ mice have elevated LDL cholesterol (41.4 mmol/L), as well as obesity, high triglyceride levels, insulin resistance, and hepatic steatosis (Hartvigsen, Binder et al. 2007). The cholesterol in the VLDL and IDL/LDL fractions were significantly greater in the Western diet fed *Ldlr*$^{-/-}$ mice compared to the high-cholesterol diet-fed mice. The extent of aortic atherosclerosis evaluated by the *en face* method was the same in high-cholesterol vs Western diet-fed mice, but the lesion areas in the aorta by cross-sectional analysis were 35-45% greater in the Western-diet fed mice (Hartvigsen, Binder et al. 2007).

1.5 Cellular Lipid metabolism

Lipid metabolism is critical for membrane synthesis and energy storage. Fatty acids make up the structural components of membrane lipids, modulate cell signalling pathways, and serve as fuel for oxidation and the tricarboxylic acid cycle. Cells can generate palmitic acid (C16:0), myristic acid (C14:0), and steric acid (C18:0) (Richard Lehner 2016). The diet supplies most fatty acids, including essential fatty acids linoleic acid (18:2n-6) and alpha-linolenic acid (18:3n-3) as these fatty acids cannot be synthesized from carbohydrates (Spector and Kim 2015, Richard Lehner 2016).

1.5.1 Adipocytes

Two types of adipose tissue exist in mammals, white (WAT) and brown (BAT). WAT depots include visceral and subcutaneous. Adipose tissue protects organs from mechanical stress and secrete several endocrine factors including adipokines and bioactive lipids that serve a physiological signals for energy metabolism in the body (Scheja and Heeren 2019). Importantly, adipose tissue serves as a site of calorie storage after feeding and a source of free fatty acids during fasting (Rosen and Spiegelman 2014). White adipocytes are unilocular, meaning they contain a single lipid droplet. Brown adipocytes contain many lipid droplets, are rich in mitochondria, and release stored chemical energy as heat (Rosen and Spiegelman 2014). Adipocytes store fatty acids as triglycerides into a single lipid droplet (Morigny, Boucher et al. 2021), preventing lipotoxicity in skeletal muscle and the liver. The venous drainage of visceral WAT converges to the portal circulation and as such directly supplies the liver with fatty acids and adipokines (Rosen and Spiegelman 2014).

1.5.1.1 Fed state

The rise in circulating insulin that follows the intake of a meal stimulates the translocation of glucose transporter GLUT4 to the adipocyte plasma membrane (Santoro, McGraw et al. 2021).

Additionally, under the sustained stimulation of insulin, GLUT4 undergoes multiple rounds of recruitment to the plasma membrane to capture glucose, internalization, and rapid recycling back to the plasma membrane (Santoro, McGraw et al. 2021). Once in the adipocyte, <5% of glucose is stored as glycogen (Flatt and Ball 1964). Glucose undergoes glycolysis in the cytoplasm, leading to the production glycerol-3-phosphate, the backbone of triacylglycerol molecules, which accounts for 50% of the glucose taken into the cell (Flatt and Ball 1964). Pyruvate from glycolysis can enter the tricarboxylic acid cycle (TCA), supplying citrate and acetyl-CoA for the *de novo* synthesis of fatty acids (Santoro, McGraw et al. 2021). Alternatively, pyruvate can be converted into lactate for systemic delivery as a fuel source or signalling metabolite.

Triglyceride-rich lipoproteins supply most of the fatty acids stored in adipocytes through the actions of LPL (Figure 1.7). While insulin modestly increases the secretion of LPL from adipocytes, it also increases the proportion of LPL molecules that dimerize to form active LPL on the endothelial cell surface of the adipose capillary bed (Karpe, Bickerton et al. 2007). As previously described, LPL hydrolyzes triacylglycerol molecules from the core of these lipoproteins. CD36 and fatty acid binding proteins capture the liberated long chain fatty acids for entry into the adipocytes. Fatty acid transport proteins and long-chain acyl-CoA synthetases activate the fatty acids with an acetyl-CoA. GPAT esterifies the glycerol-3-phosphate backbone with one fatty acid, which is then esterified once again by 1-acyl-glycerol-3-phosphate-acyltransferase (Morigny, Boucher et al. 2021). DGAT catalyzed the formation of the triglyceride molecule. The resulting triacylglycerol can be stored in the lipid droplet. Therefore, insulin promotes the storage of energy in the form of triacylglycerol molecules in adipose tissue in the fed state.

1.5.1.2 Fasted state

Energy stored as triacylglycerol molecules must be released during periods of fasting or intense exercise. Fasting increases the expression of angiopoietin-like protein 4 (ANGPTL4), where it binds to an LPL dimer and converts it to catalytically inactive monomers (Sukonina,

Lookene et al. 2006). Since triglycerides cannot pass through the plasma membrane, they must be first cleaved into free fatty acids and glycerol (Figure 1.7). Adipocyte lipid droplet coat proteins, including perilipin 1 (PLIN1), regulate the pathways that release the stored fatty acids, termed lipolysis (Morigny, Boucher et al. 2021). The accumulation of intracellular cGMP and cAMP activates protein kinases PKG and PKA, which phosphorylate PLIN1 on the lipid droplet (Morigny, Boucher et al. 2021). Phosphorylation of PLIN1 releases CGI58 (*ABHD5*), allowing it to interact and activate adipose triglyceride lipase (ATGL; *PNPLA2*). Activated ATGL catalyzes the hydrolysis one fatty acid from the triacylglycerol molecule, yielding DAG (Morigny, Boucher et al. 2021). PKG and PKA also phosphorylate hormone-sensitive lipase (HSL) in the cytosol, thereby promoting its localization to the lipid droplet. PLIN1 binds to phosphorylated HSL, which catalyzes the hydrolysis of one fatty acid from the DAG, yielding MAG (Morigny, Boucher et al. 2021). Finally, monoacylglycerol lipase catalyzes the hydrolysis of one fatty acid from MAG, yielding a glycerol molecule (Morigny, Boucher et al. 2021). The three released fatty acids from the initial triacylglycerol molecule can be released from the adipocyte to bind albumin for transport in circulation or be oxidized (Jaishy and Abel 2016). The glycerol released from the initial triacylglycerol molecule circulates primarily to the liver where it serves as a substrate for the *de novo* production of glucose. The acetyl CoA molecules derived from fatty acid oxidation serve as allosteric modulators of the first step of gluconeogenesis (Santoro, McGraw et al. 2021). Therefore, adipocyte lipolysis fuels hepatic gluconeogenesis in the fasted state, when insulin no longer inhibits this process.

Figure 1.7 Adipocyte lipid handling in the fed and fasted state. Insulin stimulates the translocation of glucose transporter GLUT4 to the adipocyte plasma membrane. Glucose undergoes glycolysis, where the production of glycerol-3-phasphate, acetyl-CoA, and citrate serve as building blocks for triglyceride synthesis. Additionally, fatty acids liberated from chylomicrons through the actions of lipoprotein lipase (LPL) and glycosylphosphatidylinositol anchored high density lipoprotein binding protein 1 (GPIHBP1). Enzymes glycerol-3-phosphate acyltransferase (GPAT), 1-acyl-sn-glycerol-3-phosphate acyltransferase (AGPAT), and coenzyme A:diacylglycerol acyltransferase (DGAT) catalyze triglyceride synthesis from these building blocks. In the fasted state, triglycerides from the lipid droplet are hydrolyzed through the actions of adipose triglyceride lipase (ATGL), hormone sensitive lipase (HSL), and monoacylglycerol lipase (MAGL). Released fatty acids and glycerol are released into circulation for transport via albumin. Created with Biorender.

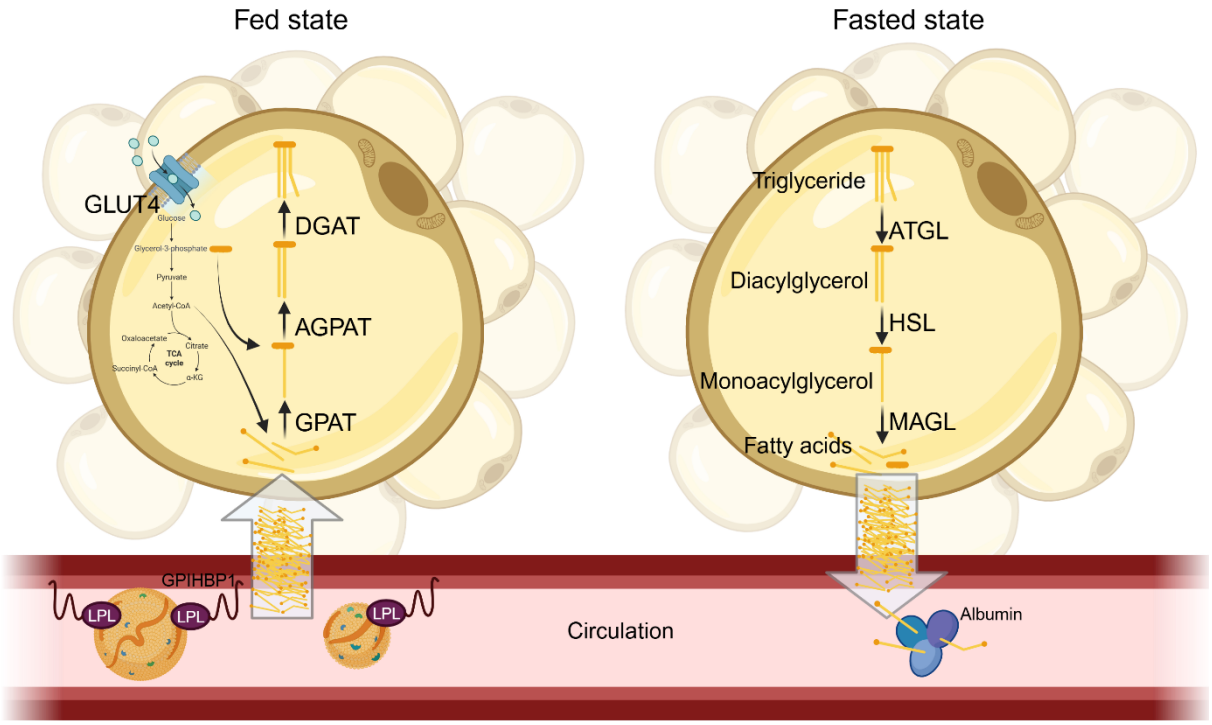
Fed state
Fasted state
GLUT4
Glucose
Glycerol-3-phosphate
Pyruvate
Acetyl-CoA
Oxaloacetate
Citrate
TCA cycle
Succinyl-CoA
α-KG
DGAT
AGPAT
GPAT
Triglyceride
ATGL
Diacylglycerol
HSL
Monoacylglycerol
MAGL
Fatty acids
GPIHBP1
LPL
LPL
LPL
Circulation
Albumin

1.5.1.3 Obesity

Fat mass accumulates by hypertrophy or by hyperplasia. Hypertrophy in adipose tissue refers to the expansion of existing adipocyte size (Ghaben and Scherer 2019). The differentiation of resident preadipocytes and subsequent formation of new adipocytes leads to hyperplasia in adipose tissue (Ghaben and Scherer 2019). Adipocytes respond to the increased caloric intake by enlarging. At the same time, they maintain their normal lipolysis rates upon fasting. Even when fasting free fatty acid levels rise, as long as skeletal muscle insulin sensitivity is intact, these fatty acids are rapidly taken up and oxidized (Guilherme, Virbasius et al. 2008). An excess of body fat mass defines the endocrine disorder that is obesity (Schwartz, Seeley et al. 2017). Adipocyte expansion leads to both mechanical stress and limited oxygen supply (hypoxia), leading to adipose tissue inflammation. Hypertrophic adipocytes display greater lipolytic activity (Laurencikiene, Skurk et al. 2011), greater inflammatory cytokine secretion, and reduced secretion of leptin and adiponectin (Skurk, Alberti-Huber et al. 2007). Contributing factors to obesity pathogenesis include molecular, genetic, developmental, behavioral, and environment (Schwartz, Seeley et al. 2017). A simplistic view of obesity pathogenesis involves the description of excess caloric consumption relative to energy expended (Schwartz, Seeley et al. 2017). More recent views are described based on the difficulty to treat obesity, owing to the complexity of the disease. Indeed, survival of humans across evolution favours the conservation of body fat. However, currently, the unlimited available calories coupled with the biological predisposition to conserve fat likely drives the global obesity epidemic (Schwartz, Seeley et al. 2017).

Leptin plays a significant role in obesity and energy homeostasis, whereby leptin deficiency leads to severe hyperphagia and obesity in rodents (Zhang, Proenca et al. 1994) and severely obese children (Montague, Farooqi et al. 1997). Recombinant leptin therapy in a child with congenital leptin deficiency led to sustained weight loss, particularly fat loss (Farooqi, Jebb et al. 1999). These individuals are extremely rare. Individuals living with obesity rather have

elevated plasma leptin levels, proportional to their body fat content (Considine, Sinha et al. 1996). The paradoxical high leptin levels but a lack of a response to its appetite-suppressing effects led to the “leptin resistance” hypothesis (Zhou and Rui 2013). This hypothesis was driven by studies demonstrating defects in the transport of leptin across the blood brain barrier (Banks 2012). This hypothesis is challenged by studies in diet-induced obese mice with high leptin levels treated with a competitive leptin receptor antagonist showing maintained cellular responses to endogenous leptin (Ottaway, Mahbod et al. 2015). To date, the definition of leptin resistance and its diagnostic use is not established (Gruzdeva, Borodkina et al. 2019). Nevertheless, these data reposition the main role of leptin-responsive neurocircuits are more sensitive to decreases rather than increases in circulating leptin levels. These circuits may then prevent body fat loss when leptin levels are lower, whereby genetics, development, and environmental factors can influence the leptin threshold below which compensatory increases in food intake and reductions in energy expenditure occur (Schwartz, Seeley et al. 2017).

1.5.2 Hepatocytes

The hepatic artery supplies blood from the aorta, rich in oxygen. The portal vein supplies most of the blood to the liver, but it is relatively oxygen-poor yet nutrient-rich (Schulze, Schott et al. 2019). Hepatocytes are unique epithelial cells, as in they may have several basolateral and apical domains. Blood flows into the liver sinusoids, which span across the basolateral surfaces of hepatocytes. As such, hepatocytes are among the first cells exposed to ingested substances. Hepatocytes secrete lipids, bile salts and degraded proteins from the apical plasma membrane into canaliculi, or small channels, that feed into the intrahepatic biliary tree that eventually drains into the gall bladder for storage (Schulze, Schott et al. 2019). The apical canalicular domains contain ABC transporters and bile acid efflux transporters. Hepatocytes secrete newly synthesized proteins and lipoproteins at the blood-facing, basolateral domain leading to dumping into circulation (Schulze, Schott et al. 2019).

The influx of free fatty acids from adipose tissue accounts for 70-80% of triglyceride synthesis in hepatocytes, whereas triglycerides from triglyceride-rich lipoproteins taken up by hepatocytes and the synthesis of triglycerides form fatty acids generated *de novo* account for 5-10% and 5-30%, respectively (van Zwol, van de Sluis et al. 2024). The predominant triglyceride synthesis pathway in the liver is through glycerol-3-phosphate, although the monoacylglycerol pathway is also used (Figure 1.8) (Farese, Cases et al. 2000). Glycerol 3-phosphate serves as a backbone for the addition of fatty acyl-CoA molecules catalyzed first by glycerol-phosphate acyl transferase and then by acylglycerol-phosphate acyl transferase. To generate DAG from this molecule, phosphatidic acid phosphorylase removes the phosphate group from the glycerol backbone, yielding the substrate for DGAT to catalyze the acylation of the third fatty acid (Sanders and Griffin 2016). Hepatocytes use triacylglycerol molecules as a source of fatty acids for oxidation and energy production as well as the secretion of VLDL. Ultimately, the goal of the cell is to limit intracellular levels of non-esterified free fatty acids as well as fatty acyl-CoA molecules to prevent lipotoxicity. Excess triacylglycerol molecules are stored in lipid droplets in the cytosol, originating from the cytosolic side of the endoplasmic reticulum (van Zwol, van de Sluis et al. 2024). Fatty acid transport protein (FATP), fatty acid translocase (FAT/CD36), and plasma membrane fatty acid-binding protein (FABPpm) facilitate the entry of fatty acids into hepatocytes. Fatty acids may also enter the cell by passive diffusion. Therefore, upon entry, cytoplasmic fatty acid binding protein (FABPc) bind long chain fatty acids (>14 carbons) and acyl-CoA synthetases (ACS) activates fatty acids to CoA esters (Yoon, Shaw et al. 2021). Intracellular fatty acids may be directed to metabolic processes or the nucleus to modulate gene expression (Nguyen, Leray et al. 2008).

1.5.2.1 Fed state

In the fed state, hepatic fatty acids originate from lipoprotein hydrolysis and *de novo* lipogenesis (Figure 1.8). In general, high carbohydrate diets induce *de novo* lipogenesis, whereas fasting or acute fat feeding inhibit *de novo* lipogenesis. Acetyl-CoA is the building block for fatty acid synthesis (Sanders and Griffin 2016). The major enzyme involved in fatty acid synthesis is fatty acid synthase (FAS), a multidomain enzyme complex. First, ATP citrate lyase (ACLY) generates acetyl-CoA from citrate generated by the TCA cycle (Yoon, Shaw et al. 2021). Acetyl-CoA carboxylase (ACC) then catalyzes the formation of malonyl-CoA from acetyl-CoA. Malonyl/acetyl transferase catalyzes the transfer of malonyl-CoA to the acyl carrier protein domain of fatty acid synthase (FASN), a multi-enzyme protein that elongates the ACP-bound malonyl-CoA moiety with additional acetyl-CoA molecules. Specifically, the β-ketoacyl synthase active site of FASN catalyzes the decarboxylative condensation of acetyl-CoA and malonyl-CoA, forming a β-ketoacyl-ACP intermediate (Richard Lehner 2016). Next, the NADPH-dependent β-ketoreductase active site of FASN reduces the ketone of the β-ketoacyl-ACP intermediate, generating a hydroxyl group that is subsequently dehydrated by the dehydratase active site of FASN, forming a trans-enoyl-ACP intermediate (Richard Lehner 2016). The NADPH-dependent enoyl-reductase then further reduces this intermediate, generating a saturated acyl-ACP chain that can be further elongated until a 16- or 18-carbon fatty acid is generated (Sanders and Griffin 2016). The thioesterase domain of FASN catalyzes the release of the 16- or 18-carbon fatty acid. In summary, FASN catalyzes the following reaction to generate palmitate (Richard Lehner 2016):

acetyl-CoA + 7malonyl-CoA + 14NADPH + $14H^+$ → palmitate + $7HCO3^-$ + 8CoA + $14NADP^+$ + $6H_2O$.

Figure 1.8 Hepatic lipid handling in the fed and fasted state. In the fed state, lipoprotein hydrolysis and de novo lipogenesis supply hepatic fatty acids. Glucose entry into glycolysis activates ChREBP while insulin signalling activates SREBP-1c. Lipoprotein lipase (LPL), anchored by glycosylphosphatidylinositol anchored high density lipoprotein binding protein 1 (GPIHBP1), liberate fatty acids from chylomicrons. Fatty acids are absorbed by fatty acid binding protein (FABPpm), fatty acid transport proteins (FATP), and fatty acid translocase/cluster determinant 36 (CD36). Glucose transporter GLUT2 transports glucose into hepatocytes, where glycolysis supplies acetyl-CoA and citrate as building blocks for fatty acid synthesis. ATP citrate lyase (ACLY) generates acetyl-CoA from the TCA cycle. Acetyl-CoA carboxylase (ACC) catalyzes the formation of malonyl-CoA from acetyl-CoA, the building blocks for fatty acid synthase by the multidomain protein fatty acid synthase (FASN). Enzymes of the smooth endoplasmic reticulum (ER) activate fatty acids and resynthesize them into triglycerides. Glycerol-3-phosphate acyltransferase 3 and 4 (GPAT3/4) to catalyze the linkage of a fatty acyl-CoA to glycerol-3-phosphate yielding lysophosphatidic acid. The enzyme 1-acyl-sn-glycerol-3-phosphate acyltransferases (AGPAT1-5) catalyze the esterification of lysophosphatidic acid into phosphatidic acid. Phosphatidic acid phosphohydrolase catalyse the hydrolysis of the phosphate group on phosphatidic acid to yield DAG, which is converted to a triglyceride through the action of DGAT 1 and/or 2. Triglycerides are temporarily stored in cytosolic lipid droplets (CLD) or are incorporated into very-low-density lipoproteins (VLDL). In the fasted state, free fatty acids from adipose tissue lipolysis enter hepatocytes by passive or active diffusion. Activated fatty acids may be esterified into triglyceride molecules, which may be stored in lipid droplets. These lipid droplets are targeted by lipases, such as adipose triglyceride lipase (ATGL), where liberated fatty acids may provide substrate for VLDL particles. Long chain fatty acids may also be catabolized in the peroxisome into shorter fatty acids. Fatty acids are oxidized in the mitochondria to generate energy for the cell. Created with Biorender.

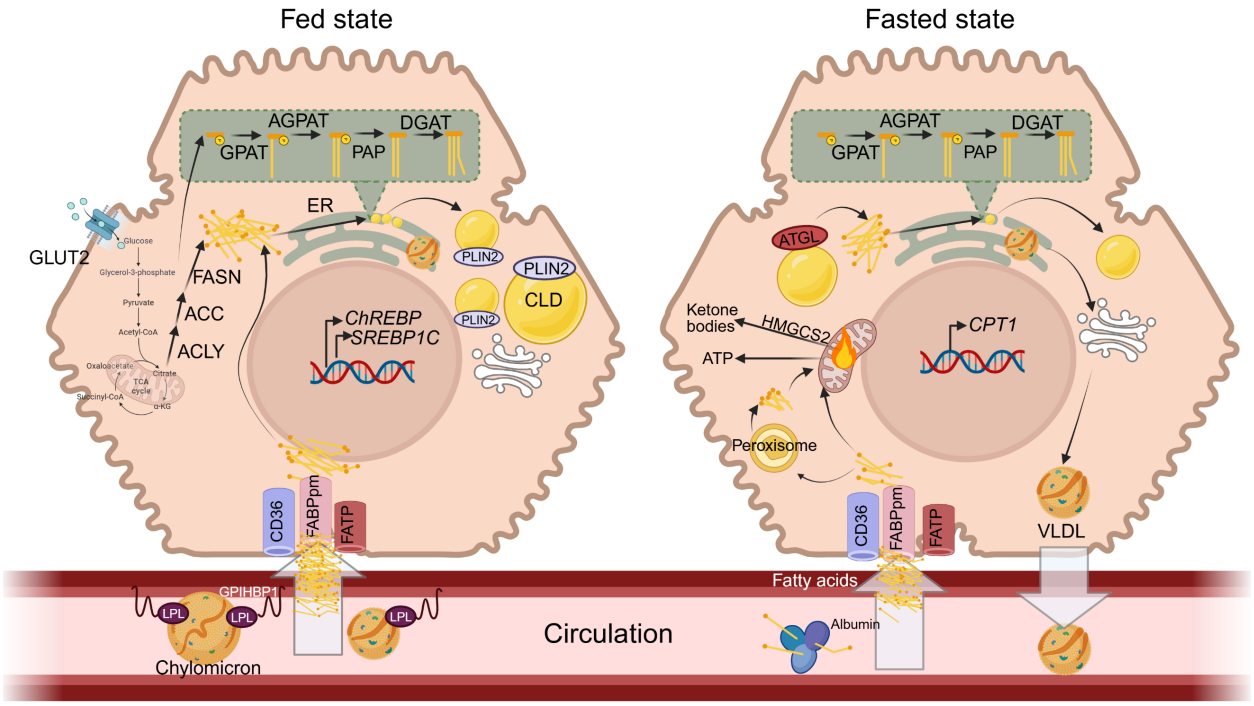
Fed state
Fasted state
AGPAT
GPAT
PAP
DGAT
ER
GLUT2
Glucose
Glycerol-3-phosphate
Pyruvate
Acetyl-CoA
Oxaloacetate
Citrate
TCA cycle
Succinyl-CoA
α-KG
FASN
ACC
ACLY
ChREBP
SREBP1C
PLIN2
CLD
ATGL
Ketone bodies
HMGCS2
ATP
CPT1
Peroxisome
CD36
FABPpm
FATP
GPIHBP1
LPL
Chylomicron
Circulation
Fatty acids
Albumin
VLDL

The fatty acids supplied by FASN are used to support membrane structure and signalling within the cell. Palmitate, produced in this reaction, can be activated by fatty acid-CoA ligase (ACS), elongated by fatty acid protein 5 (ELOVL5), desaturated by stearoyl-CoA desaturase (SCD1) and fatty acid desaturase 2 (FADS2) to generate various fatty acid species (Yoon, Shaw et al. 2021). These fatty acids can also be synthesized into triglycerides for storage through the actions of DGAT. CLD form in the endoplasmic reticulum and bud into the cytoplasm where they can continue to expand and are coated by proteins including perilipin 2 (PLIN2), which prevents access to lipases (Figure 1.8) (Mashek 2021).

Both transcriptional regulation of enzymes involved in fatty acid synthesis as well as allosteric regulation of ACC control *de novo* lipogenesis. Transcription factors carbohydrate response element binding protein (ChREBP) and sterol regulatory element-binding protein 1c (SREBP-1c) regulate the expression of genes involved in *de novo* lipogenesis (Richard Lehner 2016). Glucose entry into glycolysis activates ChREBP while insulin signalling activates SREBP-1c, leading to their entry into the nucleus to upregulate gene expression. ChREBP is retained in the cytosol by the 14-3-3 protein (Sanders and Griffin 2016). Glycolytic intermediates glucose 6-phosphate and fructose-2,6-bisphophate lead to the dephosphorylation of ChREBP. In the dephosphorylated form, ChREBP dissociates from the protein 14-3-3, allowing nuclear localization of ChREBP. Here, ChREBP upregulates the transcription of FAS, SCD1, ELOVL6, ACC, pyruvate kinase (Sanders and Griffin 2016).

Insulin signalling leads to the activation of AKT. AKT activates mammalian target of rapamycin complex 1 (mTORC1), which upregulates the activity of SREBP1c in two ways (Sanders and Griffin 2016). First, through the actions of ribosomal protein S6 kinase 1, leads to the nuclear localization of another transcription factor, liver X receptor (LXR). LXR heterodimerizes with retinoid X receptor (RXR) to turn on the transcription of *SREBP1C.* Second, mTORC1 activity leads to the inhibition of lipin1 and AKT inhibits glycogen synthase kinase 3β

(GSK3β), proteins that inhibit the maturation of SREBP1c (Sanders and Griffin 2016). The immature form of SREBP1c resides at the endoplasmic reticulum membrane in a complex with SCAP and INSIG. Insulin signalling, through PI3K/AKT leads to the phosphorylation of the immature form of SREBP1c. SCAP changes confirmation in response to sterol binding or phosphorylation itself of SREBP1c, leading to the release of the SCAP-SREBP1c complex from INSIG. The Coat protein II (COPII) trafficking complex shuttles the SCAP-SREBP1c complex to the Golgi, where SREBP1c undergoes maturation through the actions of site 1 protease (S1P) and site 2-protease (S2P) and subsequent release back into the cytosol. In the nucleus, SREBP1c promotes the transcription of FAS, stearoyl-CoA desaturase 1 (*SCD1*), *ELOVL6*, and *ACC* (Sanders and Griffin 2016).

As previously discussed, ACC catalyzes the formation of malonyl-CoA, the first committed step to *de novo* lipogenesis. In its inactive form, ACC is a dimer. Upon activation, ACC polymerizes. In response to insulin, citrate, the precursor for acetyl-CoA, promotes ACC polymerization, thereby participating in a feed forward mechanism. Glutamate also increases ACC polymerization. Insulin signalling also leads to a phosphorylation event on ACC that is required for its activation. The product of ACC, malonyl-CoA, as well as fatty acyl-CoA, serve as allosteric inhibitors of ACC, completing the negative feedback pathway. In response to glucagon or adrenaline, cellular cAMP levels rise, activating AMPK and PKA. AMPK phosphorylates ACC1 at serine 79 and ACC2 at serine 212, inhibiting its role in fatty acid synthesis (Fullerton 2016).

1.5.2.2 Fasted state

Fasting induces adipose tissue lipolysis, sending free fatty acids to the liver. Upon acetylation, acyl-CoA fatty acids may be esterified into triacylglycerol molecules, which may be stored in lipid droplets (Figure 1.8). The lipid droplet protein PLIN2 is targeted for degradation in the fasted state, allowing lipases to access CLDs (Mashek 2021). Lipid droplet lipases include ATGL with its co-activator CGI-58, HSL, and MAGL as outline in the adipocyte section. These

liberated lipid droplets may provide substrate for VLDL particles, providing fuel to the heart, skeletal muscle, and adipose tissue during the fast (Ruppert and Kersten 2024). Alternatively, fatty acids can also be transported into the mitochondria to generate energy through oxidation. First, fatty acids must be converted into a form that can enter the mitochondria. CPT1 convert acyl-CoA molecules into acyl-carnitines, enabling entry into the mitochondria by SLC24A20 transporter (Ruppert and Kersten 2024). Once in the mitochondria, CTP2 converts the acyl-carnitine back into an acyl-CoA. Fatty acid oxidation involves a series of reactions shortening the fatty acid by two carbons per cycle. Each round generates NADH, FADH2, and acetyl-CoA, where the former two can enter the electron transport chain to generate ATP. The acetyl-CoA generated from each round can enter the TCA cycle generating CO_2, H_2O, NADH and FADH2 whereby the latter two provide electrons for the generation of ATP (Ruppert and Kersten 2024). Branched and very long-chain fatty acids are oxidized in peroxisomes, rather than mitochondria. Peroxisomes degrade very long-chain fatty acids into short-chain acyl-CoA molecules, such as butyryl-CoA, propionyl-CoA, which are then converted into acyl-carnitines for mitochondrial entry and subsequent oxidation to CO_2 and H_2O (Ruppert and Kersten 2024).

Upon prolonged fasting or exercise, consumption of a low carbohydrate diet, or diabetic ketoacidosis, fatty acid delivery from adipose to the liver increases. Since the oxidation capacity and the TCA cycle flux cannot keep up with this demand, acetyl-CoA in the mitochondria is converted into ketone bodies through the actions of acetyl-CoA acetyltransferase (ACAT1), HMG-CoA synthase (HMGCS2), HMG-CoA lyase (HMGCL), and β-hydroxybutyrate dehydrogenase (BDH1) (Ruppert and Kersten 2024). β-hydroxybutyrate, acetoacetate, and acetone are ketone bodies that enter the blood stream via hepatic transporters SLC16A1 and SLC16A7 (Ruppert and Kersten 2024). Ketone bodies fuel the brain, heart, and skeletal muscle during fasting.

1.5.2.3 Insulin resistance

Insulin resistance in adipocytes, leading to unregulated lipolysis as well as upregulated hepatic d*e novo* lipogenesis contribute to pathogenic lipid accumulation, leading to metabolic dysfunction-associated steatotic liver disease (MASLD). A small study of individuals with MASLD, previously termed non-alcoholic fatty liver disease (NAFLD), revealed that 59% of hepatic triglycerides are from the influx of free fatty acids, 26% from *de novo* lipogenesis, and 15% from the diet (Donnelly, Smith et al. 2005). Additionally, malonyl-CoA inhibits fatty acid oxidation, thereby shifting the balance to greater lipid production and lower lipid catabolism in hepatocytes. The insulin signalling cascade diverges to a glucoregulatory response on one arm, and a lipogenic response on the other arm. Insulin signalling leads to the phosphorylation and nuclear exclusion of forkhead box protein O1 (FoxO1), thereby preventing the transcriptional upregulation of genes involved in gluconeogenesis. On the other arm, insulin leads to the activation of SREBP1c, leading to the transcriptional upregulation of genes involved in *de novo* lipogenesis. Therefore, in the fed state, insulin sensitivity in these cells leads to a suppression of glucose production and an increase in the conversion of dietary glucose to fatty acids and triacylglycerol molecules for storage. In the context of insulin resistance, however, insulin fails to suppress gluconeogenesis while the cell remains sensitive to the lipogenic signal of insulin (Biddinger, Hernandez-Ono et al. 2008, Brown and Goldstein 2008). Therefore, the cell is “selectively” insulin resistant, explaining the hyperglycemia, hyperinsulinemia, and hypertriglyceridemia observed in individuals living with T2DM.

The catabolism of glucose is the main substrate for *de novo* lipogenesis, whereby glycolysis is a highly regulated cellular process. In particular, phosphofructokinase-1 (PFK-1) is the first regulatory step in glycolysis sensitive to hormonal factors and cellular energy levels. Fructose from the diet, as discussed above, also contributes to acetyl-CoA production. Fructose catabolism feeds into the glycolytic pathway after the reaction catalyzed by PFK-1, thereby

bypassing this key regulatory step to generate acetyl-CoA. Fructose catabolism also feeds into the GPAT triglyceride synthesis pathway through the generation of glycerol 3-phosphate (Sanders and Griffin 2016). As such, fructose catabolism produces triacylglycerol molecules independent of insulin, a significant contributor to fatty liver disease.

1.5.3 Enterocytes

Enterocytes are columnar epithelial cells polarized with one apical membrane and one basolateral membrane. The apical membrane houses microvilli, forming the brush border of the small intestine, to increase the absorptive surface area (DeSesso and Jacobson 2001). The triacylglycerol content within an enterocyte is determined by dietary fat content, fatty acid synthesis, fatty acid oxidation, and chylomicron production. The current evidence suggests that the distribution of CLD within enterocytes is determined from the source of the lipids and will be described in the section below.

1.5.3.1 Fed state

Lipids obtained from the apical membrane and stored in CLD contain dietary fatty acids and are directed to chylomicron formation (Gangl and Ockner 1975, Ho, Delgado et al. 2002, Storch, Zhou et al. 2008). Resynthesized lipids that are not immediately incorporated into chylomicrons for secretion into the lymphatic lacteals are surrounded by a monolayer of phospholipids, free cholesterol, and coat proteins, forming CLDs. This partitioning occurs at the smooth endoplasmic reticulum. CLDs continue to accumulate triacylglycerol molecules and increase in size through triacylglycerol synthesis at the CLD surface, phospholipid synthesis for monolayer expansion and by fusing with other CLDs (D'Aquila, Hung et al. 2016). Stored fatty acids liberated from CLDs and are directed towards chylomicron synthesis, fatty acid oxidation or for other cellular purposes (D'Aquila, Hung et al. 2016). Intraduodenal, but not intravenous delivery of glucose five hours after a dietary fat challenge in rats increases triglyceride output into

lymph, thereby releasing stored lipids (Wang, Khan et al. 2025). Additionally, CLDs store fat-soluble vitamins, prostaglandins, and steroids (Demignot, Beilstein et al. 2014). CLDs are thought to control the rate of lipid absorption during the prandial phase and serve as another supply of lipids upon fasting (Beilstein, Carriere et al. 2016). CLDs are more abundant in the proximal jejunum; the number and size of CLDs increase with high-fat feeding and decrease as fasting time increases (Zhu, Lee et al. 2009).

DGAT1 and DGAT2 enzymes do not have redundant roles within enterocyte lipid partitioning. Within the intestine, *Dgat1*$^{-/-}$ mice accumulate more CLD in the enterocyte cytoplasm upon high-fat diet feeding (Buhman, Smith et al. 2002) and upon dietary fat challenge have massive CLD compared to controls (Hung, Carreiro et al. 2017). *Dgat1*$^{-/-}$ mice secrete chylomicrons with significantly smaller triglyceride content at a slower rate, leading to greater intestinal lipid storage after a dietary fat challenge compared to controls (Buhman, Smith et al. 2002, Hung, Carreiro et al. 2017). However, *Dgat1*$^{-/-}$ mice display normal dietary fat absorption (Buhman, Smith et al. 2002). Mice with an intestinal-specific overexpression of DGAT1 accumulate more lipids in the endoplasmic reticulum lumen upon a dietary fat challenge, however, this does not impact intestinal-triglyceride secretion rates (Hung, Carreiro et al. 2017). Mice with an overexpression of intestinal DGAT2 accumulate more lipids in the Golgi in this state and display the greater intestinal-triglyceride secretion rates compared to controls (Hung, Carreiro et al. 2017). Together, the proposed model for these two enzymes involves DGAT1 synthesizing triglycerides from liberated fatty acids into the endoplasmic reticulum lumen for chylomicron synthesis, thereby impacting chylomicron size and restricting CLD size. DGAT2, by contrast, synthesizes triglycerides for nascent chylomicrons and for CLD formation, thereby impacting intestinal-triglyceride secretion rates. Unlike *Dgat1*$^{-/-}$ mice, whole-body *Dgat2*$^{-/-}$ mice have abnormally low lipids and die soon after birth (Stone, Myers et al. 2004), indicating that DGAT1 cannot compensate for the loss of DGAT2.

1.5.3.2 Fasted state

Basolateral lipids are directed to fatty acid oxidation or phospholipid synthesis (Gangl and Ockner 1975, Ho, Delgado et al. 2002, Storch, Zhou et al. 2008). Experiments in primary murine enteroids, derived from intestinal crypts, revealed that lipids can be taken up from triglyceride-rich lipoproteins from the basolateral membrane, and that this uptake increases mitochondrial respiration (Li, Rodia et al. 2019). Experiments in intestinal-specific deletion of ATGL and its activator CGI-58 revealed that cytosolic hydrolysis by ATGL/CGI-58 mediate the hydrolysis of CLD formed from the uptake of fatty acids from the basolateral side and therefore from circulation (Korbelius, Vujic et al. 2019). Moreover, this intestinal-specific double knockout has normal intestinal-triglyceride secretion rates in mice fed a chow or high-fat diet, indicating that ATGL-mediated hydrolysis does not supply substrate for chylomicron formation.

1.5.3.3 Intestinal insulin resistance

Like hepatocytes, systemic insulin resistance leads to lipid accumulation in enterocytes from an influx of circulating free fatty acids and from *de novo* lipogenesis. Additionally, enterocytes are charged with absorbing over 95% of dietary fat. Therefore, in the context of diet-induced obesity and insulin resistance, post-prandial lipemia manifests. Both human and animal studies in the context of obesity and insulin resistance demonstrate an overproduction of apoB48-containing particles and delayed triglyceride clearance (Haidari, Leung et al. 2002, Duez, Lamarche et al. 2006, Federico, Naples et al. 2006, Adeli and Lewis 2008, Douglass, Malik et al. 2012, Uchida, Whitsitt et al. 2012). Additionally, intestinal insulin resistance promotes chylomicron production via enhanced microsomal triglyceride transfer protein activity (Bozzetto, Della Pepa et al. 2020). Mechanistically, enterocytes from hamsters with diet-induced insulin resistance display impaired insulin signalling downstream of the insulin receptor (Federico, Naples et al. 2006), where in the healthy state, acute insulin inhibits apoB48 secretion in chow-fed hamsters (Federico, Naples et al. 2006) and healthy individuals (Pavlic,

Xiao et al. 2010). Moreover, acute elevations of plasma free fatty acids to mimic an insulin resistant state stimulate intestinal triglyceride rich lipoprotein production in men and in male hamsters (Lewis, Naples et al. 2004, Duez, Lamarche et al. 2008), indicating an additional substrate pool of fatty acids for chylomicron production. Enhanced *de novo* lipogenesis rates as shown by radiolabelled acetate incorporation into lipids have been observed in duodenal specimens obtained from individuals undergoing bariatric surgery (Veilleux, Grenier et al. 2014), thereby contributing to the enterocyte fatty acid pool. Importantly, postprandial, but not fasting triglycerides exhibit a strong association with coronary artery disease and additionally, these individuals display significantly higher plasma triglyceride levels in response to an acute dietary fat challenge compared to healthy controls (Patsch, Miesenbock et al. 1992). Therefore, a deeper understanding the molecular mechanisms impacted by intestinal insulin resistance are required to inform therapeutic treatments.

1.6 GLP-1R+, GLP-2R+, GIPR+ cells and their function in the gastrointestinal tract

1.6.1 GLP-1R+ cells

The human GLP-1R gene consists of 7 exons and localizes to chromosome 6 band p21.1 (Stoffel, Espinosa et al. 1993). The transcriptional start site of the GLP-1R does not contain a TATA- or a CAAT-box element, however, it contains 3 putative Sp1 binding sites (Lankat-Buttgereit and Goke 1997). Within the 350 bp region, 74% of the sequence is GC nucleotides (Lankat-Buttgereit and Goke 1997). The GLP-1R is 463 amino acids in length also belongs to the class B family of 7-transmembrane-spanning, heterotrimeric G-protein-coupled receptors (Mayo,

Miller et al. 2003). GLP-1 binds to the N-terminal, extracellular region of the GLP-1R. The intracellular pathways engaged by GLP-1R activation have been elucidated using β-cells in the islet. The GLP-1R primarily couples to Gαs upon GLP-1 binding, but also to other Gα subtypes including Gαq, Gαi, and Gαo (El Eid, Reynolds et al. 2022, Capozzi, Bouslov et al. 2025). Gαs activation stimulates adenylyl cyclase to produce cAMP. The rise in cAMP activates PKA and exchange protein activated by cAMP-2 (EPAC2), leading to membrane depolarization, calcium increases and insulin exocytosis. Arrestins act as scaffolds to promote recruitment and activation of MAPK and PI-3K signal transduction pathways (Mayo, Miller et al. 2003). Genetic knockout models as well as receptor agonists and antagonists have elucidated many aspects of GLP-1R biology. In particular, exendin-4 is a GLP-1R agonist, was discovered in the saliva of the Gila monster (Eng, Kleinman et al. 1992, Raufman, Singh et al. 1992). Exendin 9-39 is the N-terminally truncated version of exendin-4 and antagonizes the GLP-1R (Mayo, Miller et al. 2003). To terminate the GLP-1R signal, the cell endocytoses GLP-1R via clathrin-dependent and independent pathways to recycling endosomes. GLP-1R can be recycled back to the plasma membrane or targeted for lysosomal degradation (Marzook, Tomas et al. 2021).

Glp1r expression determined by RNAscope *in situ* hybridization reveals the highest expression in duodenal Brunner's glands and in stomach gland parietal cells (Wismann, Barkholt et al. 2017). Consistent with this, use of a reporter mouse together with a number of validation approaches, GLP-1R was identified in chief cells, parietal cells and Brunner's glands (Andersen, Grunddal et al. 2021). A well-validated antibody to the GLP-1R (MAb 3F52) and corroborated with ^{125}I-labeled GLP-1 also demonstrated a strong signal in stomach parietal cells, basolateral epithelial cells in the duodenum, Brunner’s glands and the myenteric nerve plexus (Pyke, Heller et al. 2014). *Glp1r* mRNA expression in mice is detected in a subset of neurons of the myenteric and submucosal plexus (Andersen, Grunddal et al. 2021) that also express the neuron cytoplasmic protein 9.5 (PGP9.5) (Kedees, Guz et al. 2013). *Glp1r* mRNA expression was

detected in myenteric ganglia in the intestinal mucosa, which are excitable by GLP-1 treatment *ex vivo* (64% synaptic and 36% after-hyperpolarizing types). Indeed, 63% of *Glp1r*-fluorescent neurons in primary small intestinal cultures and 19% in colonic cultures are neuronal nitric oxide synthase positive markers for inhibitory motor neurons (Richards, Parker et al. 2014). GLP-1 receptors are expressed in the enteric nervous system and in the vagus nerve (Grasset, Puel et al. 2017), which allow for the activation of the gut-brain-periphery axis. As such, the presence of GLP-1R+cell bodies in the enteric nervous system (Figure 1.9) has been proposed to provide the signaling route to the central nervous system required for distally secreted GLP-1.

Figure 1.9 GLP-1R+, GLP-2R+, and GIPR+ cell in the small intestine identified in mice. GLP-1R is expressed in somatostatin-secreting enteroendocrine cells, smooth muscle cells, pericytes, Paneth cells, intraepithelial lymphocytes (αβ and γδ), as well as submucosal and myenteric neurons. GLP-1R is expressed in neuronal nitric oxide synthase (nNOS)+ neurons. GLP-2R is detected in smooth muscle cells and subepithelial myofibroblasts. Specifically, GLP-2R is detected in submucosal and myenteric neurons that are nNos+, vasoactive intestinal polypeptide (VIP)+, and choline-acetyltransferase (ChAT)+, and substance P (SP)+ cells. GIPR is detected in CD146+ pericytes. The relative receptor- and hormone-expressing cell density within the small intestine is depicted (inset). Studies highlighted here did not determine co-expression of GLP-1R, GLP-2R, or GIPR. Reproduced from: Morrow, N.M., Hanson, A.A. & Mulvihill, E.E. (2021). Distinct Identity of GLP-1R, GLP-2R, and GIPR Expressing Cells and Signaling Circuits Within the Gastrointestinal Tract. Front Cell Dev Biol. 9,703996.

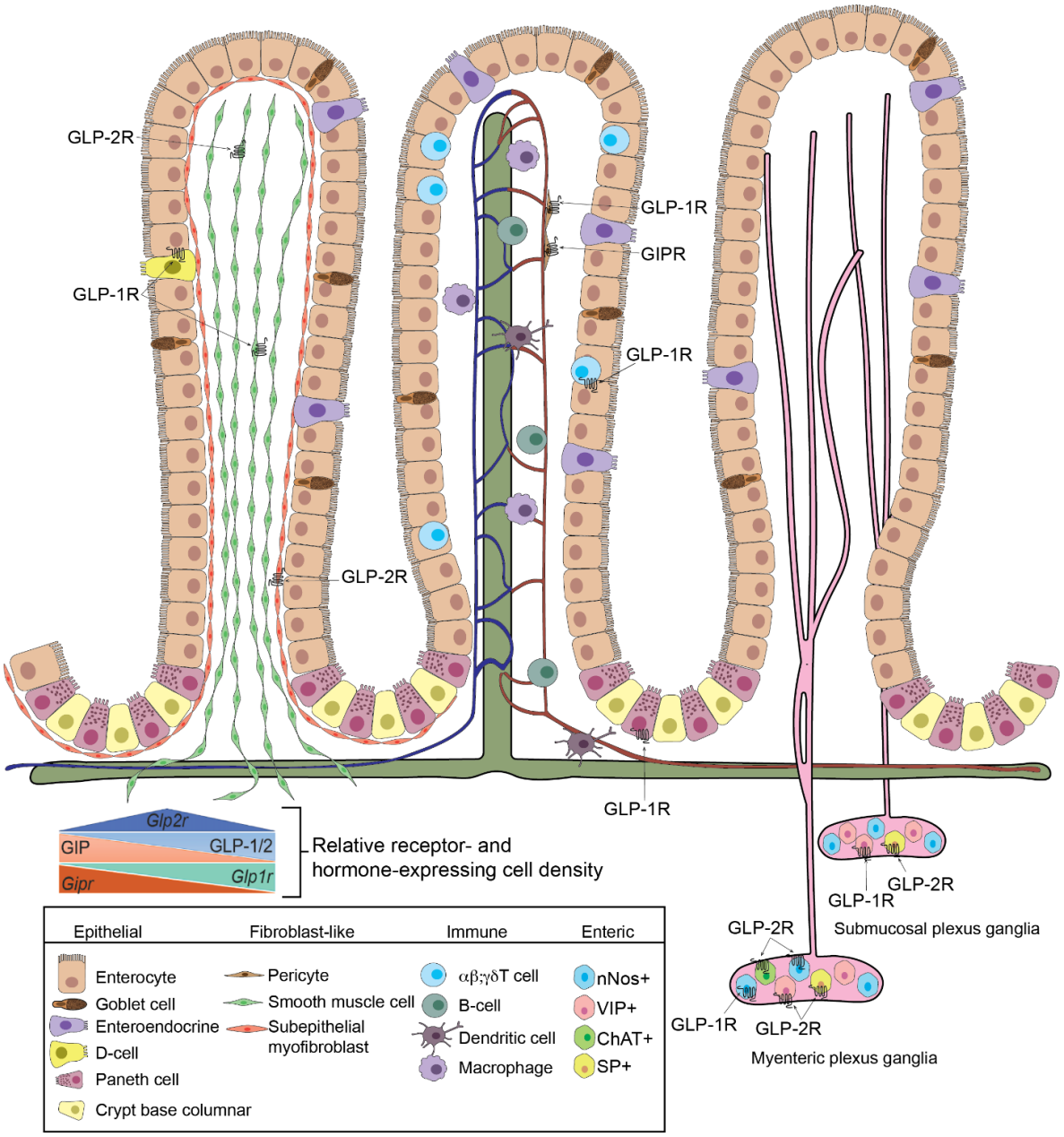
GLP-2R
GLP-1R
GLP-2R
GLP-1R
GIPR
GLP-1R
GLP-1R
Glp2r
GIP
GLP-1/2
Glp1r
Gipr
Relative receptor- and
hormone-expressing cell density
GLP-1R
GLP-2R
Submucosal plexus ganglia
GLP-2R
GLP-1R
GLP-2R
Myenteric plexus ganglia
Epithelial
Enterocyte
Goblet cell
Enteroendocrine
D-cell
Paneth cell
Crypt base columnar
Fibroblast-like
Pericyte
Smooth muscle cell
Subepithelial
myofibroblast
Immune
αβ;γδT cell
B-cell
Dendritic cell
Macrophage
Enteric
nNos+
VIP+
ChAT+
SP+

1.6.1.1 GLP-1R signalling modulates gut inflammation

Glp1r mRNA expression increases with age between 2 to 12 weeks in murine jejunum, ileum, and colon (Campos, Lee et al. 1994). *Glp1r* mRNA expression is highest in the jejunum within the epithelial fraction, followed by ileum then colon (Kedees, Guz et al. 2013). Sequential collagenase digestion of the gut reveals *Glp1r* expression to be within the epithelial fraction instead of the crypt, mesenchyme, or smooth muscle layer fractions (Yusta, Baggio et al. 2015). Within the epithelial compartment of the small intestine, intraepithelial lymphocytes (IELs) (both the Tαβ and Tγδ subsets) express *Glp1r* (Yusta, Baggio et al. 2015, He, Kahles et al. 2019) (Figure 1.9). Additionally, GLP-1R-expressing αβ and γδ T cells transit to the gut via integrin B7 (*Itgb7)* (He, Kahles et al. 2019). Indeed, IELs encode a functional GLP-1R as exendin-4 treatment in sorted activated and nonactivated IELs increases cAMP levels. However, GLP-1R in IELs is not required for IEL development or recruitment to the gut as their abundance does not change in response to GLP-1R agonist treatment or in *Glp1r*$^{-/-}$ mice (Yusta, Baggio et al. 2015). By contrast, *Glp1r*$^{-/-}$ mice lose significantly more weight, exhibit significantly increased disease activity scores and greater colon damage than wild type controls in response to chemically-induced colitis (Yusta, Baggio et al. 2015).

Glp1r is also detected in Paneth cells, identified by lysozyme expression, in the jejunum and ileum crypts but not colon, distinct from proliferating Ki67+ cells (Kedees, Guz et al. 2013). Additionally, exendin-4 treatment increases *c-fos* expression in GLP-1R+ Paneth cells, which is abolished when exendin-(9-39) is administered prior to exendin-4 treatment (Kedees, Guz et al. 2013). *Glp1r* expression is also observed in the arteries and arterioles of the intestine and colocalized with αSMA and the pericyte marker NG2 (Richards, Parker et al. 2014). In this model, *Glp1r* fluorescence was absent from the epithelial layer.

1.6.1.2 GLP-1R signalling promotes intestinal growth

Treatment with GLP-1R agonists, exendin-4 or liraglutide, for 1 week has been shown to increase small intestinal length and weight as well as large intestinal weight in a GLP-1R-dependent manner (Koehler, Baggio et al. 2015). Chronic treatment of exendin-4 increases crypt number in the proximal intestine and colon, leading to increased intestinal circumference and length (Koehler, Baggio et al. 2015). The authors demonstrate that GLP-1R agonist treatment induces expression of tyrosine kinase IGF1R/ErbB (EGFR) pathways, however, agonist treatment can still increase intestinal growth in the absence of intestinal epithelial IGF1 receptor as well as EGF receptor signaling (Koehler, Baggio et al. 2015). Acute, but not chronic, exendin-4 treatment increases *Fgf7* mRNA expression in the small intestine (Koehler, Baggio et al. 2015). The intestinotrophic effects of exendin-4 are lost in *Fgf7*$^{-/-}$ mice, effects that were not observed upon GLP-2 treatment in these mice (Koehler, Baggio et al. 2015). Despite the role of IELs in mediating intestinal mucosal repair through Fgf7/KGF (Boismenu and Havran 1994), reconstituting *Glp1r*+ IELs into *Glp1r*$^{-/-}$ mice via bone marrow transplant does not rescue the intestinotrophic effects of exendin-4 in these mice (Koehler, Baggio et al. 2015).

1.6.1.3 GLP-1R signalling participates in a feedback loop for its own secretion

L cells do not express *Glp1r* (Grigoryan, Kedees et al. 2012), however, other chromogranin A+ enteroendocrine cells do (Kedees, Guz et al. 2013, Andersen, Grunddal et al. 2021). A paracrine relationship exists between GLP-1-secreting L cells and somatostatin-secreting D-cells (Jepsen, Grunddal et al. 2019). Specifically, L cells express the somatostatin receptor, *Sstr5*, and D cells express *Glp1r.* GLP-1 secretion in response to intraduodenal infusion of glucose increases with somatostatin receptor antagonism (SSTr2 and SSTr5) (Jepsen, Grunddal et al. 2019). Similarly, somatostatin secretion is dependent on GLP-1R activation as its secretion is inhibited upon GLP-1R antagonist (exendin-9) treatment (Jepsen, Grunddal et al. 2019).

1.6.2 GLP-2R+ cells

The human *GLP2R* is localized to chromosome 17p13.3 and encodes a 550 amino acid G protein-coupled receptor, processed to become a 486 amino acid receptor (Munroe, Gupta et al. 1999). The gene at chromosome 17p13.3 encoding the human *GLP2R* receptor is also very well conserved as the rat sequence is 80% of the same amino acid sequence (Shin, Estall et al. 2005). *GLP2R* is 14 exons long and has seven transmembrane domains. The GLP-2R also belongs to the class B family of 7-transmembrane-spanning, heterotrimeric G-protein-coupled receptors (Munroe, Gupta et al. 1999, Mayo, Miller et al. 2003). Despite the similarity in amino acid sequence, GLP-2R only recognizes GLP-2 and not related members of the glucagon family (Yusta, Boushey et al. 2000). GLP-2R signalling terminates with receptor internalization in a lipid-raft-dependent manner where interactions with early endosomes occur prior to recycling back to the cell surface (Estall, Yusta et al. 2004). Studies using genetic models, GLP-2 infusions, and GLP-2(3-33), an antagonist to the GLP-2R (Shin, Estall et al. 2005), have uncovered many of the biological functions of this peptide hormone.

Immunohistochemistry experiments using a rat polyclonal antibody localized the GLP-2R to vagal afferents, enteric neurons, enteroendocrine cells, and myenteric plexus nerve fibrils (Nelson, Sharp et al. 2007). Isolated rat intestinal mucosal cells expressing *Glp2r* transcripts also expressed markers for enteroendocrine or neural cells (Walsh, Yusta et al. 2003). Human vasoactive intestinal polypeptide positive enteric neurons in the submucosal plexus and myenteric plexus express the GLP-2R (Figure 1.9) (Guan, Karpen et al. 2006). In the mouse duodenal myenteric plexus, ~18% of GLP-2R+ are neuronal nitric oxide synthase positive, 10% are vasoactive intestinal polypeptide positive, ~71% are choline-acetyltransferase positive, and 27% are substance P (SP)+ (Cinci, Faussone-Pellegrini et al. 2011). Human endothelial nitric oxide synthase positive enteric neurons in the submucosa also express the GLP-2R, supporting a direct role for GLP-2-mediated increase in endothelial nitric oxide synthase protein and release through

cAMP-dependent protein kinase A (Guan, Karpen et al. 2006). GLP-2R protein in neonatal pigs colocalizes with chromogranin A+ enteroendocrine cells in the jejunal villus (~58%) and crypt epithelium (60%) (Guan, Karpen et al. 2006). Isolated Human GLP-2R protein also colocalizes to chromogranin A+ enteroendocrine cells in both the villus and crypt epithelium (Guan, Karpen et al. 2006). Human GLP-2R protein colocalizes to 5-HT-containing cells in the epithelium, a neurotransmitter released by enteroendocrine cells (Guan, Karpen et al. 2006).

1.6.2.1 Intestinotrophic role of GLP-2

In the rat jejunum, relative *Glp2r* expression as a percentage of the expression in intact intestine is 0.07%, 33%, 256%, 392% abundant in the epithelium, mucosa, smooth muscle layer, and the intestine devoid of epithelium, respectively (Pedersen, Pedersen et al. 2015). In rats, mice, marmosets and human intestinal tissue, GLP-2R localizes to cells residing immediately below the basolateral membrane of enterocytes, which are subepithelial myofibroblasts as marked by smooth muscle actin (Figure 1.9) (Orskov, Hartmann et al. 2005). *Glp2r* expression is most abundant in the lamina propria of duodenal and jejunal villi (Wismann, Barkholt et al. 2017), wherein the jejunum its expression within the lamina propria stromal cells predominate in the upper half of villi (Yusta, Matthews et al. 2019). The receptor's location in the lamina propria is consistent with evidence that suggests the link between GLP-2 to KGF, IGF-1, and ErbB, as these growth factors are produced and secreted from stromal cells found in the lamina propria (Yusta, Matthews et al. 2019).

The intestinotrophic effects of GLP-2 have been well described since its initial characterization (Drucker, Shi et al. 1997). GLP-2 increases intestinal cell proliferation while inhibiting apoptosis, leading to increased villus height and expanding the absorptive mucosal surface (Drucker, Shi et al. 1997). GLP-2 has been shown to enhance crypt-cell proliferation, demonstrated by BrDU labelling and measuring crypt depth (Koehler, Baggio et al. 2015). GLP-2 reduces mucosal injury by stimulating intestinal growth; specifically, increasing villus height, crypt

depth, improving nutrient absorption and nutritional status (Estall and Drucker 2005). Mice fasted for 24 hours exhibit small intestinal atrophy, a decrease in intestinal weight, a decrease in crypt-villus height, and an increase in villus apoptosis (Shin, Estall et al. 2005). Refeeding restored all parameters, while co-administration of GLP-2R antagonist, GLP-2^{3-33}, prevents adaptive changes to refeeding (Shin, Estall et al. 2005). Similarly, the restoration of jejunal mucosal mass, protein, and DNA 25-65% by *ad libidum* or intragastric infusion for 2 to 4 days is blunted with 2.5 or 50 μg/kg body weight GLP-2^{3-33}, but not 10 μg/kg body weight GLP-2^{3-33}, compared to the baseline fed group (Nelson, Murali et al. 2008). Mucosal growth following refeeding is associated with increased circulating GLP-2 and jejunal *Igf-1* mRNA expression. Interestingly, GLP-2^{3-33} at any dose prevents restoration of plasma IGF-I levels in response to refeeding (Nelson, Murali et al. 2008). There is evidence for both paracrine and neuronal mechanisms for GLP-2-mediated gut growth. GLP-2R+ myofibroblasts in the small intestine and colon contain keratinocyte growth factor (KGF), whereby immunoneutralization of KGF abolishes the trophic effects of GLP-2 treatment in the colon, but not the small intestine in mice (Orskov, Hartmann et al. 2005). Mechanistically, GLP-2 activates its receptors on subepithelial myofibroblasts, which in turn increase expression and secretion of IGF-1 (Markovic and Brubaker 2019). Gut growth coincides with increased IGF-1 and IGF-2, particularly in the mucosal and muscularis regions (Dube, Forse et al. 2006). Chronic GLP-2 treatment does not increase crypt-cell proliferation, and growth of the crypt-villus is reduced in intestinal epithelial- specific IGF knockout mice (Rowland, Trivedi et al. 2011). In the nonobese diabetic (NOD) mouse, a model of type 1 diabetes, treatment with h(Gly^2)GLP-2 once daily for 14 days, increases small intestine length and weight, while also improving jejunal transepithelial resistance compared to treatment with saline (Hadjiyanni, Li et al. 2009).

1.6.3 GIPR+ cells

The human GIP receptor (GIPR) gene localizes to chromosome 19 band q13.3 and is ~13.8 kb long. The GIPR also belongs to the class B family of heterotrimeric G-protein-coupled receptors (Mayo, Miller et al. 2003). The receptor is 466 amino acids in length, including a signal peptide and 7 transmembrane domains; the gene contains 14 exons (Yamada, Hayami et al. 1995). The first 92 base pairs of the *GIPR* gene contains 88% sequence identity between rat and human; interestingly, neither promoter region contains a TATA box (Boylan, Jepeal et al. 2006). MZF1/Sp1-C (-75), Sp1-B (-57), and Sp1-A (-45) transcription factor binding sites were identified using radiolabeled synthetic probes and confirmed with CHiP analysis (Boylan, Jepeal et al. 2006). Indeed, sequence deletion between -85 and -40 decreases promoter activity by 88% (Boylan, Jepeal et al. 2006). The *GIPR* promoter contains a cAMP response element, and as such, activation of GIPR signalling is coupled to increases in cAMP and rises in cellular calcium levels. GIPR is also a $G\alpha_s$-coupled receptor, thereby activating adenylate cyclase to amplify cAMP production (Muller, Adriaenssens et al. 2025). PI-3K, PKA, AKT, MAPK, and phospholipase A2 are also coupled to GIPR activation. GIP binds to the N-terminal domain of GIPR. which is associated with the recruitment of beta arrestins and induces the internalization of its receptor involving clathrin-coated pits, AP-2, and dynamin (Ismail, Dubois-Vedrenne et al. 2015).

On a whole tissue level, *Gipr* mRNA is expressed in rat stomach, duodenum, and proximal small intestine (Usdin, Mezey et al. 1993, Coon, Schwartz et al. 2013). In the stomach, RNAseq of purified gastric somatostatin-producing D-cells from SST-Cre.ROSA26^{EYFP} mice reveal *Gipr* expression in these cells (Adriaenssens, Lam et al. 2015). GIPR is faintly detected at the protein level at multiple sizes (50, 55, 60, and 70 kDa) in jejunal mucosal cells compared to the strong signal at 50 kDa in pancreatic homogenates (Coon, Schwartz et al. 2013). In this same study, GIPR immunohistochemistry demonstrated positive staining beneath the basolateral surface of

epithelial cells of the proximal jejunum (Coon, Schwartz et al. 2013). Genetic elimination of *Gipr* in hematopoietic cell lineages, including endothelial cells (*Gipr*$^{Tie2-/-}$ mice) does not impact jejunal *Gipr* mRNA (Pujadas, Varin et al. 2020). Recently, CD146+ pericytes have been reported to express *Gipr* (Figure 1.9), whereby genetic elimination and receptor activation with D-Ala$_2$ GIP amplify and lower gut inflammation, respectively (Hammoud, Kaur et al. 2024).

1.6.4 Gut hormones in the regulation of lipid metabolism

Spearman correlations between GLP-1, GLP-2, GIP, and triglyceride responses in plasma during an oral fat tolerance test in obese men reveal a small albeit significant positive correlation (r-squared values close to zero) between all three hormone AUCs for triglyceride and apoB48 (Matikainen, Bjornson et al. 2016). In this study, these gut hormones display small contributions to explaining the variance in triglyceride AUC, where instead fasting triglyceride values serve as the largest contributor for explaining this variance (Matikainen, Bjornson et al. 2016). Still, the high concentrations of GLP-1, GLP-2, and GIP within the gut circulation relative to systemic circulation suggest that endogenous gut hormone action on chylomicron secretion may be local and underestimated.

1.6.5 *Glp1r*$^{-/-}$*Gipr*$^{-/-}$ mouse

GIP receptor knockout mice (*Gipr*$^{-/-}$ mice) display normal development and mild glucose intolerance in response to an oral glucose gavage (Miyawaki, Yamada et al. 1999, Pamir, Lynn et al. 2003). *Glp1r*$^{-/-}$ mice display impaired glucose-stimulated insulin secretion and glucose tolerance (Scrocchi, Brown et al. 1996). Together, these data suggest that loss of one incretin receptor can be compensated, at least in part, by the other incretin receptor signalling pathway. Therefore, the development of the double incretin receptor knockout (DIRKO) mouse was initiated. *Glp1r*$^{-/-}$ mice were derived on the CD1 background (Scrocchi, Brown et al. 1996), whereas *Gipr*$^{-/-}$ mice were generated on the C57BL/6 background (Miyawaki, Yamada et al.

1999). The authors backcrossed the *Glp1r*$^{-/-}$ mouse for five generations on the C57BL/6 background, which was then crossed with the *Gipr*$^{-/-}$ mouse (Hansotia, Baggio et al. 2004). Male and female mice are fertile and display normal body weight gain but significantly impaired glucose tolerance when glucose was administered by oral or intraperitoneal injection (Hansotia, Baggio et al. 2004). Importantly, these studies show that the glucose-lowering effects of GIPR and GLP-1R agonists are eliminated in the DIRKO mice (Hansotia, Baggio et al. 2004). The *Glp1r*$^{-/-}$*Glp2r*$^{-/-}$ mouse was a gift from the Drucker lab and is first described in this thesis. *Glp2r*$^{-/-}$ mice were generated on the C57BL/6 background in the Drucker lab. Exons 7-9 were replaced with a neomycin resistance cassette (Lee, Lee et al. 2012).

1.6.6 GLP-1R

1.6.6.1 Clinical studies

Multiple degradation-resistant GLP1R agonists (GLP1RAs) have been developed and are effective for glycemic control for individuals living with T2DM (Baggio and Drucker 2007, Drucker 2022). Beyond their role in diabetes management and cardiovascular safety, GLP1RAs also decrease appetite and reduce body weight, and are now prescribed for weight loss in individuals living with obesity (Pi-Sunyer, Astrup et al. 2015, Wilding, Batterham et al. 2021). Patients living with T2DM treated with metformin and the GLP-1R agonist exenatide for one year display significantly reduced circulating triglycerides, apoB48, and FFA following an early meal (50 g of fat, 75 g of carbohydrates, 35 g of protein) (Bunck, Corner et al. 2010). In patients with recent-onset T2DM, subcutaneous injection of exenatide immediately prior to meal consumption (5384 kJ) reduces post-meal serum triglycerides and remnant lipoprotein triglycerides at 2-, 4-, and 6-hours post-meal, in particular preventing the 4-hour peak in triglycerides seen in placebo controls (Schwartz, Koska et al. 2010). Similarly, exenatide significantly reduces serum apoB48 and apoC-III levels throughout the 8-hour sampling period (Schwartz, Koska et al. 2010). Two weeks of exenatide treatment twice daily, 1 hour before morning and evening meals, significantly reduces

plasma triglycerides following these meals (~50% carbohydrate, 20% protein, and 30% fat) compared to placebo (Schwartz, Ratner et al. 2008). Experiments in healthy humans maintained in a fed state via co-infusion of d3-leucine and a lipid/carbohydrate formula in a nasoduodenal tube under pancreatic clamp conditions revealed that treatment of exenatide significantly decreases the apoB48 production rate in the triglyceride-rich lipoprotein fraction, however, this did not impact plasma triglycerides, free fatty acids, or the triglyceride content of triglyceride-rich lipoproteins compared to placebo (Xiao, Bandsma et al. 2012).

1.6.6.2 Preclinical studies

Treatment with GLP-1R agonist exendin-4 in mice significantly decreases triglyceride-rich lipoproteins-fraction triglyceride accumulation at 90 minutes, and apoB48 levels at 60 and 90 minutes following an acute dietary fat challenge. This effect is significantly reversed with GLP-1R antagonist exendin(9-39) treatment (Hsieh, Longuet et al. 2010). While exendin-4 significantly increases plasma insulin levels 5-min post injection, these levels are not significantly different from PBS control after 20 minutes, suggesting that the GLP-1 mediated reduction in intestinal-triglyceride secretion is independent of the incretin effect. Indeed, the authors show that in co-administration of insulin injection and triton infusion 20 min post-olive oil gavage in mice does not significantly impact the accumulation of triglycerides in plasma (Hsieh, Longuet et al. 2010). Despite similar gastric emptying rates between *Glp1r*$^{-/-}$ mice and wild type controls (Baggio, Huang et al. 2004), pulse-chase experiments in primary suspended villi from chow-fed hamsters reveal that exendin-4 does not change cellular apoB48 levels, but significantly decreases ^{35}S-labelled apoB48 secretion in the media (Hsieh, Longuet et al. 2010).

The nodose ganglia and nerve terminals innervating the portal vein express *Glp1r.* Therefore, significant GLP-1R action occurs in the hepatic portal bed (Vahl, Tauchi et al. 2007). However, DPP4 activity is extremely high in the portal vein, limiting endogenous GLP-1 action (Vahl, Tauchi et al. 2007, Trzaskalski, Vulesevic et al. 2023). Studies in healthy hamsters

delivering GLP-1(7-36) in the portal vein or in the nodose ganglion significantly blunts intestinal-triglyceride secretion, where the opposite phenotype is observed with GLP-1R antagonism delivery in the portal vein (Hoffman, Alvares et al. 2022). The impact of GLP-1 to blunt intestinal-triglyceride secretion is prevented by vagotomy and by selective deafferenting vagal afferents that express GLP-1 via injections of neurotoxin-conjugated GLP-1R agonist (saponin-exenatide) into the nodose ganglion (Hoffman, Alvares et al. 2022). These studies are also complemented by portal vein injections and nodose ganglia injections of GLP-1 in *Glp1r*$^{-/-}$ hamsters. However, after just two weeks of high fructose diet feeding, GLP-1 fails to lower intestinal-triglyceride secretion when injected in the portal vein or in the nodose ganglion (Hoffman, Alvares et al. 2022). Therefore, diet-induced obesity appears to desensitize vagal afferent GLP-1Rs in the context of the control of post-prandial lipemia. This may be driven by the increase in DPP4 activity in diet-induced obesity. Therefore, as GLP-1R agonists still lower post-prandial lipids in individuals living with obesity and dyslipidemia, this indicates that other predominant pathways remain sensitive or are isolated from DPP4 activity to respond to this signal. However, lipid tolerance is not different in mice with genetic elimination of *Glp1r* in the hypothalamus, brain stem, and the enteric nervous system via *Wnt1-Cre2* and in neurons of the dorsal motor nucleus of the vagus, the nodose ganglia, and the nucleus of the solitary tract, targeted by *Phox2b-Cre*. Moreover, GLP-1R agonists still lower plasma triglyceride levels following an acute dietary fat challenge in *Glp1r*$^{\Delta Wnt1-/-}$ and *Glp1r*$^{\Delta Phox2b-/-}$ mice (Varin, Mulvihill et al. 2019).

1.6.7 GLP-2R

1.6.7.1 Clinical studies

Degradation-resistant GLP-2 analogues were approved for the management of short bowel syndrome in 2012 (Brubaker 2018). Subcutaneous injection of 1500 µg of GLP-2 five hours after the start of a liquid mixed macronutrient formula infusion through a nasoduodenal tube in healthy men significantly increases peak plasma triglyceride and triglyceride-rich lipoprotein-

apoB48 levels at 1 hour and area under the concentration curve for the first 3 hours of treatment (Dash, Xiao et al. 2014). GLP-2 does not increase plasma triglyceride-rich lipoprotein apoB48 levels by increasing the synthesis of new particles, nor does it decrease the clearance of triglyceride-rich lipoprotein apoB48, rather, GLP-2 stimulates the release of pre-formed triglyceride-rich lipoproteins apoB48 during the first hour of treatment (Dash, Xiao et al. 2014). Similarly, GLP-2 treatment significantly increases plasma triglyceride, triglyceride content of triglyceride-rich lipoproteins, triglyceride-rich lipoproteins retinyl palmitate, and retinyl palmitate levels in the chylomicron fraction for 2 hours when administered 7 hours after a meal containing retinyl palmitate (Dash, Xiao et al. 2014). Together, these studies demonstrate the storage capacity of the small intestine and the impact of GLP-2 to mobilize these stores.

1.6.7.2 Preclinical studies

In hamsters, acute GLP-2 analogue, hGly^{2}-GLP-2, treatment significantly increases the triglyceride content of triglyceride-rich lipoproteins. GLP-2 increases the ^{3}H-triolein radiolabel incorporation specifically into plasma triglycerides, and not cholesterol ester or fatty acids at 60- and 90-minutes post-gavage compared to controls in hamsters (Hsieh, Longuet et al. 2009). Similar to hamsters, acute GLP-2 treatment significantly increases plasma triglyceride concentration at 60- and 90-minutes post-oil gavage as well as triglyceride and apoB48 accumulation in the chylomicron fraction of plasma (Hsieh, Longuet et al. 2009). GLP-2 does not increase the protein expression of hamster intestinal FATP4 or MTP, rather it significantly increases the expression of glycosylated CD36 on the apical membrane of enterocytes, consistent with the role of apical CD36 in the absorption of dietary fat. Indeed, acute GLP-2 treatment fails to increase intestinal-triglyceride secretion in *Cd36*$^{-/-}$ mice (Hsieh, Longuet et al. 2009). ^{35}S-methionine pulse-chase experiments of jejunal fragments isolated from hamsters 1 hour after an olive oil gavage revealed that GLP-2 treatment *ex vivo* increases the secretion of the radiolabelled-apoB48 into the media with unchanged cellular concentrations (Hsieh, Longuet

et al. 2009). This experiment demonstrates that GLP-2R-expressing cell(s) mediating this indirect increase reside near enterocytes in these jejunal fragments.

GLP-2 increases intestinal blood flow and stimulates the expression of intestinal endothelial nitric oxide synthase (Guan, Stoll et al. 2003). Inhibiting nitric oxide synthase with L-NAME does not impact intestinal-triglyceride-rich lipoproteins secretion in hamsters (Hsieh, Trajcevski et al. 2015), likely due to the lymphatic fate of these particles. Still, preventing GLP-2-mediated increases in portal and intestinal blood flow via L-NAME, blocks the GLP-2-mediated increase in apoB48 in the triglyceride-rich lipoproteins fraction of plasma (Hsieh, Trajcevski et al. 2015). Mice lacking endothelial nitric oxide synthase (*eNOS*$^{-/-}$ mice) display normal radiolabel appearance into plasma as wild type controls, and GLP-2 treatment fails to increase plasma ^{3}H levels compared to wild-type mice (Hsieh, Trajcevski et al. 2015). Additionally, jejunal triglyceride mass is significantly greater in *eNOS*$^{-/-}$ mice compared to wild type mice, again independent of GLP-2, suggesting that eNOS is involved in the release of stored triglycerides as large chylomicrons rather than absorbed dietary triglycerides and this is upregulated by exogenous GLP-2 (Hsieh, Trajcevski et al. 2015).

Many studies have focused on the ability of GLP-2 to impact the release of lipids stored in the intestine from a previous meal. Indeed, GLP-2$^{1-33}$ peptide treatment 5 hours after intraduodenally administered olive oil significantly increases the triglyceride content of triglyceride-rich lipoproteins, which is inhibited by co-treatment with L-NAME. Similar to acute L-NAME treatment, L-NAME treatment alone 5 hours post acute dietary fat challenge does not change triglyceride-rich lipoproteins secretion compared to saline control (Hsieh, Trajcevski et al. 2015), suggesting that GLP-2 may influence the partitioning of dietary fatty acids from lymph to portal circulation or that endogenous gut-hormone action by GLP-1R and/or GIPR maintains normal intestinal-triglyceride-rich lipoproteins secretion. GLP-2 rapidly increases lymph flow and cumulative lymph volume in cannulated rats 300 minutes after an intraduodenal bolus of Intralipid

20% (Stahel, Xiao et al. 2019). GLP-2 does not significantly change lymph triglyceride concentration, triglyceride output (mL triglyceride per hour) or chylomicron size (triglyceride:apoB48) compared to placebo control, rather it increases the cumulative increase in lymph triglycerides in 60 minutes (Stahel, Xiao et al. 2019). Another study in rats demonstrated that vagotomy attenuates the ability of GLP-2 to increase triglyceride output in the lymph (Mukherjee, Wang et al. 2024). This was associated with identification of activated neurons in the arcuate nucleus of the hypothalamus via c-Fos staining upon GLP-2 treatment (Mukherjee, Wang et al. 2024), unveiling a gut-brain axis mediated by GLP-2R signalling.

Glp2r$^{-/-}$ mice display similar plasma-triglyceride excursion following an olive oil gavage compared to wild-type controls, although trends for decreased secretion are observed (Fuchs, Yusta et al. 2020). This may be driven by the loss of GLP-2R action or the significantly higher plasma active GLP-1 levels observed in these mice (Fuchs, Yusta et al. 2020). Similarly, a stronger phenotype for intestinal-triglyceride secretion is observed in *Glp1r*$^{-/-}$ mice (Hsieh, Longuet et al. 2010), consistent with the predominant role for endogenous GLP-1 in the control of dietary fat delivery.

1.6.8 GIPR

The impact of GIPR signalling on lipid metabolism has been largely focused on adipose tissue. Intravenous GIP infusion does not impact triglyceride levels (Holst, Windelov et al. 2016). In lean individuals under hyperglycemic-hyperinsulinemic clamp conditions, endogenous GIP action promotes triglyceride uptake in subcutaneous adipose tissue, shown with GIP infusion and GIPR antagonist GIP(3-30)NH2 infusion (Asmar, Asmar et al. 2017). GIP infusion significantly increases lipoprotein lipase activity in obese (*fa/fa*) and lean (*fa/-*) VDF Zucker rats (Kim, Nian et al. 2007). Conversely, GIPR antagonist (GIP(3-30)NH2) treatment in rats has been shown to significantly increase plasma triglyceride levels and LPL activity compared to controls (Baldassano, Gasbjerg et al. 2019). By contrast, GIPR agonist treatment with D-Ala2-GIP

treatment has been shown to significantly reduce serum LPL activity in both chow- and high-fat diet-fed mice (Szalowska, Meijer et al. 2011). However, the significance of endogenous GIP secretion as a dominant regulator of LPL secretion is uncertain. GIP, in the presence of insulin, increases LPL gene expression in 3T3-L1 adipocytes via AKT/LKB1/AMPK signaling mediated by resistin (Kim, Nian et al. 2007) and in human adipocytes by increasing TORC2 and phospho-CREB nuclear localization to bind to the CRE-II promoter region (Kim, Nian et al. 2010).

Selective deletion of *Gipr* in brown adipose tissue significantly increases both fasting (overnight) and fed (1 hour re-feed) plasma triglyceride levels of high-fat fed mice (Beaudry, Kaur et al. 2019). Diet-induced obese $Gipr^{BAT-/-}$ mice housed at room temperature display significantly increased intestinal-triglyceride secretion upon a dietary fat challenge (Beaudry, Kaur et al. 2019). Acute GIPR agonist D-Ala2-GIP treatment in mice significantly increases intestinal-triglyceride secretion and plasma apoB48 levels in response to a dietary fat challenge compared to PBS control (Hsieh, Longuet et al. 2010), suggesting a role for GIP in plasma triglycerides independent of triglyceride-rich lipoproteins clearance. It has also been recently shown in rats that intraperitoneal administration of GIP five hours after a dietary fat challenge rapidly increases lymph flow rate and volume leading to a significantly greater lymph triglyceride output (Wang, Khan et al. 2025), thereby providing evidence for GIP to promote post-absorptive release of stored lipids from a previous meal. Dietary fat absorption and intestinal-triglyceride secretion are unchanged upon K cell destruction (Pedersen, Ugleholdt et al. 2013, Holst, Windelov et al. 2016). With the recent identification of GIPR+ pericytes in the gut (Hammoud, Kaur et al. 2024), intestine-specific deletions of *Gipr* will help delineate the contribution of this cell type to intestinal lipid metabolism.

1.6.9 Endogenous gut hormone control of intestinal-triglyceride secretion

Despite having the shortest half-life, GLP-1 appears to have the greatest control of intestinal-triglyceride secretion compared to the opposing actions induced by GLP-2 and GIP.

This stems from observations raising endogenous gut hormone levels with DPP4 inhibitors and genetic elimination of DPP4, as well as co-infusion of the peptide hormones. Chronic DPP4 inhibition with sitagliptin treatment does not significantly impact plasma triglyceride levels at fasting or upon a dietary fat challenge in chow-fed hamsters. In chow-fed mice, however, acute DPP4 inhibition with sitagliptin treatment prior to a dietary fat challenge significantly reduces intestinal-triglyceride secretion (Hsieh, Longuet et al. 2010). Three weeks of DPP4 activity inhibition with sitagliptin significantly lowers plasma triglyceride levels at fasting and triglyceride-rich lipoprotein-fraction triglyceride levels during a dietary fat challenge in high-fructose fed hamsters (Hsieh, Longuet et al. 2010). Both gut selective and systemic inhibition of DPP4 lower intestinal-triglyceride secretion, which were associated with significantly greater levels of active GLP-1 ten minutes after the dietary fat challenge (Varin, Hanson et al. 2020). Whole body genetic elimination of DPP4 as well as endothelial/hematopoietic cell-specific deletion of DPP4 (*Tie2-Cre*) leads to lower intestinal-triglyceride secretion and increased post-dietary fat challenge active GLP-1 levels (Varin, Hanson et al. 2020). Moreover, the impact of DPP4 inhibition on lowering intestinal-triglyceride secretion requires DPP4 action in endothelial and hematopoietic cells. By contrast, intestinal-specific deletion of DPP4 (*Vil-Cre*) does not significantly impact intestinal-triglyceride secretion or post-dietary fat challenge active GLP-1 levels (Varin, Hanson et al. 2020).

1.7 Clinical significance

More than 2 million Canadians live with T2DM, and cardiovascular disease is the leading cause of premature death (Wu and Parhofer 2014). Risk factors for cardiovascular disease development in T2DM include hyperglycemia, obesity, dysregulated blood lipids, insulin resistance, and hypertension. The abnormal blood lipid levels in T2DM exacerbate the accumulation of lipid-rich necrotic debris, including cholesterol-overflowing immune cells and smooth muscle cells within blood vessel walls, promoting the development of atherosclerotic plaques (Lusis 2000). Heart attacks and strokes occur when these plaques block the vessel

through expansion or rupture. A causal relationship between low-density lipoprotein (LDL) cholesterol and cardiovascular risk is well established. While statin therapy lowers the risk of acute cardiovascular events by decreasing LDL cholesterol, it does not completely halt the progression of cardiovascular disease (Wu and Parhofer 2014), suggesting other fundamental drivers must exist.

The residual cardiovascular risk is likely driven by multiple factors, such as the enhanced inflammatory state of atherosclerotic lesions (Yahagi, Kolodgie et al. 2017) and the dysregulated metabolism of triglyceride-rich lipoproteins. Increased production, reduced lipolysis, and lower clearance rates of triglyceride-rich lipoproteins, either individually or in combination, can raise plasma triglyceride levels (Chait, Ginsberg et al. 2020). Several large-scale population studies suggest that elevated plasma triglyceride-rich lipoprotein levels are an independent risk factor for CVD (Toth 2016). Moreover, coronary atherosclerosis severity positively correlates with plasma triglyceride-rich lipoprotein levels in patients living with T2DM (Tkac, Kimball et al. 1997). Peripheral insulin resistance impacts intestinal-triglyceride secretion, as seen in individuals with obesity and fructose-fed hamsters, where an overproduction of triglyceride-rich, apoB48-containing chylomicrons is observed after the same meal compared to healthy controls, resulting in increased and prolonged post-prandial lipemia (Lewis, O'Meara et al. 1990, Adeli and Lewis 2008). As these lipoproteins circulate, they are hydrolyzed by lipases, yielding cholesterol-enriched, atherogenic remnant lipoprotein particles. Therefore, despite significant achievements in understanding the hormonal, nutritional, metabolic, and neural factors that modulate triglyceride-rich lipoproteins production, there remains an urgent need to unravel the fundamental biological pathways that drive lipoprotein hypersecretion.

1.8 Dietary interventions

1.8.1 Citrus flavonoids

Plants produce flavonoids for protection against UV radiation and pathogens and they represent a significant portion of our diets. Flavonoids are composed of 15 carbon atoms with two benzene rings and one heterocyclic ring. The structure of flavonoids divides them into seven categories: flavones, isoflavones, flavanones, flavanols, flavonols, anthocyanidins, and chalcones (Wang, Liu et al. 2022). Flavonoids from citrus fruits consist of five classes: flavones, flavanones, flavonols, flavans, and anthocyanins. Citrus flavonoids exist with and without a sugar moiety, glycoside or aglycone forms, respectively. Upon consumption, the gut microbiota metabolizes flavonoids to their aglycone forms for absorption and transport to the liver, where flavonoids are further metabolized depending on their structure (Mulvihill, Burke et al. 2016).

Flavonoids concentrate in the citrus peel and seeds. The pathogenic fungus *Deuterophoma tracheiphila* causes a disease in citrus fruits called “mal secco” throughout the Mediterranean. The fruits susceptible to “mal secco” include lemons and grapefruits, but curiously, not tangerines. Early experiments using methanol extracts of the tangerine peel revealed a 55% inhibition of the fungus growth rate *in vitro* at 200 parts per million. These extracts include tangeretin, nobiletin, and hesperidin. *In vivo* experiments in lemon seedlings inoculated with the fungus revealed that nobiletin prevented death of the seedlings and significantly slowed signs of disease, thereby labeling nobiletin as a fungistat (Ben-Aziz 1967). In addition to its anti-fungal properties, nobiletin and other flavonoids have been further investigated for their potential to limit oxidative stress. Since then, several studies have added to the properties of nobiletin including anti-cancer, anti-proliferative, anti-mutagenic, and metabolic protection (Chen, Liang et al. 2023, Ran, Gan et al. 2024).

Nobiletin is a polymethoxylflavone found only in the *Citrus depressa* fruit. The chemical structure is 5,6,7,8,3',3'-hexamethoxyflavonone (Wang, Liu et al. 2022). *In vitro* experiments revealed that nobiletin, like insulin (Malmstrom, Packard et al. 1997) reduces the secretion of apoB100 in the media of HepG2 cells through the activation of $MAPK^{erk}$ (Mulvihill, Assini et al. 2011). Nobiletin also dose-dependently increases the phosphorylation of ERK1/2 but does not induce tyrosine phosphorylation of the insulin receptor or IRS-1 (Mulvihill, Assini et al. 2011). Similar to insulin, nobiletin treatment of HepG2 cells led to lower mRNA abundance of *MTP, DGAT1,* and *DGAT2*. However, nobiletin treatment, and not insulin, reduced MTP activity. Nobiletin, like insulin, has been shown to increase the mRNA levels and activity of the LDLR in HepG2 cells. Unlike insulin, nobiletin did not increase the rate of fatty acid synthesis or triglyceride synthesis in HepG2 cells, leading to reduced triglyceride mass in these cells (Mulvihill, Assini et al. 2011).

After oral administration (200 mg/kg) in rats, the major urine metabolite was nobiletin with the loss of one methyl group (4'-hydroxy-3-,5,6,7,8-pentamethoxyflavone), where the amount excreted in 24 hours represented ~13% of the nobiletin dose administered (Yasuda, Yoshimura et al. 2003). *In vivo* experiments revealed that nobiletin, when added to a Western diet at 0.1% or 0.3% w/w in $Ldlr^{-/-}$ mice, prevented weight gain and adiposity despite no difference in caloric intake or intestinal triglyceride absorption. Nobiletin has been shown to reduce fasting plasma triglyceride, cholesterol, free fatty acids, and glycerol levels. Nobiletin treatment improved glucose tolerance and insulin sensitivity shown by both injection of an insulin bolus and through hyperinsulinemic-euglycemic clamps. Nobiletin lowered triglyceride storage in the muscle and has also been shown to significantly reduce the hepatic triglyceride secretion rates (Mulvihill, Assini et al. 2011). Nobiletin significantly reduces hepatic triglyceride, and cholesterol ester mass. The mRNA levels of hepatic *Srebf1c* have been shown to be significantly lower with the addition of nobiletin to the Western diet. Additionally, gene expression analysis revealed that nobiletin

normalized the expression levels of genes related to fatty acid oxidation in the liver. Accordingly, *ex vivo* analysis of hepatic fatty oxidation in these mice revealed significantly greater capacity to oxidize palmitate compared to mice fed the Western diet alone (Mulvihill, Assini et al. 2011). Additionally, nobiletin treatment restored fasting ketone body levels to that similar in chow-fed mice compared to the lower levels observed in Western-diet fed mice. Metabolic cage analyses in these mice revealed that the addition of nobiletin to the Western diet significantly increases energy expenditure. The prevention of exacerbated dyslipidemia in *Ldlr*$^{-/-}$ mice by the addition of nobiletin to the Western diet also significantly blunted atherosclerotic lesion area (Mulvihill, Assini et al. 2011).

Prevention studies with nobiletin treatment have been complemented by intervention studies. Specifically, in *Ldlr*$^{-/-}$ mice with diet-induced obesity and atherosclerosis, the addition of nobiletin to a high-fat, high-cholesterol diet has been shown to induce significant weight loss, increase energy expenditure, and increase hepatic fatty acid oxidation without impacting caloric intake compared to mice that continued on the high-fat, high-cholesterol diet alone. Moreover, intervention with nobiletin improved dyslipidemia, insulin sensitivity, hepatic steatosis. While atherosclerotic lesion size was unchanged, these plaques displayed improved stability through lower macrophage content (Burke, Sutherland et al. 2018).

Through a screen of 5,300 small molecules in fibroblasts from *Clock*$^{\Delta 19/+}$ heterozygous mice expressing a luciferase fusion protein from the endogenous *Period2* promoter, termed circadian reporter cells, nobiletin emerged as an amplifier of circadian rhythms (He, Nohara et al. 2016). Nobiletin treatment by oral gavage every other day failed to prevent obesity and metabolic dysregulation in *Clock*$^{\Delta/\Delta}$ mice fed a high-fat diet (He, Nohara et al. 2016), indicating that nobiletin confers its metabolic protection through strengthening of the circadian clock amplitude. Specifically, nobiletin was found to activate ROR nuclear receptors, stabilizing the transcriptional feedback loop of *Bmal1* and *Clock* (He, Nohara et al. 2016). Interestingly, in mice fed a Western

diet, the addition of nobiletin led to significantly lower triglyceride levels in the intestine in a fasted state compared to mice fed the Western diet alone (Mulvihill, Assini et al. 2011). This finding revealed that the handling of this Western diet is different in mice that maintain insulin sensitivity despite still consuming the same diet. The mechanisms through which nobiletin prevented the accumulation of intestinal lipids in the fasted state as well as the impact and potential mechanisms on intestinal lipid metabolism were explored in this thesis.

1.8.2 Ketogenic diet

During periods of nutrient deprivation, ketone body metabolism fuels the brain (Puchalska and Crawford 2017). Ketone bodies converge on several metabolic pathways, including fatty acid oxidation, the tricarboxylic acid cycle, gluconeogenesis, *de novo* lipogenesis, and sterol biosynthesis (Puchalska and Crawford 2017). As previously discussed, acetyl-CoA products from fatty acid oxidation serve as the building blocks for ketone body formation, predominantly in the liver. Ketone bodies are then oxidized to acetyl-CoA for entry into the tricarboxylic acid cycle in extrahepatic tissues such as the brain, heart, and skeletal muscle. Alternatively, ketone bodies in extrahepatic tissues are diverted to lipogenesis, sterol synthesis pathways, or are excreted in the urine. Ketogenesis is classically viewed as a spillover pathway downstream of fatty acid oxidation under the control of hormones and transcription factors. The rate of ketogenesis is proportional to the level of fatty acid oxidation. However, amino acids can also serve as substrates for ketone bodies (Puchalska and Crawford 2017). In healthy humans, ketone bodies contribute to 5-20% of total energy expenditure in fed, fasted, and starved states (Puchalska and Crawford 2017).

Carbohydrate restriction was commonly advised to patients living with diabetes before the use of insulin as a treatment (Westman, Yancy et al. 2006). Since 2017, Diabetes Canada, Diabetes UK, Diabetes Australia, and the American Diabetes Association have established statements of support for the use of low-carbohydrate diets and ketogenic diets with adequate protein intake for the management of T2DM under the supervision of their physician (Evert,

Dennison et al. 2019, 2020). Consumption of the ketogenic diet places the body in the state of nutritional ketosis, where fatty acids and ketone bodies serve as the main energy source. To achieve ketosis, less than 10% of dietary energy must come from carbohydrates. While macronutrient proportions are not strictly prescribed, protein and fat intake span from 10-30% and 60-80%, respectively (Dynka, Rodzen et al. 2025). As a result, most energy is derived from fatty acid oxidation. Dietary fat composition can significantly impact the ketogenesis drive upon ketogenic diet consumption. For example, diets rich in medium-chain fatty acids will lead to direct delivery from enterocytes to hepatocytes as these fatty acids will not be incorporated into chylomicrons. Indeed, octanoate induces a greater ketogenesis rate compared to oleate in the perfused mouse liver (Nakajima, Horiuchi et al. 1997). Additionally, low carbohydrate diet consumption relieves the drive for insulin production, leading to lower plasma insulin levels, thus lifting insulin's effect to slow ketogenesis (Ruppert and Kersten 2024, Dynka, Rodzen et al. 2025).

As previously discussed, however, the intestinal-triglyceride proportion as well as intestinal lipid storage is proportional to the intake of dietary fat. Indeed, the small intestine absorbs 95% of dietary fat. Therefore, increasing dietary fat intake should increase the storage of dietary fat as well as the amount of triglyceride secreted into circulation. How the intestine adapts to this increase in dietary fat is not well understood.

1.9 Scope of Thesis

The small intestine is an extremely adaptable organ to changes in the external environment including diet and metabolic demand. The handling of dietary fat is also sensitive to these changes, whereby this process is actively regulated by hormonal signals. Despite being produced in the gut, the impact of incretin receptors in different organs, particularly in the endocrine pancreas, has distracted from complete understanding of direct signalling circuits in the intestine. Agonism of GIPR, GLP-1R and GLP-2R has a clear clinical impact on nutrient

absorption and utilization; however, unravelling endogenous circuits engaged in mediating this beneficial effect is not straightforward. Gut hormones represent a signal produced by cells in direct contact with luminal nutrients and the circulation, and, as such, critically responsive to nutritional and environmental stresses. Therefore, the dynamic remodelling of intestinal structure and function upon these stresses represent opportunities to uncover fundamental gut hormone control on lipid handling, surface area expansion, and systemic metabolic responses. In this thesis, I hypothesized that hormonal signalling regulates absorptive surface area, which in turn modulates intestinal lipid metabolism in response to increases in energy intake. This hypothesis was examined using extreme models of physiology to uncover factors controlling adaptability. In Chapter 2, we characterized the impact of adding nobiletin to a high-fat, high-cholesterol diet to intestinal lipid handling and explored the requirement of gut hormone action for nobiletin's metabolic improvements. In Chapter 3, we characterize the adaptation of the small intestine to five weeks of extreme high-fat diet feeding and concomitant carbohydrate restriction. In Chapter 4, we examined the requirement of gut hormone receptor signalling in the expansion of gut surface area upon the doubling of food intake that accompanies chronic cold stress. Through the completion of these studies, we unveiled contributions of endogenous gut hormone receptor signalling to intestinal lipid metabolism, intestinal growth, and sex-specific changes to the intestinal response to metabolic challenges

1.10 References

(2020). "Diabetes Canada Position Statement on Low-Carbohydrate Diets for Adults With Diabetes: A Rapid Review." Can J Diabetes **44**(4): 295–299.

Adam, R. C., I. J. Mintah, C. A. Alexa-Braun, L. M. Shihanian, J. S. Lee, P. Banerjee, S. C. Hamon, H. I. Kim, J. C. Cohen, H. H. Hobbs, C. Van Hout, J. Gromada, A. J. Murphy, G. D. Yancopoulos, M. W. Sleeman and V. Gusarova (2020). "Angiopoietin-like protein 3 governs LDL-cholesterol levels through endothelial lipase-dependent VLDL clearance." J Lipid Res **61**(9): 1271–1286.

Adeli, K. and G. F. Lewis (2008). "Intestinal lipoprotein overproduction in insulin-resistant states." Curr Opin Lipidol **19**(3): 221–228.

Adriaenssens, A., B. Y. Lam, L. Billing, K. Skeffington, S. Sewing, F. Reimann and F. Gribble (2015). "A Transcriptome-Led Exploration of Molecular Mechanisms Regulating Somatostatin-Producing D-Cells in the Gastric Epithelium." Endocrinology **156**(11): 3924–3936.

Agellon, L. B., A. Walsh, T. Hayek, P. Moulin, X. C. Jiang, S. A. Shelanski, J. L. Breslow and A. R. Tall (1991). "Reduced high density lipoprotein cholesterol in human cholesteryl ester transfer protein transgenic mice." J Biol Chem **266**(17): 10796–10801.

Alpers, D. H. (2000). "Is glutamine a unique fuel for small intestinal cells?" Curr Opin Gastroenterol **16**(2): 155.

Andersen, D. B., K. V. Grunddal, J. Pedersen, R. E. Kuhre, M. L. Lund, J. J. Holst and C. Orskov (2021). "Using a Reporter Mouse to Map Known and Novel Sites of GLP-1 Receptor Expression in Peripheral Tissues of Male Mice." Endocrinology **162**(3).

Anini, Y. and P. L. Brubaker (2003). "Role of leptin in the regulation of glucagon-like peptide-1 secretion." Diabetes **52**(2): 252–259.

Argikar, A. A. and U. A. Argikar (2018). "The mesentery: an ADME perspective on a 'new' organ." Drug Metab Rev **50**(3): 398–405.

Asmar, M., A. Asmar, L. Simonsen, L. S. Gasbjerg, A. H. Sparre-Ulrich, M. M. Rosenkilde, B. Hartmann, F. Dela, J. J. Holst and J. Bulow (2017). "The Gluco- and Liporegulatory and Vasodilatory Effects of Glucose-Dependent Insulinotropic Polypeptide (GIP) Are Abolished by an Antagonist of the Human GIP Receptor." Diabetes **66**(9): 2363–2371.

Baggio, L. L. and D. J. Drucker (2007). "Biology of incretins: GLP-1 and GIP." Gastroenterology **132**(6): 2131–2157.

Baggio, L. L., Q. Huang, T. J. Brown and D. J. Drucker (2004). "A recombinant human glucagon-like peptide (GLP)-1-albumin protein (albugon) mimics peptidergic activation of GLP-1 receptor-dependent pathways coupled with satiety, gastrointestinal motility, and glucose homeostasis." Diabetes **53**(9): 2492–2500.

Baldassano, S., L. S. Gasbjerg, H. S. Kizilkaya, M. M. Rosenkilde, J. J. Holst and B. Hartmann (2019). "Increased Body Weight and Fat Mass After Subchronic GIP Receptor Antagonist, but Not GLP-2 Receptor Antagonist, Administration in Rats." Front Endocrinol (Lausanne) **10**: 492.

Banks, W. A. (2012). "Role of the blood-brain barrier in the evolution of feeding and cognition." Ann N Y Acad Sci **1264**(1): 13–19.

BARRE, L. (1932). "Sur les possibilities d'un traitement du diabete par. L'incretine." Bull Acad R Med Belg **12**: 620–634.

Bayliss, W. M. and E. H. Starling (1902). "The mechanism of pancreatic secretion." J Physiol **28**(5): 325–353.

Beaudry, J. L., K. D. Kaur, E. M. Varin, L. L. Baggio, X. Cao, E. E. Mulvihill, H. E. Bates, J. E. Campbell and D. J. Drucker (2019). "Physiological roles of the GIP receptor in murine brown adipose tissue." Mol Metab **28**: 14–25.

Beilstein, F., V. Carriere, A. Leturque and S. Demignot (2016). "Characteristics and functions of lipid droplets and associated proteins in enterocytes." Exp Cell Res **340**(2): 172–179.

Bell, G. I., R. Sanchez-Pescador, P. J. Laybourn and R. C. Najarian (1983). "Exon duplication and divergence in the human preproglucagon gene." Nature **304**(5924): 368–371.

Bell, G. I., R. F. Santerre and G. T. Mullenbach (1983). "Hamster preproglucagon contains the sequence of glucagon and two related peptides." Nature **302**(5910): 716–718.

Ben-Aziz, A. (1967). "Nobiletin is main fungistat in tangerines resistant to mal secco." Science **155**(3765): 1026–1027.

Bernier-Latmani, J. and T. V. Petrova (2017). "Intestinal lymphatic vasculature: structure, mechanisms and functions." Nat Rev Gastroenterol Hepatol **14**(9): 510–526.

Biddinger, S. B., A. Hernandez-Ono, C. Rask-Madsen, J. T. Haas, J. O. Aleman, R. Suzuki, E. F. Scapa, C. Agarwal, M. C. Carey, G. Stephanopoulos, D. E. Cohen, G. L. King, H. N. Ginsberg and C. R. Kahn (2008). "Hepatic insulin resistance is sufficient to produce dyslipidemia and susceptibility to atherosclerosis." Cell Metab **7**(2): 125–134.

Boden, G., X. Chen, M. Mozzoli and I. Ryan (1996). "Effect of fasting on serum leptin in normal human subjects." J Clin Endocrinol Metab **81**(9): 3419–3423.

Boismenu, R. and W. L. Havran (1994). "Modulation of epithelial cell growth by intraepithelial gamma delta T cells." Science **266**(5188): 1253–1255.

Borgstrom, B., A. Dahlqvist, G. Lundh and J. Sjovall (1957). "Studies of intestinal digestion and absorption in the human." J Clin Invest **36**(10): 1521–1536.

Boylan, M. O., L. I. Jepeal and M. M. Wolfe (2006). "Sp1/Sp3 binding is associated with cell-specific expression of the glucose-dependent insulinotropic polypeptide receptor gene." Am J Physiol Endocrinol Metab **290**(6): E1287–1295.

Bozzetto, L., G. Della Pepa, C. Vetrani and A. A. Rivellese (2020). "Dietary Impact on Postprandial Lipemia." Front Endocrinol (Lausanne) **11**: 337.

Brown, J. C., J. R. Dryburgh, S. A. Ross and J. Dupre (1975). "Identification and actions of gastric inhibitory polypeptide." Recent Prog Horm Res **31**: 487–532.

Brown, J. C. and S. C. Otte (1979). "GIP and the entero-insular axis." Clin Endocrinol Metab **8**(2): 365–377.

Brown, J. C. and R. A. Pederson (1970). "A multiparameter study on the action of preparations containing cholecystokinin-pancreozymin." Scand J Gastroenterol **5**(6): 537–541.

Brown, M. S. and J. L. Goldstein (1986). "A receptor-mediated pathway for cholesterol homeostasis." Science **232**(4746): 34–47.

Brown, M. S. and J. L. Goldstein (2008). "Selective versus total insulin resistance: a pathogenic paradox." Cell Metab **7**(2): 95–96.

Brubaker, P. L. (2018). "Glucagon-like Peptide-2 and the Regulation of Intestinal Growth and Function." Compr Physiol **8**(3): 1185–1210.

Brubaker, P. L., A. Crivici, A. Izzo, P. Ehrlich, C. H. Tsai and D. J. Drucker (1997). "Circulating and tissue forms of the intestinal growth factor, glucagon-like peptide-2." Endocrinology **138**(11): 4837–4843.

Bryant, M. G., S. R. Bloom, J. M. Polak, S. Hobbs, W. Domschke, S. Domschke, P. Mitznegg, H. Ruppin and L. Demling (1983). "Measurement of gut hormonal peptides in biopsies from human stomach and proximal small intestine." Gut **24**(2): 114–119.

Buchan, A. M., J. M. Polak, C. Capella, E. Solcia and A. G. Pearse (1978). "Electronimmunocytochemical evidence for the K cell localization of gastric inhibitory polypeptide (GIP) in man." Histochemistry **56**(1): 37–44.

Buhman, K. K., S. J. Smith, S. J. Stone, J. J. Repa, J. S. Wong, F. F. Knapp, Jr., B. J. Burri, R. L. Hamilton, N. A. Abumrad and R. V. Farese, Jr. (2002). "DGAT1 is not essential for intestinal triacylglycerol absorption or chylomicron synthesis." J Biol Chem **277**(28): 25474–25479.

Bunck, M. C., A. Corner, B. Eliasson, R. J. Heine, R. M. Shaginian, Y. Wu, P. Yan, U. Smith, H. Yki-Jarvinen, M. Diamant and M. R. Taskinen (2010). "One-year treatment with exenatide vs. insulin glargine: effects on postprandial glycemia, lipid profiles, and oxidative stress." Atherosclerosis **212**(1): 223–229.

Burant, C. F., J. Takeda, E. Brot-Laroche, G. I. Bell and N. O. Davidson (1992). "Fructose transporter in human spermatozoa and small intestine is GLUT5." J Biol Chem **267**(21): 14523–14526.

Burke, A. C., B. G. Sutherland, D. E. Telford, M. R. Morrow, C. G. Sawyez, J. Y. Edwards, M. Drangova and M. W. Huff (2018). "Intervention with citrus flavonoids reverses obesity and improves metabolic syndrome and atherosclerosis in obese Ldlr(-/-) mice." J Lipid Res **59**(9): 1714–1728.

Burks, K. H., N. O. Stitziel and N. O. Davidson (2025). "Molecular Regulation and Therapeutic Targeting of VLDL Production in Cardiometabolic Disease." Cell Mol Gastroenterol Hepatol **19**(1): 101409.

Campbell, J. E. and C. B. Newgard (2021). "Mechanisms controlling pancreatic islet cell function in insulin secretion." Nat Rev Mol Cell Biol **22**(2): 142–158.

Campos, R. V., Y. C. Lee and D. J. Drucker (1994). "Divergent tissue-specific and developmental expression of receptors for glucagon and glucagon-like peptide-1 in the mouse." Endocrinology **134**(5): 2156–2164.

Capozzi, M. E., D. Bouslov, A. Sargsyan, M. Y. Chan, S. M. Gray, K. Viloria, A. Bareja, J. D. Douros, S. L. Lewandowski, J. C. Tong, A. Hasib, F. Cuozzo, E. C. Ross, M. W. Foster, L. S. Weinstein, M. A. Hussain, M. J. Merrins, F. S. Willard, M. O. Huising, K. W. Sloop, D. J. Hodson, D. A. D'Alessio and J. E. Campbell (2025). "beta-cell Gas signaling is critical for physiological and pharmacological enhancement of insulin secretion." J Clin Invest.

Chait, A., H. N. Ginsberg, T. Vaisar, J. W. Heinecke, I. J. Goldberg and K. E. Bornfeldt (2020). "Remnants of the Triglyceride-Rich Lipoproteins, Diabetes, and Cardiovascular Disease." Diabetes **69**(4): 508–516.

Chen, S. H., G. Habib, C. Y. Yang, Z. W. Gu, B. R. Lee, S. A. Weng, S. R. Silberman, S. J. Cai, J. P. Deslypere, M. Rosseneu and et al. (1987). "Apolipoprotein B-48 is the product of a messenger RNA with an organ-specific in-frame stop codon." Science **238**(4825): 363–366.

Chen, Y. Y., J. J. Liang, D. L. Wang, J. B. Chen, J. P. Cao, Y. Wang and C. D. Sun (2023). "Nobiletin as a chemopreventive natural product against cancer, a comprehensive review." Crit Rev Food Sci Nutr **63**(23): 6309–6329.

Christensen, M., L. Vedtofte, J. J. Holst, T. Vilsboll and F. K. Knop (2011). "Glucose-dependent insulinotropic polypeptide: a bifunctional glucose-dependent regulator of glucagon and insulin secretion in humans." Diabetes **60**(12): 3103–3109.

Cinci, L., M. S. Faussone-Pellegrini, A. Rotondo, F. Mule and M. G. Vannucchi (2011). "GLP-2 receptor expression in excitatory and inhibitory enteric neurons and its role in mouse duodenum contractility." Neurogastroenterol Motil **23**(9): e383–392.

Collier, G., A. McLean and K. O'Dea (1984). "Effect of co-ingestion of fat on the metabolic responses to slowly and rapidly absorbed carbohydrates." Diabetologia **26**(1): 50–54.

Collins, J. T., A. Nguyen and M. Badireddy (2021). Anatomy, Abdomen and Pelvis, Small Intestine. StatPearls. Treasure Island (FL).

Considine, R. V., M. K. Sinha, M. L. Heiman, A. Kriauciunas, T. W. Stephens, M. R. Nyce, J. P. Ohannesian, C. C. Marco, L. J. McKee, T. L. Bauer and et al. (1996). "Serum immunoreactive-leptin concentrations in normal-weight and obese humans." N Engl J Med **334**(5): 292–295.

Coon, S. D., J. H. Schwartz, V. M. Rajendran, L. Jepeal and S. K. Singh (2013). "Glucose-dependent insulinotropic polypeptide regulates dipeptide absorption in mouse jejunum." Am J Physiol Gastrointest Liver Physiol **305**(10): G678–684.

Creutzfeldt, W., R. Ebert, B. Willms, H. Frerichs and J. C. Brown (1978). "Gastric inhibitory polypeptide (GIP) and insulin in obesity: increased response to stimulation and defective feedback control of serum levels." Diabetologia **14**(1): 15–24.

D'Alessio, D., W. Lu, W. Sun, S. Zheng, Q. Yang, R. Seeley, S. C. Woods and P. Tso (2007). "Fasting and postprandial concentrations of GLP-1 in intestinal lymph and portal plasma: evidence for selective release of GLP-1 in the lymph system." Am J Physiol Regul Integr Comp Physiol **293**(6): R2163–2169.

D'Aquila, T., Y. H. Hung, A. Carreiro and K. K. Buhman (2016). "Recent discoveries on absorption of dietary fat: Presence, synthesis, and metabolism of cytoplasmic lipid droplets within enterocytes." Biochim Biophys Acta **1861**(8 Pt A): 730–747.

Dash, S., C. Xiao, C. Morgantini, P. W. Connelly, B. W. Patterson and G. F. Lewis (2014). "Glucagon-like peptide-2 regulates release of chylomicrons from the intestine." Gastroenterology **147**(6): 1275–1284 e1274.

Davidson, N. O., A. M. Hausman, C. A. Ifkovits, J. B. Buse, G. W. Gould, C. F. Burant and G. I. Bell (1992). "Human intestinal glucose transporter expression and localization of GLUT5." Am J Physiol **262**(3 Pt 1): C795–800.

Deacon, C. F., A. H. Johnsen and J. J. Holst (1995). "Degradation of glucagon-like peptide-1 by human plasma in vitro yields an N-terminally truncated peptide that is a major endogenous metabolite in vivo." J Clin Endocrinol Metab **80**(3): 952–957.

Deacon, C. F., A. H. Johnsen and J. J. Holst (1995). "Human colon produces fully processed glucagon-like peptide-1 (7-36) amide." FEBS Lett **372**(2-3): 269–272.

Demignot, S., F. Beilstein and E. Morel (2014). "Triglyceride-rich lipoproteins and cytosolic lipid droplets in enterocytes: key players in intestinal physiology and metabolic disorders." Biochimie **96**: 48–55.

DeSesso, J. M. and C. F. Jacobson (2001). "Anatomical and physiological parameters affecting gastrointestinal absorption in humans and rats." Food Chem Toxicol **39**(3): 209–228.

Dixon, J. B. (2010). "Mechanisms of chylomicron uptake into lacteals." Ann N Y Acad Sci **1207 Suppl 1**: E52–57.

Donnelly, K. L., C. I. Smith, S. J. Schwarzenberg, J. Jessurun, M. D. Boldt and E. J. Parks (2005). "Sources of fatty acids stored in liver and secreted via lipoproteins in patients with nonalcoholic fatty liver disease." J Clin Invest **115**(5): 1343–1351.

Douglass, J. D., N. Malik, S. H. Chon, K. Wells, Y. X. Zhou, A. S. Choi, L. B. Joseph and J. Storch (2012). "Intestinal mucosal triacylglycerol accumulation secondary to decreased lipid secretion in obese and high fat fed mice." Front Physiol **3**: 25.

Drucker, D. J. (2022). "GLP-1 physiology informs the pharmacotherapy of obesity." Mol Metab **57**: 101351.

Drucker, D. J. and P. L. Brubaker (1989). "Proglucagon gene expression is regulated by a cyclic AMP-dependent pathway in rat intestine." Proc Natl Acad Sci U S A **86**(11): 3953–3957.

Drucker, D. J., T. Jin, S. L. Asa, T. A. Young and P. L. Brubaker (1994). "Activation of proglucagon gene transcription by protein kinase-A in a novel mouse enteroendocrine cell line." Mol Endocrinol **8**(12): 1646–1655.

Drucker, D. J., S. Mojsov and J. F. Habener (1986). "Cell-specific post-translational processing of preproglucagon expressed from a metallothionein-glucagon fusion gene." J Biol Chem **261**(21): 9637–9643.

Drucker, D. J., J. Philippe, S. Mojsov, W. L. Chick and J. F. Habener (1987). "Glucagon-like peptide I stimulates insulin gene expression and increases cyclic AMP levels in a rat islet cell line." Proc Natl Acad Sci U S A **84**(10): 3434–3438.

Drucker, D. J., Q. Shi, A. Crivici, M. Sumner-Smith, W. Tavares, M. Hill, L. DeForest, S. Cooper and P. L. Brubaker (1997). "Regulation of the biological activity of glucagon-like peptide 2 in vivo by dipeptidyl peptidase IV." Nat Biotechnol **15**(7): 673–677.

Dube, P. E., C. L. Forse, J. Bahrami and P. L. Brubaker (2006). "The essential role of insulin-like growth factor-1 in the intestinal tropic effects of glucagon-like peptide-2 in mice." Gastroenterology **131**(2): 589–605.

Duez, H., B. Lamarche, K. D. Uffelman, R. Valero, J. S. Cohn and G. F. Lewis (2006). "Hyperinsulinemia is associated with increased production rate of intestinal apolipoprotein B-48-containing lipoproteins in humans." Arterioscler Thromb Vasc Biol **26**(6): 1357–1363.

Duez, H., B. Lamarche, R. Valero, M. Pavlic, S. Proctor, C. Xiao, L. Szeto, B. W. Patterson and G. F. Lewis (2008). "Both intestinal and hepatic lipoprotein production are stimulated by an acute elevation of plasma free fatty acids in humans." Circulation **117**(18): 2369–2376.

Dupre, J., S. A. Ross, D. Watson and J. C. Brown (1973). "Stimulation of insulin secretion by gastric inhibitory polypeptide in man." J Clin Endocrinol Metab **37**(5): 826–828.

Dynka, D., L. Rodzen, M. Rodzen, A. Pacholak-Klimas, G. Ede, S. Sethi, D. Lojko, K. Barton, K. Berry, A. Deptula, Z. Grzywacz, P. Martin, J. Unwin and D. Unwin (2025). "Ketogenic Diets for Body Weight Loss: A Comparison with Other Diets." Nutrients **17**(6).

Ebert, R. and W. Creutzfeldt (1982). "Influence of gastric inhibitory polypeptide antiserum on glucose-induced insulin secretion in rats." Endocrinology **111**(5): 1601–1606.

Eissele, R., R. Goke, S. Willemer, H. P. Harthus, H. Vermeer, R. Arnold and B. Goke (1992). "Glucagon-like peptide-1 cells in the gastrointestinal tract and pancreas of rat, pig and man." Eur J Clin Invest **22**(4): 283–291.

El Eid, L., C. A. Reynolds, A. Tomas and J. Ben (2022). "Biased agonism and polymorphic variation at the GLP-1 receptor: Implications for the development of personalised therapeutics." Pharmacol Res **184**: 106411.

El, K. and J. E. Campbell (2020). "The role of GIP in alpha-cells and glucagon secretion." Peptides **125**: 170213.

Elrick, H., L. Stimmler, C. J. Hlad, Jr. and Y. Arai (1964). "Plasma Insulin Response to Oral and Intravenous Glucose Administration." J Clin Endocrinol Metab **24**: 1076–1082.

Eng, J., W. A. Kleinman, L. Singh, G. Singh and J. P. Raufman (1992). "Isolation and characterization of exendin-4, an exendin-3 analogue, from Heloderma suspectum venom. Further evidence for an exendin receptor on dispersed acini from guinea pig pancreas." J Biol Chem **267**(11): 7402–7405.

Ensari, A. and M. N. Marsh (2018). "Exploring the villus." Gastroenterol Hepatol Bed Bench **11**(3): 181–190.

Estall, J. L. and D. J. Drucker (2005). "Tales beyond the crypt: glucagon-like peptide-2 and cytoprotection in the intestinal mucosa." Endocrinology **146**(1): 19–21.

Estall, J. L., B. Yusta and D. J. Drucker (2004). "Lipid raft-dependent glucagon-like peptide-2 receptor trafficking occurs independently of agonist-induced desensitization." Mol Biol Cell **15**(8): 3673–3687.

Evert, A. B., M. Dennison, C. D. Gardner, W. T. Garvey, K. H. K. Lau, J. MacLeod, J. Mitri, R. F. Pereira, K. Rawlings, S. Robinson, L. Saslow, S. Uelmen, P. B. Urbanski and W. S. Yancy, Jr. (2019). "Nutrition Therapy for Adults With Diabetes or Prediabetes: A Consensus Report." Diabetes Care **42**(5): 731–754.

Farese, R. V., Jr., S. Cases and S. J. Smith (2000). "Triglyceride synthesis: insights from the cloning of diacylglycerol acyltransferase." Curr Opin Lipidol **11**(3): 229–234.

Farooqi, I. S., S. A. Jebb, G. Langmack, E. Lawrence, C. H. Cheetham, A. M. Prentice, I. A. Hughes, M. A. McCamish and S. O'Rahilly (1999). "Effects of recombinant leptin therapy in a child with congenital leptin deficiency." N Engl J Med **341**(12): 879–884.

Federico, L. M., M. Naples, D. Taylor and K. Adeli (2006). "Intestinal insulin resistance and aberrant production of apolipoprotein B48 lipoproteins in an animal model of insulin resistance and metabolic dyslipidemia: evidence for activation of protein tyrosine phosphatase-1B, extracellular signal-related kinase, and sterol regulatory element-binding protein-1c in the fructose-fed hamster intestine." Diabetes **55**(5): 1316–1326.

Feingold, K. R. (2000). Introduction to Lipids and Lipoproteins. Endotext. K. R. Feingold, B. Anawalt, M. R. Blackman et al. South Dartmouth (MA).

Flatt, J. P. and E. G. Ball (1964). "Studies on the Metabolism of Adipose Tissue. Xv. An Evaluation of the Major Pathways of Glucose Catabolism as Influenced by Insulin and Epinephrine." J Biol Chem **239**: 675–685.

Fodden, J. H. and W. O. Read (1954). "The activity of extracted pancreatic hyperglycemic-glycogenolytic factor after cobaltous chloride and synthalin A." Endocrinology **54**(3): 303–310.

Francis, G. A. (2016). Chapter 15 - High-Density Lipoproteins: Metabolism and Protective Roles Against Atherosclerosis. Biochemistry of Lipids, Lipoproteins and Membranes (Sixth Edition). R. S. M. Neale D. Ridgway, Elsevier**:** 437–457.

Fuchs, S., B. Yusta, L. L. Baggio, E. M. Varin, D. Matthews and D. J. Drucker (2020). "Loss of Glp2r signaling activates hepatic stellate cells and exacerbates diet-induced steatohepatitis in mice." JCI Insight **5**(8).

Fujita, Y., A. Asadi, G. K. Yang, Y. N. Kwok and T. J. Kieffer (2010). "Differential processing of pro-glucose-dependent insulinotropic polypeptide in gut." Am J Physiol Gastrointest Liver Physiol **298**(5): G608–614.

Fullerton, M. D. (2016). "AMP-activated protein kinase and its multifaceted regulation of hepatic metabolism." Curr Opin Lipidol **27**(2): 172–180.

Gangl, A. and R. K. Ockner (1975). "Intestinal metabolism of plasma free fatty acids. Intracellular compartmentation and mechanisms of control." J Clin Invest **55**(4): 803–813.

Gehart, H. and H. Clevers (2019). "Tales from the crypt: new insights into intestinal stem cells." Nat Rev Gastroenterol Hepatol **16**(1): 19–34.

Ghaben, A. L. and P. E. Scherer (2019). "Adipogenesis and metabolic health." Nat Rev Mol Cell Biol **20**(4): 242–258.

Gorboulev, V., A. Schurmann, V. Vallon, H. Kipp, A. Jaschke, D. Klessen, A. Friedrich, S. Scherneck, T. Rieg, R. Cunard, M. Veyhl-Wichmann, A. Srinivasan, D. Balen, D. Breljak, R. Rexhepaj, H. E. Parker, F. M. Gribble, F. Reimann, F. Lang, S. Wiese, I. Sabolic, M. Sendtner and H. Koepsell (2012). "Na(+)-D-glucose cotransporter SGLT1 is pivotal for intestinal glucose absorption and glucose-dependent incretin secretion." Diabetes **61**(1): 187–196.

Grasset, E., A. Puel, J. Charpentier, X. Collet, J. E. Christensen, F. Terce and R. Burcelin (2017). "A Specific Gut Microbiota Dysbiosis of Type 2 Diabetic Mice Induces GLP-1 Resistance through an Enteric NO-Dependent and Gut-Brain Axis Mechanism." Cell Metab **25**(5): 1075–1090 e1075.

Gribble, F. M. and F. Reimann (2019). "Function and mechanisms of enteroendocrine cells and gut hormones in metabolism." Nat Rev Endocrinol **15**(4): 226–237.

Griel, L. C., Jr. and R. D. McCarthy (1969). "Blood serum lipoproteins: a review." J Dairy Sci **52**(8): 1233–1243.

Grigoryan, M., M. H. Kedees, M. J. Charron, Y. Guz and G. Teitelman (2012). "Regulation of mouse intestinal L cell progenitors proliferation by the glucagon family of peptides." Endocrinology **153**(7): 3076–3088.

Grimelius, L., C. Capella, R. Buffa, J. M. Polak, A. G. Pearse and E. Solcia (1976). "Cytochemical and ultrastructural differentiation of enteroglucagon and pancreatic-type glucagon cells of the gastrointestinal tract." Virchows Arch B Cell Pathol **20**(3): 217–228.

Gruzdeva, O., D. Borodkina, E. Uchasova, Y. Dyleva and O. Barbarash (2019). "Leptin resistance: underlying mechanisms and diagnosis." Diabetes Metab Syndr Obes **12**: 191–198.

Guan, X., H. E. Karpen, J. Stephens, J. T. Bukowski, S. Niu, G. Zhang, B. Stoll, M. J. Finegold, J. J. Holst, D. Hadsell, B. L. Nichols and D. G. Burrin (2006). "GLP-2 receptor localizes to enteric neurons and endocrine cells expressing vasoactive peptides and mediates increased blood flow." Gastroenterology **130**(1): 150–164.

Guan, X., B. Stoll, X. Lu, K. A. Tappenden, J. J. Holst, B. Hartmann and D. G. Burrin (2003). "GLP-2-mediated up-regulation of intestinal blood flow and glucose uptake is nitric oxide-dependent in TPN-fed piglets 1." Gastroenterology **125**(1): 136–147.

Guilherme, A., J. V. Virbasius, V. Puri and M. P. Czech (2008). "Adipocyte dysfunctions linking obesity to insulin resistance and type 2 diabetes." Nat Rev Mol Cell Biol **9**(5): 367–377.

Guyard-Dangremont, V., C. Desrumaux, P. Gambert, C. Lallemant and L. Lagrost (1998). "Phospholipid and cholesteryl ester transfer activities in plasma from 14 vertebrate species. Relation to atherogenesis susceptibility." Comp Biochem Physiol B Biochem Mol Biol **120**(3): 517–525.

Hadjiyanni, I., K. K. Li and D. J. Drucker (2009). "Glucagon-like peptide-2 reduces intestinal permeability but does not modify the onset of type 1 diabetes in the nonobese diabetic mouse." Endocrinology **150**(2): 592–599.

Haeusler, R. A., T. E. McGraw and D. Accili (2018). "Biochemical and cellular properties of insulin receptor signalling." Nat Rev Mol Cell Biol **19**(1): 31–44.

Haidari, M., N. Leung, F. Mahbub, K. D. Uffelman, R. Kohen-Avramoglu, G. F. Lewis and K. Adeli (2002). "Fasting and postprandial overproduction of intestinally derived lipoproteins in an animal model of insulin resistance. Evidence that chronic fructose feeding in the hamster is accompanied by enhanced intestinal de novo lipogenesis and ApoB48-containing lipoprotein overproduction." J Biol Chem **277**(35): 31646–31655.

Hammoud, R., K. D. Kaur, J. A. Koehler, L. L. Baggio, C. K. Wong, K. E. Advani, B. Yusta, I. Efimova, F. M. Gribble, F. Reimann, S. Fishman, C. Varol and D. J. Drucker (2024). "Glucose-dependent insulinotropic polypeptide receptor signaling alleviates gut inflammation in mice." JCI Insight **10**(3).

Hansen, L., C. F. Deacon, C. Orskov and J. J. Holst (1999). "Glucagon-like peptide-1-(7-36)amide is transformed to glucagon-like peptide-1-(9-36)amide by dipeptidyl peptidase IV in the capillaries supplying the L cells of the porcine intestine." Endocrinology **140**(11): 5356–5363.

Hansotia, T., L. L. Baggio, D. Delmeire, S. A. Hinke, Y. Yamada, K. Tsukiyama, Y. Seino, J. J. Holst, F. Schuit and D. J. Drucker (2004). "Double incretin receptor knockout (DIRKO) mice reveal an essential role for the enteroinsular axis in transducing the glucoregulatory actions of DPP-IV inhibitors." Diabetes **53**(5): 1326–1335.

Hartmann, B., M. B. Harr, P. B. Jeppesen, M. Wojdemann, C. F. Deacon, P. B. Mortensen and J. J. Holst (2000). "In vivo and in vitro degradation of glucagon-like peptide-2 in humans." J Clin Endocrinol Metab **85**(8): 2884–2888.

Hartvigsen, K., C. J. Binder, L. F. Hansen, A. Rafia, J. Juliano, S. Horkko, D. Steinberg, W. Palinski, J. L. Witztum and A. C. Li (2007). "A diet-induced hypercholesterolemic murine model to study atherogenesis without obesity and metabolic syndrome." Arterioscler Thromb Vasc Biol **27**(4): 878–885.

He, B., K. Nohara, N. Park, Y. S. Park, B. Guillory, Z. Zhao, J. M. Garcia, N. Koike, C. C. Lee, J. S. Takahashi, S. H. Yoo and Z. Chen (2016). "The Small Molecule Nobiletin Targets the Molecular Oscillator to Enhance Circadian Rhythms and Protect against Metabolic Syndrome." Cell Metab **23**(4): 610–621.

He, S., F. Kahles, S. Rattik, M. Nairz, C. S. McAlpine, A. Anzai, D. Selgrade, A. M. Fenn, C. T. Chan, J. E. Mindur, C. Valet, W. C. Poller, L. Halle, N. Rotllan, Y. Iwamoto, G. R. Wojtkiewicz, R. Weissleder, P. Libby, C. Fernandez-Hernando, D. J. Drucker, M. Nahrendorf and F. K. Swirski (2019). "Gut intraepithelial T cells calibrate metabolism and accelerate cardiovascular disease." Nature **566**(7742): 115–119.

Hediger, M. A. and D. B. Rhoads (1994). "Molecular physiology of sodium-glucose cotransporters." Physiol Rev **74**(4): 993–1026.

Heinrich, G., P. Gros and J. F. Habener (1984). "Glucagon gene sequence. Four of six exons encode separate functional domains of rat pre-proglucagon." J Biol Chem **259**(22): 14082–14087.

Heinrich, G., P. Gros, P. K. Lund, R. C. Bentley and J. F. Habener (1984). "Pre-proglucagon messenger ribonucleic acid: nucleotide and encoded amino acid sequences of the rat pancreatic complementary deoxyribonucleic acid." Endocrinology **115**(6): 2176–2181.

Herrmann, C., R. Goke, G. Richter, H. C. Fehmann, R. Arnold and B. Goke (1995). "Glucagon-like peptide-1 and glucose-dependent insulin-releasing polypeptide plasma levels in response to nutrients." Digestion **56**(2): 117–126.

Higashimoto, Y. and R. A. Liddle (1993). "Isolation and characterization of the gene encoding rat glucose-dependent insulinotropic peptide." Biochem Biophys Res Commun **193**(1): 182–190.

Higashimoto, Y., E. C. Opara and R. A. Liddle (1995). "Dietary regulation of glucose-dependent insulinotropic peptide (GIP) gene expression in rat small intestine." Comp Biochem Physiol C Pharmacol Toxicol Endocrinol **110**(2): 207–214.

Higashimoto, Y., J. Simchock and R. A. Liddle (1992). "Molecular cloning of rat glucose-dependent insulinotropic peptide (GIP)." Biochim Biophys Acta **1132**(1): 72–74.

Higuchi, K., A. V. Hospattankar, S. W. Law, N. Meglin, J. Cortright and H. B. Brewer, Jr. (1988). "Human apolipoprotein B (apoB) mRNA: identification of two distinct apoB mRNAs, an mRNA with the apoB-100 sequence and an apoB mRNA containing a premature in-frame translational stop codon, in both liver and intestine." Proc Natl Acad Sci U S A **85**(6): 1772–1776.

Higuchi, K., K. Kitagawa, K. Kogishi and T. Takeda (1992). "Developmental and age-related changes in apolipoprotein B mRNA editing in mice." J Lipid Res **33**(12): 1753–1764.

Hill, M. E., S. L. Asa and D. J. Drucker (1999). "Essential requirement for Pax6 in control of enteroendocrine proglucagon gene transcription." Mol Endocrinol **13**(9): 1474–1486.

Ho, S. Y., L. Delgado and J. Storch (2002). "Monoacylglycerol metabolism in human intestinal Caco-2 cells: evidence for metabolic compartmentation and hydrolysis." J Biol Chem **277**(3): 1816–1823.

Ho, S. Y. and J. Storch (2001). "Common mechanisms of monoacylglycerol and fatty acid uptake by human intestinal Caco-2 cells." Am J Physiol Cell Physiol **281**(4): C1106–1117.

Hoffman, S., D. Alvares and K. Adeli (2022). "GLP-1 attenuates intestinal fat absorption and chylomicron production via vagal afferent nerves originating in the portal vein." Mol Metab **65**: 101590.

Holst, J. J., C. Orskov, O. V. Nielsen and T. W. Schwartz (1987). "Truncated glucagon-like peptide I, an insulin-releasing hormone from the distal gut." FEBS Lett **211**(2): 169–174.

Holst, J. J., J. A. Windelov, G. A. Boer, J. Pedersen, B. Svendsen, M. Christensen, S. Torekov, M. Asmar, B. Hartmann and A. Nissen (2016). "Searching for the physiological role of glucose-dependent insulinotropic polypeptide." J Diabetes Investig **7 Suppl 1**: 8–12.

Horton, J. D., J. L. Goldstein and M. S. Brown (2002). "SREBPs: activators of the complete program of cholesterol and fatty acid synthesis in the liver." J Clin Invest **109**(9): 1125–1131.

Hospattankar, A. V., K. Higuchi, S. W. Law, N. Meglin and H. B. Brewer, Jr. (1987). "Identification of a novel in-frame translational stop codon in human intestine apoB mRNA." Biochem Biophys Res Commun **148**(1): 279–285.

Hsieh, J., C. Longuet, C. L. Baker, B. Qin, L. M. Federico, D. J. Drucker and K. Adeli (2010). "The glucagon-like peptide 1 receptor is essential for postprandial lipoprotein synthesis and secretion in hamsters and mice." Diabetologia **53**(3): 552–561.

Hsieh, J., C. Longuet, A. Maida, J. Bahrami, E. Xu, C. L. Baker, P. L. Brubaker, D. J. Drucker and K. Adeli (2009). "Glucagon-like peptide-2 increases intestinal lipid absorption and chylomicron production via CD36." Gastroenterology **137**(3): 997–1005, 1005 e1001–1004.

Hsieh, J., K. E. Trajcevski, S. L. Farr, C. L. Baker, E. J. Lake, J. Taher, J. Iqbal, M. M. Hussain and K. Adeli (2015). "Glucagon-Like Peptide 2 (GLP-2) Stimulates Postprandial Chylomicron Production and Postabsorptive Release of Intestinal Triglyceride Storage Pools via Induction of Nitric Oxide Signaling in Male Hamsters and Mice." Endocrinology **156**(10): 3538–3547.

Hung, Y. H., A. L. Carreiro and K. K. Buhman (2017). "Dgat1 and Dgat2 regulate enterocyte triacylglycerol distribution and alter proteins associated with cytoplasmic lipid droplets in response to dietary fat." Biochim Biophys Acta Mol Cell Biol Lipids **1862**(6): 600–614.

Ikeguchi, E., N. Harada, Y. Kanemaru, A. Sankoda, S. Yamane, K. Iwasaki, M. Imajo, Y. Murata, K. Suzuki, E. Joo and N. Inagaki (2018). "Transcriptional factor Pdx1 is involved in age-related GIP hypersecretion in mice." Am J Physiol Gastrointest Liver Physiol **315**(2): G272–G282.

Ingalls, A. M., M. M. Dickie and G. D. Snell (1950). "Obese, a new mutation in the house mouse." J Hered **41**(12): 317–318.

Iqbal, J. and M. M. Hussain (2009). "Intestinal lipid absorption." Am J Physiol Endocrinol Metab **296**(6): E1183–1194.

Ishibashi, S., M. S. Brown, J. L. Goldstein, R. D. Gerard, R. E. Hammer and J. Herz (1993). "Hypercholesterolemia in low density lipoprotein receptor knockout mice and its reversal by adenovirus-mediated gene delivery." J Clin Invest **92**(2): 883–893.

Ismail, S., I. Dubois-Vedrenne, M. Laval, I. G. Tikhonova, R. D'Angelo, C. Sanchez, P. Clerc, M. J. Gherardi, V. Gigoux, R. Magnan and D. Fourmy (2015). "Internalization and desensitization of the human glucose-dependent-insulinotropic receptor is affected by N-terminal acetylation of the agonist." Mol Cell Endocrinol **414**: 202–215.

Iwasaki, K., N. Harada, K. Sasaki, S. Yamane, K. Iida, K. Suzuki, A. Hamasaki, D. Nasteska, K. Shibue, E. Joo, T. Harada, T. Hashimoto, Y. Asakawa, A. Hirasawa and N. Inagaki (2015). "Free fatty acid receptor GPR120 is highly expressed in enteroendocrine K cells of the upper small intestine and has a critical role in GIP secretion after fat ingestion." Endocrinology **156**(3): 837–846.

Jaishy, B. and E. D. Abel (2016). "Lipids, lysosomes, and autophagy." J Lipid Res **57**(9): 1619–1635.

Jeppesen, P. B., B. Hartmann, J. Thulesen, B. S. Hansen, J. J. Holst, S. S. Poulsen and P. B. Mortensen (2000). "Elevated plasma glucagon-like peptide 1 and 2 concentrations in ileum resected short bowel patients with a preserved colon." Gut **47**(3): 370–376.

Jeppesen, P. B., E. L. Sanguinetti, A. Buchman, L. Howard, J. S. Scolapio, T. R. Ziegler, J. Gregory, K. A. Tappenden, J. Holst and P. B. Mortensen (2005). "Teduglutide (ALX-0600), a dipeptidyl peptidase IV resistant glucagon-like peptide 2 analogue, improves intestinal function in short bowel syndrome patients." Gut **54**(9): 1224–1231.

Jepsen, S. L., K. V. Grunddal, N. J. Wewer Albrechtsen, M. S. Engelstoft, M. B. N. Gabe, E. P. Jensen, C. Orskov, S. S. Poulsen, M. M. Rosenkilde, J. Pedersen, F. M. Gribble, F. Reimann, C. F. Deacon, T. W. Schwartz, A. D. Christ, R. E. Martin and J. J. Holst (2019). "Paracrine crosstalk between intestinal L- and D-cells controls secretion of glucagon-like peptide-1 in mice." Am J Physiol Endocrinol Metab **317**(6): E1081–E1093.

Julve, J., J. M. Martin-Campos, J. C. Escola-Gil and F. Blanco-Vaca (2016). "Chylomicrons: Advances in biology, pathology, laboratory testing, and therapeutics." Clin Chim Acta **455**: 134–148.

Karpe, F., A. S. Bickerton, L. Hodson, B. A. Fielding, G. D. Tan and K. N. Frayn (2007). "Removal of triacylglycerols from chylomicrons and VLDL by capillary beds: the basis of lipoprotein remnant formation." Biochem Soc Trans **35**(Pt 3): 472–476.

Kedees, M. H., Y. Guz, M. Grigoryan and G. Teitelman (2013). "Functional activity of murine intestinal mucosal cells is regulated by the glucagon-like peptide-1 receptor." Peptides **48**: 36–44.

Kelesidis, T., I. Kelesidis, S. Chou and C. S. Mantzoros (2010). "Narrative review: the role of leptin in human physiology: emerging clinical applications." Ann Intern Med **152**(2): 93–100.

Kiela, P. R. and F. K. Ghishan (2016). "Physiology of Intestinal Absorption and Secretion." Best Pract Res Clin Gastroenterol **30**(2): 145–159.

Kim, S. J., C. Nian and C. H. McIntosh (2007). "Activation of lipoprotein lipase by glucose-dependent insulinotropic polypeptide in adipocytes. A role for a protein kinase B, LKB1, and AMP-activated protein kinase cascade." J Biol Chem **282**(12): 8557–8567.

Kim, S. J., C. Nian and C. H. McIntosh (2007). "Resistin is a key mediator of glucose-dependent insulinotropic polypeptide (GIP) stimulation of lipoprotein lipase (LPL) activity in adipocytes." J Biol Chem **282**(47): 34139–34147.

Kim, S. J., C. Nian and C. H. McIntosh (2010). "GIP increases human adipocyte LPL expression through CREB and TORC2-mediated trans-activation of the LPL gene." J Lipid Res **51**(11): 3145–3157.

Kimball, C. and J. R. Murlin (1923). "Aqueous extracts of pancreas: III. Some precipitation reactions of insulin." Journal of Biological Chemistry **58**(1): 337–346.

Knudsen, L. B. and L. Pridal (1996). "Glucagon-like peptide-1-(9-36) amide is a major metabolite of glucagon-like peptide-1-(7-36) amide after in vivo administration to dogs, and it acts as an antagonist on the pancreatic receptor." Eur J Pharmacol **318**(2-3): 429–435.

Koehler, J. A., L. L. Baggio, B. Yusta, C. Longuet, K. J. Rowland, X. Cao, D. Holland, P. L. Brubaker and D. J. Drucker (2015). "GLP-1R agonists promote normal and neoplastic intestinal growth through mechanisms requiring Fgf7." Cell Metab **21**(3): 379–391.

Korbelius, M., N. Vujic, V. Sachdev, S. Obrowsky, S. Rainer, B. Gottschalk, W. F. Graier and D. Kratky (2019). "ATGL/CGI-58-Dependent Hydrolysis of a Lipid Storage Pool in Murine Enterocytes." Cell Rep **28**(7): 1923–1934 e1924.

Lankat-Buttgereit, B. and B. Goke (1997). "Cloning and characterization of the 5' flanking sequences (promoter region) of the human GLP-1 receptor gene." Peptides **18**(5): 617–624.

Laurencikiene, J., T. Skurk, A. Kulyte, P. Heden, G. Astrom, E. Sjolin, M. Ryden, H. Hauner and P. Arner (2011). "Regulation of lipolysis in small and large fat cells of the same subject." J Clin Endocrinol Metab **96**(12): E2045–2049.

Lauritsen, B., J. J. Holst and A. J. Moody (1981). "Depression of insulin release by anti-GIP serum after oral glucose in rats." Scand J Gastroenterol **16**(3): 417–420.

Lee, S. J., J. Lee, K. K. Li, D. Holland, H. Maughan, D. S. Guttman, B. Yusta and D. J. Drucker (2012). "Disruption of the murine Glp2r impairs Paneth cell function and increases susceptibility to small bowel enteritis." Endocrinology **153**(3): 1141–1151.

Lewis, G. F. and P. L. Brubaker (2021). "The discovery of insulin revisited: lessons for the modern era." J Clin Invest **131**(1).

Lewis, G. F., M. Naples, K. Uffelman, N. Leung, L. Szeto and K. Adeli (2004). "Intestinal lipoprotein production is stimulated by an acute elevation of plasma free fatty acids in the fasting state: studies in insulin-resistant and insulin-sensitized Syrian golden hamsters." Endocrinology **145**(11): 5006–5012.

Lewis, G. F., N. M. O'Meara, P. A. Soltys, J. D. Blackman, P. H. Iverius, A. F. Druetzler, G. S. Getz and K. S. Polonsky (1990). "Postprandial lipoprotein metabolism in normal and obese subjects: comparison after the vitamin A fat-loading test." J Clin Endocrinol Metab **71**(4): 1041–1050.

Li, D., C. N. Rodia, Z. K. Johnson, M. Bae, A. Muter, A. E. Heussinger, N. Tambini, A. M. Longo, H. Dong, J. Y. Lee and A. B. Kohan (2019). "Intestinal basolateral lipid substrate transport is linked to chylomicron secretion and is regulated by apoC-III." J Lipid Res **60**(9): 1503–1515.

Lopez, L. C., M. L. Frazier, C. J. Su, A. Kumar and G. F. Saunders (1983). "Mammalian pancreatic preproglucagon contains three glucagon-related peptides." Proc Natl Acad Sci U S A **80**(18): 5485–5489.

Lu, W. J., Q. Yang, W. Sun, S. C. Woods, D. D'Alessio and P. Tso (2007). "The regulation of the lymphatic secretion of glucagon-like peptide-1 (GLP-1) by intestinal absorption of fat and carbohydrate." Am J Physiol Gastrointest Liver Physiol **293**(5): G963–971.

Lu, W. J., Q. Yang, W. Sun, S. C. Woods, D. D'Alessio and P. Tso (2008). "Using the lymph fistula rat model to study the potentiation of GIP secretion by the ingestion of fat and glucose." Am J Physiol Gastrointest Liver Physiol **294**(5): G1130–1138.

Lu, W. J., Q. Yang, L. Yang, D. Lee, D. D'Alessio and P. Tso (2012). "Chylomicron formation and secretion is required for lipid-stimulated release of incretins GLP-1 and GIP." Lipids **47**(6): 571–580.

Lund, P. K., R. H. Goodman, P. C. Dee and J. F. Habener (1982). "Pancreatic preproglucagon cDNA contains two glucagon-related coding sequences arranged in tandem." Proc Natl Acad Sci U S A **79**(2): 345–349.

Lund, P. K., R. H. Goodman and J. F. Habener (1981). "Pancreatic pre-proglucagons are encoded by two separate mRNAs." J Biol Chem **256**(13): 6515–6518.

Lund, P. K., R. H. Goodman, M. R. Montminy, P. C. Dee and J. F. Habener (1983). "Anglerfish islet pre-proglucagon II. Nucleotide and corresponding amino acid sequence of the cDNA." J Biol Chem **258**(5): 3280–3284.

Lusis, A. J. (2000). "Atherosclerosis." Nature **407**(6801): 233–241.

Luttrell, L. M. and R. J. Lefkowitz (2002). "The role of beta-arrestins in the termination and transduction of G-protein-coupled receptor signals." J Cell Sci **115**(Pt 3): 455–465.

Malmstrom, R., C. J. Packard, T. D. Watson, S. Rannikko, M. Caslake, D. Bedford, P. Stewart, H. Yki-Jarvinen, J. Shepherd and M. R. Taskinen (1997). "Metabolic basis of hypotriglyceridemic effects of insulin in normal men." Arterioscler Thromb Vasc Biol **17**(7): 1454–1464.

Markovic, M. A. and P. L. Brubaker (2019). "The roles of glucagon-like peptide-2 and the intestinal epithelial insulin-like growth factor-1 receptor in regulating microvillus length." Sci Rep **9**(1): 13010.

Marzook, A., A. Tomas and B. Jones (2021). "The Interplay of Glucagon-Like Peptide-1 Receptor Trafficking and Signalling in Pancreatic Beta Cells." Front Endocrinol (Lausanne) **12**: 678055.

Mashek, D. G. (2021). "Hepatic lipid droplets: A balancing act between energy storage and metabolic dysfunction in NAFLD." Mol Metab **50**: 101115.

Matikainen, N., E. Bjornson, S. Soderlund, C. Boren, B. Eliasson, K. H. Pietilainen, L. H. Bogl, A. Hakkarainen, N. Lundbom, A. Rivellese, G. Riccardi, J. P. Despres, N. Almeras, J. J. Holst, C. F. Deacon, J. Boren and M. R. Taskinen (2016). "Minor Contribution of Endogenous GLP-1 and GLP-2 to Postprandial Lipemia in Obese Men." PLoS One **11**(1): e0145890.

Mayo, K. E., L. J. Miller, D. Bataille, S. Dalle, B. Goke, B. Thorens and D. J. Drucker (2003). "International Union of Pharmacology. XXXV. The glucagon receptor family." Pharmacol Rev **55**(1): 167–194.

McCullough, A. J., L. J. Miller, F. J. Service and V. L. Go (1983). "Effect of graded intraduodenal glucose infusions on the release and physiological action of gastric inhibitory polypeptide." J Clin Endocrinol Metab **56**(2): 234–241.

McIntyre, N., C. D. Holdsworth and D. S. Turner (1964). "New Interpretation of Oral Glucose Tolerance." Lancet **2**(7349): 20–21.

Meek, C. L., H. B. Lewis, K. Burling, F. Reimann and F. Gribble (2021). "Expected values for gastrointestinal and pancreatic hormone concentrations in healthy volunteers in the fasting and postprandial state." Ann Clin Biochem **58**(2): 108–116.

Meier, J. J., O. Goetze, J. Anstipp, D. Hagemann, J. J. Holst, W. E. Schmidt, B. Gallwitz and M. A. Nauck (2004). "Gastric inhibitory polypeptide does not inhibit gastric emptying in humans." Am J Physiol Endocrinol Metab **286**(4): E621–625.

Meier, J. J., M. A. Nauck, D. Kranz, J. J. Holst, C. F. Deacon, D. Gaeckler, W. E. Schmidt and B. Gallwitz (2004). "Secretion, degradation, and elimination of glucagon-like peptide 1 and gastric inhibitory polypeptide in patients with chronic renal insufficiency and healthy control subjects." Diabetes **53**(3): 654–662.

Merrill, N. J., W. S. Davidson, Y. He, I. Diaz Ludovico, S. Sarkar, M. R. Berger, J. E. McDermott, L. J. Van Eldik, D. M. Wilcock, M. E. Monroe, J. E. Kyle, K. D. Bruce, J. W. Heinecke, T. Vaisar, J. Raber, J. F. Quinn and J. T. Melchior (2023). "Human cerebrospinal fluid contains diverse lipoprotein subspecies enriched in proteins implicated in central nervous system health." Sci Adv **9**(35): eadi5571.

Miyawaki, K., Y. Yamada, H. Yano, H. Niwa, N. Ban, Y. Ihara, A. Kubota, S. Fujimoto, M. Kajikawa, A. Kuroe, K. Tsuda, H. Hashimoto, T. Yamashita, T. Jomori, F. Tashiro, J. Miyazaki and Y. Seino (1999). "Glucose intolerance caused by a defect in the entero-insular axis: a study in gastric inhibitory polypeptide receptor knockout mice." Proc Natl Acad Sci U S A **96**(26): 14843–14847.

Mojsov, S., G. Heinrich, I. B. Wilson, M. Ravazzola, L. Orci and J. F. Habener (1986). "Preproglucagon gene expression in pancreas and intestine diversifies at the level of post-translational processing." J Biol Chem **261**(25): 11880–11889.

Montague, C. T., I. S. Farooqi, J. P. Whitehead, M. A. Soos, H. Rau, N. J. Wareham, C. P. Sewter, J. E. Digby, S. N. Mohammed, J. A. Hurst, C. H. Cheetham, A. R. Earley, A. H. Barnett, J. B. Prins and S. O'Rahilly (1997). "Congenital leptin deficiency is associated with severe early-onset obesity in humans." Nature **387**(6636): 903–908.

Moody, A. J., J. Markussen, A. S. Fries, C. Steenstrup and F. Sundby (1970). "The insulin releasing activites of extracts of pork intestine." Diabetologia **6**(2): 135–140.

Moore, B. (1906). "On the treatment of Diabetus mellitus by acid extract of Duodenal Mucous Membrane." Biochem J **1**(1): 28–38.

Morigny, P., J. Boucher, P. Arner and D. Langin (2021). "Lipid and glucose metabolism in white adipocytes: pathways, dysfunction and therapeutics." Nat Rev Endocrinol **17**(5): 276–295.

Moriya, R., T. Shirakura, J. Ito, S. Mashiko and T. Seo (2009). "Activation of sodium-glucose cotransporter 1 ameliorates hyperglycemia by mediating incretin secretion in mice." Am J Physiol Endocrinol Metab **297**(6): E1358–1365.

Mukherjee, K., R. Wang and C. Xiao (2024). "Release of Lipids Stored in the Intestine by Glucagon-Like Peptide-2 Involves a Gut-Brain Neural Pathway." Arterioscler Thromb Vasc Biol **44**(1): 192–201.

Muller, T. D., A. Adriaenssens, B. Ahren, M. Bluher, A. L. Birkenfeld, J. E. Campbell, M. P. Coghlan, D. D'Alessio, C. F. Deacon, S. DelPrato, J. D. Douros, D. J. Drucker, N. S. Figueredo Burgos, P. R. Flatt, B. Finan, R. E. Gimeno, F. M. Gribble, M. R. Hayes, C. Holscher, J. J. Holst, P. J. Knerr, F. K. Knop, C. M. Kusminski, A. Liskiewicz, G. Mabilleau, S. A. Mowery, M. A. Nauck, A. Novikoff, F. Reimann, A. G. Roberts, M. M. Rosenkilde, R. J. Samms, P. E. Scherer, R. J. Seeley, K. W. Sloop, C. Wolfrum, D. Wootten, R. D. DiMarchi and M. H. Tschop (2025). "Glucose-dependent insulinotropic polypeptide (GIP)." Mol Metab **95**: 102118.

Muller, T. D., B. Finan, S. R. Bloom, D. D'Alessio, D. J. Drucker, P. R. Flatt, A. Fritsche, F. Gribble, H. J. Grill, J. F. Habener, J. J. Holst, W. Langhans, J. J. Meier, M. A. Nauck, D. Perez-Tilve, A. Pocai, F. Reimann, D. A. Sandoval, T. W. Schwartz, R. J. Seeley, K. Stemmer, M. Tang-Christensen, S. C. Woods, R. D. DiMarchi and M. H. Tschop (2019). "Glucagon-like peptide 1 (GLP-1)." Mol Metab **30**: 72–130.

Mulvihill, E. E. (2018). "Regulation of intestinal lipid and lipoprotein metabolism by the proglucagon-derived peptides glucagon like peptide 1 and glucagon like peptide 2." Curr Opin Lipidol **29**(2): 95–103.

Mulvihill, E. E., J. M. Assini, J. K. Lee, E. M. Allister, B. G. Sutherland, J. B. Koppes, C. G. Sawyez, J. Y. Edwards, D. E. Telford, A. Charbonneau, P. St-Pierre, A. Marette and M. W. Huff (2011). "Nobiletin attenuates VLDL overproduction, dyslipidemia, and atherosclerosis in mice with diet-induced insulin resistance." Diabetes **60**(5): 1446–1457.

Mulvihill, E. E., A. C. Burke and M. W. Huff (2016). "Citrus Flavonoids as Regulators of Lipoprotein Metabolism and Atherosclerosis." Annu Rev Nutr **36**: 275–299.

Munroe, D. G., A. K. Gupta, F. Kooshesh, T. B. Vyas, G. Rizkalla, H. Wang, L. Demchyshyn, Z. J. Yang, R. K. Kamboj, H. Chen, K. McCallum, M. Sumner-Smith, D. J. Drucker and A. Crivici (1999). "Prototypic G protein-coupled receptor for the intestinotrophic factor glucagon-like peptide 2." Proc Natl Acad Sci U S A **96**(4): 1569–1573.

Murphy, R. F., D. T. Elmore and K. D. Buchanan (1971). "Isolation of glucagon-like immunoreactivity of gut by affinity chromatography." Biochem J **125**(3): 61P–62P.

Nakajima, T., M. Horiuchi, H. Yamanaka, Z. Kizaki, F. Inoue, N. Kodo, A. Kinugasa, T. Saheki and T. Sawada (1997). "The effect of carnitine on ketogenesis in perfused livers from juvenile visceral steatosis mice with systemic carnitine deficiency." Pediatr Res **42**(1): 108–113.

Nauck, M. A., N. Kleine, C. Orskov, J. J. Holst, B. Willms and W. Creutzfeldt (1993). "Normalization of fasting hyperglycaemia by exogenous glucagon-like peptide 1 (7-36 amide) in type 2 (non-insulin-dependent) diabetic patients." Diabetologia **36**(8): 741–744.

Nelson, D. W., S. G. Murali, X. Liu, M. C. Koopmann, J. J. Holst and D. M. Ney (2008). "Insulin-like growth factor I and glucagon-like peptide-2 responses to fasting followed by controlled or ad libitum refeeding in rats." Am J Physiol Regul Integr Comp Physiol **294**(4): R1175–1184.

Nelson, D. W., J. W. Sharp, M. S. Brownfield, H. E. Raybould and D. M. Ney (2007). "Localization and activation of glucagon-like peptide-2 receptors on vagal afferents in the rat." Endocrinology **148**(5): 1954–1962.

Nguyen, P., V. Leray, M. Diez, S. Serisier, J. Le Bloc'h, B. Siliart and H. Dumon (2008). "Liver lipid metabolism." J Anim Physiol Anim Nutr (Berl) **92**(3): 272–283.

Nielsen, S. and F. Karpe (2012). "Determinants of VLDL-triglycerides production." Curr Opin Lipidol **23**(4): 321–326.

Ogata, H., Y. Seino, N. Harada, A. Iida, K. Suzuki, T. Izumoto, K. Ishikawa, E. Uenishi, N. Ozaki, Y. Hayashi, T. Miki, N. Inagaki, S. Tsunekawa, Y. Hamada, S. Seino and Y. Oiso (2014). "KATP channel as well as SGLT1 participates in GIP secretion in the diabetic state." J Endocrinol **222**(2): 191–200.

Orskov, C., M. Bersani, A. H. Johnsen, P. Hojrup and J. J. Holst (1989). "Complete sequences of glucagon-like peptide-1 from human and pig small intestine." J Biol Chem **264**(22): 12826–12829.

Orskov, C., T. Buhl, L. Rabenhoj, H. Kofod and J. J. Holst (1989). "Carboxypeptidase-B-like processing of the C-terminus of glucagon-like peptide-2 in pig and human small intestine." FEBS Lett **247**(2): 193–196.

Orskov, C., B. Hartmann, S. S. Poulsen, J. Thulesen, K. J. Hare and J. J. Holst (2005). "GLP-2 stimulates colonic growth via KGF, released by subepithelial myofibroblasts with GLP-2 receptors." Regul Pept **124**(1-3): 105–112.

Orskov, C., J. J. Holst, S. Knuhtsen, F. G. Baldissera, S. S. Poulsen and O. V. Nielsen (1986). "Glucagon-like peptides GLP-1 and GLP-2, predicted products of the glucagon gene, are secreted separately from pig small intestine but not pancreas." Endocrinology **119**(4): 1467–1475.

Orskov, C., J. J. Holst and O. V. Nielsen (1988). "Effect of truncated glucagon-like peptide-1 [proglucagon-(78-107) amide] on endocrine secretion from pig pancreas, antrum, and nonantral stomach." Endocrinology **123**(4): 2009–2013.

Osborne, J. C., Jr., G. Bengtsson-Olivecrona, N. S. Lee and T. Olivecrona (1985). "Studies on inactivation of lipoprotein lipase: role of the dimer to monomer dissociation." Biochemistry **24**(20): 5606–5611.

Ottaway, N., P. Mahbod, B. Rivero, L. A. Norman, A. Gertler, D. A. D'Alessio and D. Perez-Tilve (2015). "Diet-induced obese mice retain endogenous leptin action." Cell Metab **21**(6): 877–882.

Pamir, N., F. C. Lynn, A. M. Buchan, J. Ehses, S. A. Hinke, J. A. Pospisilik, K. Miyawaki, Y. Yamada, Y. Seino, C. H. McIntosh and R. A. Pederson (2003). "Glucose-dependent insulinotropic polypeptide receptor null mice exhibit compensatory changes in the enteroinsular axis." Am J Physiol Endocrinol Metab **284**(5): E931–939.

Pan, X. and M. M. Hussain (2012). "Gut triglyceride production." Biochim Biophys Acta **1821**(5): 727–735.

Paternoster, S. and M. Falasca (2018). "Dissecting the Physiology and Pathophysiology of Glucagon-Like Peptide-1." Front Endocrinol (Lausanne) **9**: 584.

Patsch, J. R., G. Miesenbock, T. Hopferwieser, V. Muhlberger, E. Knapp, J. K. Dunn, A. M. Gotto, Jr. and W. Patsch (1992). "Relation of triglyceride metabolism and coronary artery disease. Studies in the postprandial state." Arterioscler Thromb **12**(11): 1336–1345.

Pavlic, M., C. Xiao, L. Szeto, B. W. Patterson and G. F. Lewis (2010). "Insulin acutely inhibits intestinal lipoprotein secretion in humans in part by suppressing plasma free fatty acids." Diabetes **59**(3): 580–587.

Pedersen, J., N. B. Pedersen, S. W. Brix, K. V. Grunddal, M. M. Rosenkilde, B. Hartmann, C. Orskov, S. S. Poulsen and J. J. Holst (2015). "The glucagon-like peptide 2 receptor is expressed in enteric neurons and not in the epithelium of the intestine." Peptides **67**: 20–28.

Pedersen, J., R. K. Ugleholdt, S. M. Jorgensen, J. A. Windelov, K. V. Grunddal, T. W. Schwartz, E. M. Fuchtbauer, S. S. Poulsen, P. J. Holst and J. J. Holst (2013). "Glucose metabolism is altered after loss of L cells and alpha-cells but not influenced by loss of K cells." Am J Physiol Endocrinol Metab **304**(1): E60–73.

Pederson, R. A., H. E. Schubert and J. C. Brown (1975). "Gastric inhibitory polypeptide. Its physiologic release and insulinotropic action in the dog." Diabetes **24**(12): 1050–1056.

Phan, B. A., T. D. Dayspring and P. P. Toth (2012). "Ezetimibe therapy: mechanism of action and clinical update." Vasc Health Risk Manag **8**: 415–427.

Pi-Sunyer, X., A. Astrup, K. Fujioka, F. Greenway, A. Halpern, M. Krempf, D. C. Lau, C. W. le Roux, R. Violante Ortiz, C. B. Jensen, J. P. Wilding, S. Obesity and N. N. S. G. Prediabetes (2015). "A Randomized, Controlled Trial of 3.0 mg of Liraglutide in Weight Management." N Engl J Med **373**(1): 11–22.

Powell, L. M., S. C. Wallis, R. J. Pease, Y. H. Edwards, T. J. Knott and J. Scott (1987). "A novel form of tissue-specific RNA processing produces apolipoprotein-B48 in intestine." Cell **50**(6): 831–840.

Psichas, A., P. F. Larraufie, D. A. Goldspink, F. M. Gribble and F. Reimann (2017). "Chylomicrons stimulate incretin secretion in mouse and human cells." Diabetologia **60**(12): 2475–2485.

Puchalska, P. and P. A. Crawford (2017). "Multi-dimensional Roles of Ketone Bodies in Fuel Metabolism, Signaling, and Therapeutics." Cell Metab **25**(2): 262–284.

Pujadas, G., E. M. Varin, L. L. Baggio, E. E. Mulvihill, K. W. A. Bang, J. A. Koehler, D. Matthews and D. J. Drucker (2020). "The gut hormone receptor GIPR links energy availability to the control of hematopoiesis." Mol Metab **39**: 101008.

Pyke, C., R. S. Heller, R. K. Kirk, C. Orskov, S. Reedtz-Runge, P. Kaastrup, A. Hvelplund, L. Bardram, D. Calatayud and L. B. Knudsen (2014). "GLP-1 receptor localization in monkey and human tissue: novel distribution revealed with extensively validated monoclonal antibody." Endocrinology **155**(4): 1280–1290.

Rader, D. J. (2006). "Molecular regulation of HDL metabolism and function: implications for novel therapies." J Clin Invest **116**(12): 3090–3100.

Ran, Q., Q. Gan, Y. Zhu, L. Song, L. Shen, X. Duan, X. Zhu and W. Huang (2024). "Mechanism insights into the pleiotropic effects of nobiletin as a potential therapeutic agent on non-alcoholic fatty liver disease (NAFLD)." Biomed Pharmacother **173**: 116322.

Raufman, J. P., L. Singh, G. Singh and J. Eng (1992). "Truncated glucagon-like peptide-1 interacts with exendin receptors on dispersed acini from guinea pig pancreas. Identification of a mammalian analogue of the reptilian peptide exendin-4." J Biol Chem **267**(30): 21432–21437.

Reimann, F., A. M. Habib, G. Tolhurst, H. E. Parker, G. J. Rogers and F. M. Gribble (2008). "Glucose sensing in L cells: a primary cell study." Cell Metab **8**(6): 532–539.

Ribeiro-Parenti, L., A. C. Jarry, J. B. Cavin, A. Willemetz, J. Le Beyec, A. Sannier, S. Benadda, A. L. Pelletier, M. Hourseau, T. Leger, B. Morlet, A. Couvelard, Y. Anini, S. Msika, J. P. Marmuse, S. Ledoux, M. Le Gall and A. Bado (2021). "Bariatric surgery induces a new gastric mucosa phenotype with increased functional glucagon-like peptide-1 expressing cells." Nat Commun **12**(1): 110.

Richard Lehner, A. D. Q. (2016). Fatty Acid Handling in Mammalian Cells. Biochemistry of Lipids, Lipoproteins and Membranes (Sixth Edition). R. S. M. Neale D. Ridgway, Elsevier**:** 149–184.

Richards, P., H. E. Parker, A. E. Adriaenssens, J. M. Hodgson, S. C. Cork, S. Trapp, F. M. Gribble and F. Reimann (2014). "Identification and characterization of GLP-1 receptor-expressing cells using a new transgenic mouse model." Diabetes **63**(4): 1224–1233.

Roberge, J. N. and P. L. Brubaker (1993). "Regulation of intestinal proglucagon-derived peptide secretion by glucose-dependent insulinotropic peptide in a novel enteroendocrine loop." Endocrinology **133**(1): 233–240.

Roberge, J. N., K. A. Gronau and P. L. Brubaker (1996). "Gastrin-releasing peptide is a novel mediator of proximal nutrient-induced proglucagon-derived peptide secretion from the distal gut." Endocrinology **137**(6): 2383–2388.

Robertson, M. D., M. Parkes, B. F. Warren, D. J. Ferguson, K. G. Jackson, D. P. Jewell and K. N. Frayn (2003). "Mobilisation of enterocyte fat stores by oral glucose in humans." Gut **52**(6): 834–839.

Rocca, A. S. and P. L. Brubaker (1999). "Role of the vagus nerve in mediating proximal nutrient-induced glucagon-like peptide-1 secretion." Endocrinology **140**(4): 1687–1694.

Rosen, E. D. and B. M. Spiegelman (2014). "What we talk about when we talk about fat." Cell **156**(1-2): 20–44.

Rowland, K. J., S. Trivedi, D. Lee, K. Wan, R. N. Kulkarni, M. Holzenberger and P. L. Brubaker (2011). "Loss of glucagon-like peptide-2-induced proliferation following intestinal epithelial insulin-like growth factor-1-receptor deletion." Gastroenterology **141**(6): 2166–2175 e2167.

Ruppert, P. M. M. and S. Kersten (2024). "Mechanisms of hepatic fatty acid oxidation and ketogenesis during fasting." Trends Endocrinol Metab **35**(2): 107–124.

Sanders, F. W. and J. L. Griffin (2016). "De novo lipogenesis in the liver in health and disease: more than just a shunting yard for glucose." Biol Rev Camb Philos Soc **91**(2): 452–468.

Santer, R., R. Schneppenheim, A. Dombrowski, H. Gotze, B. Steinmann and J. Schaub (1997). "Mutations in GLUT2, the gene for the liver-type glucose transporter, in patients with Fanconi-Bickel syndrome." Nat Genet **17**(3): 324–326.

Santoro, A., T. E. McGraw and B. B. Kahn (2021). "Insulin action in adipocytes, adipose remodeling, and systemic effects." Cell Metab **33**(4): 748–757.

Sato, S., R. Hokari, C. Kurihara, H. Sato, K. Narimatsu, H. Hozumi, T. Ueda, M. Higashiyama, Y. Okada, C. Watanabe, S. Komoto, K. Tomita, A. Kawaguchi, S. Nagao and S. Miura (2013). "Dietary lipids and sweeteners regulate glucagon-like peptide-2 secretion." Am J Physiol Gastrointest Liver Physiol **304**(8): G708–714.

Scheja, L. and J. Heeren (2019). "The endocrine function of adipose tissues in health and cardiometabolic disease." Nat Rev Endocrinol **15**(9): 507–524.

Schonfeld, P. and L. Wojtczak (2016). "Short- and medium-chain fatty acids in energy metabolism: the cellular perspective." J Lipid Res **57**(6): 943–954.

Schulthess, G., G. Lipka, S. Compassi, D. Boffelli, F. E. Weber, F. Paltauf and H. Hauser (1994). "Absorption of monoacylglycerols by small intestinal brush border membrane." Biochemistry **33**(15): 4500–4508.

Schulze, R. J., M. B. Schott, C. A. Casey, P. L. Tuma and M. A. McNiven (2019). "The cell biology of the hepatocyte: A membrane trafficking machine." J Cell Biol **218**(7): 2096–2112.

Schwartz, E. A., J. Koska, M. P. Mullin, I. Syoufi, D. C. Schwenke and P. D. Reaven (2010). "Exenatide suppresses postprandial elevations in lipids and lipoproteins in individuals with

impaired glucose tolerance and recent onset type 2 diabetes mellitus." Atherosclerosis **212**(1): 217–222.

Schwartz, M. W., R. J. Seeley, L. M. Zeltser, A. Drewnowski, E. Ravussin, L. M. Redman and R. L. Leibel (2017). "Obesity Pathogenesis: An Endocrine Society Scientific Statement." Endocr Rev **38**(4): 267–296.

Schwartz, S. L., R. E. Ratner, D. D. Kim, Y. Qu, L. L. Fechner, S. M. Lenox and J. H. Holcombe (2008). "Effect of exenatide on 24-hour blood glucose profile compared with placebo in patients with type 2 diabetes: a randomized, double-blind, two-arm, parallel-group, placebo-controlled, 2-week study." Clin Ther **30**(5): 858–867.

Scott Kiss, R. and A. Sniderman (2017). "Shunts, channels and lipoprotein endosomal traffic: a new model of cholesterol homeostasis in the hepatocyte." J Biomed Res **31**(2): 95–107.

Scrocchi, L. A., T. J. Brown, N. MaClusky, P. L. Brubaker, A. B. Auerbach, A. L. Joyner and D. J. Drucker (1996). "Glucose intolerance but normal satiety in mice with a null mutation in the glucagon-like peptide 1 receptor gene." Nat Med **2**(11): 1254–1258.

Shibue, K., S. Yamane, N. Harada, A. Hamasaki, K. Suzuki, E. Joo, K. Iwasaki, D. Nasteska, T. Harada, Y. Hayashi, Y. Adachi, Y. Owada, R. Takayanagi and N. Inagaki (2015). "Fatty acid-binding protein 5 regulates diet-induced obesity via GIP secretion from enteroendocrine K cells in response to fat ingestion." Am J Physiol Endocrinol Metab **308**(7): E583–591.

Shin, E. D., J. L. Estall, A. Izzo, D. J. Drucker and P. L. Brubaker (2005). "Mucosal adaptation to enteral nutrients is dependent on the physiologic actions of glucagon-like peptide-2 in mice." Gastroenterology **128**(5): 1340–1353.

Skurk, T., C. Alberti-Huber, C. Herder and H. Hauner (2007). "Relationship between adipocyte size and adipokine expression and secretion." J Clin Endocrinol Metab **92**(3): 1023–1033.

Spector, A. A. and H. Y. Kim (2015). "Discovery of essential fatty acids." J Lipid Res **56**(1): 11–21.

Spreckley, E. and K. G. Murphy (2015). "The L-Cell in Nutritional Sensing and the Regulation of Appetite." Front Nutr **2**: 23.

Stahel, P., C. Xiao, X. Davis, P. Tso and G. F. Lewis (2019). "Glucose and GLP-2 (Glucagon-Like Peptide-2) Mobilize Intestinal Triglyceride by Distinct Mechanisms." Arterioscler Thromb Vasc Biol **39**(8): 1565–1573.

Stoffel, M., R. Espinosa, 3rd, M. M. Le Beau and G. I. Bell (1993). "Human glucagon-like peptide-1 receptor gene. Localization to chromosome band 6p21 by fluorescence in situ hybridization and linkage of a highly polymorphic simple tandem repeat DNA polymorphism to other markers on chromosome 6." Diabetes **42**(8): 1215–1218.

Stone, S. J., H. M. Myers, S. M. Watkins, B. E. Brown, K. R. Feingold, P. M. Elias and R. V. Farese, Jr. (2004). "Lipopenia and skin barrier abnormalities in DGAT2-deficient mice." J Biol Chem **279**(12): 11767–11776.

Storch, J., Y. X. Zhou and W. S. Lagakos (2008). "Metabolism of apical versus basolateral sn-2-monoacylglycerol and fatty acids in rodent small intestine." J Lipid Res **49**(8): 1762–1769.

Stumpel, F., R. Burcelin, K. Jungermann and B. Thorens (2001). "Normal kinetics of intestinal glucose absorption in the absence of GLUT2: evidence for a transport pathway requiring

glucose phosphorylation and transfer into the endoplasmic reticulum." Proc Natl Acad Sci U S A **98**(20): 11330–11335.

Sukonina, V., A. Lookene, T. Olivecrona and G. Olivecrona (2006). "Angiopoietin-like protein 4 converts lipoprotein lipase to inactive monomers and modulates lipase activity in adipose tissue." Proc Natl Acad Sci U S A **103**(46): 17450–17455.

Suzuki, K., N. Harada, S. Yamane, Y. Nakamura, K. Sasaki, D. Nasteska, E. Joo, K. Shibue, T. Harada, A. Hamasaki, K. Toyoda, K. Nagashima and N. Inagaki (2013). "Transcriptional regulatory factor X6 (Rfx6) increases gastric inhibitory polypeptide (GIP) expression in enteroendocrine K-cells and is involved in GIP hypersecretion in high fat diet-induced obesity." J Biol Chem **288**(3): 1929–1938.

Sykes, S., L. M. Morgan, J. English and V. Marks (1980). "Evidence for preferential stimulation of gastric inhibitory polypeptide secretion in the rat by actively transported carbohydrates and their analogues." J Endocrinol **85**(2): 201–207.

Szalowska, E., K. Meijer, N. Kloosterhuis, F. Razaee, M. Priebe and R. J. Vonk (2011). "Sub-chronic administration of stable GIP analog in mice decreases serum LPL activity and body weight." Peptides **32**(5): 938–945.

Takeda, J., Y. Seino, K. Tanaka, H. Fukumoto, T. Kayano, H. Takahashi, T. Mitani, M. Kurono, T. Suzuki, T. Tobe and et al. (1987). "Sequence of an intestinal cDNA encoding human gastric inhibitory polypeptide precursor." Proc Natl Acad Sci U S A **84**(20): 7005–7008.

Tartaglia, L. A., M. Dembski, X. Weng, N. Deng, J. Culpepper, R. Devos, G. J. Richards, L. A. Campfield, F. T. Clark, J. Deeds, C. Muir, S. Sanker, A. Moriarty, K. J. Moore, J. S. Smutko, G. G. Mays, E. A. Wool, C. A. Monroe and R. I. Tepper (1995). "Identification and expression cloning of a leptin receptor, OB-R." Cell **83**(7): 1263–1271.

Thorens, B., M. T. Guillam, F. Beermann, R. Burcelin and M. Jaquet (2000). "Transgenic reexpression of GLUT1 or GLUT2 in pancreatic beta cells rescues GLUT2-null mice from early death and restores normal glucose-stimulated insulin secretion." J Biol Chem **275**(31): 23751–23758.

Tkac, I., B. P. Kimball, G. Lewis, K. Uffelman and G. Steiner (1997). "The severity of coronary atherosclerosis in type 2 diabetes mellitus is related to the number of circulating triglyceride-rich lipoprotein particles." Arterioscler Thromb Vasc Biol **17**(12): 3633–3638.

Toth, P. P. (2016). "Triglyceride-rich lipoproteins as a causal factor for cardiovascular disease." Vasc Health Risk Manag **12**: 171–183.

Trzaskalski, N. A., B. Vulesevic, M. A. Nguyen, N. Jeraj, E. Fadzeyeva, N. M. Morrow, C. A. Locatelli, N. Travis, A. A. Hanson, J. R. Nunes, C. O'Dwyer, J. N. van der Veen, I. Lorenzen-Schmidt, R. Seymour, S. M. Pulente, A. C. Clement, A. M. Crawley, R. L. Jacobs, M. A. Doyle, C. L. Cooper, K. H. Kim, M. D. Fullerton and E. E. Mulvihill (2023). "Hepatocyte-derived DPP4 regulates portal GLP-1 bioactivity, modulates glucose production, and when absent influences NAFLD progression." JCI Insight **8**(2).

Tseng, C. C., L. A. Jarboe, S. B. Landau, E. K. Williams and M. M. Wolfe (1993). "Glucose-dependent insulinotropic peptide: structure of the precursor and tissue-specific expression in rat." Proc Natl Acad Sci U S A **90**(5): 1992–1996.

Tsujita, M., J. T. Melchior and S. Yokoyama (2024). "Lipoprotein Particles in Cerebrospinal Fluid." Arterioscler Thromb Vasc Biol **44**(5): 1042–1052.

Turner, J. R. (2009). "Intestinal mucosal barrier function in health and disease." Nat Rev Immunol **9**(11): 799–809.

Uchida, A., M. C. Whitsitt, T. Eustaquio, M. N. Slipchenko, J. F. Leary, J. X. Cheng and K. K. Buhman (2012). "Reduced triglyceride secretion in response to an acute dietary fat challenge in obese compared to lean mice." Front Physiol **3**: 26.

Ugleholdt, R., M. L. Poulsen, P. J. Holst, J. C. Irminger, C. Orskov, J. Pedersen, M. M. Rosenkilde, X. Zhu, D. F. Steiner and J. J. Holst (2006). "Prohormone convertase 1/3 is essential for processing of the glucose-dependent insulinotropic polypeptide precursor." J Biol Chem **281**(16): 11050–11057.

Unger, R. H., A. M. Eisentraut, C. M. Mc, S. Keller, H. C. Lanz and L. L. Madison (1959). "Glucagon antibodies and their use for immunoassay for glucagon." Proc Soc Exp Biol Med **102**: 621–623.

Unger, R. H., H. Ketterer and A. M. Eisentraut (1966). "Distribution of immunoassayable glucagon in gastrointestinal tissues." Metabolism **15**(10): 865–867.

Unger, R. H., A. Ohneda, I. Valverde, A. M. Eisentraut and J. Exton (1968). "Characterization of the responses of circulating glucagon-like immunoreactivity to intraduodenal and intravenous administration of glucose." J Clin Invest **47**(1): 48–65.

Usdin, T. B., E. Mezey, D. C. Button, M. J. Brownstein and T. I. Bonner (1993). "Gastric inhibitory polypeptide receptor, a member of the secretin-vasoactive intestinal peptide receptor family, is widely distributed in peripheral organs and the brain." Endocrinology **133**(6): 2861–2870.

Vahl, T. P., M. Tauchi, T. S. Durler, E. E. Elfers, T. M. Fernandes, R. D. Bitner, K. S. Ellis, S. C. Woods, R. J. Seeley, J. P. Herman and D. A. D'Alessio (2007). "Glucagon-like peptide-1 (GLP-1) receptors expressed on nerve terminals in the portal vein mediate the effects of endogenous GLP-1 on glucose tolerance in rats." Endocrinology **148**(10): 4965–4973.

van Zwol, W., B. van de Sluis, H. N. Ginsberg and J. A. Kuivenhoven (2024). "VLDL Biogenesis and Secretion: It Takes a Village." Circ Res **134**(2): 226–244.

Varin, E. M., A. A. Hanson, J. L. Beaudry, M. A. Nguyen, X. Cao, L. L. Baggio, E. E. Mulvihill and D. J. Drucker (2020). "Hematopoietic cell- versus enterocyte-derived dipeptidyl peptidase-4 differentially regulates triglyceride excursion in mice." JCI Insight **5**(16).

Varin, E. M., E. E. Mulvihill, L. L. Baggio, J. A. Koehler, X. Cao, R. J. Seeley and D. J. Drucker (2019). "Distinct Neural Sites of GLP-1R Expression Mediate Physiological versus Pharmacological Control of Incretin Action." Cell Rep **27**(11): 3371–3384 e3373.

Veilleux, A., E. Grenier, P. Marceau, A. C. Carpentier, D. Richard and E. Levy (2014). "Intestinal lipid handling: evidence and implication of insulin signaling abnormalities in human obese subjects." Arterioscler Thromb Vasc Biol **34**(3): 644–653.

Vuylsteke, C. A., G. Cornelis and C. De Duve (1952). "Influence du traitement au cobalt sur le contenu en facteur HG du pancreas de Cobaye." Archives Internationales de Physiologie **60**(1): 128–131.

Walsh, N. A., B. Yusta, M. P. DaCambra, Y. Anini, D. J. Drucker and P. L. Brubaker (2003). "Glucagon-like peptide-2 receptor activation in the rat intestinal mucosa." Endocrinology **144**(10): 4385–4392.

Wang, R., M. S. A. Khan, K. Mukherjee, M. Ghanem and C. Xiao (2025). "Glucose-dependent insulinotropic polypeptide stimulates post-absorptive lipid secretion in the intestine." Front Physiol **16**: 1549392.

Wang, Y., X. J. Liu, J. B. Chen, J. P. Cao, X. Li and C. D. Sun (2022). "Citrus flavonoids and their antioxidant evaluation." Crit Rev Food Sci Nutr **62**(14): 3833–3854.

Westman, E. C., W. S. Yancy, Jr. and M. Humphreys (2006). "Dietary treatment of diabetes mellitus in the pre-insulin era (1914-1922)." Perspect Biol Med **49**(1): 77–83.

Wewer Albrechtsen, N. J., J. J. Holst, A. D. Cherrington, B. Finan, L. L. Gluud, E. D. Dean, J. E. Campbell, S. R. Bloom, T. M. Tan, F. K. Knop and T. D. Muller (2023). "100 years of glucagon and 100 more." Diabetologia **66**(8): 1378–1394.

Wilding, J. P. H., R. L. Batterham, S. Calanna, M. Davies, L. F. Van Gaal, I. Lingvay, B. M. McGowan, J. Rosenstock, M. T. D. Tran, T. A. Wadden, S. Wharton, K. Yokote, N. Zeuthen, R. F. Kushner and S. S. Group (2021). "Once-Weekly Semaglutide in Adults with Overweight or Obesity." N Engl J Med **384**(11): 989–1002.

Wismann, P., P. Barkholt, T. Secher, N. Vrang, H. B. Hansen, P. B. Jeppesen, L. L. Baggio, J. A. Koehler, D. J. Drucker, D. A. Sandoval and J. Jelsing (2017). "The endogenous preproglucagon system is not essential for gut growth homeostasis in mice." Mol Metab **6**(7): 681–692.

Wu, L. and K. G. Parhofer (2014). "Diabetic dyslipidemia." Metabolism **63**(12): 1469–1479.

Xiao, C., R. H. Bandsma, S. Dash, L. Szeto and G. F. Lewis (2012). "Exenatide, a glucagon-like peptide-1 receptor agonist, acutely inhibits intestinal lipoprotein production in healthy humans." Arterioscler Thromb Vasc Biol **32**(6): 1513–1519.

Xiao, C., P. Stahel, A. L. Carreiro, Y. H. Hung, S. Dash, I. Bookman, K. K. Buhman and G. F. Lewis (2019). "Oral Glucose Mobilizes Triglyceride Stores From the Human Intestine." Cell Mol Gastroenterol Hepatol **7**(2): 313–337.

Yahagi, K., F. D. Kolodgie, C. Lutter, H. Mori, M. E. Romero, A. V. Finn and R. Virmani (2017). "Pathology of Human Coronary and Carotid Artery Atherosclerosis and Vascular Calcification in Diabetes Mellitus." Arterioscler Thromb Vasc Biol **37**(2): 191–204.

Yamada, Y., T. Hayami, K. Nakamura, P. J. Kaisaki, Y. Someya, C. Z. Wang, S. Seino and Y. Seino (1995). "Human gastric inhibitory polypeptide receptor: cloning of the gene (GIPR) and cDNA." Genomics **29**(3): 773–776.

Yamane, S., N. Harada, A. Hamasaki, A. Muraoka, E. Joo, K. Suzuki, D. Nasteska, D. Tanaka, M. Ogura, S. Harashima and N. Inagaki (2012). "Effects of glucose and meal ingestion on incretin secretion in Japanese subjects with normal glucose tolerance." J Diabetes Investig **3**(1): 80–85.

Yasuda, T., Y. Yoshimura, H. Yabuki, T. Nakazawa, K. Ohsawa, Y. Mimaki and Y. Sashida (2003). "Urinary metabolites of nobiletin orally administered to rats." Chem Pharm Bull (Tokyo) **51**(12): 1426–1428.

Yoon, H., J. L. Shaw, M. C. Haigis and A. Greka (2021). "Lipid metabolism in sickness and in health: Emerging regulators of lipotoxicity." Mol Cell **81**(18): 3708–3730.

Yusta, B., L. L. Baggio, J. Koehler, D. Holland, X. Cao, L. J. Pinnell, K. C. Johnson-Henry, W. Yeung, M. G. Surette, K. W. Bang, P. M. Sherman and D. J. Drucker (2015). "GLP-1R Agonists

Modulate Enteric Immune Responses Through the Intestinal Intraepithelial Lymphocyte GLP-1R." Diabetes **64**(7): 2537–2549.

Yusta, B., R. P. Boushey and D. J. Drucker (2000). "The glucagon-like peptide-2 receptor mediates direct inhibition of cellular apoptosis via a cAMP-dependent protein kinase-independent pathway." J Biol Chem **275**(45): 35345–35352.

Yusta, B., D. Matthews, J. A. Koehler, G. Pujadas, K. D. Kaur and D. J. Drucker (2019). "Localization of Glucagon-Like Peptide-2 Receptor Expression in the Mouse." Endocrinology **160**(8): 1950–1963.

Zeigerer, A., R. Sekar, M. Kleinert, S. Nason, K. M. Habegger and T. D. Muller (2021). "Glucagon's Metabolic Action in Health and Disease." Compr Physiol **11**(2): 1759–1783.

Zhang, Y., R. Proenca, M. Maffei, M. Barone, L. Leopold and J. M. Friedman (1994). "Positional cloning of the mouse obese gene and its human homologue." Nature **372**(6505): 425–432.

Zhou, Y. and L. Rui (2013). "Leptin signaling and leptin resistance." Front Med **7**(2): 207–222.

Zhu, J., B. Lee, K. K. Buhman and J. X. Cheng (2009). "A dynamic, cytoplasmic triacylglycerol pool in enterocytes revealed by ex vivo and in vivo coherent anti-Stokes Raman scattering imaging." J Lipid Res **50**(6): 1080–1089.

Chapter 2 : Nobiletin prevents high-fat diet induced dysregulation of intestinal lipid metabolism and attenuates post-prandial lipemia

Publication information:

Morrow, N.M., Trzaskalski, N.A., Hanson, A.A., Fadzeyeva, E., Telford, D.E., Chhoker, S.S., Sutherland, B.G., Edwards, J.Y., Huff, M.W. & Mulvihill, E.E. *Nobiletin Prevents High-Fat Diet-Induced Dysregulation of Intestinal Lipid Metabolism and Attenuates Postprandial Lipemia.* Arterioscler Thromb Vasc Biol. 2022. Issue 2 Pages 127-144. DOI: 10.1161/ATVBAHA.121.316896

Part of this manuscript was published in the following thesis:

"Nobiletin Corrects Intestinal Insulin Resistance and Lipid Metabolism in Ldlr$^{-/-}$ Mice Fed a High-fat Diet" by Nadya Morrow, The University of Western Ontario, Master of Science, under the supervision of Dr. Murray W. Huff.

Abstract

Objective: Nobiletin is a dietary flavonoid that improves insulin resistance and atherosclerosis in mice with metabolic dysfunction. Dysregulation of intestinal lipoprotein metabolism contributes to atherogenesis. The objective of the study was to determine if nobiletin targets the intestine to improve metabolic dysregulation in both male and female mice. Approach: Triglyceride rich lipoprotein (TRL) secretion, intracellular triglyceride kinetics, and intestinal morphology were determined in male and female low-density lipoprotein receptor knockout, and male wild-type mice fed a standard laboratory diet or high-fat, high-cholesterol diet ± nobiletin using an olive-oil gavage, radiotracers, and electron microscopy. Results: Nobiletin attenuated post-prandial TRL levels in plasma and enhanced TRL clearance. Nobiletin reduced fasting jejunal triglyceride accumulation through accelerated TRL secretion and lower jejunal fatty-acid synthesis with no impact on fatty-acid oxidation. Fasting-refeeding experiments revealed that nobiletin led to higher levels of phosphorylated AKT and FoxO1 and normal *Srebf1-c* expression indicating increased insulin sensitivity. Intestinal length and weight were diminished by high-fat feeding and restored by nobiletin. Both fasting and post-prandial plasma glucagon-like peptide-1

(GLP-1) (and likely GLP-2) were elevated in response to nobiletin. Treatment with a GLP-2 receptor antagonist, GLP-2(3-33), reduced villus length in high-fat-fed mice but did not impact TRL secretion in any diet group. In contrast to males, nobiletin did not improve post-prandial lipid parameters in female mice. Conclusions: Nobiletin opposed the effects of the high-fat diet by normalizing intestinal *de novo* lipogenesis through improved insulin sensitivity. Nobiletin prevents post-prandial lipemia because the enhanced TRL clearance more than compensates for increased TRL secretion. Nobiletin improves post-prandial lipid metabolism in mice fed a high-fat, high-cholesterol diet by enhancing intestinal insulin sensitivity

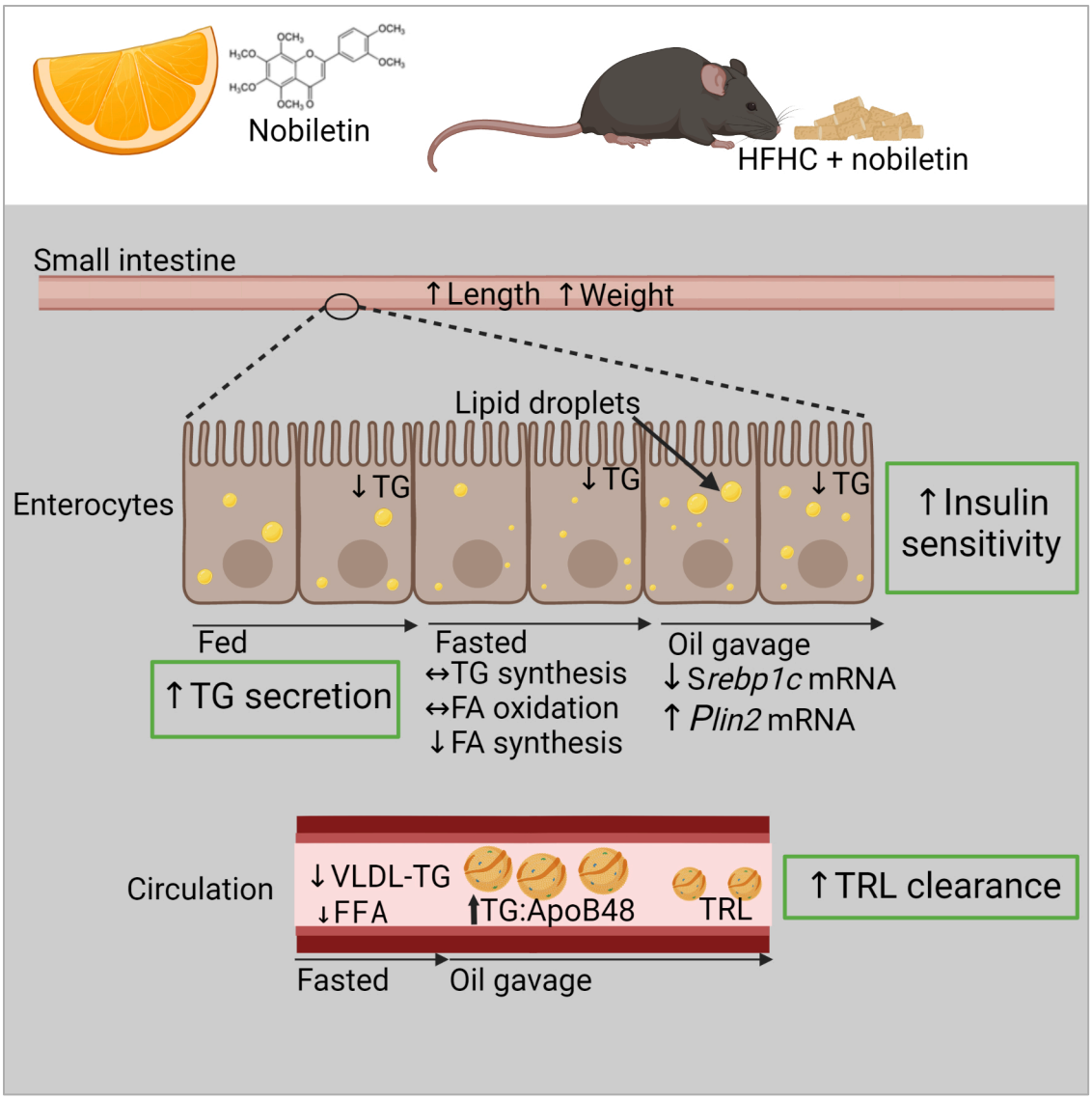

Graphical Abstract i.

2.1 List of Abbreviations

apoB48: Apolipoprotein B48

CLD: Cytoplasmic lipid droplet

HFHC: High-fat, high-cholesterol

FA: Fatty acid

GLP-1: Glucagon-like peptide 1

GLP-2: Glucagon-like peptide 2

Ldlr: Low-density lipoprotein receptor

MTP: Microsomal triglyceride transfer protein

NEFA: Non-esterified fatty acid

TG: Triglyceride

TRL: Triglyceride-rich lipoproteins

SLD: Standard laboratory diet

WT: Wild-type

LTT: Lipid tolerance test

FPLC: Fast protein liquid chromatography

AUC: Area under the curve

CE: Cholesteryl ester

DAPI: 4',6-diamidino-2-phenylindole (nuclear stain)

OCT: Optimal cutting temperature (embedding medium)

PBS: Phosphate-buffered saline

i.p.: Intraperitoneal

i.v.: Intravenous

SDS-PAGE: Sodium dodecyl sulfate–polyacrylamide gel electrophoresis

TEM: Transmission electron microscopy

SEM: Standard error of the mean

ANOVA: Analysis of variance

mTORC1: Mammalian target of rapamycin complex 1

FoxO1: Forkhead box protein O1

Srebf1-c: Sterol regulatory element binding protein 1c

Plin2: Perilipin 2

Atgl: Adipose triglyceride lipase

Cd36: Cluster of differentiation 36

Dgat2: Diacylglycerol O-acyltransferase 2

Fabp2: Fatty acid binding protein 2

Mogat2: Monoacylglycerol O-acyltransferase 2

Acox1: Acyl-CoA oxidase 1

Cpt1α: Carnitine palmitoyltransferase 1 alpha

GLPDRKO: *Glp1r*$^{-/-}$*Glp2r*$^{-/-}$ mouse

VLDL: Very low-density lipoprotein

LPL: Lipoprotein lipase

Apoc3: Apolipoprotein C3

Fasn: Fatty acid synthase

2.2 Introduction

Central to the metabolic syndrome is insulin resistance, which drives the predominance of small, dense LDL particles, the reduction of HDL-cholesterol, and increased fasting and post-prandial concentrations of apolipoprotein B (apoB)-containing triglyceride-rich lipoproteins (TRL) (Wu and Parhofer 2014). In the setting of diabetes, where dyslipidemia is exacerbated, statin therapy achieves target LDL-cholesterol levels. Still, it does not eliminate cardiovascular risk (Wu and Parhofer 2014, Xiao, Dash et al. 2016, Fan, Philip et al. 2019). Analysis from the Reduction of Cardiovascular Events with Icosapent Ethyl-Intervention Trial (REDUCE-IT) has demonstrated that patients on statins with elevated triglyceride levels can further reduce their cardiovascular risk through targeting triglyceride concentrations (Bhatt, Steg et al. 2019).

Intestinal enterocytes absorb and package dietary lipids for storage in cytoplasmic lipid droplets (CLD) or into chylomicrons (Iqbal and Hussain 2009). It is increasingly appreciated that intestinal lipid handling and lipoprotein synthesis are regulated by dietary lipid supply, hormonal signaling (Mulvihill 2018), and circulating fatty acids (FA) (Duez, Lamarche et al. 2006, Pavlic, Xiao et al. 2010). In wild-type (WT) mice, acute insulin injection following an olive-oil gavage reduced plasma triglyceride through increased phosphorylation of intestinal AKT as well as reduced microsomal triglyceride transfer protein (MTP) expression and activity (Tran, Postal et al. 2016). Chronic high-fat feeding induces changes in intestinal nutrient metabolism; however, it is debated whether they result from adaptation or obesity-induced dysregulation (Haidari, Leung et al. 2002, Zoltowska, Ziv et al. 2003, Uchida, Whitsitt et al. 2012, D'Aquila, Hung et al. 2016). In WT mice, these changes include a shortening of the small intestine, decreased secretion rate of intestinally-derived TRL, and increased lipid retention (Zhu, Lee et al. 2009, Douglass, Malik et al. 2012, Uchida, Whitsitt et al. 2012, Dalby, Ross et al. 2017), extending the post-prandial period (Sairyo, Kobayashi et al. 2018). Therefore, it remains unclear how the kinetics of intestinal triglyceride mass and triglyceride secretion are dysregulated in the post-prandial state in insulin resistance.

In the liver, insulin resistance drives upregulation of forkhead box protein O1 (FoxO1) through a lack of phosphorylation. Unlike the FoxO1 pathway, the mammalian target of rapamycin complex 1 (mTORC1) signalling remains insulin-sensitive (Brown and Goldstein 2008). As such, prolonged and elevated circulating insulin levels upregulate sterol regulatory element binding protein 1c (SREBP-1c) expression, leading to inappropriately accelerated FA synthesis (Brown and Goldstein 2008). Together, enhanced hepatic de novo FA synthesis and increased circulating non-esterified FA (NEFA) provide the substrate for hepatic triglyceride synthesis, which can be stored or packaged in VLDL particles for secretion (Brown and Goldstein 2008, Sears and Perry 2015, Czech 2017). The contribution of this bifurcation in insulin signalling to the kinetics of intestinal triglyceride mass and post-prandial triglyceride-secretion is unclear.

Epidemiologically, a higher intake of flavonoids correlates with lower cardiovascular risk (Mulvihill, Burke et al. 2016). We and others have reported that nobiletin, a tangerine-derived flavonoid, prevents high fat-diet-induced metabolic dysregulations in WT mice (Lee, Cha et al. 2013, He, Nohara et al. 2016, Kim, Choi et al. 2017, Morrow, Burke et al. 2020) through actions in a variety of tissues in addition to its clock amplitude enhancing properties (He, Nohara et al. 2016). Nobiletin administered as either prevention (Mulvihill, Assini et al. 2011) or intervention (Burke, Sutherland et al. 2018) treatment in *Ldlr*$^{-/-}$ mice reduces atherosclerosis, VLDL-triglyceride secretion, and hepatic triglyceride accumulation. Mechanistically, nobiletin reduces hepatic-FA synthesis and enhances hepatic-FA oxidation (Mulvihill, Assini et al. 2011, Burke, Sutherland et al. 2018). Nobiletin also attenuates fasting intestinal triglyceride accumulation in *Ldlr*$^{-/-}$ mice (Mulvihill, Assini et al. 2011). However, the specific mechanism(s) by which nobiletin may influence intestinal lipid metabolism in models of atherogenesis (*Ldlr*$^{-/-}$) remains unclear. The purpose of these studies was to examine the development of intestinal insulin resistance, intestinal lipid accumulation, and post-prandial chylomicron secretion in both male and female mice fed a high-fat, high-cholesterol (HFHC) diet +/- nobiletin.

2.3 Materials and methods

Animals and Diets

Male and female *Ldlr*$^{-/-}$, male C57BL/6J (WT) (The Jackson Laboratory, Bar Harbor, MA), and male *Glp1r*$^{-/-}$*Glp2r*$^{-/-}$ (GLPDRKO) mice (Lee, Lee et al. 2012) kindly provided by Dr. Daniel Drucker (Toronto, ON) were housed in standard cages at 23˚C on a 12h light and dark cycle with littermate controls. Mice were cared for following the Canadian Guide for the Care and Use of Laboratory Animals. Approval was obtained for all procedures (Western University-AUP-2016-057, UOHI-AUP-2909). Mice (10-12 weeks) were fed ad libitum one of three diets for 10-12 weeks: a purified standard laboratory diet (SLD) (Teklad-8604, Envigo, Madison WI), HFHC diet (Teklad-TD09268, Envigo), or HFHC-diet supplemented with 0.3% nobiletin (#10236-47-2, R&S PharmChem, Hangzhou City, China). The dose of 0.3% has been previously shown to prevent metabolic dysregulation and atherosclerosis in *Ldlr*$^{-/-}$ mice (Mulvihill, Assini et al. 2011). Synthetic mouse GLP-2(3-33) (Chi Scientific Maynard, MA) was injected daily (30 ng/day) for 14 days following 10-weeks of HFHC-diet.

Blood and tissue collection

Metabolic studies, blood collection, FPLC, and sacrifice were as previously described (Assini, Mulvihill et al. 2013). Briefly, the small intestine was divided into duodenum, jejunum, ileum (1:3:2 ratio), and flushed with 0.5 mM sodium taurocholate (37˚C) followed by ice-cold saline. Whole intestinal tissue was used for analysis unless otherwise indicated. Plasma lipids, insulin (Mulvihill, Assini et al. 2011), tissue lipids (Assini, Mulvihill et al. 2013), and gene expression (Burke, Sutherland et al. 2018) were measured as previously described. For glucagon like peptide 1 (GLP-1) measurement (total-K1503PD-2, active-K1526LK, Mesoscale) 5000KIU/mL Trasylol, 1.2mg/mL EDTA, 0.1nmol/L Diprotin A was added.

Lipid tolerance test and Plasma ultracentrifugation

Mice were fasted for 6 hours and gavaged with 200 µl olive-oil (±10 µCi 3H-triolein, Amersham, Oakville, ON; ±30 µg BODIPY-C16-FA, Molecular Probes, Eugene, OR; ± 3mg acetaminophen). In indicated experiments, mice were also injected with 100mg/kg poloxamer-407 (P407) (*i.p.*) 30min before the oil gavage. TRL were isolated by ultracentrifugation (#344625 TLA-120.2, Beckman Coulter, Mississauga, ON) (17000rpm, 12^{o}C, 30min-chylomicrons (<1.006) followed by 40000 rpm, 12^{o}C 2h-VLDL fraction (<1.006). For fasting samples only, body-weight matched mice were pooled. Triglyceride values in the chylomicron and VLDL-fraction were corrected for plasma volume spun and respective fraction volume collected. In WT mice, plasma triglyceride was measured using the Infinity Triglycerides assay. For gastric emptying measurements, plasma acetaminophen was measured (Sekisui Diagnostics, Charlottetown, PE).

Chylomicron clearance and glucose tolerance

Mice were fasted for 5 hours and administered 5,310 µg ULDL chylomicrons (LeeBio) in 100µL PBS *i.v*. and samples were taken every 2min post-injection. An oral glucose tolerance test was performed following a 6 hour fast (1 g/kg body weight) and blood glucose was measured by glucometer (MediCure Canada, Ajax, ON).

Plasma immunoblotting

Samples from *Ldlr*$^{-/-}$ mice were run on 10% SDS-PAGE gels (BioRad #456-1086), transferred onto nitrocellulose membranes, and incubated with apoB primary antibodies (Midland AB_2734118) or albumin (Novus Biologicals NB 600-41532) and secondary IRDye® 800CW (#925-32214-LI-COR Biosciences, Lincoln, NE), imaged (LI-COR Biosciences Odyssey), and quantitated (ImageStudio Software 5.0). Plasma from WT mice was run on 4% SDS-PAGE gels, transferred onto nitrocellulose membranes, incubated with apoB antibodies (Midland AB_2734118) and mouse-anti-goat IgG-HRP (Santa Cruz Biotechnologies, sc-2354;

RRID:AB_628490), visualized (SuperSignal WestPico PLUS, Thermo Scientific, P134577), imaged (ChemiDoc XRS+; Bio-Rad) and quantitated (ImageLab).

Tissue immunoblotting

Samples were homogenized in RIPA buffer (Sigma R0278 with P8340, P5726) and DTT. Protein concentrations were determined as described (Assini, Mulvihill et al. 2013) (mTORC1-12.5 µg, AKT-6.25 µg, and FoxO1-50 µg), were visualized using enhanced chemiluminescence reagent (Roche Diagnostics) and quantified using an Imaging Densitometer (GS-700; Bio-Rad).

2.3.7 Jejunal FA/triglyceride synthesis and FA oxidation

FA synthesis was measured 30min following an (*i.p.*) injection of 20µCi [1-14C]-acetate (Amersham). Incorporation into FA was measured as described (Mulvihill, Allister et al. 2009). Triglyceride synthesis was measured by incubating jejunal homogenates with [14C]oleoyl-CoA (Amersham). [3H]cholesteryl-oleate (Amersham) was used as an internal standard (Mulvihill, Allister et al. 2009). For FA oxidation, jejunal mucosa was homogenized. Two µCi of [1-14C]palmitic acid (PerkinElmer: NEC075H250UC) and 150 µM unlabeled palmitic acid was complexed with 3% FA-free BSA and $14CO_2$ in the filter pads. The incorporation of tracers was measured by liquid scintillation counting (Mulvihill, Allister et al. 2009).

Microscopy

Transmission electron microscopy: jejunal segments were fixed in 1% paraformaldehyde and 1% glutaraldehyde, post-fixed in 1% osmium tetroxide, dehydrated, and immersed in acetone. The tissue was infiltrated with epon-araldite resin, embedded, and polymerized (Electron Microscopy Sciences, Hatfield PA). Sections (Reichert Ultracut) were stained with paraphenylenediamine (Shirai, Geoly et al. 2016) and imaged (Leica Aperio At2 slide scanner). Ultrathin sections were stained with Reynold's lead citrate and imaged (Philips 420 TEM, AMT-4KMP XR41S-B camera; Woburn, MA). The identification of CLDs was based on previous characterizations (D'Aquila,

Hung et al. 2016, Hung, Carreiro et al. 2017). For fluorescence microscopy, jejunal segments were fixed in 4% paraformaldehyde, incubated in 30% sucrose, embedded in OCT, sectioned (10 µm), counterstained with DAPI, and imaged (Zeiss AxioScope) where autofluorescence was captured to define tissue outline. CLD area quantification was performed using CellProfiler (version-4.2.0) using a modified pipeline (Adomshick, Pu et al. 2020).

Statistical analysis

Data are presented as mean±SEM. Statistical analyses were performed using One- or Two-Way ANOVA (indicated) with post-hoc Tukey's test following Brown-Forsythe test and Barlett's test for normality and equal variance. A p-value <0.05 was considered significant, and p-values are listed where appropriate. A notation of N.S. indicates no statistically significant difference. All data were analyzed using GraphPad Prism 8.

2.4 Results

2.4.1 Nobiletin attenuates triglyceride accumulation in the circulation and the jejunum during fasted and post-prandial states in male and female *Ldlr*$^{-/-}$ mice.

Nobiletin has previously been shown to attenuate dyslipidemia in HFHC-fed male WT (Lee, Cha et al. 2013, He, Nohara et al. 2016, Kim, Choi et al. 2017, Morrow, Burke et al. 2020) and *Ldlr*$^{-/-}$ mice (Mulvihill, Assini et al. 2011, Burke, Sutherland et al. 2018). FPLC analyses of plasma from both male and female *Ldlr*$^{-/-}$ mice demonstrated elevated triglyceride levels in HFHC-fed mice following a 6h fast (Figure 2.1A,B). Nobiletin significantly reduced VLDL-triglyceride in female *Ldlr*$^{-/-}$ mice, however, these levels remained significantly higher than SLD-fed female mice (Figure 2.1A). Nobiletin significantly reduced VLDL-triglyceride to levels not different from SLD-fed male *Ldlr*$^{-/-}$ controls (Figure 2.1B). To determine if dietary triglycerides are handled differently

in HFHC vs HFHC+nobiletin mice, plasma from *Ldlr*$^{-/-}$ males obtained after 6h fast and 2h post-oil gavage was separated by FPLC. At 2h post-gavage, the triglyceride-AUC in the FPLC fractions of male HFHC-fed *Ldlr*$^{-/-}$ mice did not change from the elevated baseline, suggesting delayed intestinal-triglyceride excursion (Figure 2.1C,D). By contrast, the triglyceride-AUC of nobiletin-treated male *Ldlr*$^{-/-}$ mice increased significantly from baseline to triglyceride levels significantly lower than HFHC-fed mice (Figure 2.1C,D). HFHC-fed male *Ldlr*$^{-/-}$ mice displayed significantly elevated jejunal triglyceride in the fed state compared to SLD-fed mice, suggesting an accumulation of dietary triglyceride in the jejunum (Figure 1E). By contrast, nobiletin-treated male *Ldlr*$^{-/-}$ mice did not accumulate jejunal triglyceride at any time point (Figure 2.1E).

To assess an extended view of the post-prandial period, a lipid tolerance test (LTT) was performed in male *Ldlr*$^{-/-}$ mice. Despite significantly elevated fasting plasma triglyceride in HFHC-fed mice, the incremental change in plasma triglyceride from the olive oil gavage was not significantly different compared to SLD-controls (Figure 2.1F). Nobiletin-treatment elevated triglyceride levels to a greater extent compared to HFHC and SLD-fed mice, particularly at 2 hours post-gavage (Figure 2.1F). In another set of mice, separating triglyceride-rich plasma lipoprotein fractions by ultracentrifugation revealed significantly elevated chylomicron-triglyceride in HFHC-fed mice compared to SLD-fed mice at fasting, 2h and 4h post-oil (Figure 2.1G). Chylomicron-triglyceride levels in nobiletin-treated mice were intermediate and not significantly different from HFHC-fed or SLD-fed mice at any time point (Figure 2.1G). Plasma VLDL-triglyceride were significantly elevated in HFHC-fed mice at fasting, 1h, 2h, and 4h post-gavage compared to SLD-fed mice (Figure 2.1H). Nobiletin treatment led to significantly lower VLDL-triglyceride at fasting, 2 h, and 4 h post-oil compared to HFHC-fed mice (Figure 2.1H). Comparisons within diet groups revealed that only HFHC-fed mice displayed significant increases in chylomicron-triglyceride (4h) or VLDL-triglyceride (2 h and 4 h) compared to their baselines, suggesting either a delayed secretion or impaired clearance in HFHC-fed mice is prevented by nobiletin.

Nobiletin prevented HFHC-induced weight gain in male and female *Ldlr*$^{-/-}$ mice (Figure 2-IA,C Data Supplement). In male *Ldlr*$^{-/-}$ mice, caloric intake was unchanged across diet groups, however, nobiletin-treated female *Ldlr*$^{-/-}$ mice consumed significantly more calories (~1.2-fold) than standard laboratory diet (SLD)-fed mice (Figure 2-IB, D Data Supplement). As in males(Mulvihill, Assini et al. 2011), nobiletin also prevented hepatic triglyceride accumulation in female *Ldlr*$^{-/-}$ mice (Figure 2-IE, Data Supplement).

Figure 2.1 Nobiletin attenuates triglyceride (TG) accumulation in circulation and in the jejunum during the fasted and post-prandial state in male Ldlr$^{-/-}$ mice. Fasting (6 h) plasma in (A) female *Ldlr*$^{-/-}$ mice and (B) male *Ldlr*$^{-/-}$ mice for fast protein liquid chromatography (FPLC); TG was measured in each fraction with area under the curve (AUC) calculations of the VLDL (very-low-density lipoprotein)-TG (fractions 5–10; n=8–13/group). (C) FPLC-TG 2-h post gavage in the same male mice as in (B). (D) AUC calculations of fasting and 2-h post gavage VLDL-TG from FPLC fractions and absolute change from baseline (Δ). (E) Male *Ldlr*$^{-/-}$ mice were sacrificed in fed state (0) or after 3, 6, and 9 h of fasting for jejunal TG (n=4/time point). (F) Lipid tolerance test (LTT) plasma TG with incremental AUC (n=8/time point). In another set of male *Ldlr*$^{-/-}$ mice, fasting plasma from 2 mice per group was pooled and mice were euthanized at 1-, 2-, and 4-h post gavage for ultracentrifugation (n=4–6/time point). TG measured in the (G) chylomicron- and (H) VLDL-fractions. Values are mean±SEM. ANOVA with post hoc Tukey test was used to calculate statistical significance and p-values are labeled in each graph. In secretion curves (E and F) statistical differences over time were determined by 2-way ANOVA, where p-values for each time point are indicated for statistical differences between high-fat, high-cholesterol (HFHC)+nobiletin and HFHC-fed (gray) and standard laboratory diet (SLD)-fed compared with HFHC-fed (black). NS indicates nonsignificant.

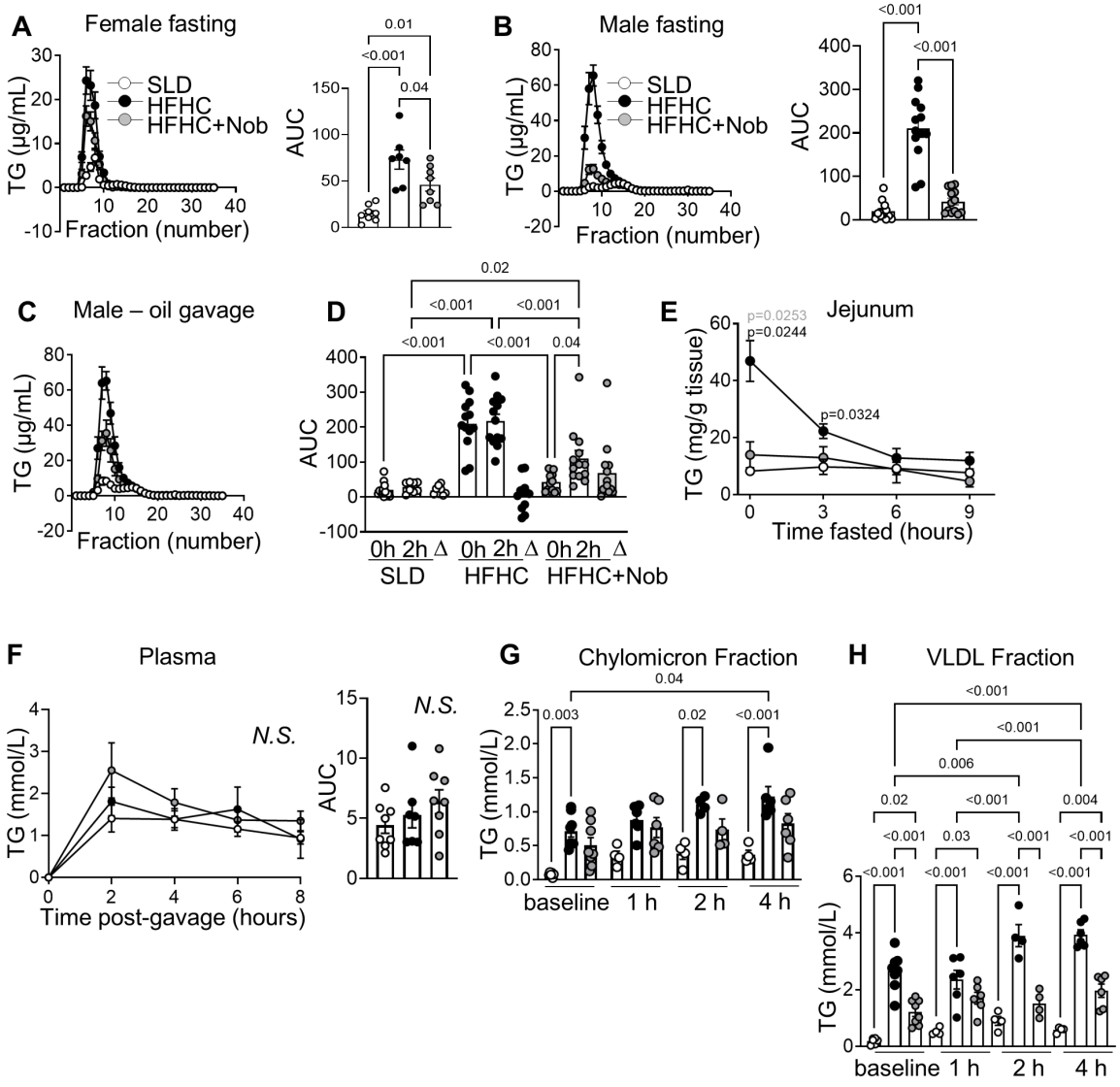
A
Female fasting
TG (µg/mL)
SLD
HFHC
HFHC+Nob
Fraction (number)
AUC
0.01
<0.001
0.04
B
Male fasting
TG (µg/mL)
SLD
HFHC
HFHC+Nob
Fraction (number)
AUC
<0.001
<0.001
C
Male – oil gavage
TG (µg/mL)
Fraction (number)
D
AUC
0.02
<0.001
<0.001
<0.001
<0.001
0.04
0h 2h Δ
SLD
0h 2h Δ
HFHC
0h 2h Δ
HFHC+Nob
E
Jejunum
TG (mg/g tissue)
p=0.0253
p=0.0244
p=0.0324
Time fasted (hours)
F
Plasma
TG (mmol/L)
N.S.
Time post-gavage (hours)
AUC
N.S.
G
Chylomicron Fraction
TG (mmol/L)
0.04
0.003
0.02
<0.001
baseline
1 h
2 h
4 h
H
VLDL Fraction
TG (mmol/L)
<0.001
<0.001
0.006
0.02
<0.001
0.004
<0.001
0.03
<0.001
<0.001
<0.001
<0.001
<0.001
<0.001
baseline
1 h
2 h
4 h

2.4.2 Nobiletin increases the rate of intestinal-triglyceride secretion in male WT and *Ldlr*$^{-/-}$ mice but not in female *Ldlr*$^{-/-}$ mice

To assess intestinal-triglyceride secretion rates, mice were treated with poloxamer-407 (P407) to block lipoprotein lipase (LPL) activity before the LTT. Male *Ldlr*$^{-/-}$ mice additionally received ^{3}H-triolein in the olive-oil gavage. HFHC-fed *Ldlr*$^{-/-}$ males displayed significantly lower plasma triglyceride at 1h, 2h, and 4h and radioactivity at 1h and 2h, compared to SLD-fed mice (Figure 2.2A,B). Secretion into plasma of triglyceride and radioactivity were significantly higher in nobiletin-treated male *Ldlr*$^{-/-}$ mice compared to HFHC-fed mice (Figure 2.2A,B). Plasma apoB48 levels were not significantly different in nobiletin-treated compared to HFHC-fed mice (Figure 2.2C). HFHC-fed-female *Ldlr*$^{-/-}$ mice, similar to male *Ldlr*$^{-/-}$ mice, displayed significantly delayed triglyceride secretion (Figure 2.2D). However, nobiletin treatment did not normalize triglyceride secretion in female mice (Figure 2.2D). Consistently, HFHC-fed male WT mice had lower plasma triglyceride at 1h post-gavage compared to SLD controls (Figure 2.2E). Plasma triglyceride at 1h in nobiletin-treated mice was intermediate between HFHC- and SLD-fed mice but was significantly higher over 4h (Figure 2.2E). HFHC-fed WT mice trended to elevated plasma apoB48 signal despite similar plasma triglyceride secretion compared to SLD-fed mice (Figure 2.2F). Nobiletin treatment attenuated plasma apoB48 secretion compared to HFHC-fed mice to levels similar to SLD-fed mice (Figure 2.2F).

Figure 2.2 Nobiletin increases the rate of intestinal-triglyceride (TG) secretion in male Ldlr$^{-/-}$ mice and wild-type (WT) male mice but not in female Ldlr$^{-/-}$ mice. Lipid tolerance test (LTT) was performed in male *Ldlr$^{-/-}$* mice with P407 and olive oil containing [^{3}H]triolein. LTT plasma (A) TG and (B) [^{3}H]TG (n=8 37/time point) displayed as a difference from baseline with area under the curve (AUC) calculations on the right. (C) LTT plasma apoB48 (n=4–26/time point) displayed as a difference from baseline where samples were normalized to albumin, and this ratio was normalized to the 2-h apoB48/albumin signal of a standard laboratory diet (SLD)-fed mouse, run on each gel (n=4–27/time point) with AUC calculations. LTT was performed in female *Ldlr$^{-/-}$* mice with P407. (D) LTT plasma TG displayed as a difference from baseline with AUC calculations. LTT in male WT mice with P407 and olive oil containing BODIPY-C16-fatty acid (FA). LTT (E) plasma TG. (F) Plasma apoB48 (n=3–4/group) with AUC calculations. Values are mean±SEM. ANOVA with post hoc Tukey test was used to calculate statistical significance and p-values are labeled in each graph. In secretion curves statistical differences over time were determined by 2-way ANOVA. In A, B, E, and F, p-values for each time point are indicated for statistical differences between high-fat, high-cholesterol (HFHC)+nobiletin and HFHC-fed (gray) and SLD-fed compared with HFHC-fed (black). In C and D, p-values indicate statistical differences between HFHC+nobiletin and SLD (gray) and HFHC compared with SLD (black). NS indicates nonsignificant.

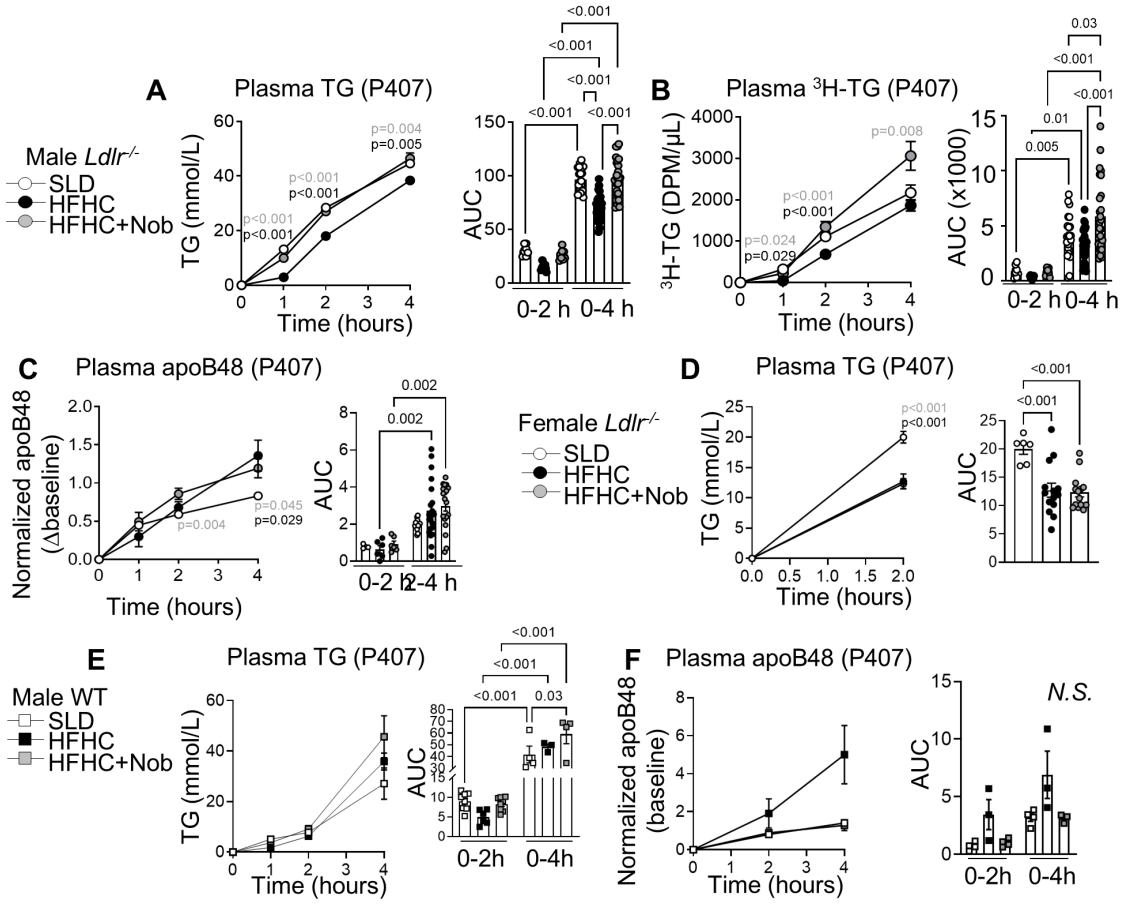
A
Plasma TG (P407)
Male Ldlr-/-
SLD
HFHC
HFHC+Nob
TG (mmol/L)
Time (hours)
AUC
0-2 h
0-4 h
B
Plasma 3H-TG (P407)
3H-TG (DPM/µL)
AUC (x1000)
C
Plasma apoB48 (P407)
Normalized apoB48 (Δbaseline)
D
Plasma TG (P407)
Female Ldlr-/-
E
Plasma TG (P407)
Male WT
F
Plasma apoB48 (P407)
Normalized apoB48 (baseline)
N.S.

2.4.3 Nobiletin increases the triglyceride content of chylomicron particles in male but not female *Ldlr*$^{-/-}$ mice.

To determine if nobiletin alters the number or triglyceride-enrichment of TRL-particles secreted, TRL fractions were isolated at fasting and 2h post-oil and P047. HFHC-fed-male *Ldlr*$^{-/-}$ mice displayed significantly reduced chylomicron-triglyceride secretion compared to SLD-fed mice (Figure 2.3A). Nobiletin treatment restored chylomicron-triglyceride secretion to a rate not significantly different from SLD-fed mice (Figure 2.3A). Despite similar fasting chylomicron-triglyceride values between diet groups (Figure 2.3A), HFHC-fed mice displayed significantly elevated fasting apoB48 (Figure 2.3B). Nobiletin-treated mice were the only diet group to display a significant increase in chylomicron-apoB48 from baseline (Figure 2.3B). Triglyceride:apoB48 calculations (particle size) revealed a significant post-prandial enrichment in all diet groups (Figure 2.3C). Still, post-oil chylomicron-triglyceride:apoB48 from HFHC-fed mice was significantly lower compared to SLD-fed mice (Figure 2.3C). Nobiletin treatment led to significantly higher chylomicron-triglyceride:apoB48 relative to HFHC-fed mice, but it did not entirely correct this defect. In female *Ldlr*$^{-/-}$ mice fed a HFHC or SLD, the patterns of response for secretion of chylomicron-triglyceride, chylomicron-apoB48, and chylomicron-triglyceride:apoB48 (Figure 2.3D-F) were similar to those of male *Ldlr*$^{-/-}$ mice (Figure 2.3A-C); however, in contrast to male *Ldlr*$^{-/-}$ mice, nobiletin did not prevent HFHC-diet-induced changes to these parameters (Figure 2.3D-F). Post oil gavage, VLDL-triglyceride levels in male *Ldlr*$^{-/-}$ mice increased significantly at 2h in all diet groups compared to their respective baseline (Figure 2.3G). Nobiletin treatment led to significantly greater VLDL-triglyceride secretion compared to HFHC-fed male *Ldlr*$^{-/-}$ mice (Figure 2.3G). VLDL-apoB48 secretion and VLDL-triglyceride:apoB48 ratios were similar among groups (Figure 2.3H,I). In female *Ldlr*$^{-/-}$ mice, HFHC-feeding led to significantly lower VLDL-triglyceride secretion at 2h compared to SLD-fed controls, while nobiletin-treated mice displayed an

intermediate VLDL-triglyceride secretion rate that was not different from HFHC-fed or SLD-controls (Figure 2.3J).

Figure 2.3 Nobiletin increases the triglyceride (TG) content of chylomicron particles in male but not female Ldlr$^{-/-}$ mice. Lipid tolerance test (LTT) with P407 was performed in *Ldlr*$^{-/-}$ mice. Fasting plasma from 2 mice per group was pooled and mice were euthanized 2-h post-gavage (n=16–30/time point) for plasma ultracentrifugation. In male *Ldlr*$^{-/-}$ mice, (A) chylomicron-TG, (B) chylomicron apoB48, and (C) ratio of chylomicron-TG to chylomicron-apoB48 signal. In female *Ldlr*$^{-/-}$ mice, (D) chylomicron-TG, (E) chylomicron-apoB48, and (F) ratio of chylomicron-TG to chylomicron apoB48. In male *Ldlr*$^{-/-}$ mice, (G) VLDL (very-low-density lipoprotein)-TG, (H) VLDL-apoB48 signal, and (I) ratio of VLDL-TG to apoB48 signal. In female *Ldlr*$^{-/-}$ mice, (J) VLDL-TG. Values are mean±SEM. ANOVA with post hoc Tukey test was used to calculate statistical significance and p-values are labeled in each graph when appropriate. HFHC indicates high-fat, high cholesterol; and SLD, standard laboratory diet.

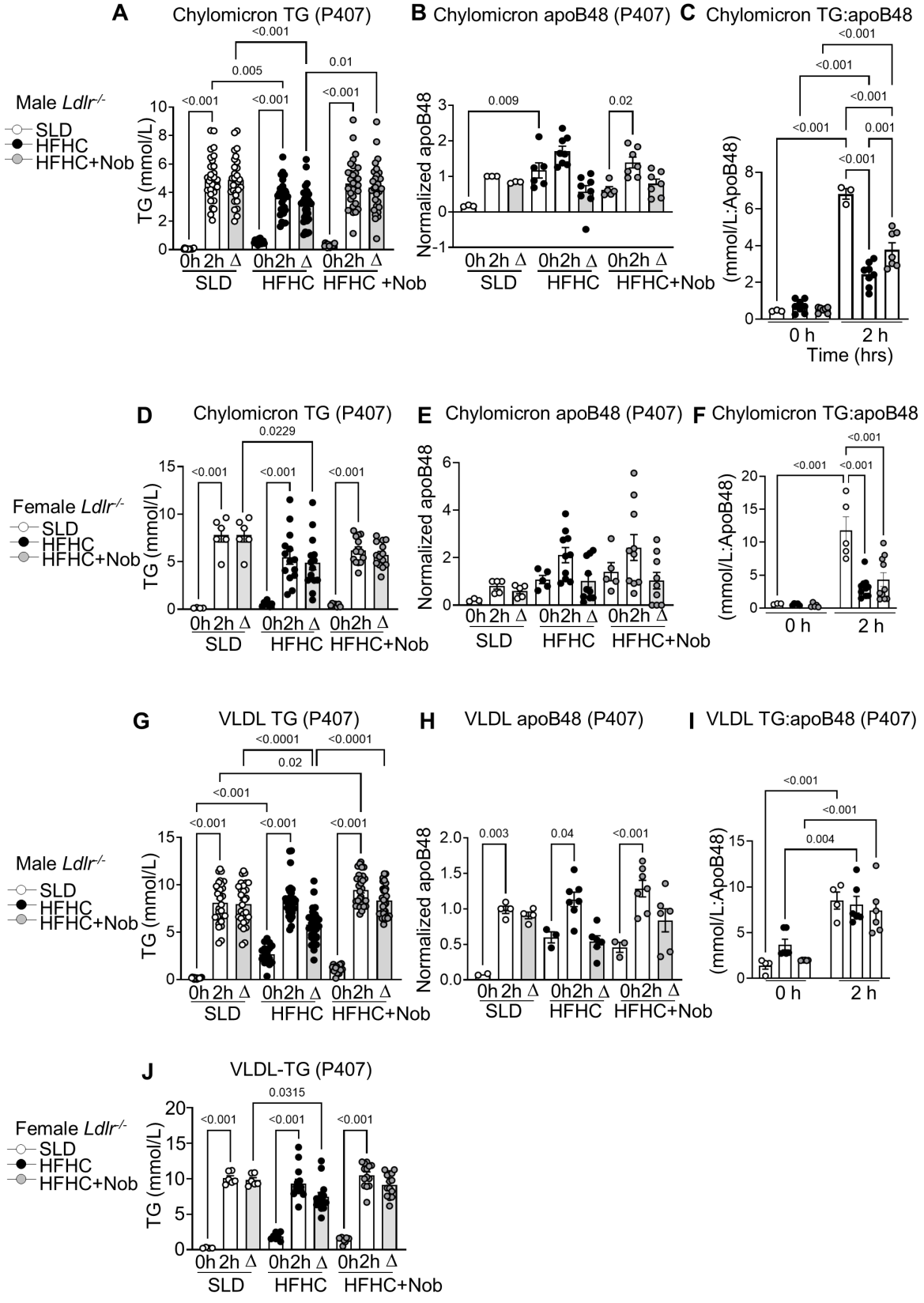
A
Chylomicron TG (P407)
B Chylomicron apoB48 (P407)
C Chylomicron TG:apoB48
Male Ldlr-/-
SLD
HFHC
HFHC+Nob
TG (mmol/L)
Normalized apoB48
(mmol/L:ApoB48)
0h 2h Δ
SLD
HFHC
HFHC +Nob
HFHC+Nob
0 h
2 h
Time (hrs)
D
Chylomicron TG (P407)
E Chylomicron apoB48 (P407)
F Chylomicron TG:apoB48
Female Ldlr-/-
G
VLDL TG (P407)
H VLDL apoB48 (P407)
I VLDL TG:apoB48 (P407)
J
VLDL-TG (P407)

2.4.4 TRL clearance is elevated by nobiletin.

To estimate the plasma-triglyceride clearance rate in male mice, we compared triglyceride-secretion rates with and without P407 treatment in the same set of male *Ldlr*$^{-/-}$ mice. We observed a significantly lower clearance rate in HFHC-fed mice compared to SLD-controls (Figure 2.4A,B). Nobiletin treatment led to a significantly higher clearance rate compared to HFHC-fed mice (Figure 2.4A,B). In male WT mice, the same significantly lower clearance rate in HFHC-fed mice compared to SLD-fed controls was observed (Figure 2.4C,D), whereas triglyceride-clearance in nobiletin-treated WT mice was intermediate between and not statistically different from the other two groups (Figure 2.4D). A more direct assessment of chylomicron-triglyceride clearance was measured in all three dietary groups of WT male mice (Figure 2.4E). Triglyceride mass rapidly decreased in all groups within the first 2 minutes. AUC calculations revealed enhanced triglyceride clearance in nobiletin-treated mice compared to HFHC-fed mice (Figure 2.4E). In WT male mice, *Ldlr* mRNA expression in jejunum and liver was not different among groups (Figure 2.4F,G). Jejunal *Apoc3* mRNA, an inhibitor of LPL activity and regulator of hepatic TRL clearance(Ramms and Gordts 2018), was significantly higher in HFHC-fed WT male mice compared to both SLD-fed and nobiletin-treated mice (Figure 2.4H). Moreover, we observed significantly greater gastric emptying in nobiletin-treated WT male mice compared to SLD-controls, suggesting enhanced nutrient transit into circulation (Figure 2.4I). Therefore, in addition to enhanced intestinal-triglyceride secretion, nobiletin accelerated plasma-triglyceride clearance.

Figure 2.4 Assessing chylomicron clearance particle rates in male Ldlr$^{-/-}$ and male wild-type (WT) mice. (A) Comparison of plasma triglyceride (TG) secretion rates in male *Ldlr*$^{-/-}$ mice treated ±P407 (n=12–14/group). (B) Estimated plasma TG clearance rate calculated from the difference in TG secretion ±P407. (C) Comparison of plasma TG secretion rates and (D) estimated plasma TG clearance rate in male WT mice without P407 (bottom) and with P407 (top; n=7–8). E, Male WT mice were injected with human chylomicrons (intravenous) following a 5-h fast and blood samples were taken for TG measurements, normalized to 4% body weight, and area under the curve (AUC) calculations. Post-prandial mRNA expression of *Ldlr* in (F) jejunum and (G) liver samples. (H) Post-prandial jejunal mRNA expression of Apoc3. I, Gastric emptying in male WT mice was assessed during a lipid tolerance test (LTT; +3 mg acetaminophen) by measuring plasma acetaminophen post-gavage and AUC calculations. Values are mean±SEM. ANOVA with post hoc Tukey test was used to calculate statistical significance and p-values are labeled in each graph when appropriate. HFHC indicates high-fat, high-cholesterol; NS indicates nonsignificant; and SLD, standard laboratory diet.

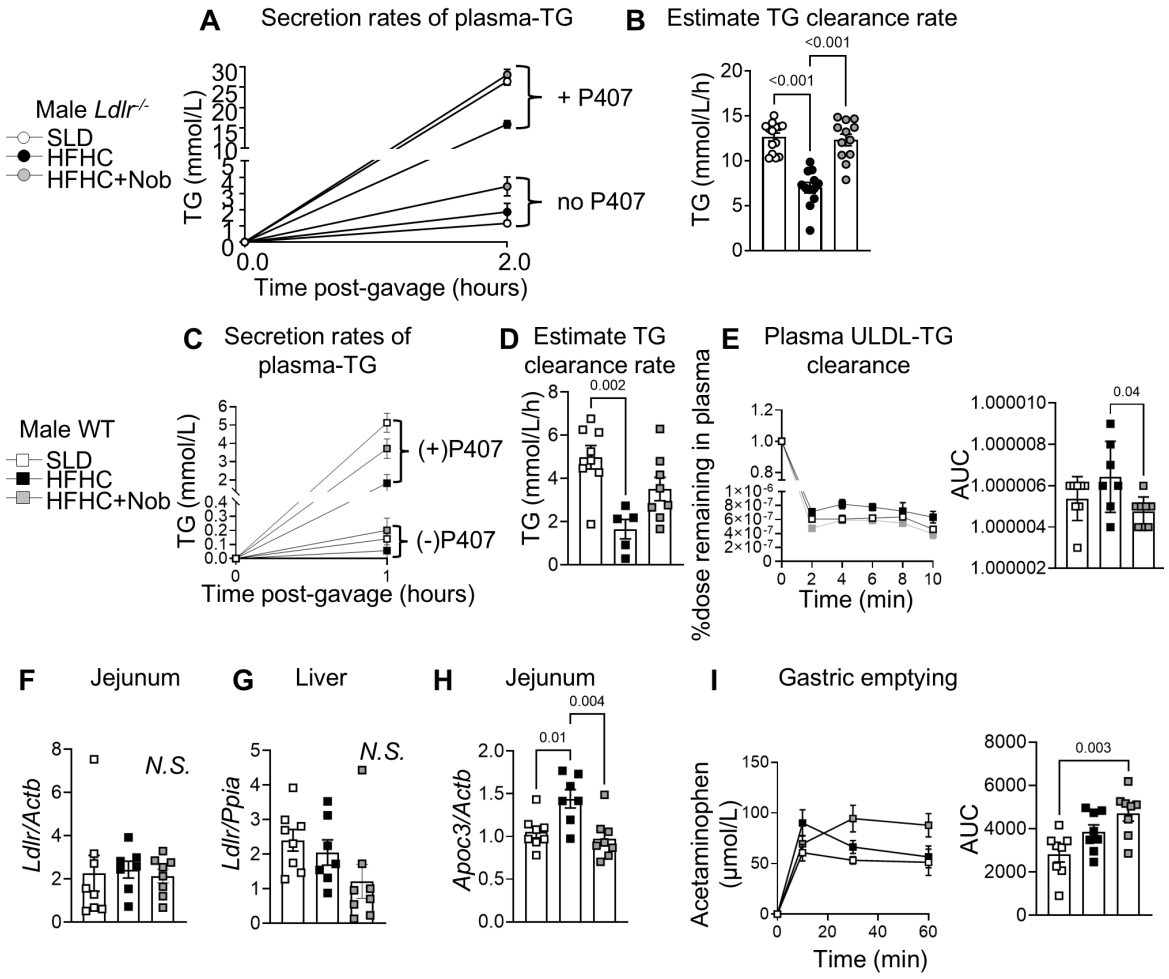
A
Secretion rates of plasma-TG
Male Ldlr-/-
SLD
HFHC
HFHC+Nob
TG (mmol/L)
+ P407
no P407
Time post-gavage (hours)
B
Estimate TG clearance rate
<0.001
<0.001
TG (mmol/L/h)
C
Secretion rates of plasma-TG
Male WT
SLD
HFHC
HFHC+Nob
TG (mmol/L)
(+)P407
(-)P407
Time post-gavage (hours)
D
Estimate TG clearance rate
0.002
TG (mmol/L/h)
E
Plasma ULDL-TG clearance
%dose remaining in plasma
Time (min)
0.04
AUC
F
Jejunum
Ldlr/Actb
N.S.
G
Liver
Ldlr/Ppia
N.S.
H
Jejunum
0.01
0.004
Apoc3/Actb
I
Gastric emptying
Acetaminophen (µmol/L)
Time (min)
0.003
AUC

2.4.5 Nobiletin attenuates intestinal lipid storage in male but not female *Ldlr*$^{-/-}$ mice.

During fat absorption, re-synthesized triglyceride within enterocytes can be stored in CLDs as reservoirs for later export (Adeli and Lewis 2008). Moreover, high fat diet-fed mice have been reported to have more abundant and larger intestinal CLDs post-oil gavage compared to SLD-fed mice (Lee, Zhu et al. 2009, Douglass, Malik et al. 2012). In male *Ldlr*$^{-/-}$ mice, levels of the radiolabel 2h post-^{3}H-triolein/oil gavage was not significantly different among diet groups, suggesting that tracer uptake was similar, however, differences in tracer metabolism cannot be excluded (Figure 2.5A). Total jejunal triglyceride mass was significantly higher in HFHC-fed *Ldlr*$^{-/-}$ male mice 2h post-gavage compared to SLD-fed controls (Figure 2.5B). In contrast, jejunal triglyceride mass in nobiletin-treated mice was significantly lower compared to HFHC-fed mice (Figure 2.5B). Intestinal triglyceride levels were similar among groups by 4h post-oil gavage (Figure IF, Data Supplement). In contrast to male *Ldlr*$^{-/-}$ mice, jejunal triglyceride mass 2h post-gavage was not significantly different among groups in female *Ldlr*$^{-/-}$ mice (Figure 2.5C).

Neutral lipid accumulation was observed in light micrographs of enterocytes 2h post-oil gavage of male *Ldlr*$^{-/-}$ HFHC-fed mice, and this signal appeared diminished in nobiletin-treated mice (Figure 2.5D). Electron micrographs revealed an abundance of large CLDs in enterocytes of a HFHC-fed *Ldlr*$^{-/-}$ male mouse (Figure 2.3E). By contrast, large CLDs appeared less frequent with nobiletin-treatment while smaller CLDs were abundant (Figure 2.3E). In male WT male mice, jejunal sections 2h post-BODIPY-C16 gavage revealed dietary fat-derived CLDs in all diet groups (Figure 2.5F). Image quantification of BODIPY-CLD area revealed a significantly greater CLD size in HFHC-fed mice compared to SLD-fed controls (Figure 2.5G). Lipid droplet size in nobiletin-treated mice was not statistically different from HFHC-or SLD-fed mice (Figure 2.5G).

Quantification of BODIPY-CLD area 4h post-gavage revealed no significant differences among groups (Figure 1G,H, Data Supplement).

Gene expression of enzymes involved in intestinal FA trafficking, triglyceride synthesis, and chylomicron assembly (Iqbal and Hussain 2009) was measured in jejunal tissue post-oil gavage. Jejunal *Srebf1-c* mRNA expression was significantly higher in HFHC-fed male and female *Ldlr*$^{-/-}$ mice and male WT mice compared to SLD-fed mice (Figure 2.5H). Nobiletin treatment led to significantly lower *Srebf1-c* mRNA expression but only in male *Ldlr*$^{-/-}$ mice (Figure 2.5H). *Plin2* is involved in lipid absorption and CLD stabilization (Frank, Bales et al. 2015), and compared to SLD, nobiletin led to significantly higher post-prandial jejunal mRNA expression of *Plin2* in all models tested (Figure 2.5I). *Atgl* mediates triglyceride hydrolysis from CLDs, and its jejunal expression is reduced in high-fat diet fed WT mice 2h post-oil gavage (Uchida, Whitsitt et al. 2012). Consistent with this, *Atgl* mRNA expression was significantly lower in male and female *Ldlr*$^{-/-}$ HFHC-fed mice compared to SLD-controls (Figure 2.5J). Nobiletin did not significantly change *Atgl* mRNA expression in male *Ldlr*$^{-/-}$ mice, whereas in female *Ldlr*$^{-/-}$ mice, this expression was significantly lower compared to in SLD-fed mice (Figure 2.5J). In male WT mice, no differences in jejunal *Atgl* mRNA were observed among diet groups (Figure 2.5J). In male *Ldlr*$^{-/-}$ mice, post-prandial mRNA expression of jejunal *Cd36, Dgat2* and *Mttp* were not different among groups (Figure II, Data Supplement). In male WT mice, jejunal *Apob, Fabp2,* and *Mogat2* mRNA expression were not significantly different among diets (Figure 2.IJ, Data Supplement).

Figure 2.5 Nobiletin attenuates post-prandial lipid accumulation in male but not female Ldlr$^{-/-}$ mice or male wild-type (WT) mice. Lipid tolerance test (LTT) in male and female *Ldlr*$^{-/-}$ mice with P407; male mice received a gavage of olive oil containing [^{3}H]triolein. (A) Distribution of [^{3}H]triolein uptake or (B) triglyceride (TG) mass along the small intestine axis from pylorus to the ileocecal junction 2-h post-gavage and area under the curve (AUC) calculations in male *Ldlr*$^{-/-}$ mice (n=7–8/group) and (C) in the jejunum of female *Ldlr*$^{-/-}$ mice. (D) Representative paraphenylenediamine-stained micrographs of jejunal segments (2-h post-gavage); arrows point to lipid droplets. (E) Representative electron micrographs of jejunal segments (n=2/group; 2-h post-gavage); stars indicate cytoplasmic lipid droplets. LTT in male WT mice with P407 and olive oil containing BODIPY-C16 fatty acid (FA). (F) Representative images of jejunal sections 2-h post-gavage visualizing BODIPY-labeled lipid droplets, DAPI-stained-nuclei, and tissue autofluorescence (orange). (G) Quantification of lipid droplet area in jejunal epithelium (n=3–4). (H) Post-prandial jejunal expression of *Srebf1c*, (I) *Plin2*, (J) *Atgl* mRNA in male and female *Ldlr*$^{-/-}$ mice and male WT mice. Values are mean±SEM. ANOVA with post hoc Tukey test was used to calculate statistical significance and p-values are labeled in each graph when appropriate. HFHC indicates high-fat, high-cholesterol; NS, non significant; and SLD, standard laboratory diet.

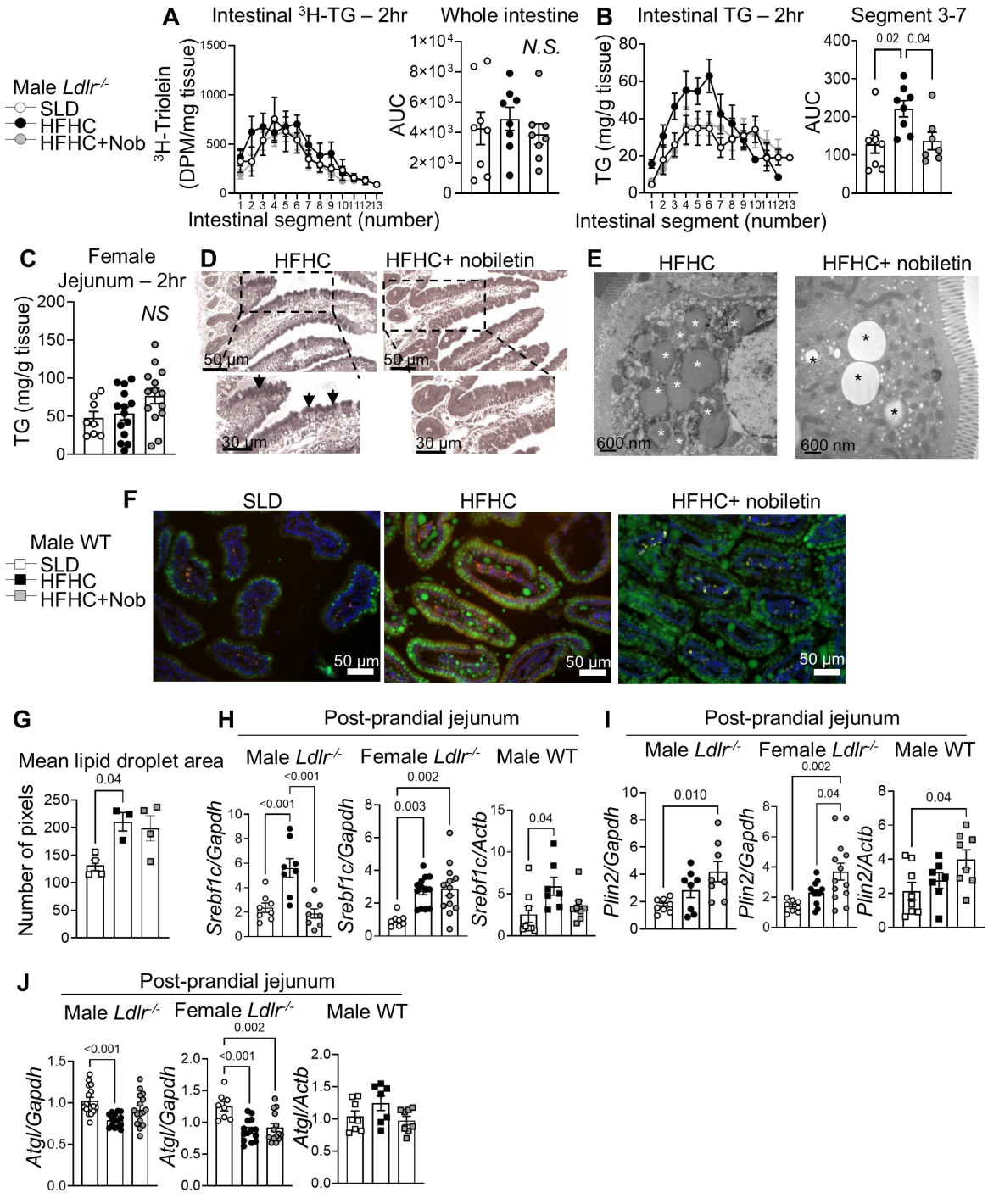
A
Intestinal ^{3}H-TG – 2hr
Whole intestine
Male *Ldlr*$^{-/-}$
SLD
HFHC
HFHC+Nob
^{3}H-Triolein (DPM/mg tissue)
Intestinal segment (number)
AUC
N.S.
B
Intestinal TG – 2hr
Segment 3-7
TG (mg/g tissue)
0.02
0.04
C
Female
Jejunum – 2hr
NS
D
HFHC
HFHC+ nobiletin
50 μm
30 μm
E
HFHC
HFHC+ nobiletin
600 nm
F
SLD
HFHC
HFHC+ nobiletin
Male WT
SLD
HFHC
HFHC+Nob
50 μm
G
Mean lipid droplet area
Number of pixels
0.04
H
Post-prandial jejunum
Male *Ldlr*$^{-/-}$
Female *Ldlr*$^{-/-}$
Male WT
Srebf1c/Gapdh
Srebf1c/Actb
<0.001
0.002
0.003
0.04
I
Post-prandial jejunum
Male *Ldlr*$^{-/-}$
Female *Ldlr*$^{-/-}$
Male WT
Plin2/Gapdh
Plin2/Actb
0.010
0.002
0.04
J
Post-prandial jejunum
Male *Ldlr*$^{-/-}$
Female *Ldlr*$^{-/-}$
Male WT
Atgl/Gapdh
Atgl/Actb
<0.001
0.002

2.4.6 Nobiletin does not attenuate fasting lipid accumulation by increasing FA oxidation.

Consistent with the time-course shown in Figure 1 and previous results (Mulvihill, Assini et al. 2011), at 6h of fasting, representative oil-red-O staining of jejunal sections reveal marked neutral lipid accumulation in male *Ldlr*$^{-/-}$ HFHC-fed mice but not in SLD-fed or nobiletin-treated mice (Figure 2.6A). Nobiletin treatment led to lower fasting jejunal triglyceride in male (significantly) and female (trend, p=0.0628) *Ldlr*$^{-/-}$ mice compared to mice fed the HFHC diet alone (Figure 2.6B,C). HFHC feeding led to significantly higher fasting jejunal cholesteryl ester (CE) in male (~5-fold) and female (~1.7-fold) *Ldlr*$^{-/-}$ mice compared to SLD-fed mice, which was significantly reduced by nobiletin treatment but only in male *Ldlr*$^{-/-}$ mice (Figure 2.6D,E). Nobiletin reduces HFHC diet-induced hepatic triglyceride mass by increasing FA oxidation in the liver (Mulvihill, Assini et al. 2011). To determine if nobiletin attenuates intestinal lipid accumulation in male *Ldlr*$^{-/-}$ mice through a similar mechanism, jejunal FA oxidation was measured *ex vivo.* Jejunal FA oxidation was significantly higher in both HFHC-fed and nobiletin-treated *Ldlr*$^{-/-}$ male mice compared to SLD-fed controls (Figure 2.6F,G). In *Ldlr*$^{-/-}$ male mice, fasting (6h) jejunal mRNA expression of genes related to FA oxidation, *Cpt1α, Acox1,* and *Atgl* mRNA were not significantly different among diet groups (Figure 2.6H). Jejunal *Plin2* mRNA was significantly higher in fasted HFHC-fed and nobiletin-treated mice compared to SLD-fed controls (Figure 2.6H). Nobiletin treatment led to significantly higher *Dgat2* mRNA expression compared to both HFHC- and SLD-fed mice, whereas no significant differences in mRNA expression of other lipid synthesis genes such as *Fasn, Cd36, Dgat1*, and *Mttp* were observed among groups (Figure 2.6H).

Figure 2.6 Nobiletin prevents high-fat, high-cholesterol (HFHC) diet-induced jejunal lipid accumulation in Ldlr$^{-/-}$ mice independent of fatty acid (FA) oxidation. Mice were fasted for 6 h. (A) Representative Oil-Red-O staining of jejunal sections in male *Ldlr*$^{-/-}$ mice. Jejunal triglyceride (TG) mass in (B) male (n=13–14/group) and (C) female *Ldlr*$^{-/-}$ mice (n=6–8/group). Jejunal cholesteryl ester (CE) mass in (D) male and (E) female *Ldlr*$^{-/-}$ mice. Jejunal FA oxidation was assessed in male *Ldlr*$^{-/-}$ mice by measuring (F) 14CO2 released and (G) acid soluble metabolites (n=7–8/group). (H) Fasting jejunal mRNA expression of *Cpt1α*, *Acox1*, *Atgl*, *Plin2*, *Dgat2*, *Fasn*, *Cd36*, *Dgat1*, and *Mttp* (n=4/group). Values are mean±SEM. ANOVA with post hoc Tukey test was used to calculate statistical significance and p-values are labeled in each graph when appropriate. SLD indicates standard laboratory diet.

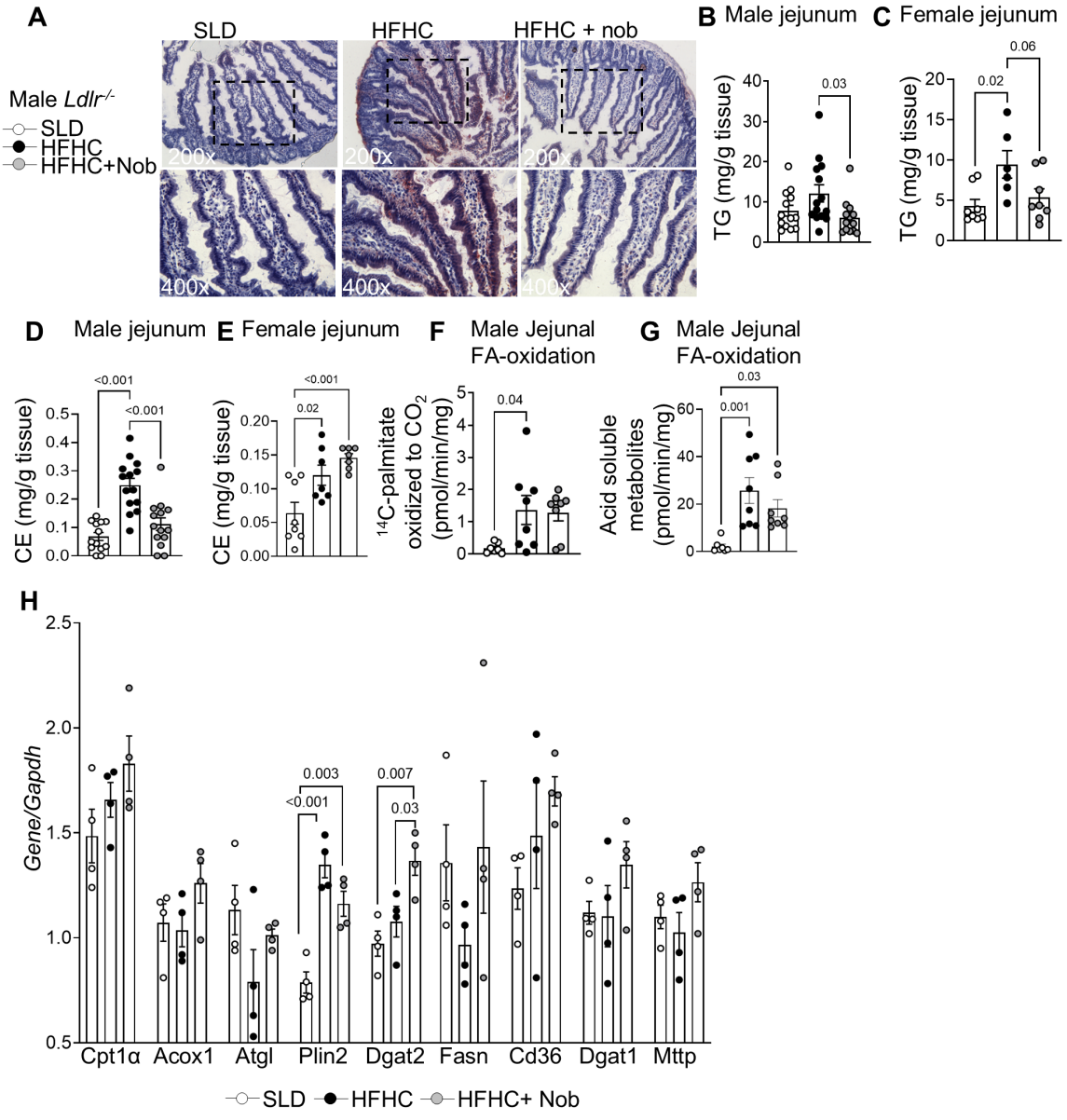
A
SLD
HFHC
HFHC + nob
Male Ldlr-/-
SLD
HFHC
HFHC+Nob
200x
400x
B Male jejunum
TG (mg/g tissue)
0.03
C Female jejunum
TG (mg/g tissue)
0.02
0.06
D Male jejunum
CE (mg/g tissue)
<0.001
<0.001
E Female jejunum
CE (mg/g tissue)
<0.001
0.02
F Male Jejunal FA-oxidation
14C-palmitate oxidized to CO2 (pmol/min/mg)
0.04
G Male Jejunal FA-oxidation
Acid soluble metabolites (pmol/min/mg)
0.03
0.001
H
Gene/Gapdh
0.003
<0.001
0.007
0.03
Cpt1α
Acox1
Atgl
Plin2
Dgat2
Fasn
Cd36
Dgat1
Mttp
SLD
HFHC
HFHC+ Nob

2.4.7 Nobiletin improves intestinal insulin signalling in *Ldlr*$^{-/-}$ mice and decreases *de novo* lipogenesis.

To determine if intestinal insulin resistance contributes to the observed intestinal lipid accumulation in HFHC-fed male *Ldlr*$^{-/-}$ mice, we assessed intestinal insulin signalling in response to physiological insulin using a 6h fasting, 2h refeeding protocol. Plasma insulin increased in all groups upon refeeding and to a greater extent in nobiletin-treated mice compared to SLD- and HFHC-fed mice (Figure 2.7A). Nobiletin led to significantly lower fasting plasma NEFA compared to HFHC-fed mice (Figure 2.7B). In HFHC-fed mice, refeeding failed to suppress plasma NEFA, whereas with nobiletin, NEFA suppression was similar to levels observed in SLD-fed mice (Figure 2.7B). Jejunal AKT phosphorylation increased in all groups with refeeding, and to a greater extent with nobiletin treatment compared to HFHC-fed mice, consistent with nobiletin's insulin-sensitizing properties (Figure 2.7C). Jejunal FOXO1 phosphorylation did not significantly change in SLD-fed or HFHC-fed mice with refeeding (Figure 2.7D). In contrast, HFHC+nobiletin refeeding significantly increased jejunal FOXO1 phosphorylation from baseline (Figure 2.7D). Both fasting and refeeding mTORC1 phosphorylation levels were not significantly different among diet groups (Figure 2.7E). However, the mRNA expression of a downstream target of mTORC1, *Srebf1-c*, increased significantly with refeeding in both HFHC-fed and nobiletin-treated mice (Figure 2.7F), however, the increase with nobiletin was significantly attenuated compared to HFHC alone (Figure 2.7F). HFHC-feeding led to significantly higher jejunal FA synthesis 1.6-fold compared to SLD in male mice (Figure 2.7G), which was significantly attenuated by nobiletin. Jejunal triglyceride synthesis, evaluated *ex vivo,* was significantly higher in both HFHC-fed and nobiletin-treated mice compared to that in SLD fed-mice (Figure 2.7H). In female *Ldlr*$^{-/-}$ mice, there was no significant difference in jejunal triglyceride synthesis capacity among diet groups (Figure 2.7I). Collectively, these results suggest that in male *Ldlr*$^{-/-}$ mice nobiletin enhances intestinal insulin sensitivity to reduce *Srebf-1c*-mediated jejunal FA synthesis.

Figure 2.7 Nobiletin improves dysregulated intestinal insulin signaling. Male Ldlr$^{-/-}$ mice were fasted for 6 h and euthanized in the fasted (F) or 2 h after refeeding (RF) their respective diets. Plasma (A) insulin and (B) nonesterified fatty acid (NEFA) levels (n=8/group). Jejunal (C), AKT (D) FoxO1 (forkhead box O1), and (E) mTORC1 (mammalian target of rapamycin complex 1) presented as a ratio of phosphorylated to total protein (n=8/group). (F) Jejunal Srebf1c expression (n=7–8/group). (G) Jejunal FA synthesis, determined by measuring 14C-acetic acid incorporation into FA (n=8/group). Jejunal triglyceride (TG) synthesis, determined by 14C-oleate incorporation (n=8/group) in (H) male and (I) female *Ldlr*$^{-/-}$ mice. Values are mean±SEM. ANOVA with post hoc Tukey test was used to calculate statistical significance, and p-values are labeled in each graph when appropriate. HFHC indicates high-fat, high-cholesterol; NS indicates nonsignificant; and SLD, standard laboratory diet.

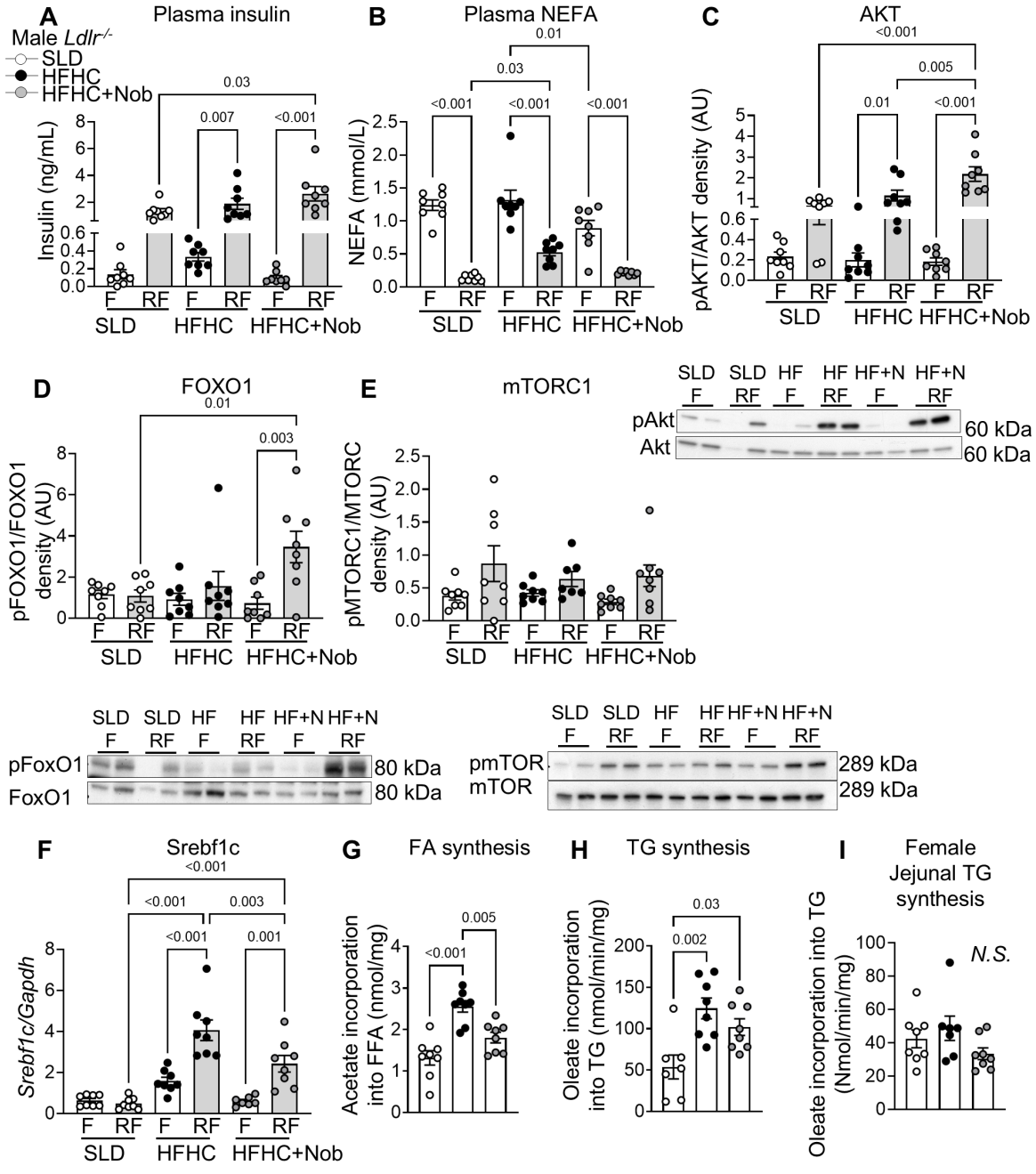
A
Plasma insulin
Male Ldlr-/-
SLD
HFHC
HFHC+Nob
Insulin (ng/mL)
0.03
0.007
<0.001
F RF F RF F RF
SLD HFHC HFHC+Nob
B
Plasma NEFA
NEFA (mmol/L)
0.01
0.03
<0.001
<0.001
<0.001
C
AKT
pAKT/AKT density (AU)
<0.001
0.005
0.01
<0.001
D
FOXO1
pFOXO1/FOXO1 density (AU)
0.01
0.003
E
mTORC1
pMTORC1/MTORC density (AU)
SLD SLD HF HF HF+N HF+N
F RF F RF F RF
pAkt
Akt
60 kDa
60 kDa
pFoxO1
FoxO1
80 kDa
80 kDa
pmTOR
mTOR
289 kDa
289 kDa
F
Srebf1c
Srebf1c/Gapdh
<0.001
<0.001
0.003
<0.001
0.001
G
FA synthesis
Acetate incorporation into FFA (nmol/mg)
<0.001
0.005
H
TG synthesis
Oleate incorporation into TG (nmol/min/mg)
0.03
0.002
I
Female Jejunal TG synthesis
Oleate incorporation into TG (Nmol/min/mg)
N.S.

2.4.8 Nobiletin prevents HFHC diet-induced shortening of the small intestine and increases plasma GLP-1.

We next evaluated nobiletin as a nutritional signal to increase the secretion of gut hormones that also regulate intestinal lipid metabolism (Mulvihill 2018), namely, glucagon-like peptides 1 (GLP-1) and GLP-2. Reliable assays for plasma GLP-2 in mice are not currently available (Drucker, Habener et al. 2017). However, as GLP-1 and GLP-2 are processing products of the same gene, an increase in plasma GLP-1 is likely accompanied by increased GLP-2. In male *Ldlr*$^{-/-}$ mice, total plasma GLP-1 increased significantly 10min post-oil in all diet groups, however, absolute levels were significantly greater with nobiletin (Figure 2.8A). In female *Ldlr*$^{-/-}$ mice, fasting plasma GLP-1 was not different (Figure 2.8B). As previously reported (Soares, Beraldi et al. 2015, Tanaka, Nemoto et al. 2020), HFHC-feeding significantly reduced small intestinal weight in male and female *Ldlr*$^{-/-}$ mice, which was prevented with nobiletin treatment (Figure 2.8C,D), consistent with increased GLP-1 (Koehler, Baggio et al. 2015) and/or GLP-2 intestinotrophic action(Drucker and Yusta 2014). HFHC-feeding significantly shortened small intestinal length (Figure 2.8E,F), whereas nobiletin attenuated this shortening in both sexes in *Ldlr*$^{-/-}$ mice (Figure 2.8E,F,G). In male WT mice, plasma active GLP-1 significantly increased in both HFHC-fed and nobiletin-treated mice post-oil, however, no significant differences in absolute levels were observed (Figure 2.8H). HFHC-feeding also shortened the small intestinal length of male WT mice (Figure 2.8I) and displayed a non-significant ($p=0.07$) trend for increased jejunal villi length (Figure 2.8J). Overall, these data suggested increased GLP-1 and/or GLP-2 as a potential mechanism of nobiletin-treatment. Since nobiletin treatment enhanced intestinal-triglyceride secretion in male *Ldlr*$^{-/-}$ mice, and that GLP-2R signalling also enhances dietary triglyceride mobilization (Stahel, Xiao et al. 2019), we hypothesized that nobiletin increased TRL secretion in a GLP-2-dependent manner.

Figure 2.8 Nobiletin increases plasma GLP-1 (glucagon-like peptide-1) and improves physical gut parameters in male and female Ldlr$^{-/-}$ mice and in male wild-type (WT) mice. Plasma GLP-1 was measured following a 6-h fast (0) and 10-min postoil gavage (10), and the difference from baseline was calculated (Δ) in (A) male *Ldlr*$^{-/-}$ mice (n=12–14/time point). Fasting (6 h) GLP-1 was measured in (B) female *Ldlr*$^{-/-}$ mice (n=6–9/group). Small intestinal weight in (C) male and (D) female *Ldlr*$^{-/-}$ mice (n=14–20/group). Small intestinal length in (E) male (F) female *Ldlr*$^{-/-}$ mice. (G) Representative images of small intestines from male *Ldlr*$^{-/-}$ mice. (H) Active GLP-1 in plasma from fasting blood samples (6 h) and 10-min postgavage in male WT mice (n=8/group). Small intestinal (I) length and (J) jejunal villi length in male WT mice. Values are mean±SEM. ANOVA with post hoc Tukey test was used to calculate statistical significance, and p-values are labeled in each graph when appropriate. HFHC indicates high-fat, high-cholesterol; NS, non significant; and SLD, standard laboratory diet.

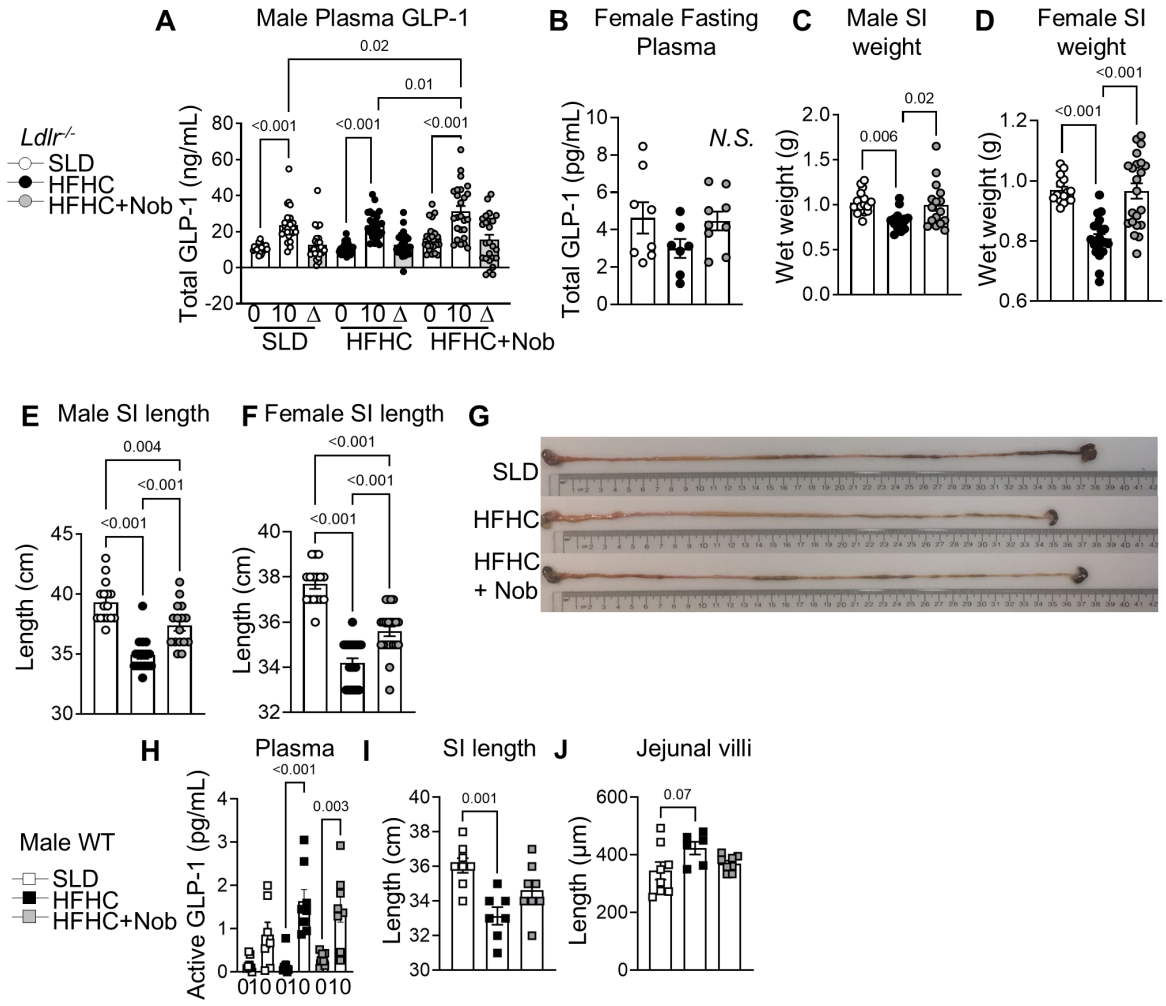
A
Male Plasma GLP-1
Ldlr-/-
SLD
HFHC
HFHC+Nob
Total GLP-1 (ng/mL)
0.02
0.01
<0.001
<0.001
<0.001
0 10 Δ 0 10 Δ 0 10 Δ
SLD
HFHC
HFHC+Nob
B
Female Fasting Plasma
Total GLP-1 (pg/mL)
N.S.
C
Male SI weight
Wet weight (g)
0.006
0.02
D
Female SI weight
Wet weight (g)
<0.001
<0.001
E
Male SI length
Length (cm)
0.004
<0.001
<0.001
F
Female SI length
Length (cm)
<0.001
<0.001
<0.001
G
SLD
HFHC
HFHC + Nob
H
Plasma
Male WT
SLD
HFHC
HFHC+Nob
Active GLP-1 (pg/mL)
<0.001
0.003
010 010 010
I
SI length
Length (cm)
0.001
J
Jejunal villi
Length (μm)
0.07

2.4.9 Nobiletin does not require intact GLP-2R signalling to increase the rate of intestinal triglyceride secretion.

To determine if nobiletin enhanced endogenous GLP-2R signalling, two dietary groups of male *Ldlr*$^{-/-}$ mice were treated with the GLP-2R antagonist, GLP-2 (3-33), or PBS for 14-days. GLP-2 (3-33) did not affect body weight (Figure 2-2A,B, Data Supplement). GLP-2(3-33) reduced jejunal villi length in HFHC-fed mice compared to PBS controls (Figure 2-2C, Data Supplement), as previously reported (Baldassano, Amato et al. 2013), suggesting that the GLP-2(3-33) was systemically active. GLP-2(3-33) did not change jejunal villi length in nobiletin-treated mice compared to PBS controls (Figure 2-2C, Data Supplement). GLP-2(3-33), previously shown to worsen hepatic steatosis (Baldassano, Amato et al. 2016) led to higher hepatic triglyceride mass in HFHC-fed mice and nobiletin-treated mice, but not significantly, and did not affect hepatic CE or free cholesterol (Figure 2-2D, E,F, Data supplement). Upon LTT with P407 treatment, nobiletin led to significantly greater chylomicron-triglyceride secretion compared to SLD-fed mice and HFHC-fed mice, but this difference was lost with GLP-2(3-33) treatment (Figure 2.9A). Nobiletin led to significantly greater VLDL-triglyceride secretion compared to HFHC-fed mice, but this difference was lost with GLP-2(3-33) treatment (Figure 2.9B). GLP-2(3-33) treatment did not significantly change fasting or post-prandial chylomicron-apoB48 levels within diet groups (Figure 2.9C). GLP-2(3-33) did not impact nobiletin's ability to reduce post-prandial jejunal triglyceride mass and increase small intestinal length (Figure 2.9D,E). However, the diet-induced differences in small intestinal weight were lost (Figure 2.9F). Collectively, these results suggest that 14-days of GLP-2R antagonism did not significantly impact post-prandial hepatic, intestinal, or plasma lipid metabolism in male *Ldlr*$^{-/-}$ mice.

To evaluate the requirement for proglucagon peptide signalling pathways for nobiletin to improve intestinal lipid metabolism in WT male mice, we treated HFHC-fed *Glp1r*$^{-/-}$*Glp2r*$^{-/-}$

(GLPDRKO) male mice with nobiletin. Before HFHC-feeding, GLPDRKO mice on a SLD displayed a trend for elevated intestinal-triglyceride secretion compared to WT controls (Figure 2.9G). GLPDRKO displayed worsened glucose tolerance compared to HFHC-fed WT mice, which was significantly improved by nobiletin (Figure 2-2G, Data Supplement). Nobiletin attenuated HFHC diet-induced weight gain and adiposity in WT (significantly) and GLPDRKO mice (trend) (Figure 2-2H,I Data Supplement). Jejunal expression of *Glp2r* and *Glp1r* were low or undetectable in this model (Figure 2.9H,I), confirming the knockout. Mice were challenged to an LTT, where the responses were similar between diet groups or genotypes (Figure 2.9J). Nobiletin treatment trended to enhanced gastric emptying, independent of GLP-1R/GLP-2R signalling (Figure 2.9L). Loss of GLP-1R/GLP-2R signalling shortened jejunal villi length and enhanced intestinal length, independent of nobiletin treatment (Figure 2.9L,M). Overall, these data suggest that in *Ldlr*$^{-/-}$ or WT mice nobiletin treatment does not require GLP-1R or GLP-2R signalling to prevent HFHC-induced metabolic dysregulation.

Figure 2.9 Nobiletin does not require intact GLP-1R (glucagon-like peptide-1 receptor) or GLP-2R signaling to increase the rate of chylomicron-triglyceride (TG) secretion. Male *Ldlr*$^{-/-}$ mice were fed a standard laboratory diet (SLD), high-fat, high-cholesterol (HFHC), or HFHC+nobiletin diet for 10 wk (n=16/group) and then treated with GLP-2(3-33) (30 ng) or PBS for 14 d. Lipid tolerance test (LTT) with P407 where fasting plasma was pooled and mice were euthanized 2-h postoil for plasma ultracentrifugation. (A) Chylomicron-TG secretion with area under the curve (AUC). (B) VLDL (Very-low-density lipoprotein)-TG secretion with AUC calculations (n=7–8/group). (C) Chylomicron-apoB48 signal and difference from baseline (Δ; n=3–5/time point). (D) Jejunal TG mass 2-h postgavage (n=7–8/group). Small intestinal (E) length and (F) weight (n=8/group). LTT in SLD-fed male *Glp1r*$^{-/-}$*Glp2r*$^{-/-}$ (GLPDRKO) mice and WT controls (n=7–9/group). (G) Plasma TG with AUC calculations. Mice were fed a HFHC diet for 10 wk. Jejunal expression of (H) Glp2r and (I) Glp1r mRNA. LTT in HFHC-fed mice with acetaminophen. (J) Plasma TG with AUC calculations. (K) Plasma acetaminophen with AUC calculations. (L) Jejunal villi length. (M) Small intestinal length. Values are mean±SEM. ANOVA with post hoc Tukey test was used to calculate statistical significance, and p-values are labeled in each graph when appropriate. NS indicates nonsignificant.

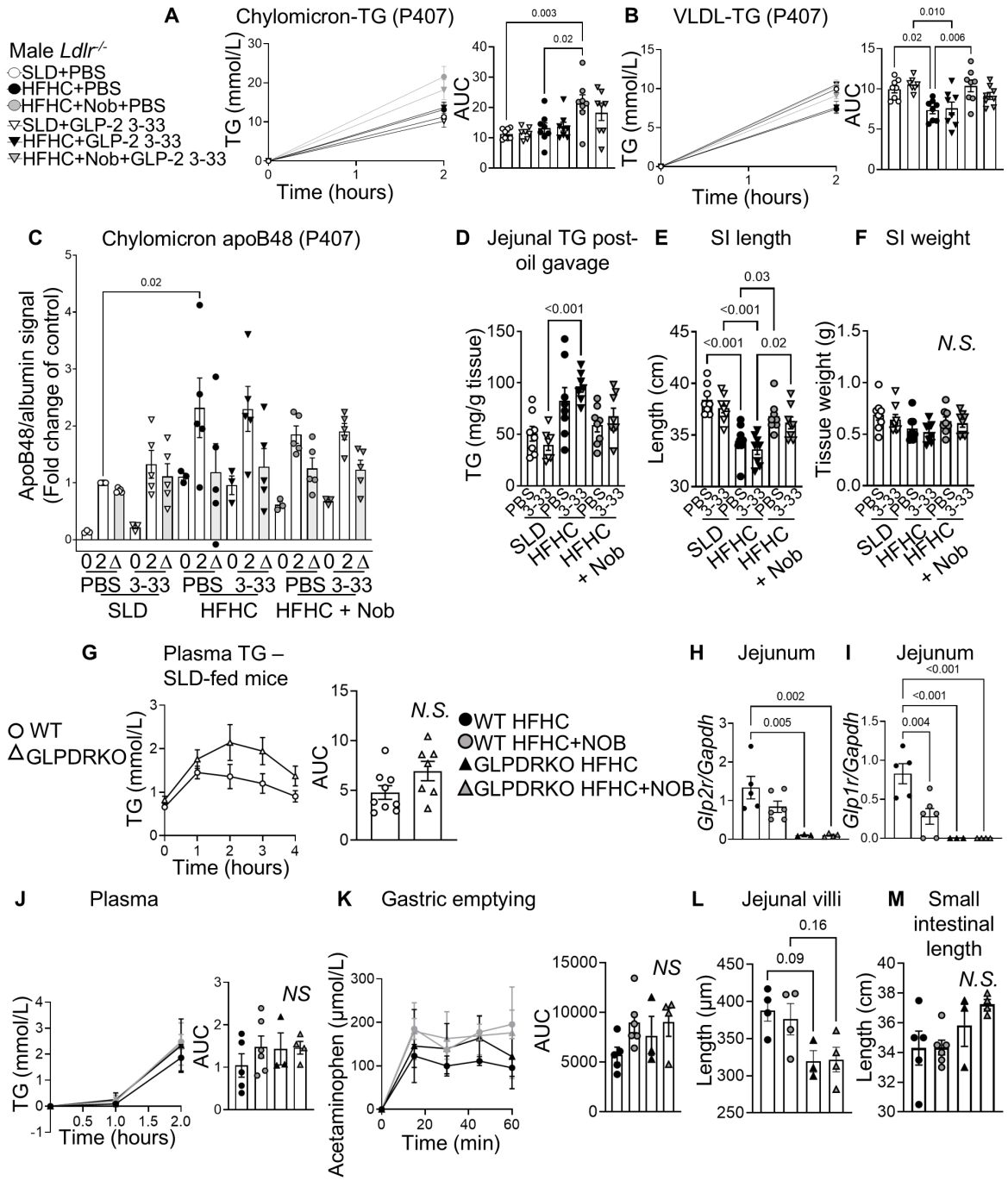
A
Chylomicron-TG (P407)
Male Ldlr-/-
SLD+PBS
HFHC+PBS
HFHC+Nob+PBS
SLD+GLP-2 3-33
HFHC+GLP-2 3-33
HFHC+Nob+GLP-2 3-33
TG (mmol/L)
Time (hours)
AUC
0.003
0.02
B
VLDL-TG (P407)
TG (mmol/L)
Time (hours)
AUC
0.010
0.02
0.006
C
Chylomicron apoB48 (P407)
ApoB48/albumin signal (Fold change of control)
0.02
0 2 Δ 0 2 Δ 0 2 Δ 0 2 Δ 0 2 Δ 0 2 Δ
PBS 3-33 PBS 3-33 PBS 3-33
SLD HFHC HFHC + Nob
D
Jejunal TG post-oil gavage
TG (mg/g tissue)
<0.001
PBS 3-33 PBS 3-33 PBS 3-33
SLD HFHC HFHC + Nob
E
SI length
Length (cm)
0.03
<0.001
<0.001
0.02
PBS 3-33 PBS 3-33 PBS 3-33
SLD HFHC HFHC + Nob
F
SI weight
Tissue weight (g)
N.S.
PBS 3-33 PBS 3-33 PBS 3-33
SLD HFHC HFHC + Nob
G
Plasma TG – SLD-fed mice
O WT
Δ GLPDRKO
TG (mmol/L)
Time (hours)
AUC
N.S.
WT HFHC
WT HFHC+NOB
GLPDRKO HFHC
GLPDRKO HFHC+NOB
H
Jejunum
Glp2r/Gapdh
0.002
0.005
I
Jejunum
Glp1r/Gapdh
<0.001
<0.001
0.004
J
Plasma
TG (mmol/L)
Time (hours)
AUC
NS
K
Gastric emptying
Acetaminophen (μmol/L)
Time (min)
AUC
NS
L
Jejunal villi
Length (μm)
0.16
0.09
M
Small intestinal length
Length (cm)
N.S.

2.5 Discussion

Previous studies have demonstrated that nobiletin lowered fasting plasma triglyceride levels through reduced apoB-VLDL secretion, restored hepatic insulin sensitivity, reduced hepatic FA synthesis, enhanced hepatic FA oxidation, and prevented HFHC diet-induced body weight gain in male WT mice (Lee, Cha et al. 2013, He, Nohara et al. 2016, Kim, Choi et al. 2017, Morrow, Burke et al. 2020) and male *Ldlr*$^{-/-}$ mice (Mulvihill, Assini et al. 2011) as well as atherosclerosis in male *Ldlr*$^{-/-}$ mice (Mulvihill, Assini et al. 2011, Burke, Sutherland et al. 2018). Given the renewed appreciation for TRL to contribute atherogenesis, we sought to evaluate the effect of nobiletin on intestinal TRL metabolism in both *Ldlr*$^{-/-}$ and WT mice. In the present study, HFHC-feeding in male *Ldlr*$^{-/-}$ mice reduced intestinal insulin sensitivity leading to enhanced intestinal *de novo* lipogenesis, which, together with dietary lipids, led to greater triglyceride storage resulting in prolonged post-prandial lipemia. The addition of nobiletin to the HFHC diet in male *Ldlr*$^{-/-}$ mice improved intestinal insulin sensitivity, attenuated *de novo* synthesis pathways, promoting efficient dietary triglyceride excursion from the intestine into plasma. Correspondingly, we observed a shortened period of post-prandial lipemia with nobiletin-treatment compared to *Ldlr*$^{-/-}$mice fed the HFHC diet alone, which may contribute to nobiletin's protection from atherosclerosis. Many of these results were reproduced in male WT mice but not in female *Ldlr*$^{-/-}$ mice (Table 1, Data Supplement).

Studies in humans and hamsters reveal an over-production of apoB48-containing particles in the context of insulin resistance (Haidari, Leung et al. 2002, Federico, Naples et al. 2006, Adeli and Lewis 2008). In HFHC-fed *Ldlr*$^{-/-}$ mice, higher post-prandial plasma apoB48 was only observed 4h post-gavage. Several studies indicate a delayed intestinal-triglyceride secretion rate in diet-induced obese mice (Douglass, Malik et al. 2012, Uchida, Whitsitt et al. 2012), which we now demonstrate is prevented by nobiletin. Despite this nobiletin-enhanced excursion, we did not detect a difference in plasma apoB48 secretion compared to HFHC alone. This data suggested

that the same number of particles are secreted and our triglyceride:apoB48 ratio analyses revealed that nobiletin treatment leads to a greater amount of triglyceride per intestinal lipoprotein particle compared to HFHC-fed mice. The VLDL fraction, post-gavage, was assumed to be predominantly intestinally derived, by the rapid rise in plasma VLDL-triglyceride following the oil gavage. However, a noted limitation of our study is unlike hamster models, we cannot differentiate the origin of apoB48 as hepatic or enterocyte in mice (Haidari, Leung et al. 2002). Nevertheless, we have previously shown that nobiletin decreased the fasting VLDL-triglyceride secretion rate to less than 1 mmol/L/h (Mulvihill, Assini et al. 2011), representing <20% of the post-oil gavage VLDL-triglyceride secretion rate observed in the present study.

In our HFHC-fed WT mice, however, higher plasma apoB48 was observed at 2h and 4h post-gavage compared to nobiletin-treated mice and SLD-controls. Still, nobiletin treatment led to enhanced intestinal-triglyceride secretion, suggesting a possible dysregulation of the LDLR with HFHC-feeding that is prevented by nobiletin. Indeed, basolateral re-uptake of chylomicrons via the LDLR has been shown in enterocytes; a process inhibited by apoC-III (Li, Rodia et al. 2019). While we did not measure circulating apoC-III, we did observe a significantly higher mRNA expression of jejunal *Apoc3* in HFHC-fed WT mice that was prevented by nobiletin. Whether enhanced post-prandial chylomicron secretion contributes to nobiletin's ability to prevent diet-induced obesity or is secondary to weight gain prevention could not be deduced from this study. Moreover, whether HFHC diet-induced changes in intestinal-triglyceride secretion rates correspond to structural changes in the small intestine (longer villi and shorter gut length) requires further investigation, particularly given that nobiletin-treatment attenuates these changes.

The peak post-prandial triglyceride levels with nobiletin, which occurred 1h earlier compared to HFHC-fed mice, were consistent with measures of enhanced triglyceride clearance in nobiletin-treated mice. Enhanced LPL-activity has been reported in Western-diet fed *Ldlr* $^{-/-}$ supplemented with the citrus flavonoid naringenin (Mulvihill, Allister et al. 2009). While our study

did not directly measure LPL-activity, VLDL and chylomicrons compete for LPL-mediated hydrolysis, where the latter is the preferred substrate due to their greater size (Julve, Martin-Campos et al. 2016). In WT mice, nobiletin treatment enhanced the clearance of injected chylomicrons. Therefore, the delayed, yet prolonged chylomicron secretion exhibited by HFHC-fed mice likely extends the retention of hepatic and/or intestinal VLDL-sized particles in the circulation. Conversely, the accelerated gastric emptying, efficient intestinal-triglyceride secretion, together with enhanced triglyceride clearance in nobiletin-treated mice suggests improved systemic energy utilization resulting in lower fasting plasma triglyceride.

HFHC-fed mice accumulated jejunal triglyceride in the fed state, which eventually cleared after 9h of fasting. We previously reported that nobiletin significantly reduced fasting liver and jejunal triglyceride; importantly, these studies demonstrated that caloric intake and intestinal triglyceride absorption were not affected by nobiletin (Mulvihill, Assini et al. 2011). The present study demonstrated that nobiletin-treated mice do not accumulate jejunal triglyceride more than SLD-fed mice, even in the fed state. Despite the limited jejunal triglyceride storage, nobiletin enhanced *Plin2* mRNA expression in all models tested compared to HFHC-fed mice. PLIN2 localization to CLD is a response to chronic high-fat feeding (Lee, Zhu et al. 2009), and in our study, electron micrographs reveal the presence of smaller CLD in nobiletin-treated mice. Furthermore, the consistently higher expression of *Plin2* by nobiletin in all models tested appears to be independent of changes in post-prandial lipid metabolism. Consistent with a previous study (Kondo, Minegishi et al. 2006), we showed that HFHC-fed mice have a greater jejunal FA oxidation capacity compared to SLD-fed mice, which remained high with nobiletin treatment. Therefore, in contrast to the liver, enhanced FA oxidation is not the dominant mechanism for triglyceride reduction in the intestine. Instead, LTT experiments in this study revealed that nobiletin limited intestinal lipid stores by enhancing the rate at which total triglyceride mass (from

stored and acute dietary pools) and radiolabelled-triglyceride (traces only dietary triglyceride) were secreted into plasma compared to HFHC-fed mice.

These studies also assessed the potential for HFHC-induced bifurcation in insulin signalling in the intestine of male *Ldlr* $^{-/-}$ mice, a mechanism well-characterized in the liver (Brown and Goldstein 2008). The insulin-sensitizing properties of nobiletin were apparent in the jejunum with higher levels of phosphorylated AKT and FOXO1 upon refeeding compared to HFHC- and SLD-fed mice. While the relationship between increased intestinal-triglyceride secretion rate and increased FOXO1 phosphorylation is unclear, these data support a different role for FOXO1 in the intestine compared to the liver (Rajas, Bruni et al. 1999). Downstream of mTORC1, improved insulin sensitivity by nobiletin led to lower jejunal *Srebf1-c* mRNA expression in the refed and post-olive oil states compared to HFHC-fed mice, leading to reduced FA synthesis. Nobiletin also reduced NEFA availability, contributing to smaller intestinal triglyceride stores. Despite higher plasma GLP-1, and presumably GLP-2, in nobiletin-treated mice, signaling through GLP-1R or GLP-2R did not significantly impact intestinal-triglyceride secretion or other aspects of metabolic protection, including prevention of HFHC diet-induced shortening of the small intestine. Collectively, these results suggest that the prevention of diet-induced insulin resistance exerted by nobiletin in the atherogenic model of *Ldlr*$^{-/-}$ male mice played an important role in limiting excess FA and triglyceride substrate for intestinal lipid storage and in promoting accelerated TRL secretion.

In summary, nobiletin prevents diet-induced intestinal lipid accumulation in male mice by normalizing *de novo* lipogenesis through improved insulin sensitivity and increases post-prandial TRL-triglyceride intestinal secretion and plasma triglyceride clearance. Furthermore, the nobiletin-induced enhancement of plasma triglyceride clearance more than compensates for the accelerated TRL-triglyceride secretion, resulting in the prevention of post-prandial lipemia which may contribute to the anti-atherogenic effects of nobiletin treatment.

2.6 Acknowledgements

We would like to thank the UWO Biotron for sample preparation, sectioning, staining and electron microscopy, the Molecular Pathology Core Facility at the University of Western Ontario for assistance with histology. M.W.H. and E.E.M are the guarantors of this work and, as such, had full access to all the data in the study and take responsibility for the integrity of the data and the accuracy of the data analysis.

2.7 Sources of Funding

This work was supported by Canadian Institutes of Health Research Grants, ARJ-162628 and Project Grant 156136 to E.E.M., MOP-126045 and MOP-119350 to M.W.H., NSERC grant 551669-152199-2004 to E.E.M. and Heart and Stroke Foundation of Canada Grant G-14-0006179 to M.W.H. E.E.M. is the recipient of a Diabetes Canada New Investigator Award.

2.8 Disclosure

The Mulvihill lab receives funding from the Merck IISP program for pre-clinical studies unrelated to this work. The other authors have no disclosures.

2.9 Supplemental Materials

Supplemental Figure 2-1 Nobiletin prevents HFHC-diet induced weight gain in male and female mice. Male and female Ldlr$^{-/-}$ mice were fed a chow, HFHC, or HFHC + nobiletin diet for 10 weeks. (A) Body weight gain and (B) caloric intake expressed as kcal/mouse/day in male *Ldlr*$^{-/-}$ mice. (C) Body weight gain and (D) caloric intake in female *Ldlr*$^{-/-}$ mice. (E) Hepatic TG mass in female *Ldlr*$^{-/-}$mice (n=7-8/group). (F) Whole intestinal TG mass 4h post-gavageolive-oil gavage in male *Ldlr*$^{-/-}$ mice (n=7-8/group) with AUC calculations on the right. (G) Representative images of jejunal sections 4h post-BODIPY-C16-FA olive-oil gavage visualizing BODIPY-labelled CLD and DAPI-stained-nuclei. (H) Quantification of lipid droplet area in jejunal epithelium (n=3-4/group). (I) Post-prandial expression of jejunal *Cd36, Dgat2*, and *Mttp* mRNA in male *Ldlr*$^{-/-}$ mice. Post-prandial expression of (J) *Apob* (K) *Fabp2*, and (L) *Mogat2* mRNA in male WT mice. Values are the mean±SEM. In (A,C) stars indicate statistical differences between HFHC and HFHC+nob over time by Two-Way ANOVA ($p<0.05$). Values are mean±SEM. In (B,D-G), stars indicate statistical difference between diets by ANOVA with post-hoc Tukey test.

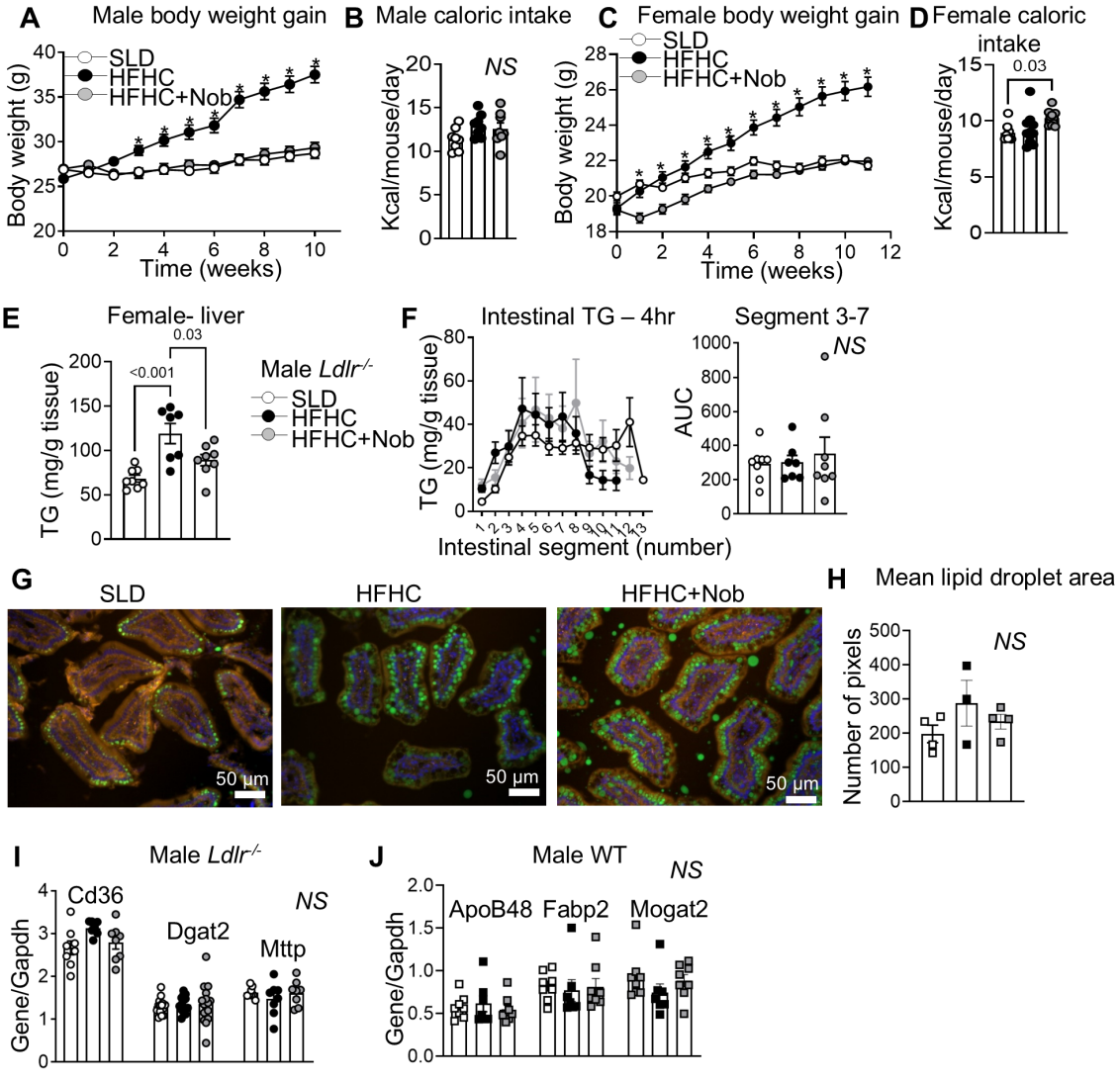
A
Male body weight gain
SLD
HFHC
HFHC+Nob
Body weight (g)
Time (weeks)
B
Male caloric intake
NS
Kcal/mouse/day
C
Female body weight gain
SLD
HFHC
HFHC+Nob
Body weight (g)
Time (weeks)
D
Female caloric intake
0.03
Kcal/mouse/day
E
Female- liver
<0.001
0.03
TG (mg/g tissue)
Male Ldlr-/-
SLD
HFHC
HFHC+Nob
F
Intestinal TG – 4hr
TG (mg/g tissue)
Intestinal segment (number)
Segment 3-7
NS
AUC
G
SLD
HFHC
HFHC+Nob
50 µm
H
Mean lipid droplet area
NS
Number of pixels
I
Male Ldlr-/-
Cd36
Dgat2
Mttp
NS
Gene/Gapdh
J
Male WT
NS
ApoB48
Fabp2
Mogat2
Gene/Gapdh

Supplemental Figure 2-2. Male *Ldlr*$^{-/-}$ mice were fed a SLD, HFHC, or HFHC + nobiletin diet for 10 weeks (n=16/group) then treated with GLP-2(3-33) or PBS (control) for 14d. Body weight gain (A) before and (B) throughout the GLP-2(3-33) treatment period. (C) Jejunal villi length plotted as the mean of ≥16 villi/mouse (n=3-6/group). Hepatic (D) TG and (E) CE and (F) free cholesterol (FC) were quantified following the 14d treatment (n=7-8/treatment group/diet). (G) Oral glucose tolerance in WT and GLPDRKO mice with AUC calculations. Final (H) body weight and (I) epididymal fat weight of WT and GLPDRKO mice. In (A,B) stars indicate statistical differences between HFHC and HFHC+nob over time by Two-Way ANOVA ($p<0.05$). Values are mean±SEM. In (C-F), stars indicate statistical difference between diets by ANOVA with post-hoc Tukey test. In (G) stars on top of symbols indicate statistical difference compared to GLPDRKO nobiletin-treated mice while stars bellow symbols indicate statistical difference compared to WT HFHC-fed mice.

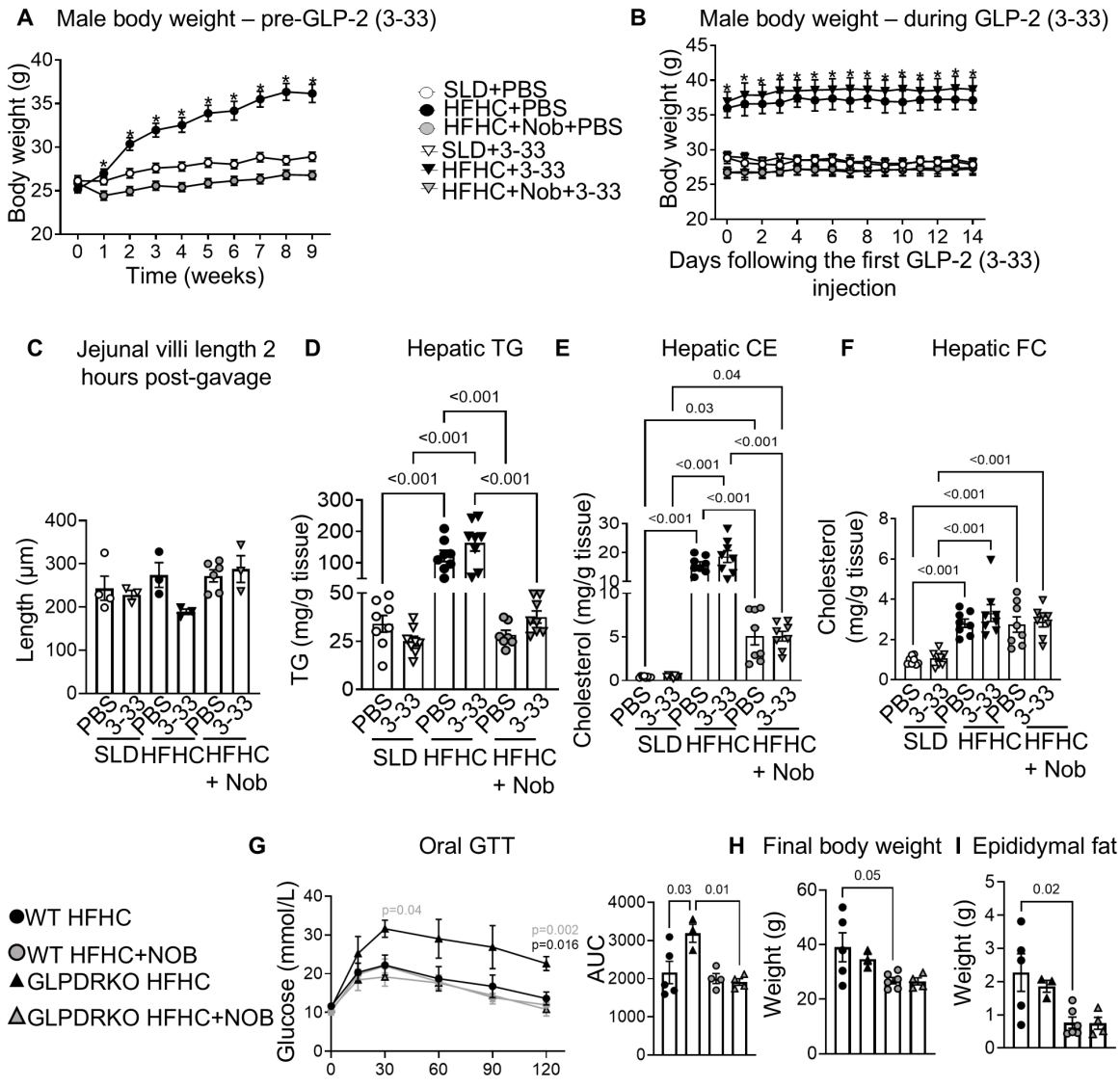
A Male body weight – pre-GLP-2 (3-33)
Body weight (g)
Time (weeks)
SLD+PBS
HFHC+PBS
HFHC+Nob+PBS
SLD+3-33
HFHC+3-33
HFHC+Nob+3-33
B Male body weight – during GLP-2 (3-33)
Body weight (g)
Days following the first GLP-2 (3-33) injection
C Jejunal villi length 2 hours post-gavage
Length (µm)
D Hepatic TG
TG (mg/g tissue)
E Hepatic CE
Cholesterol (mg/g tissue)
F Hepatic FC
Cholesterol (mg/g tissue)
PBS
3-33
SLD
HFHC
HFHC + Nob
G Oral GTT
Glucose (mmol/L)
p=0.04
p=0.002
p=0.016
WT HFHC
WT HFHC+NOB
GLPDRKO HFHC
GLPDRKO HFHC+NOB
H Final body weight
AUC
Weight (g)
I Epididymal fat
Weight (g)

Table 1 Summary of metabolic parameters changed with nobiletin treatment in the current study.

Nobiletin vs HFHC	Male *Ldlr*$^{-/-}$	Female *Ldlr*$^{-/-}$	Male WT
Prevents HFHC diet-induced weight gain	Yes	Yes	Yes
Reduces fasting plasma FPLC VLDL-TG	Yes	Yes but still higher than SLD-controls	No applicable (N/A)
Increases intestinal-TG secretion into plasma	Yes	No	Yes but only 0-2 hours not 0-4 hours
Increases intestinal-TG tracer secretion into plasma	Yes	N/A	No
Increases intestinal apoB48 secretion into plasma	No	N/A	No
Increases chylo-TG secretion	Yes	No	N/A
Increases chylo-TG:B48	Yes	No	N/A
Increases intestinal VLDL-TG secretion	Yes	No	N/A
Increases post-prandial plasma TG clearance rate	Yes	N/A	Yes and ULDL clearance
Reduces 2h post-prandial jejunal TG	Yes	No	No based on CLD analysis
Reduces 4 hour post-gavage jejunal TG	No	N/A	No based on CLD analysis
Reduces jejunal *Srebf1c* mRNA 2 hours post-gavage	Yes	No	No
Increases *Plin2* vs SLD	Yes	Yes and vs HFHC	Yes
Reduces fasting jejunal TG	Yes	Yes	N/A
Reduces fasting jejunal CE	Yes	No	N/A
Increases jejunal TG synthesis vs SLD	Yes	No	N/A
Increases total GLP-1	Yes	Yes (trend fasting)	Trend increased fasting active
Increases small intestinal weight	Yes	Yes	N/A
Increases small intestinal length	Yes	Yes	Yes (trend)
Reduces hepatic TG	N/A	Yes	N/A

2.10 References

Adeli, K. and G. F. Lewis (2008). "Intestinal lipoprotein overproduction in insulin-resistant states." Curr Opin Lipidol **19**(3): 221–228.

Adomshick, V., Y. Pu and A. Veiga-Lopez (2020). "Automated lipid droplet quantification system for phenotypic analysis of adipocytes using CellProfiler." Toxicol Mech Methods **30**(5): 378–387.

Assini, J. M., E. E. Mulvihill, B. G. Sutherland, D. E. Telford, C. G. Sawyez, S. L. Felder, S. Chhoker, J. Y. Edwards, R. Gros and M. W. Huff (2013). "Naringenin prevents cholesterol-induced systemic inflammation, metabolic dysregulation, and atherosclerosis in *Ldlr*(-)/(-) mice." J Lipid Res **54**(3): 711–724.

Baldassano, S., A. Amato, F. Cappello, F. Rappa and F. Mule (2013). "Glucagon-like peptide-2 and mouse intestinal adaptation to a high-fat diet." J Endocrinol **217**(1): 11–20.

Baldassano, S., A. Amato, F. Rappa, F. Cappello and F. Mule (2016). "Influence of endogenous glucagon-like peptide-2 on lipid disorders in mice fed a high-fat diet." Endocr Res **41**(4): 317–324.

Bhatt, D. L., P. G. Steg and M. Miller (2019). "Cardiovascular Risk Reduction with Icosapent Ethyl. Reply." N Engl J Med **380**(17): 1678.

Brown, M. S. and J. L. Goldstein (2008). "Selective versus total insulin resistance: a pathogenic paradox." Cell Metab **7**(2): 95–96.

Burke, A. C., B. G. Sutherland, D. E. Telford, M. R. Morrow, C. G. Sawyez, J. Y. Edwards, M. Drangova and M. W. Huff (2018). "Intervention with citrus flavonoids reverses obesity and improves metabolic syndrome and atherosclerosis in obese *Ldlr*($^{-/-}$) mice." J Lipid Res **59**(9): 1714–1728.

Czech, M. P. (2017). "Insulin action and resistance in obesity and type 2 diabetes." Nat Med **23**(7): 804–814.

D'Aquila, T., Y. H. Hung, A. Carreiro and K. K. Buhman (2016). "Recent discoveries on absorption of dietary fat: Presence, synthesis, and metabolism of cytoplasmic lipid droplets within enterocytes." Biochim Biophys Acta **1861**(8 Pt A): 730–747.

Dalby, M. J., A. W. Ross, A. W. Walker and P. J. Morgan (2017). "Dietary Uncoupling of Gut Microbiota and Energy Harvesting from Obesity and Glucose Tolerance in Mice." Cell Rep **21**(6): 1521–1533.

Douglass, J. D., N. Malik, S. H. Chon, K. Wells, Y. X. Zhou, A. S. Choi, L. B. Joseph and J. Storch (2012). "Intestinal mucosal triacylglycerol accumulation secondary to decreased lipid secretion in obese and high fat fed mice." Front Physiol **3**: 25.

Drucker, D. J., J. F. Habener and J. J. Holst (2017). "Discovery, characterization, and clinical development of the glucagon-like peptides." J Clin Invest **127**(12): 4217–4227.

Drucker, D. J. and B. Yusta (2014). "Physiology and pharmacology of the enteroendocrine hormone glucagon-like peptide-2." Annu Rev Physiol **76**: 561–583.

Duez, H., B. Lamarche, K. D. Uffelman, R. Valero, J. S. Cohn and G. F. Lewis (2006). "Hyperinsulinemia is associated with increased production rate of intestinal apolipoprotein B-48-containing lipoproteins in humans." Arterioscler Thromb Vasc Biol **26**(6): 1357–1363.

Fan, W., S. Philip, C. Granowitz, P. P. Toth and N. D. Wong (2019). "Residual Hypertriglyceridemia and Estimated Atherosclerotic Cardiovascular Disease Risk by Statin Use in U.S. Adults With Diabetes: National Health and Nutrition Examination Survey 2007-2014." Diabetes Care **42**(12): 2307–2314.

Federico, L. M., M. Naples, D. Taylor and K. Adeli (2006). "Intestinal insulin resistance and aberrant production of apolipoprotein B48 lipoproteins in an animal model of insulin resistance and metabolic dyslipidemia: evidence for activation of protein tyrosine phosphatase-1B, extracellular signal-related kinase, and sterol regulatory element-binding protein-1c in the fructose-fed hamster intestine." Diabetes **55**(5): 1316–1326.

Frank, D. N., E. S. Bales, J. Monks, M. J. Jackman, P. S. MacLean, D. Ir, C. E. Robertson, D. J. Orlicky and J. L. McManaman (2015). "Perilipin-2 Modulates Lipid Absorption and Microbiome Responses in the Mouse Intestine." PLoS One **10**(7): e0131944.

Haidari, M., N. Leung, F. Mahbub, K. D. Uffelman, R. Kohen-Avramoglu, G. F. Lewis and K. Adeli (2002). "Fasting and postprandial overproduction of intestinally derived lipoproteins in an animal model of insulin resistance. Evidence that chronic fructose feeding in the hamster is accompanied by enhanced intestinal de novo lipogenesis and ApoB48-containing lipoprotein overproduction." J Biol Chem **277**(35): 31646–31655.

He, B., K. Nohara, N. Park, Y. S. Park, B. Guillory, Z. Zhao, J. M. Garcia, N. Koike, C. C. Lee, J. S. Takahashi, S. H. Yoo and Z. Chen (2016). "The Small Molecule Nobiletin Targets the Molecular Oscillator to Enhance Circadian Rhythms and Protect against Metabolic Syndrome." Cell Metab **23**(4): 610–621.

Hung, Y. H., A. L. Carreiro and K. K. Buhman (2017). "Dgat1 and Dgat2 regulate enterocyte triacylglycerol distribution and alter proteins associated with cytoplasmic lipid droplets in response to dietary fat." Biochim Biophys Acta Mol Cell Biol Lipids **1862**(6): 600–614.

Iqbal, J. and M. M. Hussain (2009). "Intestinal lipid absorption." Am J Physiol Endocrinol Metab **296**(6): E1183–1194.

Julve, J., J. M. Martin-Campos, J. C. Escola-Gil and F. Blanco-Vaca (2016). "Chylomicrons: Advances in biology, pathology, laboratory testing, and therapeutics." Clin Chim Acta **455**: 134–148.

Kim, Y. J., M. S. Choi, J. T. Woo, M. J. Jeong, S. R. Kim and U. J. Jung (2017). "Long-term dietary supplementation with low-dose nobiletin ameliorates hepatic steatosis, insulin resistance, and inflammation without altering fat mass in diet-induced obesity." Mol Nutr Food Res **61**(8).

Koehler, J. A., L. L. Baggio, B. Yusta, C. Longuet, K. J. Rowland, X. Cao, D. Holland, P. L. Brubaker and D. J. Drucker (2015). "GLP-1R agonists promote normal and neoplastic intestinal growth through mechanisms requiring Fgf7." Cell Metab **21**(3): 379–391.

Kondo, H., Y. Minegishi, Y. Komine, T. Mori, I. Matsumoto, K. Abe, I. Tokimitsu, T. Hase and T. Murase (2006). "Differential regulation of intestinal lipid metabolism-related genes in obesity-resistant A/J vs. obesity-prone C57BL/6J mice." Am J Physiol Endocrinol Metab **291**(5): E1092–1099.

Lee, B., J. Zhu, N. E. Wolins, J. X. Cheng and K. K. Buhman (2009). "Differential association of adipophilin and TIP47 proteins with cytoplasmic lipid droplets in mouse enterocytes during dietary fat absorption." Biochim Biophys Acta **1791**(12): 1173–1180.

Lee, S. J., J. Lee, K. K. Li, D. Holland, H. Maughan, D. S. Guttman, B. Yusta and D. J. Drucker (2012). "Disruption of the murine Glp2r impairs Paneth cell function and increases susceptibility to small bowel enteritis." Endocrinology **153**(3): 1141–1151.

Lee, Y. S., B. Y. Cha, S. S. Choi, B. K. Choi, T. Yonezawa, T. Teruya, K. Nagai and J. T. Woo (2013). "Nobiletin improves obesity and insulin resistance in high-fat diet-induced obese mice." J Nutr Biochem **24**(1): 156–162.

Li, D., C. N. Rodia, Z. K. Johnson, M. Bae, A. Muter, A. E. Heussinger, N. Tambini, A. M. Longo, H. Dong, J. Y. Lee and A. B. Kohan (2019). "Intestinal basolateral lipid substrate transport is linked to chylomicron secretion and is regulated by apoC-III." J Lipid Res **60**(9): 1503–1515.

Morrow, N. M., A. C. Burke, J. P. Samsoondar, K. E. Seigel, A. Wang, D. E. Telford, B. G. Sutherland, C. O'Dwyer, G. R. Steinberg, M. D. Fullerton and M. W. Huff (2020). "The citrus flavonoid nobiletin confers protection from metabolic dysregulation in high-fat-fed mice independent of AMPK." J Lipid Res **61**(3): 387–402.

Mulvihill, E. E. (2018). "Regulation of intestinal lipid and lipoprotein metabolism by the proglucagon-derived peptides glucagon like peptide 1 and glucagon like peptide 2." Curr Opin Lipidol **29**(2): 95–103.

Mulvihill, E. E., E. M. Allister, B. G. Sutherland, D. E. Telford, C. G. Sawyez, J. Y. Edwards, J. M. Markle, R. A. Hegele and M. W. Huff (2009). "Naringenin prevents dyslipidemia, apolipoprotein B overproduction, and hyperinsulinemia in LDL receptor-null mice with diet-induced insulin resistance." Diabetes **58**(10): 2198–2210.

Mulvihill, E. E., J. M. Assini, J. K. Lee, E. M. Allister, B. G. Sutherland, J. B. Koppes, C. G. Sawyez, J. Y. Edwards, D. E. Telford, A. Charbonneau, P. St-Pierre, A. Marette and M. W. Huff (2011). "Nobiletin attenuates VLDL overproduction, dyslipidemia, and atherosclerosis in mice with diet-induced insulin resistance." Diabetes **60**(5): 1446–1457.

Mulvihill, E. E., A. C. Burke and M. W. Huff (2016). "Citrus Flavonoids as Regulators of Lipoprotein Metabolism and Atherosclerosis." Annu Rev Nutr **36**: 275–299.

Pavlic, M., C. Xiao, L. Szeto, B. W. Patterson and G. F. Lewis (2010). "Insulin acutely inhibits intestinal lipoprotein secretion in humans in part by suppressing plasma free fatty acids." Diabetes **59**(3): 580–587.

Rajas, F., N. Bruni, S. Montano, C. Zitoun and G. Mithieux (1999). "The glucose-6 phosphatase gene is expressed in human and rat small intestine: regulation of expression in fasted and diabetic rats." Gastroenterology **117**(1): 132–139.

Ramms, B. and P. Gordts (2018). "Apolipoprotein C-III in triglyceride-rich lipoprotein metabolism." Curr Opin Lipidol **29**(3): 171–179.

Sairyo, M., T. Kobayashi, D. Masuda, K. Kanno, Y. Zhu, T. Okada, M. Koseki, T. Ohama, M. Nishida, Y. Sakata and S. Yamashita (2018). "A Novel Selective PPARalpha Modulator (SPPARMalpha), K-877 (Pemafibrate), Attenuates Postprandial Hypertriglyceridemia in Mice." J Atheroscler Thromb **25**(2): 142–152.

Sears, B. and M. Perry (2015). "The role of fatty acids in insulin resistance." Lipids Health Dis **14**: 121.

Shirai, N., F. J. Geoly, W. F. Bobrowski and C. Okerberg (2016). "The Application of Paraphenylenediamine Staining for Assessment of Phospholipidosis." Toxicol Pathol **44**(8): 1160–1165.

Soares, A., E. J. Beraldi, P. E. Ferreira, R. B. Bazotte and N. C. Buttow (2015). "Intestinal and neuronal myenteric adaptations in the small intestine induced by a high-fat diet in mice." BMC Gastroenterol **15**: 3.

Stahel, P., C. Xiao, X. Davis, P. Tso and G. F. Lewis (2019). "Glucose and GLP-2 (Glucagon-Like Peptide-2) Mobilize Intestinal Triglyceride by Distinct Mechanisms." Arterioscler Thromb Vasc Biol **39**(8): 1565–1573.

Tanaka, S., Y. Nemoto, Y. Takei, R. Morikawa, S. Oshima, T. Nagaishi, R. Okamoto, K. Tsuchiya, T. Nakamura, S. Stutte and M. Watanabe (2020). "High-fat diet-derived free fatty acids impair the intestinal immune system and increase sensitivity to intestinal epithelial damage." Biochem Biophys Res Commun **522**(4): 971–977.

Tran, T. T., B. G. Postal, S. Demignot, A. Ribeiro, C. Osinski, J. P. Pais de Barros, A. Blachnio-Zabielska, A. Leturque, M. Rousset, P. Ferre, E. Hajduch and V. Carriere (2016). "Short Term Palmitate Supply Impairs Intestinal Insulin Signaling via Ceramide Production." J Biol Chem **291**(31): 16328–16338.

Uchida, A., M. C. Whitsitt, T. Eustaquio, M. N. Slipchenko, J. F. Leary, J. X. Cheng and K. K. Buhman (2012). "Reduced triglyceride secretion in response to an acute dietary fat challenge in obese compared to lean mice." Front Physiol **3**: 26.

Wu, L. and K. G. Parhofer (2014). "Diabetic dyslipidemia." Metabolism **63**(12): 1469–1479.

Xiao, C., S. Dash, C. Morgantini, R. A. Hegele and G. F. Lewis (2016). "Pharmacological Targeting of the Atherogenic Dyslipidemia Complex: The Next Frontier in CVD Prevention Beyond Lowering LDL Cholesterol." Diabetes **65**(7): 1767–1778.

Zhu, J., B. Lee, K. K. Buhman and J. X. Cheng (2009). "A dynamic, cytoplasmic triacylglycerol pool in enterocytes revealed by ex vivo and in vivo coherent anti-Stokes Raman scattering imaging." J Lipid Res **50**(6): 1080–1089.

Zoltowska, M., E. Ziv, E. Delvin, D. Sinnett, R. Kalman, C. Garofalo, E. Seidman and E. Levy (2003). "Cellular aspects of intestinal lipoprotein assembly in Psammomys obesus: a model of insulin resistance and type 2 diabetes." Diabetes **52**(10): 2539–2545.

Chapter 3 : Adaptation to short-term extreme fat consumption alters intestinal lipid handling in male and female mice

Publication information:

Morrow*, N.M., Locatelli*, C.A.A., Trzaskalski, N.A., Klein, C.T., Hanson, A.A., Alhadi, H., Tripathi, I., Clement, A.C., Imran, S., Lorenzen-Schmidt, I. & Mulvihill, E.E. Adaptation to short-term extreme fat consumption alters intestinal lipid handling in male and female mice. Biochim Biophys Acta Mol Cell Biol Lipids. 2022. Issue 11 Pages 159208. DOI: 10.1016/j.bbalip.2022.159208

*co-first authors

3.1 Abstract

The small intestine is a highly adaptable organ serving as both a barrier to the external environment and a conduit for nutrient absorption. Enterocytes package dietary triglycerides (TG) into chylomicrons for transport into circulation; the remaining TGs are stored in cytosolic lipid droplets (CLDs). The current study aimed to characterize the impact of diet composition on intestinal lipid handling in male and female wild-type mice. Mice were continued on their grain-based diet (GBD) and switched to a high-fat, high-cholesterol Western-style diet (WD) or a ketogenic diet (KD) for 3 or 5 weeks. KD-fed mice displayed significantly higher plasma TG levels in response to an olive oil gavage than WD- and GBD-fed mice; TG levels were ~2-fold higher in male KD-fed mice than female KD-fed mice. Poloxamer-407 experiments revealed enhanced intestinal-TG secretion rates in male mice fed a KD upon olive oil gavage, whereas secretion rates were unchanged in female mice. Surprisingly, jejunal CLD size and TG mass after oil gavage were similar among the groups. At fasting, TG mass was significantly higher in the jejunum of male KD-fed mice and the duodenum of female KD-fed mice, providing increased substrate for chylomicron formation. In addition to greater fasting intestinal TG stores, KD-fed male mice displayed longer small intestinal lengths, while female mice displayed markedly longer jejunal villi lengths. After 5 weeks of diet, 12 hr fasting-2 hr refeeding experiments revealed jejunal TG levels

were similar between diet groups in male mice; however, in female mice, jejunal TG mass was significantly higher in KD-fed mice compared to GBD- and WD-fed mice. These experiments reveal that KD feeding promotes distinct morphological and functional changes to the small intestine compared to the WD diet. Moreover, changes to intestinal lipid handling in response to carbohydrate and protein restriction manifest differently in male and female mice.

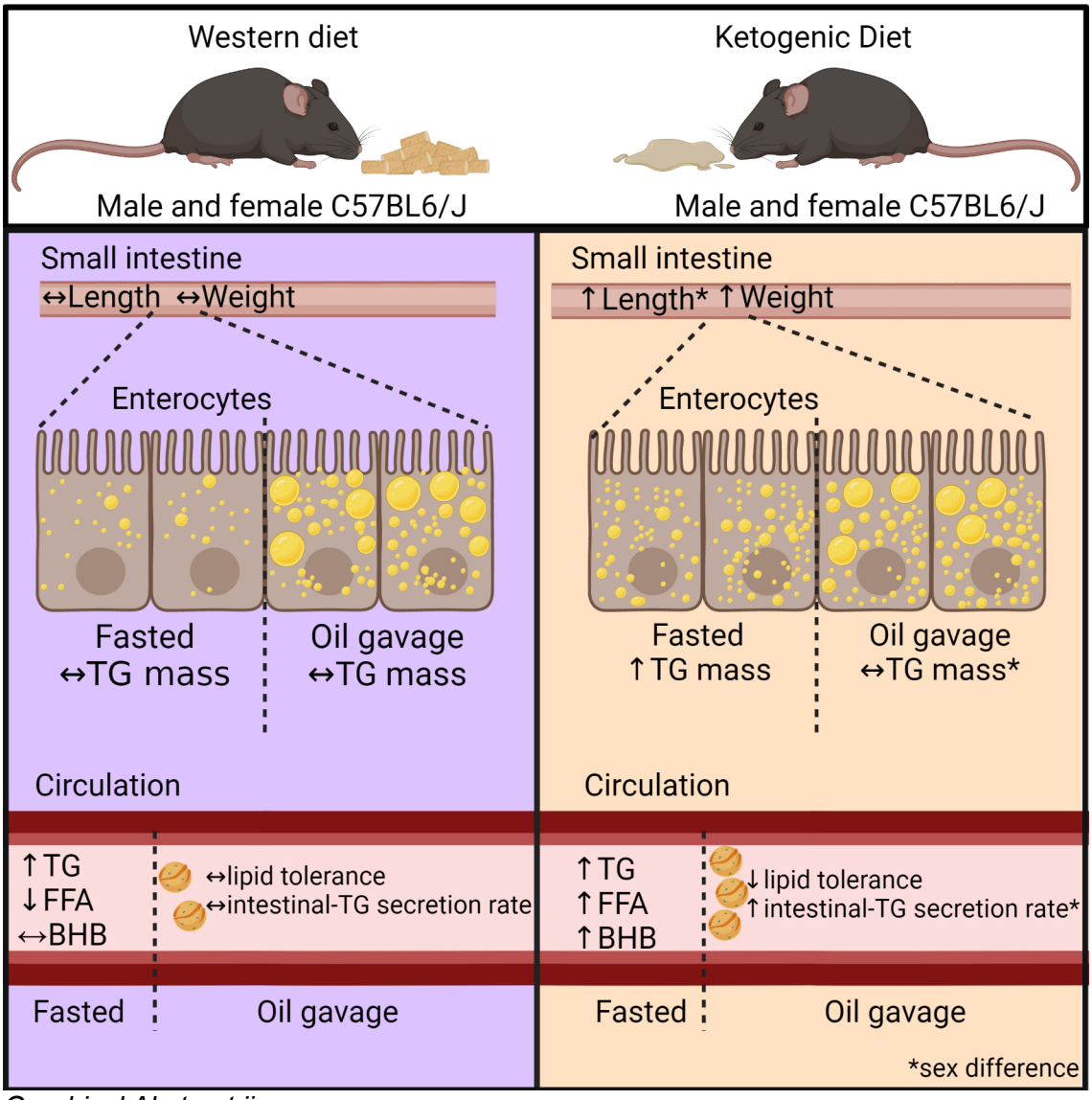

Graphical Abstract ii.

3.2 List of Abbreviations

apoB48: Apolipoprotein B48

BHB: Beta-hydroxybutyrate

CLD: Cytosolic lipid droplet

DAG: Diacylglycerol

DGAT: Diacylglycerol acyltransferase

FA: Fatty acid

GBD: Grain-based diet

KD: Ketogenic diet

LPL: Lipoprotein lipase

MAG: Monoacylglycerol

MGAT: Monoacylglycerol acyltransferase

MTP: Microsomal triacylglycerol transfer protein

NEFA: Non-esterified fatty acid

TAG: Triacylglycerol

TG: Triglyceride

TRL: Triglyceride-rich lipoproteins

VLDL: Very low-density lipoprotein

WD: Western-style diet

3.3 Introduction

Triacylglycerols (TAG) are a dominant metabolic storage unit due to their high energy density (9 kcal/g vs 3.75 kcal for glucose) (Merrill 1955, Pan and Hussain 2012). The small intestine absorbs greater than 95% of dietary fat (Pan and Hussain 2012) for distribution throughout the body (Phan and Tso 2001). As such, the small intestine continuously adapts to extremes in the external environment, including diet composition (Phan and Tso 2001, Ko, Qu et al. 2020).

The small intestinal lumen is lined with finger-like projections called villi, each lined with absorptive epithelial cells, called enterocytes, which facilitate nutrient absorption. Intestinal crypts between each villus harbour stem cells and transit-amplifying cells responsible for providing new epithelial cells (Bernier-Latmani and Petrova 2017). Enterocytes receive the products of both physically and enzymatically degraded dietary fats, namely, 2-monoacylglycerols, free fatty acids (FFA), and free cholesterol in the form of mixed micelles (Pan and Hussain 2012). Micelles facilitate the passive diffusion or active transport of hydrolyzed fats across the apical membrane of enterocytes. Once in the cytosol, fatty acids (FA) are re-esterified in the endoplasmic reticulum (ER) for further assembly and secretion in lipoproteins or storage in cytosolic lipid droplets (CLDs) to prevent lipotoxicity (Iqbal and Hussain 2009, Bernier-Latmani and Petrova 2017, Hung, Carreiro et al. 2017, Mulvihill 2018). FA are reassembled into TAG predominantly via acyl-coenzyme A:monoacylglycerol acyltransferase (MGAT), which catalyzes the covalent linkage of one fatty acyl-CoA to monoacylglycerol (MG), yielding diacylglycerol (DG), which is then acylated to form one TG molecule by acyl-coenzyme A, diacylglycerol acyltransferase 1 and 2 (DGAT 1 and 2) (Yen, Nelson et al. 2015). The second and minor pathway of TG synthesis within enterocytes is the synthesis of DG from glucose. Once assembled, TG, along with cholesterol esters, are either incorporated into chylomicrons or are temporarily stored in CLDs (Iqbal and Hussain 2009, Hung, Carreiro et al. 2017, Mulvihill 2018). Whether the flux of the MAG versus

glycerol-3-phosphate (G3P) pathways is influenced by dietary composition within the intestine remains elusive (Coleman, Lewin et al. 2000).

TG molecules occupy the majority (~80-95%) of the hydrophobic core of chylomicrons, where chylomicron size is proportional to dietary fat content (D'Aquila, Hung et al. 2016, Mulvihill 2018). Microsomal triacylglycerol transfer protein (MTP) assists in the folding of the chylomicron scaffold protein, apolipoprotein B48 (apoB48) by catalyzing the transfer of TG, cholesteryl esters, and phospholipids onto its structure as apoB48 is translated into the ER lumen (Julve, Martin-Campos et al. 2016). Following detachment of apoB48 from the ER membrane, primordial chylomicrons continue to grow by MTP-mediated lipidation or by fusing with CLDs until their release from the basolateral membrane (Pan and Hussain 2012). Chylomicrons enter the lymphatic lacteal for transport to peripheral tissues where they enter the blood circulation at the thoracic duct as the largest circulating class of lipoproteins (Pan and Hussain 2012, Bernier-Latmani and Petrova 2017). Remaining TG and cholesteryl ester molecules reside in enterocyte CLDs, which are surrounded by a monolayer of phospholipids, free cholesterol and proteins, including perilipins; the abundance and size of CLDs increase with high-fat feeding and decrease as fasting time increases (D'Aquila, Hung et al. 2016).

Several factors modulate intestinal lipoprotein secretion rates. Glucose promotes chylomicron secretion from enterocyte lipid stores (Stahel, Xiao et al. 2019, Xiao, Stahel et al. 2019). Insulin resistance in humans and fructose feeding in hamsters drive an overproduction of TAG-rich chylomicrons (Lewis, O'Meara et al. 1990, Haidari, Leung et al. 2002, Adeli and Lewis 2008). Moreover, fasting plasma insulin positively correlates to post-prandial TG and chylomicron remnant levels (Boquist, Hamsten et al. 2000). In mice, high-fat diet (HFD) feeding enhances TG levels in response to an oil gavage compared to grain-based diet (GBD) (62.1% of calories from carbohydrate (starch), 24.7% from protein, and 13.2% from fat. PicoLab 5053) -fed controls (Uchida, Whitsitt et al. 2012). However, in experiments blocking lipase-mediated hydrolysis of

circulating lipoproteins with poloxamer or tyloxapol, secretion rates are significantly reduced in HFD-fed mice after both ten weeks (Uchida, Whitsitt et al. 2012) and three weeks (Douglass, Malik et al. 2012) of feeding compared to GBD-fed controls, suggesting that TAG partitioning at the level of the CLD is perturbed. Indeed, jejunal CLDs are larger in the fed state when mice are fed a HFD compared to GBD-fed mice (Zhu, Lee et al. 2009, Uchida, Whitsitt et al. 2012). Additionally, intestinal CLD size is proportional to the volume of oil gavaged, where 300 µL versus 50 µL of olive oil leads to greater lipid droplet accumulation (Zhu, Lee et al. 2009). The underlying mechanisms in the adaptability of the small intestine to store dietary fat for later delivery is not fully understood. Moreover, the impacts of macronutrient proportions on intestinal lipid handling remain unresolved. Diets extremely high in fat including the ketogenic diet (KD) (>90 % of kcal), are severely carbohydrate-restricted and moderately protein-restricted, which can induce ketogenesis in rodents (Hu, Wang et al. 2018). 3-Hydroxy-3-Methylglutaryl-CoA Synthase 2 (HMGCS2), the rate-limiting enzyme in the production of β-hydroxybutyrate (BHB), mRNA and protein are enriched in *Lgr5*+ intestinal stem cells, particularly during fasting, and is critical for epithelium regeneration following intestinal injury in a Notch signalling-dependent manner (Cheng, Biton et al. 2019). KD feeding enhances crypt BHB levels as well as intestinal stem cell number and function (Cheng, Biton et al. 2019). Whether KD-induced increased intestinal stem cell self renewal improves intestinal lipid handling has not been explored.

Our study evaluates intestinal lipid storage and TG secretion rates with common gross dietary manipulations including Western diet (WD) and the extreme fat KD in the fasted and post-prandial state and in response to an acute dietary fat challenge in male and female mice. Additionally, we evaluate the diet-specific impacts on intestinal morphology throughout the small intestine prior to the development of obesity and insulin resistance.

3.4 Materials and methods

Animals and Diets

Male and female wild-type C57BL6/J mice were purchased (The Jackson Laboratory, Bar Harbor, MA) and bred in-house. Mice were housed in groups of 2-5 mice in standard cages at 23˚C on a 12 h light and dark cycle. Mice were cared for in accordance with the Canadian Guide for the Care and Use of Laboratory Animals. The Animal Care Committee approved all experimental procedures (UOHI-AUP-2909). At 12-18 weeks of age, mice were split into diet groups and fed a grain-based laboratory diet (GBD) (22% kcal from fat, 55% kcal from carbohydrates, 23% kcal from protein, 0% cholesterol; 2019, Envigo), a purified high fat, high cholesterol Western diet (WD) (42% kcal from fat, 42.7% kcal from carbohydrates, 15.2% kcal from protein, 0.2% weight from cholesterol: TD88137, Envigo), or purified ketogenic diet (KD) (90.5% kcal from fat, 0.4% kcal from carbohydrates, 9.2% kcal from protein, 0.2% weight from cholesterol; TD190587, Envigo) for the remainder of the study (Figure 1A). Fatty acid compositions (Supplemental Table 1) are presented in Figure 1B as a percentage of total fatty acids. Table 1 contains a more detailed breakdown of the nutrient composition of each diet. An estimate of food intake was measured in kcal as an average based on intake per cage divided the number of mice in the cage. Mice used for the terminal lipid tolerance experiment were fed the GBD, WD, or KD for three weeks and were fasted for 5 hours prior to the lipid tolerance test. Mice used for fasting experiments were fed one of the three diets for three weeks and were sacrificed following a 5 hour fast. Mice used for the 12-hour fasting 2-hour refeeding experiment were fed one of the three diets for five weeks. The fasting/refeeding paradigm was chosen to evaluate the changes in gene expression rapidly changing in response to feeding (Holt and DuBois 1991) but cannot discern changes persisting from the 12 hour fast. Mice were sacrificed by CO_2 inhalation.

Table 2 Diet composition of WD, KD, and GBD. The proportion of macronutrients and ingredients in the three diets. *Designed based on WD diet: vitamins, minerals, and cholesterol are altered in proportion to caloric density. **Contains: crude fiber 2.6%, natural detergent fibre 12.1% and ash 5%.

Diet	**Western Diet**		**Ketogenic Diet ***		**Grain Based Diet**	
	% kcal	%By weight	% kcal	%By weight	% kcal	% By weight
Carbohydrate	42.7	48.5	0.4	0.6	55	64.6**
Fat	42.0	21.2	90.5	67.3	22	9.0
Protein	15.2	17.3	9.2	15.3	23	19.0
Kcal/g	4.5		6.7		3.3	
Ingredients		g/Kg		g/Kg	(in descending order of inclusion)	
Casein		195.0		173.0	Ground wheat, ground corn, corn gluten meal, wheat middlings, soybean oil, calcium carbonate, dicalcium phosphate, brewers dried yeast, L-lysine, iodized salt, magnesium oxide, choline chloride, DL-methionine, calcium propionate, L-tryptophan, vitamin E acetate, menadione sodium bisulfite complex (source of vitamin K activity), manganous oxide, ferrous sulfate, zinc oxide, niacin, calcium pantothenate, copper sulfate, pyridoxine hydrochloride, riboflavin, thiamin mononitrate, vitamin A acetate, calcium iodate, vitamin B12 supplement, folic acid, biotin, vitamin D3 supplement, cobalt carbonate.	
DL-Methionine		3.0		2.6		
Sucrose		341.46		0		
Corn Oil		0		20.0		
Corn Starch		150.0		0		
Anhydrous Milkfat		210.0		651.0		
Cholesterol		1.5		1.31		
Cellulose		50.0		76.14		
Mineral Mix, AIN-76 (170915)		35.0		0		
Mineral Mix, Ca-P Deficient (79055)		0		19.72		
Calcium carbonate		4.0		14.15		
Calcium Phosphate, monobasic, monohydrate		0		27.2		
Vitamin Mix, Teklad (40060)		10.0		14.76		
Ethoxyquin		0.04		0.12		

Blood and Tissue Collection

Blood glucose and BHB were measured using MediSure Blood Glucose Meter and Freestyle Precision B-Ketone Test Stripes. Blood was taken at sacrifice via cardiac puncture in EDTA coated syringes. Blood was centrifuged at 4°C and 12000 rpm for 10 minutes. Plasma was stored at -80°C until analyses were performed (Ultra Sensitive Mouse Insulin ELISA Kit- ALPCO, Free Fatty Acid Quantification Kit Sigma Aldrich, Infinity Triglycerides Liquid Stable Reagent). The small intestine was divided into duodenum, proximal jejunum, distal jejunum, and ileum (1:1:1:1 ratio) and flushed with cold phosphate-buffered saline (PBS). For sample collection after oil gavage, the intestine was flushed with 0.5 mM sodium taurocholate (37ºC) followed by cold PBS. Samples of the proximal jejunum were collected for histological analyses and intestinal samples were snap frozen for quantitative real-time PCR (qRT-PCR) and lipid extractions. Snap frozen perigonadal adipose tissue extracts were analyzed for LPL activity (ab204721 Lipoprotein Lipase Activity Assay Kit).

Insulin Tolerance Test

Mice were fasted for 5 hours before *i.p.* injection with 0.6 IU/kg body weight insulin (Humalog, VL7533, DIN: 02229704) and blood glucose measurements were performed via tail snip for 90 minutes as previously described (Mulvihill, Assini et al. 2011).

Lipid Tolerance Test

After 3 weeks of feeding, mice in the first group were fasted for 5 hours at the start of the light cycle and gavaged with 200 µL olive oil (approximate fatty acid composition (in 15 mL or 14 g): saturated (palmitic and stearic 2 g), polyunsaturated (linoleic and linolenic 1.5 g) and monounsaturated (oleic 10 g) and blood was collected via tail bleed at baseline, 1- , 2-, 3-, and 4-hours after oil gavage. After 3 weeks of feeding, mice in the second group were fasted for 5 hours at the start of the light cycle and were injected *i.p.* with 100 mg/kg poloxamer-407 30 minutes

before an olive oil gavage containing 30 µg BODIPY-C16 FA (Thermo Scientific D3821). Blood was collected via tail bleed at baseline, 1-, and 2-hours post-gavage and by cardiac puncture 4 hours post-gavage. Plasma TG was measured using the colorimetric TAG assay with Infinity Triglyceride Liquid Stable Reagent and plasma fluorescence was measured in diluted samples (1:100 in PBS) on a fluorescence plate reader (BioTek).

EchoMRI

Fat and lean mass were determined by EchoMRI (EchoMRI-100 machine, Echo Medical Systems, Houston, TX, USA) in awake mice.

Histological analyses

In mice sacrificed following a 5-hour fast, a 2 cm sample from the start of all 4 segments of the intestine were flash frozen and the remaining ~4-7 cm of the segments were flushed with cold PBS then 4% paraformaldehyde prior to Swiss rolling starting from the proximal end of each segment (Bialkowska, Ghaleb et al. 2016). Intestinal rolls were fixed for 24 hours before paraffin embedding. In mice used in the fasting-refeeding experiments, two cm segments from the start of the duodenum, proximal jejunum, and ileum were flushed with 4% paraformaldehyde and fixed for 24 hours before paraffin embedding. For analysis, five-micron sections of all samples were stained with hematoxylin and eosin. Photomicrographs were obtained with a Leica Aperio Versa slide scanner. Villi length (15-30/mouse) and crypt depth (35/mouse) measurements were performed using ImageScope software as described (Koehler, Baggio et al. 2015). In the Swiss rolls, mean villi length was calculated in 1 cm regions using ImageJ. Adipocyte area was measured using the Adiposoft pluggin available in ImageJ software where 300 adipocytes were analyzed per mouse.

Cytosolic Lipid Droplet analysis

Jejunal samples were fixed in 4% paraformaldehyde, incubated in 30% sucrose overnight or until the tissue sunk and then embedded in Optimal Cutting Temperature (OCT) compound. (Tissue-Tek®). Samples were sectioned (10 microns) and stored at –20˚C until further analyses. For samples from the fasting-refeeding experiments, sections were dried for 1 hour, washed once in dH_2O, twice in PBS, and stained with BODIPY 493/503 (1.0 µg/mL; Invitrogen, D3922) for 30 minutes. Sections were washed with PBS three times and counterstained with DAPI. For BODIPY-C16 FA gavage experiments, sections were washed as above and stained with neutral lipid AUTODOT Visualization Dye (1:1000; Acepta, SM1000b). Images were captured on a Zeiss LSM880 confocal microscope with a 63X objective (NA 1.4) and the Airyscan module. Z-stacks (0.17 micron Z-axis spacing) of multiple slices were obtained, and image analyses were performed in orthogonal projections (Zen Blue). CLD area quantification was performed using CellProfiler (version-4.2.0) using a modified pipeline (Adomshick, Pu et al. 2020) where six fields of view containing one villus tip each were quantitated and averaged to generate a quantitation per mouse.

Gene Expression

Jejunal RNA was isolated with TRIzol Reagent (Ambion) as per manufacturers protocol, and cDNA was reverse transcribed using a High-Capacity cDNA Reverse Transcription Kit (Fisher Scientific 43-688-14). mRNA was quantified by the standard curve qRT-PCR method (QuantStudio 5) using Applied Biosystems TaqMan Gene Expression Master Mix (4369016). Abundance was normalized to the housekeeping gene beta-actin (*Actb)* and denoted as absolute mRNA.

Western Blotting

Plasma samples (1:100) from mice were run on 4.5% SDS-PAGE gels, transferred onto Pierce PVDF Transfer Membranes (ThermoFisher, 88518), and incubated with apoB primary

antibodies (Midland AB_2734118) and mouse-anti-goat IgG-HRP (Santa Cruz Biotechnologies, sc-2354; RRID:AB_628490), visualized (SuperSignal WestPico PLUS, Thermo Scientific, P134577), imaged (ChemiDoc XRS+; Bio-Rad), and quantitated using Image Lab 6.1 Software (Bio-Rad).

TG Mass Analysis

Intestinal lipids were extracted from ~50-100 mg segments in the duodenum, proximal jejunum, distal jejunum, ileum, and liver using a modified Folch method through homogenization in chloroform/methanol (2:1, v/v) and processed as described previously (Patel, Patel et al. 2011). Lipids were quantified using Infinity Triglyceride reagent. Each tube was vortexed and plated, then read immediately at 540 nm.

Statistical Analysis

Statistical analysis was performed using GraphPad Prism (version 9.2). Data are shown as mean +/- SEM. One-way ANOVA with post-hoc Tukey's test were used to determine significant (>0.05) differences between diet groups. Two-way ANOVA with post-hoc Tukey's multiple comparisons was performed for metabolic measures taken over time and for mean villi length measurements across gut segment length (Figure 4 and 5). The Kolmogorov–Smirnov test evaluated statistical differences in average CLD size and adipocyte size distribution (Figure 3E,K; Figure 6J, and Figure 7J; Supplemental Figure 3-4K, and Supplemental Figure 3-7K). Statistical differences between groups, not within a group over time, are represented on the graphs unless otherwise indicated (Supplemental Figure 3-5).

3.5 Results

3.5.1 Three weeks of KD feeding, but not WD feeding, induces post-prandial lipemia

To evaluate the contribution of carbohydrate restriction to the metabolic and molecular adaptations induced by KD feeding, fifteen- to eighteen-week-old male and female mice were maintained on a grain-based chow diet (GBD), fed a Western diet (WD), or a KD for three weeks (Figure 3.1, Supplemental Figure 3-1A). Food intake was similar between diet groups in male and female mice after one week of the diet acclimatization (Supplemental Figure 3-1B,C); however, body weight was significantly greater (17.4%) in WD-fed male mice compared to KD-fed male mice up to three weeks of diet feeding (Supplemental Figure 3-1D). In females, there were no significant differences in body weight (Supplemental Figure 3-1E).

To evaluate the effects of short-term WD or KD feeding on intestinal lipid handling, a lipid tolerance test was performed. Plasma TG excursions were similar in WD-fed and GBD-fed male mice (Figure 3.2A). KD-fed male mice, by contrast, displayed higher plasma TG levels at 1 hour and 2 hours post-gavage compared to WD-fed mice, which returned to baseline by 4 hours (Figure 3.2A). Similar to males, WD- and GBD-fed female mice displayed similar plasma TG levels throughout the experiment, and KD-fed mice displayed significantly higher plasma TG levels at both 1 and 2 hours post-gavage (Figure 3.2B). Interestingly, the rise in plasma TG levels from baseline was ~2-fold higher in male diet groups compared to female diet groups, despite receiving the same amount of oil (Figure 3.2A,B).

Figure 3.1 The carbohydrate restricted ketogenic diet is mainly composed of saturated fatty acid. (A) Macronutrient composition of the 3 diets: grain-based, standard laboratory chow diet (GBD), Western diet (WD), and ketogenic diet (KD). (B) Fatty acid composition as percent of total fatty acids. GBD: Grain-based diet, WD: Western diet, KD: Ketogenic diet

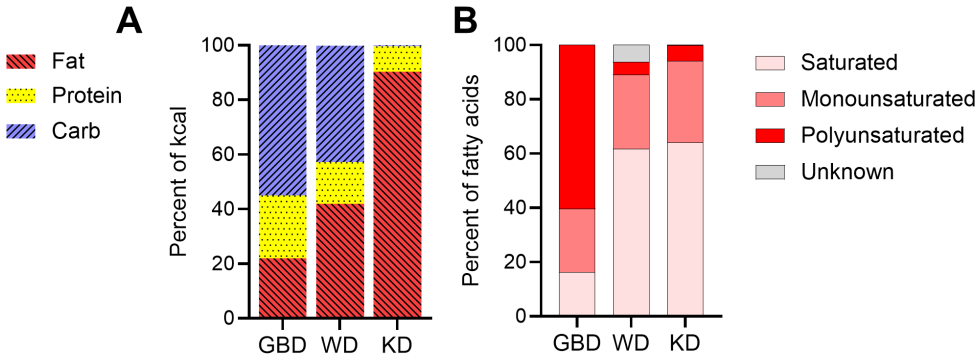
A
Fat
Protein
Carb
Percent of kcal
100
80
60
40
20
0
GBD
WD
KD
B
Percent of fatty acids
100
80
60
40
20
0
GBD
WD
KD
Saturated
Monounsaturated
Polyunsaturated
Unknown

To determine if KD-feeding enhanced intestinal-TG secretion rates, another cohort of mice were injected *i.p.* with poloxamer-407 to block lipase-mediated hydrolysis of lipoproteins prior to an olive oil gavage containing BODIPY-C16 FA after 3 weeks of feeding. KD-fed male mice displayed significantly greater TG secretion rates at 2 hours and overall, as shown in AUC, compared to GBD- and WD-fed mice (Figure 3.2C). Plasma fluorescence, originating from the BODIPY-C16 FA gavage, was also significantly greater in KD-fed male mice compared to GBD-controls over the time course (Figure 3.2D). Plasma apoB48 were not significantly different among diet groups in male mice (Figure 3.2E), suggesting that KD-fed mice secreted larger particles in response to the oil gavage. In female mice, by contrast, secretion rates were not significantly different as observed by plasma TG (Figure 3.2F), plasma fluorescence (Figure 3.2G) or plasma apoB48 levels (Figure 3.2H). However, the change in TG from baseline was significantly different between WD and GBD at 4 hours after oil gavage (Figure 3.2F). Interestingly, these data demonstrate that secretion rates are similar between male and female mice fed a WD for 3 weeks compared to continuation on the GBD. By contrast, KD-fed male mice secretion rates are 1.5-fold greater than KD-fed female mice, suggesting that the partitioning of absorbed dietary FA for secretion versus storage manifests differently in male and female mice.

Figure 3.2 Ketogenic diet feeding increases intestinal TG excursion in response to oil bolus. After 3 weeks of GBD, WD diet, or KD, mice were fasted and then given oil gavage. Plasma TG and AUC after oil gavage compared to baseline in males (A) and females (B). (C) Change in plasma TG and AUC after poloxamer-407 injection followed by oil gavage in male mice. (D) BODIPY-labelled plasma fatty acids and AUC before and 1, 2, and 4 hours after oil gavage in males. (E) ApoB48 quantification and AUC over time after poloxamer-407 injection and oil gavage in males. (F) Change in plasma TG and AUC after poloxamer-407 injection followed by oil gavage in female mice. (G) BODIPY-labelled plasma fatty acids and AUC before and 1, 2, and 4 hours after oil gavage in females. (H) ApoB48 quantification and AUC over time after poloxamer-407 injection and oil gavage in females. Data are shown as mean +/- SEM. Significance determined by one-way ANOVA (AUC) or two-way ANOVA with Tukey's multiple comparisons. Differences between diet groups are represented by colour (grey: KD and GBD, blue: KD and WD, black: WD and GBD) or line and the p-value is indicated. GBD: Grain-based diet, WD: Western diet, KD: Ketogenic diet.

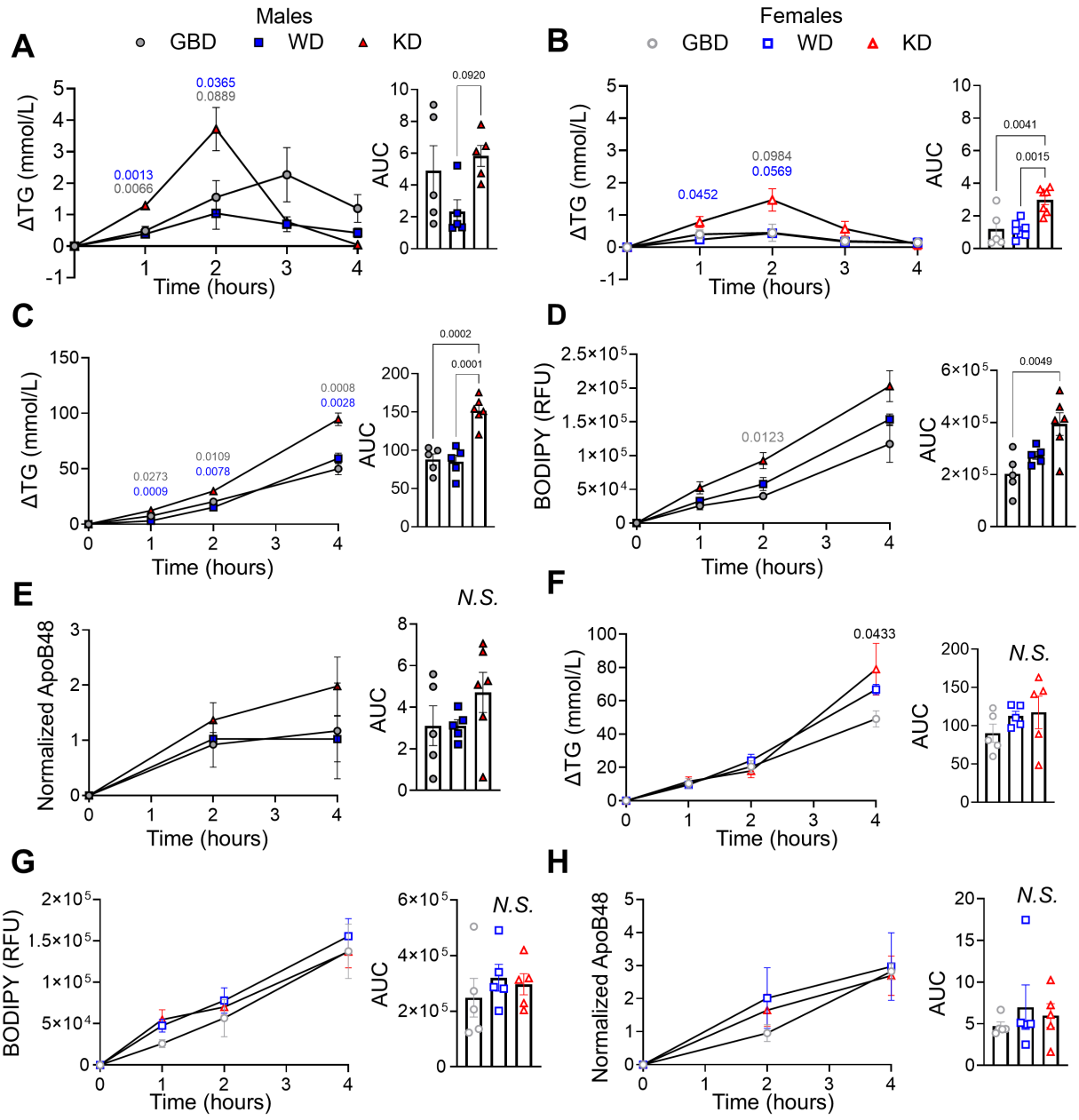
Males
Females
GBD
WD
KD
A
B
C
D
E
F
G
H
ΔTG (mmol/L)
Time (hours)
AUC
BODIPY (RFU)
Normalized ApoB48
0.0013
0.0066
0.0365
0.0889
0.0920
0.0452
0.0984
0.0569
0.0041
0.0015
0.0273
0.0009
0.0109
0.0078
0.0008
0.0028
0.0002
0.0001
0.0123
0.0049
0.0433
N.S.

3.5.2 KD impacts CLD storage in response to oil in a sex-dependent manner

To determine if the increased intestinal-TG secretion rates observed in male mice reduced dietary fat storage, CLD analyses were performed on dietary-derived lipid droplets (BODIPY-labelled) in jejunal samples 4 hours post-oil gavage. Small intestinal length was not significantly different among diet groups 4 hours post-gavage (Figure 3.3A). CLD abundance, labelled by the orally administered BODIPY-C16 FA, at the villus tip in male mice was not significantly different among diets (Figure 3.3B,C); consistent with this, jejunal TG mass was not significantly different among diet groups (Figure 3.3D). The size distribution of CLDs was similar in all diet groups (Figure 3.3E). DGAT1 is involved in TG re-assembly for chylomicron synthesis, whereas DGAT2 has been shown to catalyze TG assembly for storage in CLDs (Hung, Carreiro et al. 2017). In our study, jejunal mRNA expression for *Dgat1* was higher in KD-fed males, whereas *Dgat2* mRNA expression was not significantly different among diet groups (Figure 3.3F, Supplemental Figure 3-2A), consistent with the similar level of dietary TG storage observed. KD-fed mice had significantly higher *ApoB*, *Fasn*, *Atgl*, and *Cd36* mRNA levels compared to WD-fed mice (Figure 3.3F), consistent with enhanced intestinal-TG secretion rate. *Plin2* and *Mttp* mRNA expression was not significantly different among diet groups (Supplemental Figure 3-2A). *Srebf1c* mRNA expression was significantly lower in KD-fed mice compared to WD-fed mice, suggesting a suppression in *de novo* lipogenesis at this time point (Figure 3.3F). However, the percent overlap in signals from BODIPY-gavage and a total lipid stain suggested that the presence of CLDs derived from a previous meal or *de novo* lipogenesis was not significantly different among diet groups (Supplemental Figure 3-2B,C). *Cpt1α* mRNA expression was not significantly different among diet groups (Figure 3.3F). *Glp1r* mRNA expression was significantly lower in KD-fed mice compared to GBD-fed mice while *Glp2r* mRNA expression was similar among diet groups (Figure 3.3F, Supplemental Figure 3.2A), suggesting that the enhanced intestinal-TG secretion rates with KD feeding are independent of these gut hormone receptors signalling pathways. Additionally,

hepatic TG mass was not significantly different among diet groups (Supplemental Figure 3-2D), suggesting that the higher TG levels accumulated in these poloxamer-treated mice are largely intestinally-derived. Taken together, KD-feeding in male mice appears to prime chylomicron assembly gene expression pathways in response to an oil meal to a greater extent than background WD-feeding while jejunal dietary FA storage remains unchanged.

Small intestinal length was similar among diet groups 4 hours post-gavage in female mice (Figure 3.3G). CLD abundance at the villus tip was similar among diet groups (Figure 3.3H,I). Similar to male mice, jejunal TG mass was not significantly different among diet groups (Figure 3.3J). Compared to male mice, the percent of CLDs in the smallest size range was doubled in female mice; however, the size distribution of CLDs was similar in all diet groups (Figure 3.3K). The similar CLD size profile and intestinal-TG secretion rates in female mice were accompanied by unchanged jejunal *Dgat1*, *ApoB*, and *Fasn* mRNA levels among diet groups (Figure 3.3L). Still, *Atgl* and *Cd36* mRNA expression was significantly higher in KD-fed mice compared to both GBD- and WD-fed mice (Figure 3.3L). Additionally, *Dgat2*, *Mttp*, *Plin2*, and *Plin3* mRNA expression was not different among diet groups (Figure 3.3L, Supplemental Figure 3-2E). *Srebf1c* mRNA expression was not different among diet groups (Figure 3.3L) and the signal overlap ratio of BODIPY to total signal was similar among diet groups (Supplemental Figure 3-2F,G). In contrast to males, *Cpt1α* mRNA expression was significantly higher in KD-fed mice compared to both GBD- and WD-fed mice (Figure 3.3L). Interestingly, hepatic TG mass was greater in GBD-fed females compared to both WD- and KD-fed female mice (Supplemental Figure 3-2H), suggesting downregulated *de novo* lipogenesis in WD- and KD-fed mice or that hepatic lipid export may contribute to circulating TG levels at the 4-hour time point in WD- and KD-feeding. Therefore, in females, despite previous extreme dietary fat consumption with KD-feeding, the response to an acute dietary fat challenge in terms of the amount of TG stored in the jejunum 4 hours post-oil gavage and intestinal-TG secretion rates are similar to that in GBD- and WD-fed mice.

Figure 3.3 Small intestine length and jejunum TG are not different between diet groups after oil gavage. After 3 weeks of GBD, WD, or KD feeding male and female mice were fasted and then administered poloxamer-407 and BOPIDY-C16 labelled oil gavage four hours before sacrifice. (A) Small intestinal length in males. (B) Representative images of jejunal epithelium cytosolic lipid droplets (CLD) 4 hours post-oil in male mice. (C) Total BODIPY signal per image in males. (D) Total TG mass from jejunal extract in males. (E) Mean and binned jejunal epithelium CLD size from micrographs in males. (F) Jejunal mRNA abundance of *Dgat1, ApoB, Fasn, Atgl, Cd36, Plin3, Srebf1 and Glp1r* normalized to *Actb* in males. (G) Small intestinal length in females. (H) Representative images of jejunal epithelium CLD 4 hours post-oil in female mice. (I) Total BODIPY signal per image in females. (J) Total TG mass from jejunal extract in females. (K) Mean and binned jejunal epithelium CLD size from micrographs in females. (L) Jejunal mRNA abundance *of Dgat1, ApoB, Fasn, Atgl, Cd36, Plin3, Srebf1* and *Glp1r*, normalized to *Actb* in females. Data are shown as mean +/- SEM. Significance determined by one way ANOVA with Tukey's multiple comparisons or Kolmogorov–Smirnov test (E,K). Significance indicated between groups with lines and P value. GBD: Grain-based diet, WD: Western diet, KD: Ketogenic diet.

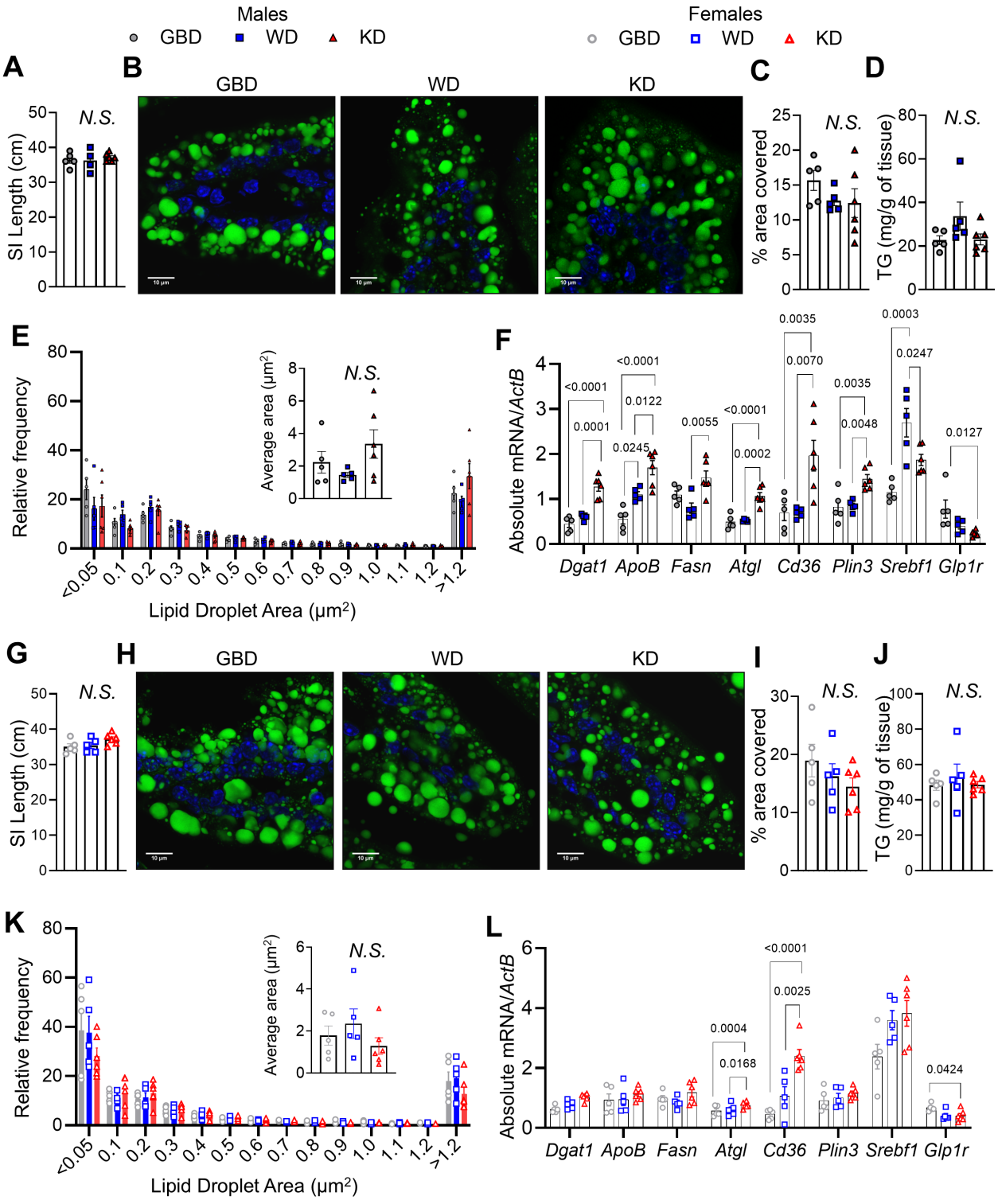
Males
GBD
WD
KD
Females
GBD
WD
KD
A
B
C
D
SI Length (cm)
N.S.
% area covered
TG (mg/g of tissue)
E
F
Relative frequency
Average area (μm²)
Lipid Droplet Area (μm²)
Absolute mRNA/ActB
Dgat1
ApoB
Fasn
Atgl
Cd36
Plin3
Srebf1
Glp1r
G
H
I
J
K
L

3.5.3 Three-week KD-fed male mice have longer small intestines and increased fasted jejunal TG

To determine if three weeks of KD-feeding impacts intestinal TG storage and absorptive surface area at baseline before the olive oil gavage, another set of mice was sacrificed following a 5 hour fast. Blood BHB levels were significantly higher in KD-fed males compared to both GBD- and WD-fed mice at baseline (Supplemental Figure 3.3A). Blood BHB levels increased with fasting in GBD- and WD-fed mice, these levels were reduced by ~0.5 mM with fasting in KD-fed mice (Supplemental Figure 3-3B) but remain significantly elevated compared to GBD- and WD-fed mice. Blood glucose levels were not significantly different at baseline or after a 5 hour fast among diet groups (Supplemental Figure 3-3C, D). Body weight was not significantly different among diet groups at either time point; however, KD-fed mice were the most resistant to weight loss induced with fasting (Supplemental Figure 3-3E,F). Despite similar body weights, small intestinal length was significantly greater in KD-fed compared to WD-fed male mice (Figure 3.4A), suggesting greater absorptive surface area. Duodenal TG mass was unchanged among diet groups (Figure 3.4B). However, TG mass in the proximal jejunum and distal jejunum was significantly greater in KD-fed mice than GBD- and WD-fed mice (Figure 3.4C,D), suggesting that the intestine adapts to the increased fat consumption by storing more dietary FA for later release. TG mass in the ileum was not significantly different among diet groups (Figure 3.4E). Consistent with a previous study highlighting the requirement of intestinal *Pparα* for villi length elongation (Stojanovic, Altirriba et al. 2021), KD-fed male mice display elevated (trend, p=0.0558) jejunal *Pparα* mRNA expression four hours post-oil gavage compared to GBD-fed mice (Figure 3.4F). To determine if specific regions of the small intestine morphologically adapted to this increased TG storage, we performed the Swiss Roll technique (Bialkowska, Ghaleb et al. 2016) to measure villi length throughout each intestinal segment (Figure 3.4G-O). Mean villi length was not significantly different between diet groups in the duodenum or proximal jejunum (Figure 3.4G,H,I,L). However, in the distal jejunum, mean villi length was significantly greater mid-segment in KD compared to

GBD mice (Figure 3.4J), suggesting an extension of the absorptive length of the intestine. In the ileum, mean villi length was greater in GBD than WD-fed males in two regions (Figure 3.4K), however, mean villi length was not statistically different with KD compared to GBD- or WD-fed mice.

Figure 3.4 Fasted male ketogenic diet-fed mice have elevated jejunal TG mass and intestinal length. Male mice were fed GBD, WD, or KD for 3 weeks and sacrificed after 5 hours of fasting. (A) Small intestinal length. Tissue TG mass in the duodenum (B), proximal jejunum (C), distal jejunum (D), and ileum (E). (F) mRNA abundance of Pparα normalized to ActB in male mice 4 hours post-oil gavage. (G) Villi lengths were quantitated in the duodenum, proximal jejunum, distal jejunum, and ileum from Swiss roll photomicrographs. Average villi lengths from 1 cm regions in (H) duodenum, (I), proximal jejunum, (J) distal jejunum, and (K) ileum. (L) Representative images of duodenal, proximal jejunal, distal jejunal, and ileal Swiss rolls. Data are shown as mean +/- SEM. Significance determined was by one-way ANOVA or two-way ANOVA (H-K) with Tukey's multiple comparisons. Differences between diet groups are represented by colour (grey: KD and GBD, black: GBD and WD) or line and the p-value is indicated. GBD: Grain-based diet, WD: Western diet, KD: Ketogenic diet. Scale bar = 2 mm.

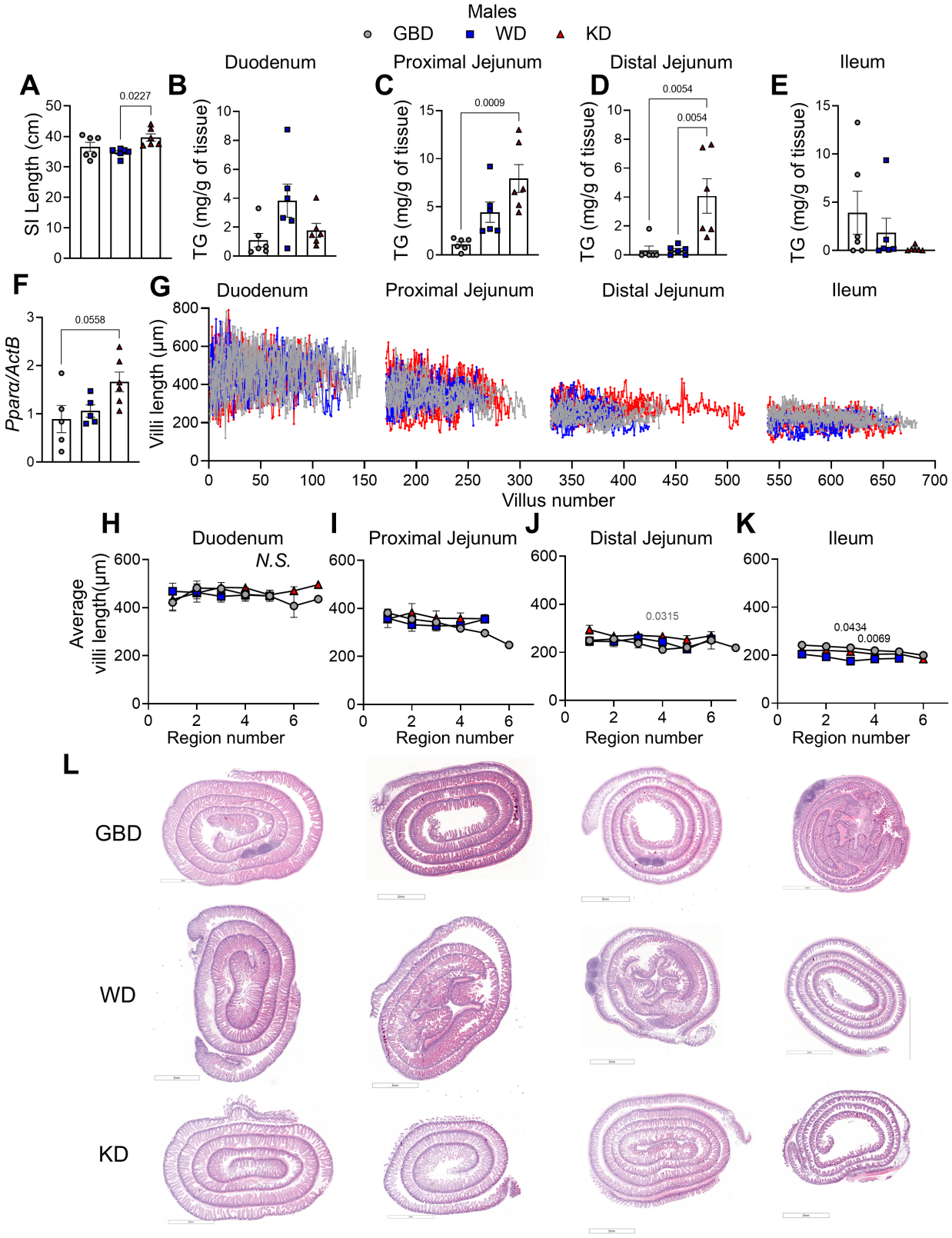
Males
GBD
WD
KD
A
SI Length (cm)
0.0227
B
Duodenum
TG (mg/g of tissue)
C
Proximal Jejunum
0.0009
D
Distal Jejunum
0.0054
0.0054
E
Ileum
F
Ppara/ActB
0.0558
G
Villi length (µm)
Villus number
H
Duodenum
N.S.
Average villi length(µm)
Region number
I
Proximal Jejunum
J
Distal Jejunum
0.0315
K
Ileum
0.0434
0.0069
L
GBD
WD
KD

3.5.4 Three-week KD-fed female mice have increased fasted intestinal TG and jejunal villi length

Fasting intestinal TG mass and villi length was also measured in female mice after 3 weeks of diet. At baseline and at 5 hours of fasting, blood BHB levels were significantly higher in KD-fed mice compared to both GBD- and WD-fed mice (Supplemental Figure 3.-3G), where similar to males, blood BHB levels decreased with fasting in KD-fed mice (Supplemental Figure 3.-3H). Additionally, similar to males, blood glucose levels were not significantly different at baseline or fasting in female mice (Supplemental Figure 3-3I,J). Body weight was significantly greater in WD-fed females compared to GBD-fed mice at baseline and fasting (Supplemental Figure 3-3K). In KD-fed females, body weight was not significantly different compared to GBD- and WD-fed mice but they were more resistant to fasting induced weight loss than GBD-fed mice (Supplemental Figure 3-3K, L). In contrast to males, small intestinal length was not different between groups after a 5 hour fast (Figure 3.5A). Duodenal, proximal jejunal, and distal jejunal TG mass, however, was significantly elevated in KD-fed mice compared to GBD and WD-fed mice (Figure 3.5B-D). TG mass in the ileum was not significantly different among diet groups (Figure 5E). Additionally, similar to male mice, KD-fed female mice display significantly elevated jejunal *Pparα* mRNA expression (Figure 3.5F). Villi length measurements in the Swiss Rolls revealed that KD-feeding did not change mean duodenal villi length (Figure 3.5G,H,L). In the proximal jejunum, however, mean villi length was significantly greater in KD-fed mice compared to both GBD- and WD-fed mice in the first four regions (Figure 3.5G,I,M). Unlike in male mice, villi length was not significantly different among groups in the distal jejunum (Figure 3.5G,J,N). Villi length was significantly greater in the first region of the ileum in KD-fed mice compared to WD-fed mice (Figure 3.5G,K,O). Similar to males, KD-feeding increases fasting intestinal TG stores, induces morphological changes to the small intestine, and attenuate weight loss with fasting.

Figure 3.5 Fasted female ketogenic diet fed mice have elevated jejunal TG mass and villi length. Female mice were fed GBD, WD, or KD for 3 weeks and tissue was collected after 5 hours of fasting. (A) Small intestinal length. Tissue TG mass in the duodenum (B), proximal jejunum (C), distal jejunum (D), and ileum (E). (F) mRNA abundance of Pparα normalized to ActB in male mice 4 hours post-oil gavage. (G) Villi lengths were quantitated in the duodenum, proximal jejunum, distal jejunum, and ileum from Swiss roll photomicrographs. Average villi lengths in 1 cm regions in (H) duodenum, (I), proximal jejunum, (J) distal jejunum, and (K) ileum. (L) Representative images of duodenal, proximal jejunal, distal jejunal, and ileal Swiss rolls. Data are shown as mean +/- SEM. Significance determined was by one-way ANOVA or two-way ANOVA (H-K) with Tukey's multiple comparisons. Differences between diet groups are represented by colour (grey: KD and GBD, blue: KD and WD) or line and the p-value is indicated. GBD: Grain-based diet, WD: Western diet, KD: Ketogenic diet. Scale bar = 2mm.

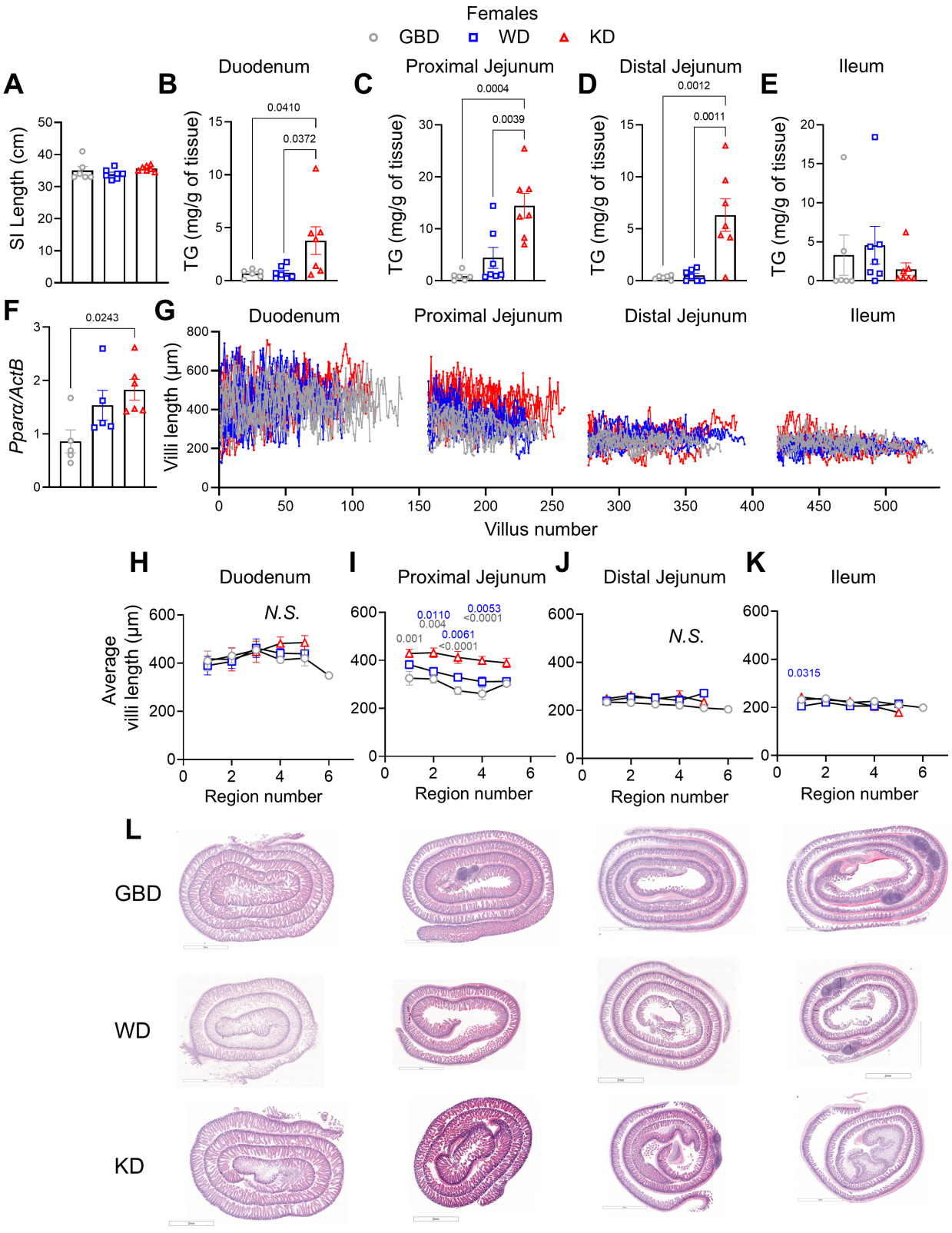
Females
GBD
WD
KD
A
SI Length (cm)
B
Duodenum
TG (mg/g of tissue)
0.0410
0.0372
C
Proximal Jejunum
0.0004
0.0039
D
Distal Jejunum
0.0012
0.0011
E
Ileum
F
Ppara/ActB
0.0243
G
Villi length (μm)
Villus number
H
Average villi length (μm)
N.S.
Region number
I
0.0110
0.004
0.001
0.0053
<0.0001
0.0061
<0.0001
J
N.S.
K
0.0315
L
GBD
WD
KD

3.5.5 KD feeding in males promotes high circulating TG and FFA but does not increase fasted-refed intestinal lipid storage after 2-hour refeeding

To evaluate the impact of the respective diets on post-prandial parameters and intestinal lipid storage, male mice were subjected to a 12-hour fasting-2-hour refeeding protocol after 5 weeks of dietary intervention. Surprisingly, WD- and KD-fed male mice demonstrated greater insulin sensitivity than GBD-fed controls after four weeks of diet (Supplemental Figure 3-4A). In two-hour refed male mice, small intestinal length was greater in KD compared to WD-fed males (Figure 3.6A). Consistently, KD-fed males also had significantly greater small intestinal weight than GBD but not WD-fed males (Figure 3.6B), which may be driven by increased villi length (trend, $p = 0.0788$) (Supplemental Figure 3.6C). Fasting blood BHB levels were not different among groups (Supplemental Figure 3-4B). As expected, refeeding decreased blood BHB in both GBD- and WD-fed mice (Supplemental Figure 3-4B,C). By contrast, blood BHB levels increased from fasting levels in KD-fed males, confirming a state of nutritional ketogenesis in these mice (Supplemental Figure 3-4B,C). Additionally, refeeding insignificantly increased blood glucose and plasma insulin levels in male GBD- and WD-fed mice but not in KD-fed mice (Supplemental Figure 3-4D-G). Fasting plasma TG was similar among diet groups in male mice (Figure 6C). Refeeding in males led to higher plasma TG levels in KD-fed mice compared to GBD-fed mice (Figure 3.6C,D). Fasting plasma FFA levels (8 carbons in length and longer) were similar in male GBD- and WD-fed mice, whereas in KD-fed mice, levels were significantly lower (Figure 3.6E). As expected, refeeding reduced plasma FFA levels in male GBD-fed and, to a lesser extent in WD-fed mice, whereas KD-fed males maintained similar FFA in the refed state (Figure 3.6E,F). Body mass was significantly greater in both the 12-hour fasted and 2-hour refed state in WD compared to GBD male mice (Supplemental Figure 3-4H). The percent body mass change from baseline revealed that KD-fed mice were more resistant to fasting induced weight loss compared to both GBD- and WD-fed mice (Supplemental Figure 3-4H,I). However, 2 hours of refeeding did not induce weight gain to baseline levels before fasting among diet groups (Supplemental Figure 3-

4I). To gain further insight in the organ responsible for the maintenance of plasma FFA levels in the refed state, perigonadal adipose tissue was analyzed for morphology and LPL activity. As anticipated with WD feeding, perigonadal adipose tissue weight was significantly increased between WD-refed mice and GBD-refed mice, however no significant differences were noted between KD-refed mice and either dietary group (Supplemental Figure 3-4J). Similar to WD-refed mice, however, KD-fed mice had significantly greater abundance of larger adipocytes compared to GBD-fed mice (WD vs GBD, p=0.0005; KD vs GBD, p=0.0016) (Supplemental Figure 3-4K). Despite these differences, LPL activity was not significantly different among diet groups in the refed state (Supplemental Figure 3-4L). These data suggest that post-prandial circulating glucose or lipid levels in the pro-lipogenic, fasting-refeeding experiment are relative to meal composition.

To further explore body composition during the fasting-refeeding experiment, EchoMRI was performed on another set of mice after 12 days of diet (Supplemental Figure 3-5A). Once again, KD-fed mice were more resistant to 12-hour fasting-induced weight loss compared to GBD- and WD-fed mice (Supplemental Figure 3-5B,C). Additionally, body weight was not recovered after two hours of refeeding among diet groups (Supplemental Figure 3-5C). Fasting significantly lowered adiposity in GBD- and KD-fed mice but not WD-fed mice (Supplemental Figure 3-5D), suggesting a greater capacity to mobilize lipids that was not restored with refeeding. The change in adiposity was similar among diet groups and a similar deficit was observed from baseline even after 2 hours of refeeding (Supplemental Figure 3-5E). Fasting lowered lean mass weight in WD- and KD-fed mice but not GBD-fed mice (Supplemental Figure 3-5F). The change in lean mass from baseline was the smallest in KD-fed mice, however, the fasting induced deficit in lean mass from baseline was significantly reduced with GBD-refeeding only (Supplemental Figure 3-5G). During refeeding, GBD-fed mice consumed the most food by weight but calorie intake was not different between diet groups (Supplemental Figure 3-5H). Taken together, these data highlight

the impact of background diet on body weight composition throughout a fasting-refeeding protocol.

CLD abundance at the villus tip was not different between diet groups (Figure 3.6G,H). Moreover, jejunal TG mass was not significantly different among diet groups (Figure 3.6I). Similarly, the size distribution of CLDs was unchanged between groups but shifted toward the smallest (<0.05 μm) and away from the largest (>1.2 μm) compared to 4 hours after oil gavage (Figure 6J). Unlike in post-oil gavage mice, *ApoB* expression was reduced in KD compared to WD mice and *Mttp* expression was increased in KD compared to GBD-fed mice (Figure 3.6K). *Dgat1* and *Atgl* expression were increased in WD, not KD, compared to GBD mice (Figure 3.6K). Expression of *Pparα* mRNA was significantly greater in KD-fed mice compared to GBD-fed mice (Figure 3.6K). *Cpt1α*, *Srebf1*, and *Plin2* mRNA expression was not significantly different between groups (Figure 3.6K) and neither was mRNA expression of *Dgat2*, *Fasn*, *Plin3*, *or Hmgcs2* (Supplemental Figure 3.6A). Expression of *Cd36* was also greater in KD compared to GBD-fed mice (Figure 3.6K). Intestinotrophic *Igf1* mRNA and *Glp2r* mRNA expression was not different among diet groups, however, *Glp1r* mRNA expression was lower in KD than WD-fed males (Figure 3.6K). Villi length and crypt depth were not significantly different in the duodenum, proximal jejunum (trend, p=0.0788), or ileum (Supplemental Figure 3-6B-G)

Figure 3.6 Ketogenic diet feeding increases small intestinal length and circulating TG in male mice. Male mice were fed GBD, WD, or KD for 5 weeks then fasted for 12 hours and refed their diet for 2 hours before sacrifice. Small intestinal (A) length and (B) weight. (C) Fasting and refed plasma TG levels and (D) the change in plasma TG levels between time points. (E) Fasting and refed free fatty acid levels with (F) the change in plasma free fatty acids levels between time points. (G) Representative images of jejunal epithelium cytosolic lipid droplets (CLD) after refeeding in male mice. (H) Quantification of total BODIPY stain signal per micrograph. (I) Total TG mass from jejunal extract. (J) Mean and binned jejunal epithelium CLD size from micrographs. (K) Jejunal mRNA abundance of *ApoB, Mttp, Dgat1, Atgl, Pparα, Cpt1α, CD36, Plin2, Srebf1, Igf1, Glp1r,* and *Glp2r* normalized to *Actb*. Data are shown as mean +/- SEM. Significance was determined by one-way ANOVA with multiple comparisons (A, B, D, F, H, I, J (mean), and K), Kolmogorov–Smirnov test (J), or two-way ANOVA with Tukey's multiple comparisons. Differences between diet groups are represented with lines and P values are indicated. GBD: Grain-based diet, WD: Western diet, KD: Ketogenic diet.

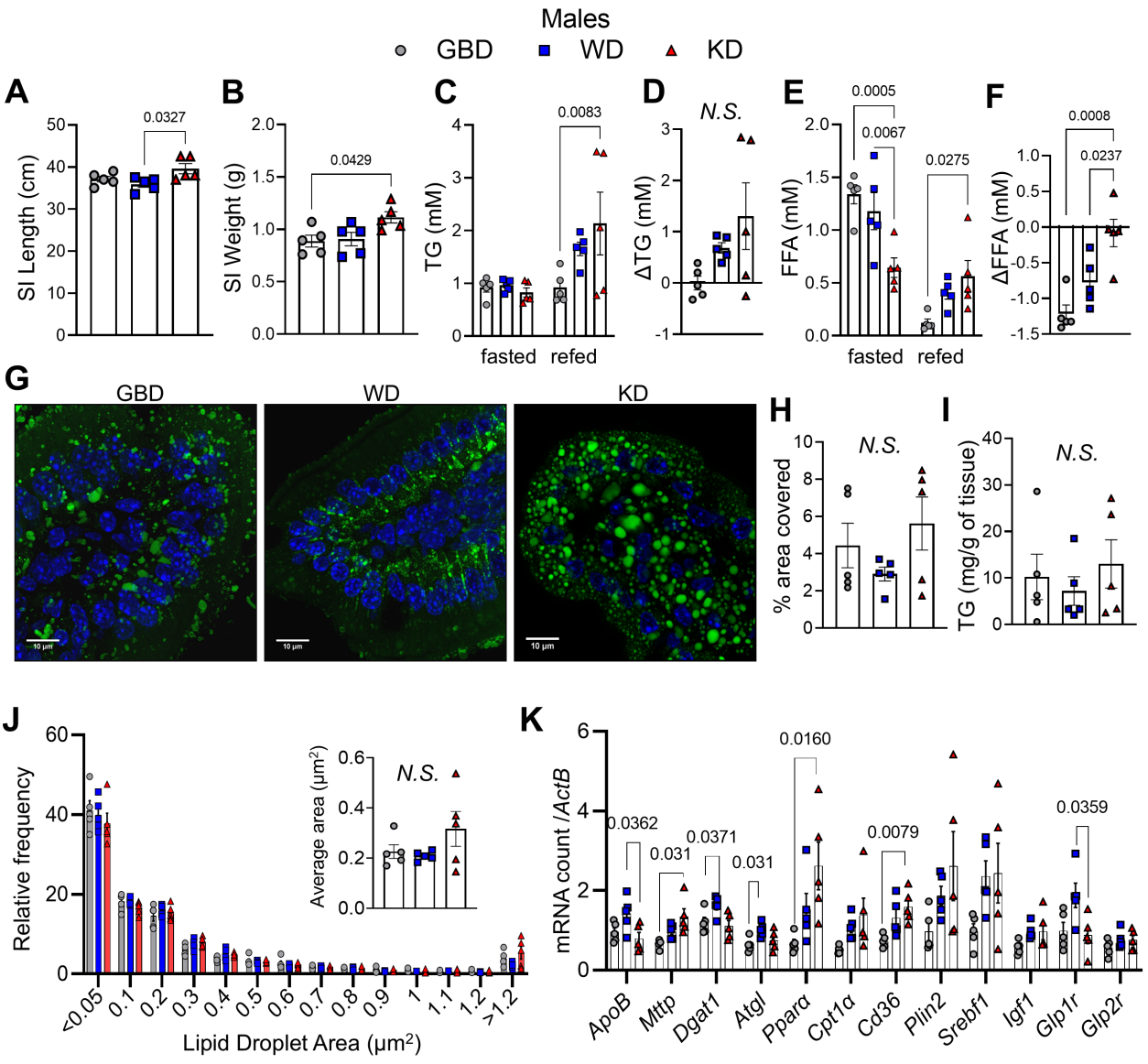
Males
GBD
WD
KD
A
SI Length (cm)
0.0327
B
SI Weight (g)
0.0429
C
TG (mM)
0.0083
fasted
refed
D
N.S.
ΔTG (mM)
E
FFA (mM)
0.0005
0.0067
0.0275
fasted
refed
F
ΔFFA (mM)
0.0008
0.0237
G
GBD
WD
KD
10 µm
H
% area covered
N.S.
I
TG (mg/g of tissue)
N.S.
J
Relative frequency
Lipid Droplet Area (µm²)
<0.05
0.1
0.2
0.3
0.4
0.5
0.6
0.7
0.8
0.9
1
1.1
1.2
>1.2
Average area (µm²)
N.S.
K
mRNA count /ActB
0.0362
0.031
0.0371
0.031
0.0160
0.0079
0.0359
ApoB
Mttp
Dgat1
Atgl
Pparα
Cpt1α
Cd36
Plin2
Srebf1
Igf1
Glp1r
Glp2r

3.5.6 KD feeding in females promotes high circulating FFA and increases fasting-refed intestinal lipid storage after 2 hours of refeeding

Insulin sensitivity was not significantly different among diet groups in female mice after four weeks of diet (Supplemental Figure 3-7A). Unlike in males, small intestinal length was not different in females in the refed state (Figure 3.7A). However, small intestine weight was increased in KD-fed females compared to WD (Figure 3.7B). Fasting blood BHB was not different between groups (Supplemental Figure 3-7B,C). Refeeding reduced BHB in GBD and WD females while KD-fed females maintained elevated BHB after refeeding, indicating ketosis (Supplemental Figure 3-7C). Blood glucose was not different between groups in the fasted or refed state although KD-fed females had more minor increases in blood glucose than GBD (Supplemental Figure 3-7D,E). There were no significant differences in plasma insulin levels (Supplemental Figure 3-7F,G). Plasma TG were not significantly different among diet groups in the fasted or fed state, but plasma FFA levels were increased in KD compared to GBD-fed females in the refed state (Figure 3.7C-F). Unlike male mice, the 12-hour fasting- 2-hour refeeding protocol did not reveal diet-specific changes in weight maintenance (Supplemental Figure 3-7H,I). Perigonadal adipose tissue weight was not significantly different among female diet groups (Supplemental Figure 3-7J). Unlike male mice, adipocyte diameter was similar among female diet groups with a shift towards larger adipocytes (Supplemental Figure 3-7K). Similar to males, LPL activity in adipose tissue was not significantly different among diet groups in the refed state (Supplemental Figure 3-7L). CLD abundance at the villus tip was greater in KD than GBD-fed females (Figure 3.7G,H). In contrast to males, jejunal TG mass was significantly higher in female KD-fed mice compared to both GBD- and WD-fed mice (Figure 3.7I). CLD size distribution was unchanged between groups but shifted to smaller sizes compared to those in post-oil gavage females (Figure 3.7J). Similar to male refed mice, female KD-fed mice had greater *Mttp* and *Pparα* expression than GBD mice but no differences in *ApoB*, *Dgat1*, or *Atgl* (Figure 3.7K). *Cpt1α*, *Cd36*, and *Srebf1* expression were greater in KD than GBD and *Plin2* expression in KD females was greater than

in GBD and WD-fed mice, consistent with increased CLD abundance (Figure 3.7K). While *Igf1* expression was not different between groups, *Glp1r* expression was lower in KD than GBD-fed females and *Glp2r* expression was lower in KD than both GBD and WD-fed females (Figure 3.7K). Similar to males, *Dgat2*, *Fasn*, *Plin3*, and *Hmgcs2* mRNA abundance were not different between groups (Supplemental Figure 3-8A). Villi length and crypt depth were unchanged between diets in duodenum, jejunum, and ileum (Supplemental Figure 3-8B-G). Taken together, these data suggest KD-feeding in females promotes intestinal lipid storage to control intestinal-TG secretion rates.

Figure 3.7 Ketogenic diet feeding increases small intestinal weight and lipid stores in female mice. Female mice were fed GBD, WD, or KD for 5 weeks then fasted for 12 hours and refed their diet for 2 hours before sacrifice. Small intestine (A) length and (B) weight. (C) Fasting and refed plasma TG levels with (D) the change in plasma TG levels between time points. (E) Fasting and refed free fatty acid levels with (F) the difference in plasma free fatty acid levels between time points. (G) Representative images of jejunal epithelium cytosolic lipid droplets (CLD) after refeeding. (H) Quantification of total BODIPY stain signal per micrograph. (I) Total TG mass from jejunal extract. (J) Mean and binned jejunal epithelium CLD size from micrographs. (K) Jejunal mRNA abundance of *ApoB, Mttp, Dgat1, Atgl, Pparα, Cpt1α, CD36, Plin2, Srebf1, Igf1, Glp1r, Glp2r* normalized to *Actb*. Data are shown as mean +/- SEM. Significance was determined by one-way ANOVA with multiple comparisons (A , B, D, F, H, I, J (mean), and K), Kolmogorov–Smirnov test (J), or two-way ANOVA with Tukey's multiple comparisons. Differences between diet groups are represented by lines with P values indicated. GBD: Grain-based diet, WD: Western diet, KD: Ketogenic diet.

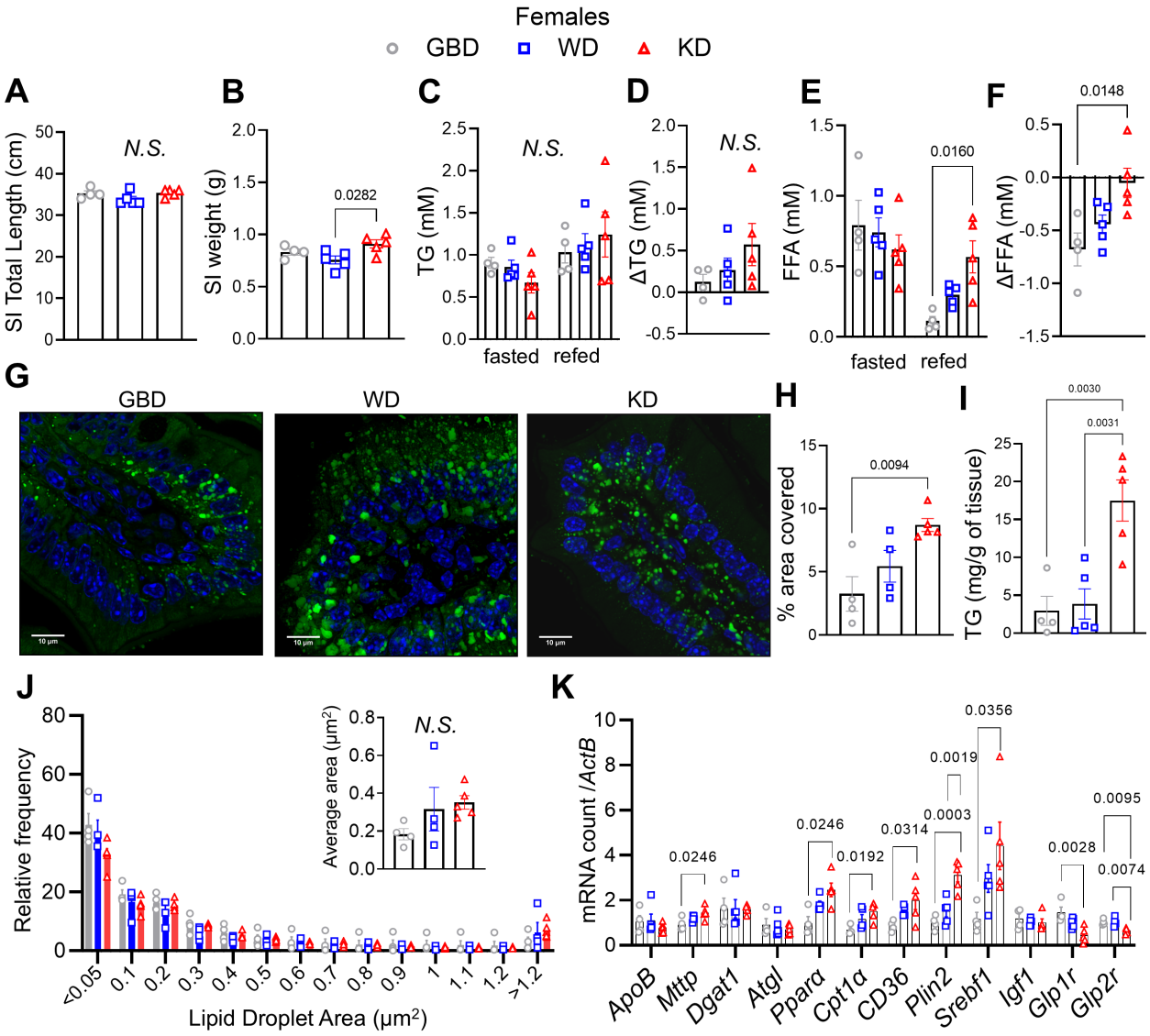
Females
GBD
WD
KD
A
SI Total Length (cm)
N.S.
B
SI weight (g)
0.0282
C
TG (mM)
N.S.
fasted
refed
D
ΔTG (mM)
N.S.
E
FFA (mM)
0.0160
fasted
refed
F
ΔFFA (mM)
0.0148
G
GBD
WD
KD
H
% area covered
0.0094
I
TG (mg/g of tissue)
0.0030
0.0031
J
Relative frequency
Lipid Droplet Area (μm²)
Average area (μm²)
N.S.
K
mRNA count /ActB
0.0246
0.0246
0.0192
0.0314
0.0003
0.0019
0.0356
0.0028
0.0095
0.0074
ApoB
Mttp
Dgat1
Atgl
Pparα
Cpt1α
CD36
Plin2
Srebf1
Igf1
Glp1r
Glp2r

3.6 Discussion

Small intestinal morphology is highly sensitive to nutrient availability (Yamauchi, Kamisoyama et al. 1996) and dietary composition, where chronic high-fat feeding significantly shortens small intestinal length (Dalby, Ross et al. 2017, Morrow, Trzaskalski et al. 2022) yet lengthens jejunal villi (Wang, Tang et al. 2020, Morrow, Trzaskalski et al. 2022). This study evaluated WD and KD-fed mice previously maintained on a GBD to uncover the influence of gross dietary manipulation in the context of a very high saturated fat, carbohydrate restriction, and moderate protein restriction on short-term intestinal adaptations to high-fat feeding. After three weeks of feeding, KD-fed male and female mice displayed significantly worsened lipid tolerance compared to GBD- and WD-fed mice, whereas lipid tolerance was unchanged in WD-fed mice compared to GBD-fed mice. Jejunal lipid droplet size and TG mass were similar among diet groups following an acute dietary fat challenge. In the fasted state, intestinal TG stores were not significantly different between WD- and GBD-fed male and female mice. However, TG stores in the proximal jejunum and distal jejunum were significantly greater in KD-fed male mice than in GBD-fed mice. TG stores were elevated in the duodenum, proximal jejunum, and distal jejunum of female KD-fed mice compared to both GBD-fed and WD-fed mice. KD-induced elevations in intestinal TG stores in male mice were accompanied by increases in small intestinal length and villi length in the distal jejunum. In female mice, KD-induced elevations in intestinal TG stores were associated with marked increases in villi length in the proximal jejunum but no changes in small intestinal length. By contrast, three weeks of WD feeding did not significantly impact small intestinal length or absorptive surface area. Fasting-refeeding experiments in male mice led to a similar level of jejunal TG mass accumulation as well as CLD size distribution. However, refeeding with a KD led to significantly higher jejunal TG mass accumulation in female mice than GBD- and WD-fed mice. Additionally, KD-feeding significantly attenuated 12 hour fasting-induced weight loss but only in male mice.

Impaired lipid tolerance with WD-feeding is well characterized (Haidari, Leung et al. 2002, Federico, Naples et al. 2006, Adeli and Lewis 2008, Douglass, Malik et al. 2012, Uchida, Whitsitt et al. 2012). Ten weeks of HFD-feeding in mice led to higher plasma TG values 2 hours post-oil gavage compared to GBD-fed controls (Uchida, Whitsitt et al. 2012). However, in poloxamer or tyloxapol experiments, secretion rates are significantly lower in HFD-fed mice after ten weeks (Uchida, Whitsitt et al. 2012) and three weeks (Douglass, Malik et al. 2012) of feeding compared to GBD-fed controls. In our study, three weeks of WD-feeding in both male and female mice did not significantly change lipid tolerance in response to an olive oil gavage or intestinal secretion rates with poloxamer relative to GBD-fed mice. This suggests that despite significant adiposity at this time point, control of intestinal lipoprotein remains intact. In contrast, we observed significant post-prandial lipemia in KD-fed male and female mice 2-hours post-oil gavage compared to both GBD-fed and WD-fed mice. In both male and female mice, jejunal mRNA expression of *Cd36* was significantly elevated with KD-feeding compared to both GBD- and WD-fed mice, consistent with increased capacity to absorb dietary fat (Drover, Ajmal et al. 2005). In male mice, post-prandial lipemia was driven by significant increases in intestinal-TG secretion rates compared to GBD-fed mice, whereas in female mice, intestinal-TG secretion rates were unchanged among diet groups. However, plasma apoB48 levels were not significantly different among diet groups in male or female mice, suggesting that the assembly of larger chylomicrons drove the increased TG secretion rates in male mice. Indeed, KD-fed mice had increased substrate for chylomicron synthesis as shown by the elevated fasting jejunal TG levels in male and fasting duodenal and jejunal TG levels in female KD-fed mice. Moreover, this may explain the unchanged post-oil TG mass and CLD size distribution in KD-fed male mice despite enhanced TG secretion rates. The mechanism underlying an unchanged intestinal-TG secretion rate in female KD-fed mice compared to GBD and WD-fed mice in our poloxamer experiment despite higher fasting intestinal TG stores is unclear. Unlike in male mice, we did not observe differences in mRNA expression of genes involved in chylomicron assembly or secretion, including *Dgat1* and *Apob*. Instead, both

Atgl and *Cpt1a* mRNA expression was significantly higher in female KD-fed mice compared to both GBD- and WD-fed mice suggesting that the unchanged post-oil TG mass and CLD abundance in female KD-fed mice despite higher fasting intestinal TG stores may be driven by enhanced oxidation of FA stored from a previous meal.

Several studies indicate intestinal adaptations to short-term, high-fat feeding studies. Four weeks of 10, 20, 30, or 45% energy derived from fat demonstrated a dose-dependent influence on gene expression, enriching transcript abundance for lipid transport and FA catabolism (de Wit, Boekschoten et al. 2011). HFD-induced obesity, but not HFD feeding in equal kcal as GBD-fed mice, drives crypt depth and villus lengthening (Zhou, Davis et al. 2018); this increased surface area is proposed to contribute to obesity. In GBD mice, CLD size is the largest in the proximal intestine and decreases distally; in HFD-fed mice, however, CLD size is consistent throughout the length of the intestine (Zembroski, D'Aquila et al. 2021), suggesting a greater capacity to store FA and/or more significant contributions from endogenous or circulating FA. In our study, 3 weeks of WD-feeding did not significantly change intestinal length or villi length throughout the small intestine compared to GBD-fed mice, suggesting that HFD-induced intestinal morphological adaptations, in line with intestinal secretion rates, occur after obesity development. Moreover, insulin sensitivity as assessed by an insulin tolerance test was still maintained in these WD-fed mice. Therefore, despite the high sucrose, high fat, high cholesterol composition of the WD, the unchanged fasting intestinal TG stores and *Srebf1c* mRNA expression in WD-fed mice compared to GBD-fed mice may be explained by the lack of intestinal insulin resistance, previously shown to enhance TG accumulation through *de novo* lipogenesis (Morrow, Trzaskalski et al. 2022). Additionally, 10-12 weeks of HFD feeding increases intestinal FA oxidation potential (D'Aquila, Zembroski et al. 2019, Morrow, Trzaskalski et al. 2022) to reduce TG stores when both dietary fat and carbohydrates are in excess, which we did not detect by gene expression at this time point. Moreover, CLD size and TG levels were similar to that of GBD-fed mice. By contrast, 3 weeks of

KD-feeding induced significant morphological changes to the small intestine. Previously, 4-6 weeks of KD-feeding led to a trend for decrease in small intestinal length (Cheng, Biton et al. 2019). In our study, KD-feeding in males increased small intestinal length and expanded the jejunal absorptive surface area distally. Interestingly, small intestinal length normalized in KD-fed mice post-oil gavage compared to the fasted state. The impact of fasting on intestinal length shortening has been documented in fish (Gaucher, Vidal et al. 2012) and chickens (Yamauchi, Kamisoyama et al. 1996), where the flexibility of intestinal length is regulated to conserve energy during nutrient scarcity. As the KD-fed mice were more resistant to fasting-induced weight loss, they may not as readily trigger length shortening. While the small intestinal length was not different in female mice fed the KD, the villi length in the proximal jejunal was significantly greater throughout the segment, potentially accounting for the significant increase in the weight of the small bowel. Interestingly, KD-fed male and female mice displayed significantly higher mRNA expression levels of *Pparα*, which plays a direct role for intestinal villi length elongation (Stojanovic, Altirriba et al. 2021). Insulin sensitivity was also maintained in KD-fed mice despite the worsened lipid tolerance test in male and female mice. We propose that the small intestine adapts to the KD by providing increased intestinal length in males to accelerate chylomicron synthesis from incoming dietary FA given the higher jejunal TG storage and in females increases proximal jejunal villi length to enable higher duodenal and jejunal TG storage. However, the rate at which these lipid stores are mobilized is greater in male compared to female mice for reasons that could not be elucidated in our study. Additionally, our study's mechanisms through which KD modulates intestinal length are unclear and whether liberation of intestinal lipid stores facilitates the resistance to fasting-induced weight loss in KD-fed mice has yet to be determined. Taken together, these experiments reveal both structural and metabolic remodelling of the intestine in a diet- and sex-specific manner. Although, delineating the sex differences, particularly in the intestinal absorption capacity in male and female mice on a KD, will require future experiments.

After refeeding their respective diet for 2 hours after a 12-hour fast, jejunal CLD size and abundance was similar among groups, suggesting that a similar amount of dietary fat is stored in the enterocyte, independent of the meal composition. However, refeeding also increased plasma TG levels in male WD- (0.967 vs 1.653 mmol/L) and KD-fed mice (0.800 vs 2.133 mmol/L) but not in GBD-fed mice (0.920 vs 0.922 mmol/L). Glucose, by contrast, only increased in both GBD- (5.4 vs 7.7 mmol/L) and WD-fed mice (6.06 vs 8.64 mmol/L) but not KD-fed mice (7.86 vs 6.48 mmol/L). Therefore, glucose availability following a 12-hour fast in GBD-fed mice may influence enterocytes to hold dietary fat in CLDs as reserves rather than to reassemble it into chylomicrons. While this would contradict the pro-chylomicron secretion effect of glucose (Xiao, Stahel et al. 2019), the 12-hour fast in GBD mice likely depletes TG storage in the intestine. In GBD-fed mice, CLD reserves have been detected in the intestine for up to 12 hours (Zhu, Lee et al. 2009), but this was following an oil gavage rather than a physiological refeeding period, highlighting the nutrient load-specific impact on CLD dynamics. Therefore, while similar CLD reserves were observed in WD- and KD-refed mice, the increased proportion of dietary fat with WD- and KD-refeeding shifted a proportion of dietary fat to chylomicron synthesis, as observed in the rise in plasma TG levels.

KD feeding after a 12 hour fast led to higher plasma TG and FFA levels compared to refeeding with the GBD or WD diet. These changes in plasma metabolites were independent of body weight compared to GBD-fed mice indicating a rapidly induced metabolic switch that mimics a fasting profile. Given the strong drive for gluconeogenesis in mice, a limitation of this study is that rodent KD must contain almost no carbohydrate and extreme fat proportion compared to human ketogenic diets to maintain elevated ketones (Hu, Wang et al. 2018). This diet, having reduced protein and <1% kcal from carbohydrates, is not representative of human KD feeding, rather a state of elevated circulating ketones and extreme dietary fat. Additionally, we can only evaluate gross differences in dietary composition as the carbohydrate source for the WD was

sucrose and not matched to the grain-based composition observed in standard laboratory chow on which the mice were normally maintained.

The influence of carbohydrate sources in intestinal physiology and early phases of obesity development is increasingly appreciated. Both high-fat diets (60% of calories from fat) and high-fat, high-sucrose diets (60% calories from fat, 25% from sucrose) increase jejunal *Pparα* mRNA expression and shorten the small intestine (Stojanovic, Altirriba et al. 2021). Four weeks of high-fat, high-sucrose feeding increases duodenal villi length and serum TG levels post-oil gavage without changing intestinal length (Taylor, Ramsamooj et al. 2021). Additionally, in chow-fed mice, high-fructose corn syrup supplementation in drinking water for four weeks increases both duodenal and proximal jejunal villus length, which is associated with weight gain and increased intestinal-TG secretion rates in poloxamer experiments in a pyruvate kinase M2-dependent manner (Taylor, Ramsamooj et al. 2021). Therefore, the lack of difference in our GBD and WD-fed mice could be driven by differences in carbohydrate sources. Additionally, our GBD may be obesogenic and induce some liver steatosis particularly in male mice as previously seen (Zhang, Leveille et al. 2020). This may explain the worsened insulin tolerance in males on the GBD. Differences in other known dietary factors, including fiber, micronutrient profiles, and texture, were also not completely matched among the 3 diets. Although nutrient sources were matched between WD and KD, protein content was necessarily reduced to achieve nutritional ketosis, therefore, the proportions of all three macronutrients are distinct and as such, differentially impact intestinal homeostasis. Indeed, both essential and non-essential amino acids are critical for maintaining intestinal mucosal barrier function through the synthesis of mucosal epithelial proteins such as mucins, epithelial permeability through upregulation of tight junction protein expression, mucosal homeostasis through the downregulation of inflammatory cytokines, and providing metabolic fuel for the rapidly dividing intestinal epithelial cells (Yang and Liao 2019, Beaumont and Blachier 2020).

In our study, 5 weeks of WD-feeding did not significantly change post-prandial TG responses to olive oil gavages with or without poloxamer compared to GBD-fed mice. Nor did the WD induce insulin resistance in comparison to the GBD. Different dietary compositions of the GBD may explain these differences. In our study, the GBD was 55% kcal from carbohydrates, 22% kcal from fat, and 23% kcal from protein, compared to the GBD used in Douglass *et al.*, which was 70% kcal from carbohydrate, 10% kcal from fat, and 20% kcal from protein (Douglass, Malik et al. 2012) and the GBD used in Uchida *et al.*, which was 62.1% kcal from carbohydrate, 13.2% kcal from fat, and 24.7% from protein (Uchida, Whitsitt et al. 2012). The decreased proportion of kcal from carbohydrate and relative increase in kcal from fat (double) as other background control diets may explain the reduced relative post-prandial lipid response as dietary fat is a key driver of adiposity in mice (Hu, Wang et al. 2018).

Overall, these data demonstrate diet- and meal-dependent effects on plasma TG levels and intestinal gene expression levels of intestinal TG re-assembly pathways. While metabolic benefits of KD feeding have been attributed to a shift toward hepatic lipid catabolism and reductions in obesity and fatty liver in humans (Schugar and Crawford 2012, Puchalska and Crawford 2017, Gershuni, Yan et al. 2018, Watanabe, Tozzi et al. 2020), our data demonstrate that the small intestinal adaptation to KD feeding in mice plays an important role in the delivery of increased dietary fat. Particularly, while both male and female KD-fed mice have increased TG excursion after oil gavage, FA absorption and background diet intestinal lipid stores exhibited sex differences. Future studies will be required to investigate the impact of sex-dependent increases in intestinally-TG secretion rates on atherosclerosis progression in long-term KD feeding.

3.7 Sources of Funding

This work was supported by Canadian Institutes of Health Research Grants, ARJ-162628, NSERC grant 551669-152199-2004 to E.E.M. C.A.A.L. was supported by a Queen Elizabeth II scholarship and N.M.M. was supported by CIHR Canada Graduate Scholarship Frederick Banting

and Charles Best Doctoral Award. N.A.T. was supported by a UOHI Cardiac Endowment scholarship. A.C.C was supported by a University of Ottawa Centre for Infection, Immunity and Inflammation scholarship. S.I. was supported by the uOttawa undergraduate research opportunity scholarship. C.T.K and H.A.H were supported by NSERC undergraduate student research awards.

3.8 Supplemental materials

Supplemental Figure 3-1 Ketogenic diet does not induce obesity after 5 weeks of feeding. Male and female mice were fed a GBD, WD, or KD for 3 or 5 weeks. (A) Schematic of the experimental outline. (B,C) Estimated mean kcal intake of group housed mice on each diet by week of experiment. (D, E) Total body weight of male mice over diet intervention. Data are shown as mean +/- SEM. Significance determined by mixed effects analysis with Tukey's multiple comparisons. Differences between diet groups are represented by colour (grey: KD and GBD, blue: KD and WD, black: GBD and WD) or line and the p-value is indicated. GBD: Grain-based diet, WD: Western diet, KD: Ketogenic diet.

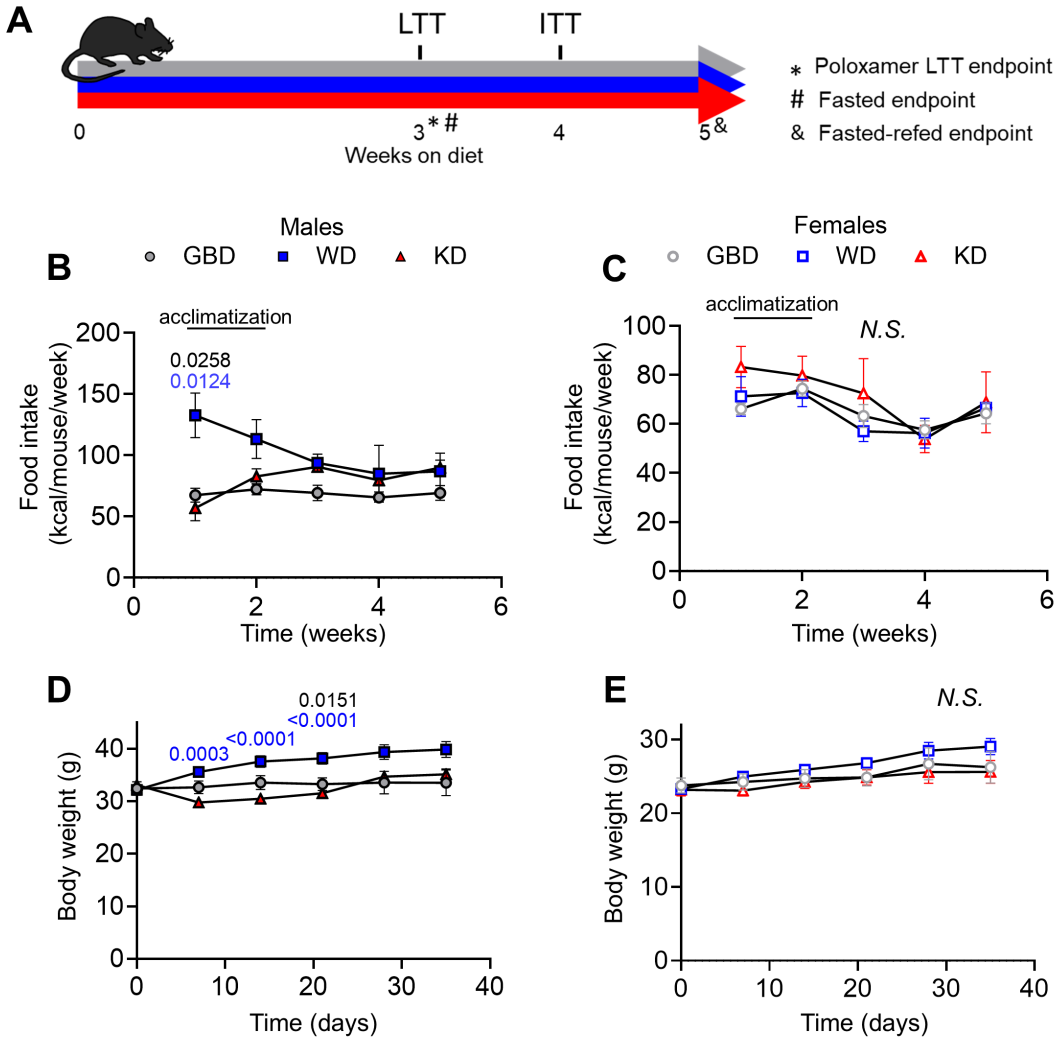
A
LTT
ITT
0
3 * #
4
5 &
Weeks on diet
* Poloxamer LTT endpoint
# Fasted endpoint
& Fasted-refed endpoint
B
Males
GBD
WD
KD
acclimatization
0.0258
0.0124
Food intake (kcal/mouse/week)
Time (weeks)
C
Females
GBD
WD
KD
acclimatization
N.S.
Food intake (kcal/mouse/week)
Time (weeks)
D
0.0151
<0.0001
<0.0001
0.0003
Body weight (g)
Time (days)
E
N.S.
Body weight (g)
Time (days)

Supplemental Figure 3-2 Ketogenic diet-feeding does not impact ratio of total to gavage-derived lipid in males or females or hepatic TG mass compared to WD-fed mice. (A) Jejunal mRNA abundance of *Dgat2, Mttp, Plin2, Cpt1α, Igf1, Glp2r* normalized to *Actb* in male mice 4 hours post-oil gavage. (B) Representative images of total (Autodot) and gavage-derived (BODIPY-C16) cytosolic lipid droplets (CLD) in male mice with (C) the calculated ratio of gavage to total neutral lipid stain. (D) Male relative liver weight to total body weight and (E) hepatic TG mass. (F) Jejunal mRNA abundance *of Dgat2, Mttp, Plin2, Cpt1α, Igf1*, and *Glp2r* normalized to *Actb* in female mice 4 hours post-oil gavage. (G) Representative images of total (Autodot) and gavage-derived (BODIPY-C16) CLD in females with (H) the calculated ratio of gavage to total neutral lipid stain. (I) Female relative liver weight to total body weight with (J) hepatic TG mass. Data are shown as mean +/- SEM. Significance determined by one way ANOVA with Tukey's multiple comparisons. GBD: Grain-based diet, WD: Western diet, KD: Ketogenic diet.

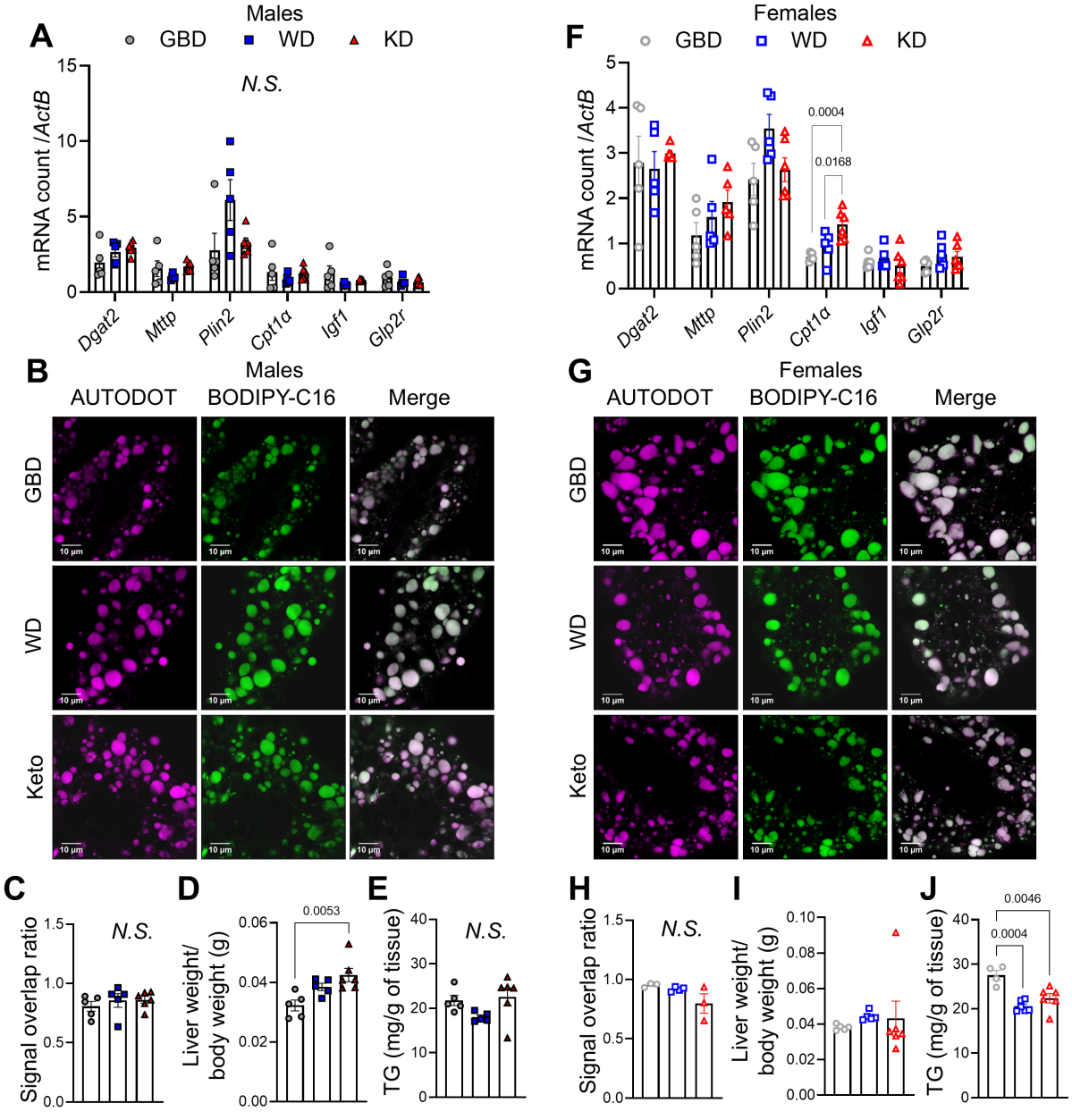
A
Males
GBD
WD
KD
N.S.
mRNA count /ActB
Dgat2
Mttp
Plin2
Cpt1α
Igf1
Glp2r
F
Females
0.0004
0.0168
B
AUTODOT
BODIPY-C16
Merge
GBD
WD
Keto
10 μm
G
C
Signal overlap ratio
D
Liver weight/ body weight (g)
0.0053
E
TG (mg/g of tissue)
H
I
J
0.0046
0.0004

Supplemental Figure 3-3 Male and female ketogenic diet-fed mice maintain elevated ketones in the fed state and are more resistant to fasting-induced weight loss. Male and female mice were fed a GBD, WD, or KD for 3 weeks and sacrificed after a 5 hour fast. (A) Male fed and 5-hour fasted blood BHB with (B) the change in blood BHB between time points. (C) Male fed and 5-hour fasted blood glucose with (D) the change in blood glucose between time points. (E) Male fed and 5-hour fasted total body weight with (F) the percent change in body weight between time points. Another set of male mice underwent EchoMRI analysis at 9 and 16 days after beginning WD or KD, where (G) total body weight (H) fat mass, (I) and lean mass were measured. (J) Female fed and 5-hour fasted blood BHB with (K) the change in blood BHB between time points. (L) Female fed and 5-hour fasted blood glucose with (M) the change in blood glucose between time points. (N) Female fed and 5-hour fasted total body weight with (O) the percent change in body weight between time points. Data are shown as mean +/- SEM. Significance was determined by one-way ANOVA or two-way ANOVA (A,C,E,G,I,K) with Tukey's multiple comparisons. Differences between diet groups are represented by lines with the p-value. GBD: Grain-based diet, WD: Western diet, KD: Ketogenic diet.

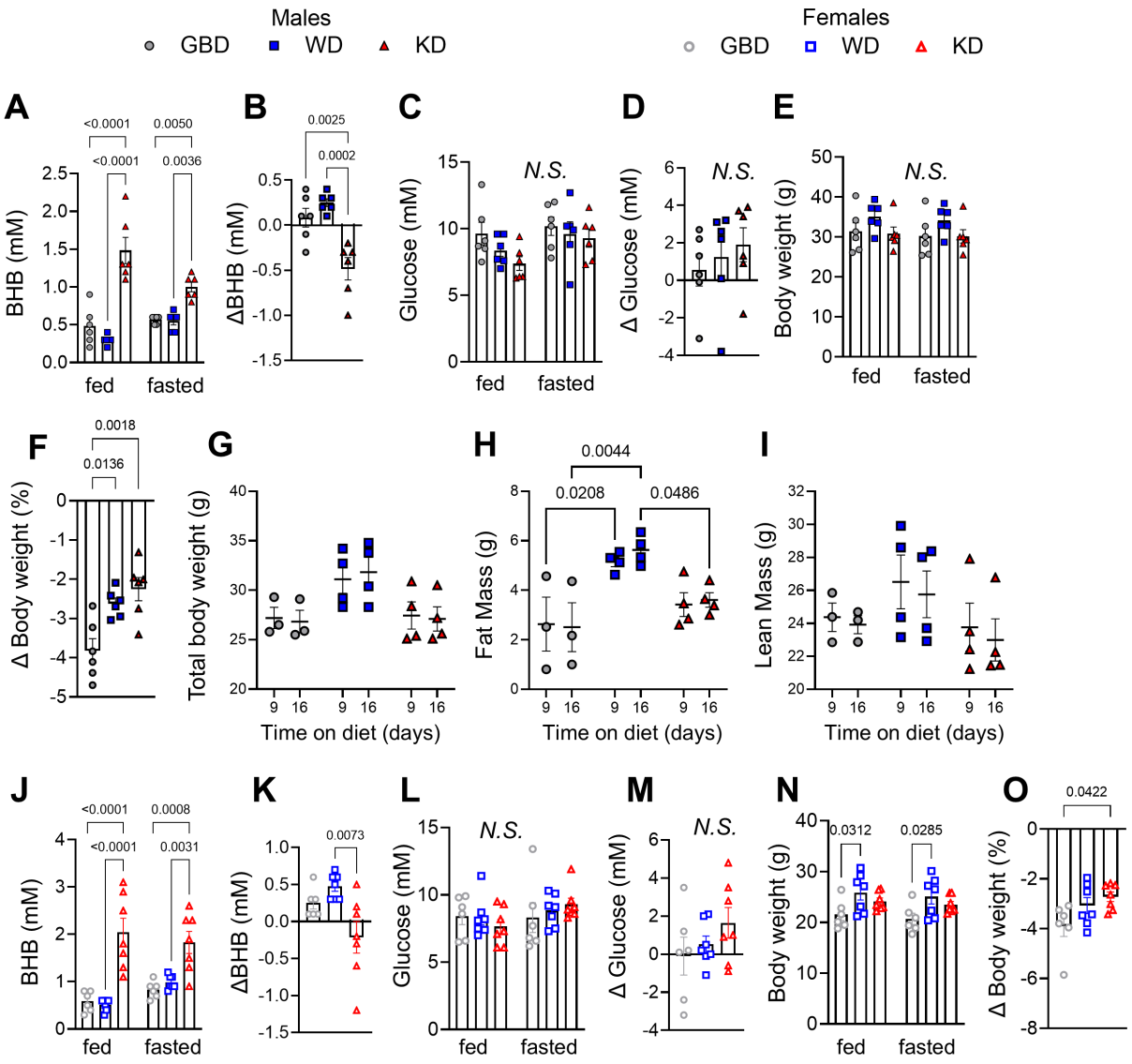
Males
GBD
WD
KD
Females
GBD
WD
KD
A
BHB (mM)
<0.0001
<0.0001
0.0050
0.0036
fed
fasted
B
ΔBHB (mM)
0.0025
0.0002
C
Glucose (mM)
N.S.
fed
fasted
D
Δ Glucose (mM)
N.S.
E
Body weight (g)
N.S.
fed
fasted
F
Δ Body weight (%)
0.0018
0.0136
G
Total body weight (g)
Time on diet (days)
H
Fat Mass (g)
0.0044
0.0208
0.0486
Time on diet (days)
I
Lean Mass (g)
Time on diet (days)
J
BHB (mM)
<0.0001
<0.0001
0.0008
0.0031
fed
fasted
K
ΔBHB (mM)
0.0073
L
Glucose (mM)
N.S.
fed
fasted
M
Δ Glucose (mM)
N.S.
N
Body weight (g)
0.0312
0.0285
fed
fasted
O
Δ Body weight (%)
0.0422

Supplemental Figure 3-4 Ketogenic diet refeeding maintains insulin sensitivity but does not impact villi length or crypt depth in male mice. Male mice were fed GBD, WD, or KD for 5 weeks. At 4 weeks on diet mice underwent an insulin tolerance test. (A) Post-i.p. insulin injection glycemia over time and area under the curve normalized to fasted glucose after 4 weeks of diet in males. At 5 weeks mice were fasted for 12 hours and refed their diet for 2 hours before sacrifice. (B) Blood BHB and (C) change in blood BHB in refed compared to fasted state. (D) Fasted and refed blood glucose and (E) change in blood glucose from fasted to refed in males. (F) Fasted and refed plasma insulin and (G) change in plasma insulin from fasted to refed state. (H) Perigonadal fat pad weight. (I) Percent frequency of adipocyte sizes and mean adipocyte size. (J) LPL activity over 60 minutes and AUC activity in perigonadal adipose tissue extracts. Data are shown as mean +/- SEM. Significance determined by one-way ANOVA or two-way ANOVA (A,B,D,F,J) with Tukey's multiple comparisons. Differences between diet groups are represented by colour (grey: KD and GBD, black: WD and GBD) or line and the p-value is indicated. GBD: Grain-based diet, WD: Western diet, KD: Ketogenic diet.

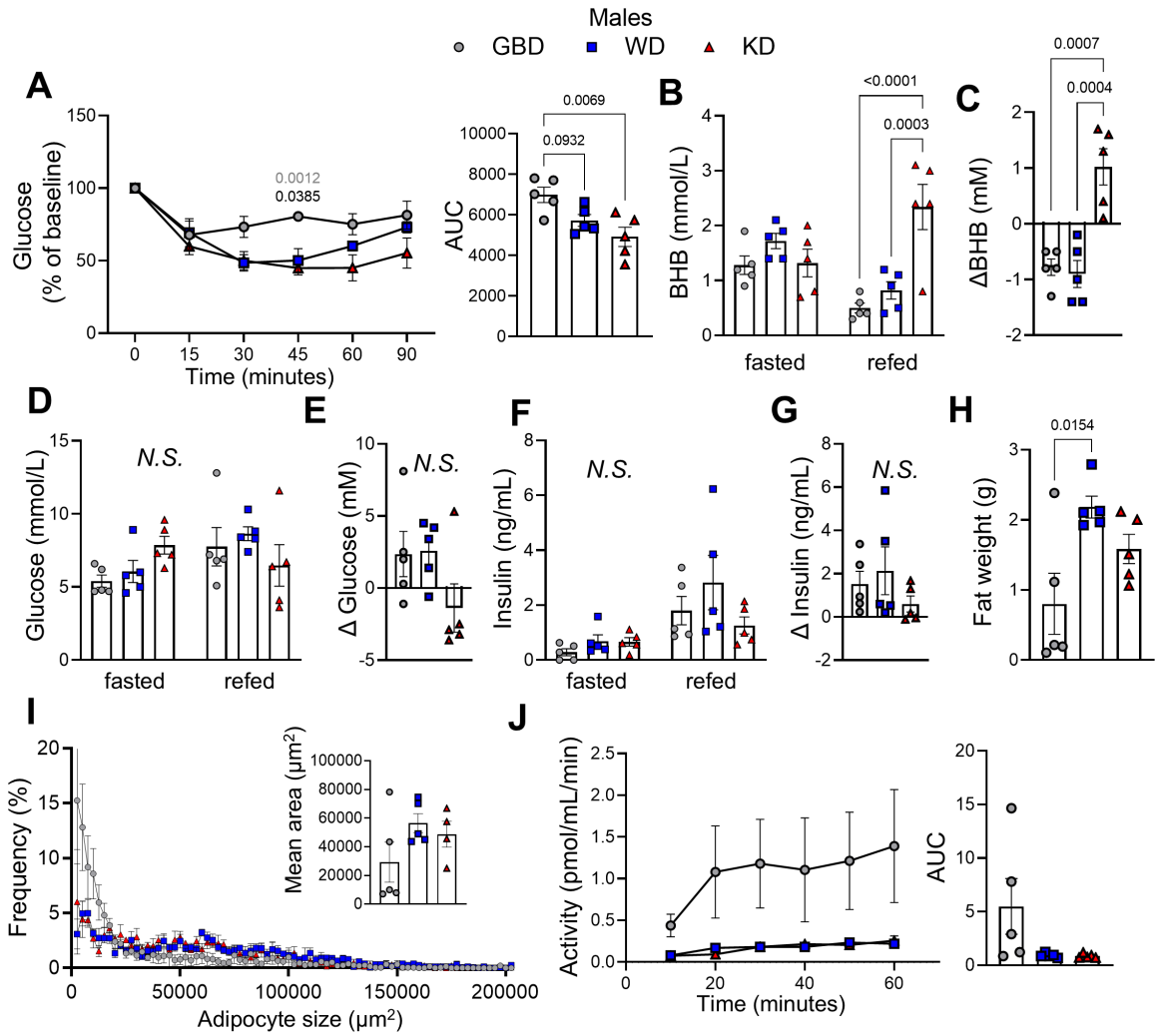
Males
GBD
WD
KD
A
Glucose (% of baseline)
Time (minutes)
0.0012
0.0385
AUC
0.0069
0.0932
B
BHB (mmol/L)
fasted
refed
<0.0001
0.0003
C
ΔBHB (mM)
0.0007
0.0004
D
Glucose (mmol/L)
N.S.
fasted
refed
E
Δ Glucose (mM)
N.S.
F
Insulin (ng/mL)
N.S.
fasted
refed
G
Δ Insulin (ng/mL)
N.S.
H
Fat weight (g)
0.0154
I
Frequency (%)
Adipocyte size (μm²)
Mean area (μm²)
J
Activity (pmol/mL/min)
Time (minutes)
AUC

Supplemental Figure 3-5 Short term KD-fed mice resist weight loss during 12 hour fast. Male mice were fed a GBD, WD, or KD. After 12 days on diet, body composition was determined by EchoMRI in fed, fasted, and refer time points. (A) Total body weight after 5 weeks on diet after a 12 hour fast and 2 hours of refeeding. (B) Percent change in body weight after fasting and refeeding. (C) Schematic of EchoMRI fasting refeeding timeline in another set of mice. (D) Baseline (end of light cycle), 12-hour fasted, and 2-hour refed body weight. (E) Body weight change at 12 hours fasted and 2 hours refed compared to baseline weight. (F) Baseline (end of light cycle), 12-hour fasted, and 2-hour refed fat mass. (G) Fat mass change at 12 hours fasted and 2 hours refed compared to baseline. (H) Baseline (end of light cycle), 12 hours fasted, and 2 hour rsefed lean mass. (I) Lean mass change at 12 hours fasted and 2 hours refed compared to baseline. Estimated food intake during the 2 hour refeed period in grams (J) and kcal (K). Data are shown as mean +/- SEM. Significance determined by one (B, J, K) or 2-way ANOVA with Tukey's multiple comparisons. Significant differences within a group over time are represented by different letters.

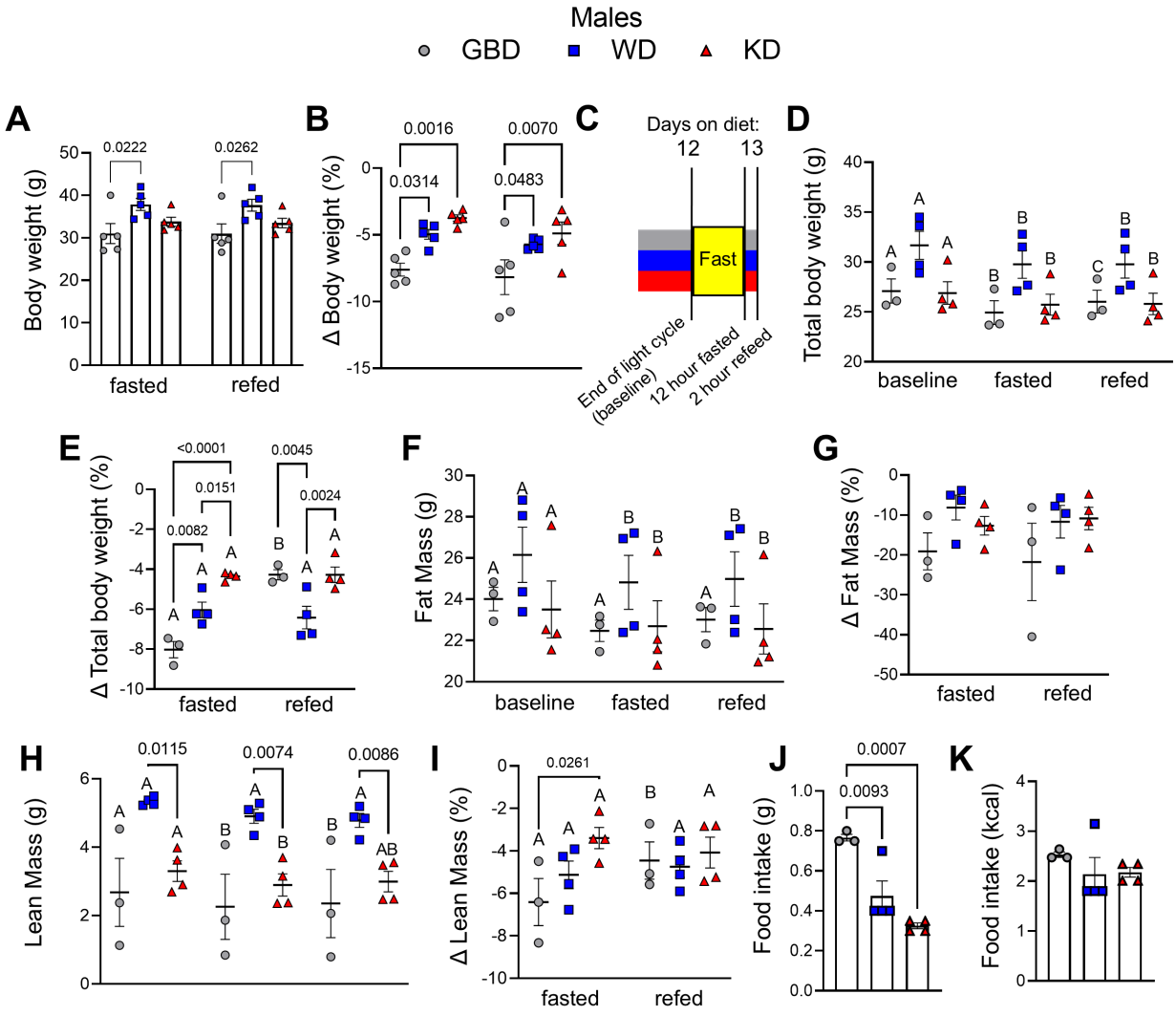
Males
GBD
WD
KD
A
Body weight (g)
0.0222
0.0262
fasted
refed
B
Δ Body weight (%)
0.0016
0.0070
0.0314
0.0483
C
Days on diet:
12
13
Fast
End of light cycle (baseline)
12 hour fasted
2 hour refeed
D
Total body weight (g)
baseline
fasted
refed
E
Δ Total body weight (%)
<0.0001
0.0151
0.0082
0.0045
0.0024
F
Fat Mass (g)
G
Δ Fat Mass (%)
H
Lean Mass (g)
0.0115
0.0074
0.0086
I
Δ Lean Mass (%)
0.0261
J
Food intake (g)
0.0007
0.0093
K
Food intake (kcal)

Supplemental Figure 3-6 Villi length and crypt depth are not changed with diet in males in the refed state. (A) Total mRNA abundance of *Dgat2, Fasn, Plin3*, and *Hmgcs2* normalized to *Actb*. Villi length in the (B) duodenum, (C) jejunum, and (D) ileum of male mice. Crypt depth in the (E) duodenum, (F) jejunum, and (G) ileum. Data are shown as mean +/- SEM. Significance determined by one way ANOVA with Tukey's multiple comparisons. GBD: Grain-based diet, WD: Western diet, KD: Ketogenic diet.

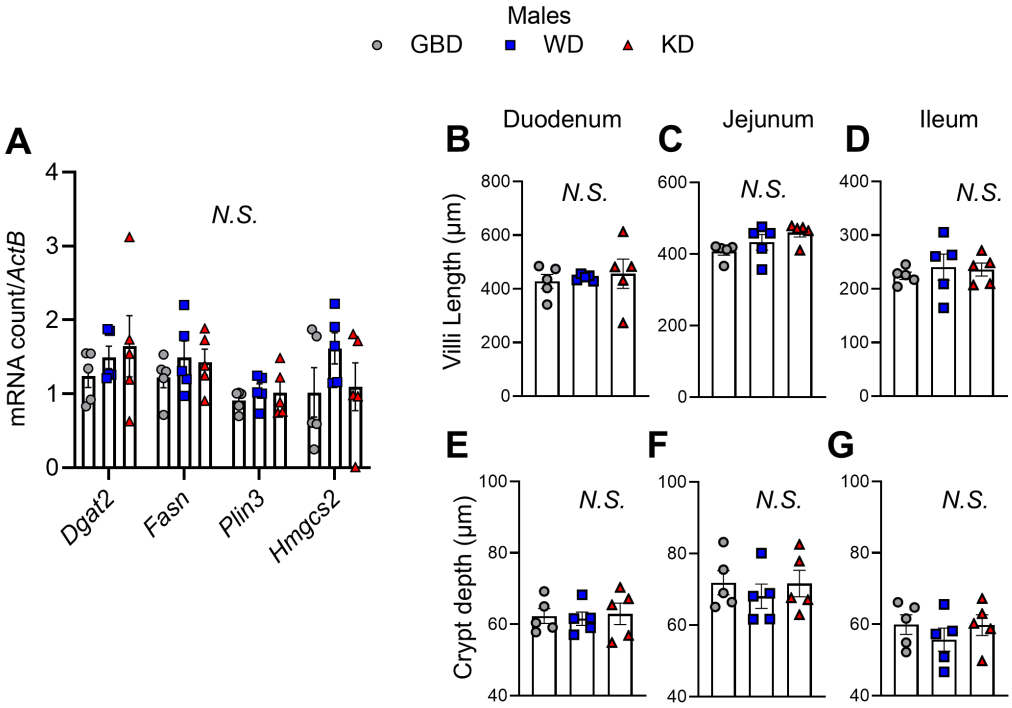
Males
GBD
WD
KD
A
mRNA count/ActB
N.S.
Dgat2
Fasn
Plin3
Hmgcs2
B
Duodenum
C
Jejunum
D
Ileum
Villi Length (µm)
N.S.
E
F
G
Crypt depth (µm)

Supplemental Figure 3-7 Ketogenic diet refeeding maintains ketosis, does not impact adipose LPL activity or body weight in female mice. Female mice were fed GBD, WD, or KD for 5 weeks. At 4 weeks on diet mice underwent an insulin tolerance test. (A) Post-i.p. insulin injection glycemia over time and area under the curve normalized to fasted glucose after 4 weeks of diet in males. At 5 weeks mice were fasted for 12 hours and refed their diet for 2 hours before sacrifice. (B) Blood BHB and (C) change in blood BHB in refed compared to fasted state. (D) Fasted and refed blood glucose and (E) change in blood glucose from fasted to refed in males. (F) Fasted and refed plasma insulin and (G) change in plasma insulin from fasted to refed state. (H) Perigonadal fat pad weight. (I) Percent frequency of adipocyte sizes and mean adipocyte size. (J) LPL activity over 60 minutes and AUC activity in perigonadal adipose tissue extracts. (K) Total body weight after 5 weeks on diet after a 12 hour fast and 2 hours of refeeding. (L) Percent change in body weight after fasting a refeeding compared to baseline. Data are shown as mean +/- SEM. Significance determined by one-way ANOVA or two-way ANOVA (A,B,D,F,J) with Tukey's multiple comparisons. Differences between diet groups are represented by line and the p-value is indicated. GBD: Grain-based diet, WD: Western diet, KD: Ketogenic diet.

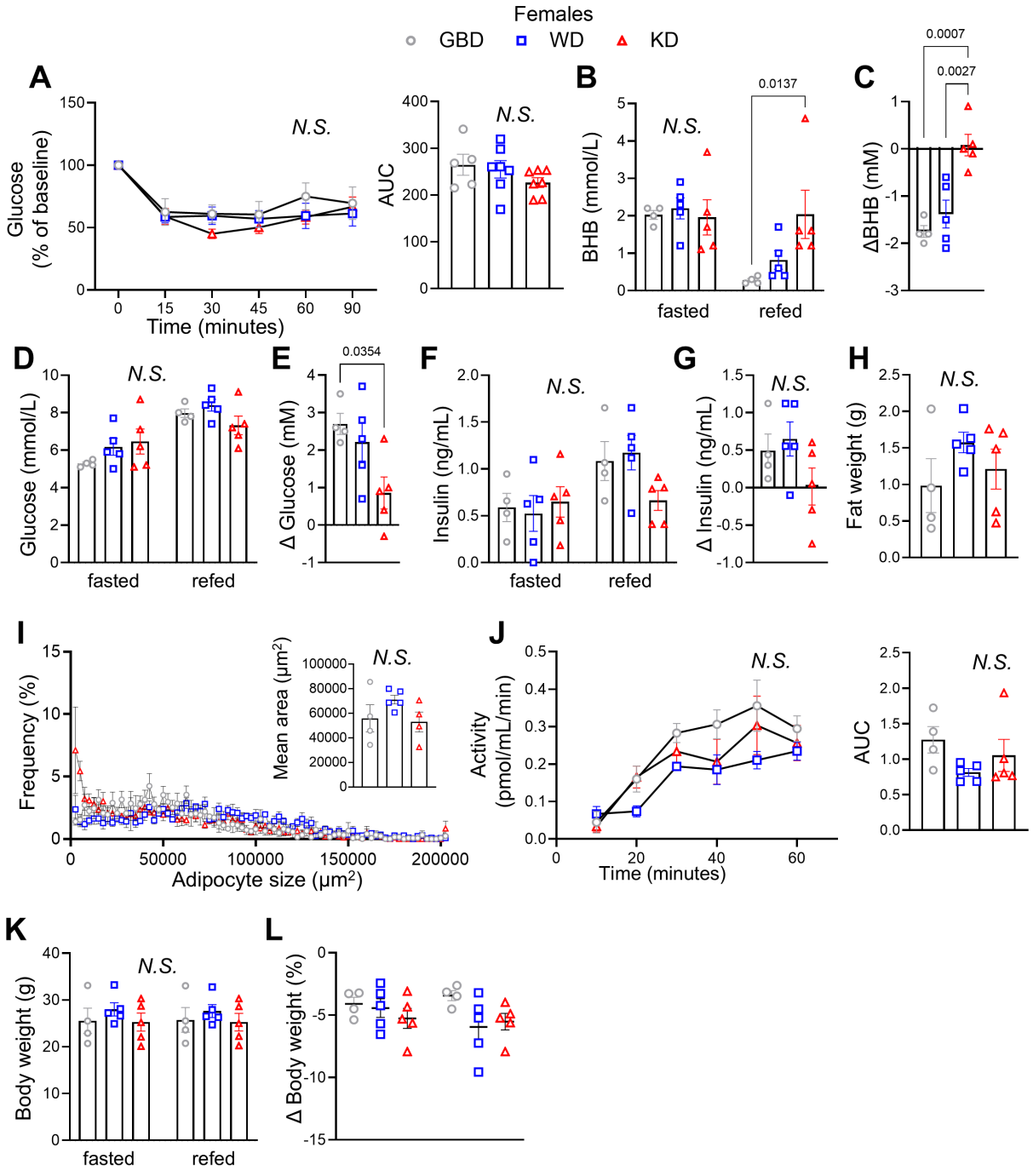
Females
GBD
WD
KD
A
Glucose (% of baseline)
Time (minutes)
N.S.
AUC
B
BHB (mmol/L)
0.0137
fasted
refed
C
ΔBHB (mM)
0.0007
0.0027
D
Glucose (mmol/L)
E
Δ Glucose (mM)
0.0354
F
Insulin (ng/mL)
G
Δ Insulin (ng/mL)
H
Fat weight (g)
I
Frequency (%)
Adipocyte size (μm²)
Mean area (μm²)
J
Activity (pmol/mL/min)
AUC
K
Body weight (g)
L
Δ Body weight (%)

Supplemental Figure 3-8 Short term KD does not significantly impact villi length or crypt depth in female mice. (A) Total mRNA abundance of *Dgat2, Fasn, Plin3*, and *Hmgcs2* normalized to *Actb*. Villi length in the (B) duodenum, (C) jejunum, and (D) ileum of male mice. Crypt depth in the (E) duodenum, (F) jejunum, and (G) ileum. Data are shown as mean +/- SEM. Significance determined by one way ANOVA with Tukey's multiple comparisons. GBD: Grain-based diet, WD: Western diet, KD: Ketogenic diet.

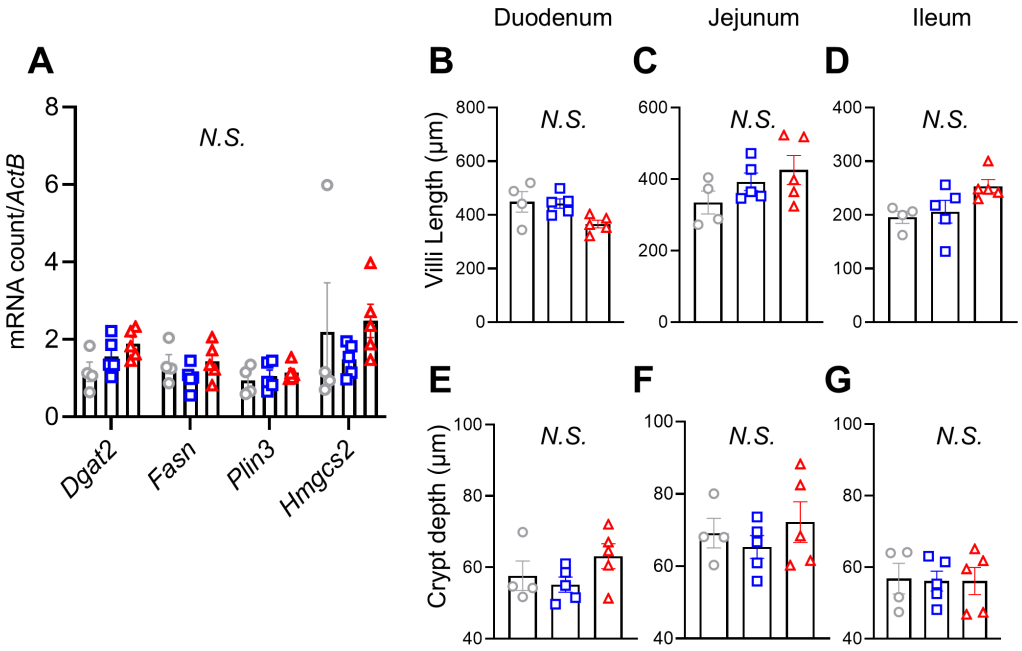
A
B
C
D
E
F
G
Duodenum
Jejunum
Ileum
mRNA count/ActB
Villi Length (μm)
Crypt depth (μm)
N.S.
Dgat2
Fasn
Plin3
Hmgcs2

3.9 References

Adeli, K. and G. F. Lewis (2008). "Intestinal lipoprotein overproduction in insulin-resistant states." Curr Opin Lipidol **19**(3): 221–228.

Adomshick, V., Y. Pu and A. Veiga-Lopez (2020). "Automated lipid droplet quantification system for phenotypic analysis of adipocytes using CellProfiler." Toxicol Mech Methods **30**(5): 378–387.

Beaumont, M. and F. Blachier (2020). "Amino Acids in Intestinal Physiology and Health." Adv Exp Med Biol **1265**: 1–20.

Bernier-Latmani, J. and T. V. Petrova (2017). "Intestinal lymphatic vasculature: structure, mechanisms and functions." Nat Rev Gastroenterol Hepatol **14**(9): 510–526.

Bialkowska, A. B., A. M. Ghaleb, M. O. Nandan and V. W. Yang (2016). "Improved Swiss-rolling Technique for Intestinal Tissue Preparation for Immunohistochemical and Immunofluorescent Analyses." J Vis Exp(113).

Boquist, S., A. Hamsten, F. Karpe and G. Ruotolo (2000). "Insulin and non-esterified fatty acid relations to alimentary lipaemia and plasma concentrations of postprandial triglyceride-rich lipoproteins in healthy middle-aged men." Diabetologia **43**(2): 185–193.

Cheng, C. W., M. Biton, A. L. Haber, N. Gunduz, G. Eng, L. T. Gaynor, S. Tripathi, G. Calibasi-Kocal, S. Rickelt, V. L. Butty, M. Moreno-Serrano, A. M. Iqbal, K. E. Bauer-Rowe, S. Imada, M. S. Ulutas, C. Mylonas, M. T. Whary, S. S. Levine, Y. Basbinar, R. O. Hynes, M. Mino-Kenudson, V. Deshpande, L. A. Boyer, J. G. Fox, C. Terranova, K. Rai, H. Piwnica-Worms, M. M. Mihaylova, A. Regev and O. H. Yilmaz (2019). "Ketone Body Signaling Mediates Intestinal Stem Cell Homeostasis and Adaptation to Diet." Cell **178**(5): 1115–1131 e1115.

Coleman, R. A., T. M. Lewin and D. M. Muoio (2000). "Physiological and nutritional regulation of enzymes of triacylglycerol synthesis." Annu Rev Nutr **20**: 77–103.

D'Aquila, T., Y. H. Hung, A. Carreiro and K. K. Buhman (2016). "Recent discoveries on absorption of dietary fat: Presence, synthesis, and metabolism of cytoplasmic lipid droplets within enterocytes." Biochim Biophys Acta **1861**(8 Pt A): 730–747.

D'Aquila, T., A. S. Zembroski and K. K. Buhman (2019). "Diet Induced Obesity Alters Intestinal Cytoplasmic Lipid Droplet Morphology and Proteome in the Postprandial Response to Dietary Fat." Front Physiol **10**: 180.

Dalby, M. J., A. W. Ross, A. W. Walker and P. J. Morgan (2017). "Dietary Uncoupling of Gut Microbiota and Energy Harvesting from Obesity and Glucose Tolerance in Mice." Cell Rep **21**(6): 1521–1533.

de Wit, N. J., M. V. Boekschoten, E. M. Bachmair, G. J. Hooiveld, P. J. de Groot, I. Rubio-Aliaga, H. Daniel and M. Muller (2011). "Dose-dependent effects of dietary fat on development of obesity in relation to intestinal differential gene expression in C57BL/6J mice." PLoS One **6**(4): e19145.

Douglass, J. D., N. Malik, S. H. Chon, K. Wells, Y. X. Zhou, A. S. Choi, L. B. Joseph and J. Storch (2012). "Intestinal mucosal triacylglycerol accumulation secondary to decreased lipid secretion in obese and high fat fed mice." Front Physiol **3**: 25.

Drover, V. A., M. Ajmal, F. Nassir, N. O. Davidson, A. M. Nauli, D. Sahoo, P. Tso and N. A. Abumrad (2005). "CD36 deficiency impairs intestinal lipid secretion and clearance of chylomicrons from the blood." J Clin Invest **115**(5): 1290–1297.

Federico, L. M., M. Naples, D. Taylor and K. Adeli (2006). "Intestinal insulin resistance and aberrant production of apolipoprotein B48 lipoproteins in an animal model of insulin resistance and metabolic dyslipidemia: evidence for activation of protein tyrosine phosphatase-1B, extracellular signal-related kinase, and sterol regulatory element-binding protein-1c in the fructose-fed hamster intestine." Diabetes **55**(5): 1316–1326.

Gaucher, L., N. Vidal, A. D'Anatro and D. E. Naya (2012). "Digestive flexibility during fasting in the characid fish Hyphessobrycon luetkenii." J Morphol **273**(1): 49–56.

Gershuni, V. M., S. L. Yan and V. Medici (2018). "Nutritional Ketosis for Weight Management and Reversal of Metabolic Syndrome." Curr Nutr Rep **7**(3): 97–106.

Haidari, M., N. Leung, F. Mahbub, K. D. Uffelman, R. Kohen-Avramoglu, G. F. Lewis and K. Adeli (2002). "Fasting and postprandial overproduction of intestinally derived lipoproteins in an animal model of insulin resistance. Evidence that chronic fructose feeding in the hamster is accompanied by enhanced intestinal de novo lipogenesis and ApoB48-containing lipoprotein overproduction." J Biol Chem **277**(35): 31646–31655.

Holt, P. R. and R. N. DuBois, Jr. (1991). "In vivo immediate early gene expression induced in intestinal and colonic mucosa by feeding." FEBS Lett **287**(1-2): 102–104.

Hu, S., L. Wang, D. Yang, L. Li, J. Togo, Y. Wu, Q. Liu, B. Li, M. Li, G. Wang, X. Zhang, C. Niu, J. Li, Y. Xu, E. Couper, A. Whittington-Davies, M. Mazidi, L. Luo, S. Wang, A. Douglas and J. R. Speakman (2018). "Dietary Fat, but Not Protein or Carbohydrate, Regulates Energy Intake and Causes Adiposity in Mice." Cell Metab **28**(3): 415–431 e414.

Hung, Y. H., A. L. Carreiro and K. K. Buhman (2017). "Dgat1 and Dgat2 regulate enterocyte triacylglycerol distribution and alter proteins associated with cytoplasmic lipid droplets in response to dietary fat." Biochim Biophys Acta Mol Cell Biol Lipids **1862**(6): 600–614.

Iqbal, J. and M. M. Hussain (2009). "Intestinal lipid absorption." Am J Physiol Endocrinol Metab **296**(6): E1183–1194.

Julve, J., J. M. Martin-Campos, J. C. Escola-Gil and F. Blanco-Vaca (2016). "Chylomicrons: Advances in biology, pathology, laboratory testing, and therapeutics." Clin Chim Acta **455**: 134–148.

Ko, C. W., J. Qu, D. D. Black and P. Tso (2020). "Regulation of intestinal lipid metabolism: current concepts and relevance to disease." Nat Rev Gastroenterol Hepatol **17**(3): 169–183.

Koehler, J. A., L. L. Baggio, B. Yusta, C. Longuet, K. J. Rowland, X. Cao, D. Holland, P. L. Brubaker and D. J. Drucker (2015). "GLP-1R agonists promote normal and neoplastic intestinal growth through mechanisms requiring Fgf7." Cell Metab **21**(3): 379–391.

Lewis, G. F., N. M. O'Meara, P. A. Soltys, J. D. Blackman, P. H. Iverius, A. F. Druetzler, G. S. Getz and K. S. Polonsky (1990). "Postprandial lipoprotein metabolism in normal and obese subjects: comparison after the vitamin A fat-loading test." J Clin Endocrinol Metab **71**(4): 1041–1050.

Merrill, A. L. W. B. K. (1955). Energy value of foods; basis and derivation. Washington, Human Nutrition Research Branch, Agricultural Research Service, U.S. Dept. of Agriculture.

Morrow, N. M., N. A. Trzaskalski, A. A. Hanson, E. Fadzeyeva, D. E. Telford, S. S. Chhoker, B. G. Sutherland, J. Y. Edwards, M. W. Huff and E. E. Mulvihill (2022). "Nobiletin Prevents High-Fat Diet-Induced Dysregulation of Intestinal Lipid Metabolism and Attenuates Postprandial Lipemia." Arterioscler Thromb Vasc Biol **42**(2): 127–144.

Mulvihill, E. E. (2018). "Regulation of intestinal lipid and lipoprotein metabolism by the proglucagon-derived peptides glucagon like peptide 1 and glucagon like peptide 2." Curr Opin Lipidol **29**(2): 95–103.

Mulvihill, E. E., J. M. Assini, J. K. Lee, E. M. Allister, B. G. Sutherland, J. B. Koppes, C. G. Sawyez, J. Y. Edwards, D. E. Telford, A. Charbonneau, P. St-Pierre, A. Marette and M. W. Huff (2011). "Nobiletin attenuates VLDL overproduction, dyslipidemia, and atherosclerosis in mice with diet-induced insulin resistance." Diabetes **60**(5): 1446–1457.

Pan, X. and M. M. Hussain (2012). "Gut triglyceride production." Biochim Biophys Acta **1821**(5): 727–735.

Patel, R., M. Patel, R. Tsai, V. Lin, A. L. Bookout, Y. Zhang, L. Magomedova, T. Li, J. F. Chan, C. Budd, D. J. Mangelsdorf and C. L. Cummins (2011). "LXRbeta is required for glucocorticoid-induced hyperglycemia and hepatosteatosis in mice." J Clin Invest **121**(1): 431–441.

Phan, C. T. and P. Tso (2001). "Intestinal lipid absorption and transport." Front Biosci **6**: D299–319.

Puchalska, P. and P. A. Crawford (2017). "Multi-dimensional Roles of Ketone Bodies in Fuel Metabolism, Signaling, and Therapeutics." Cell Metab **25**(2): 262–284.

Schugar, R. C. and P. A. Crawford (2012). "Low-carbohydrate ketogenic diets, glucose homeostasis, and nonalcoholic fatty liver disease." Curr Opin Clin Nutr Metab Care **15**(4): 374–380.

Stahel, P., C. Xiao, X. Davis, P. Tso and G. F. Lewis (2019). "Glucose and GLP-2 (Glucagon-Like Peptide-2) Mobilize Intestinal Triglyceride by Distinct Mechanisms." Arterioscler Thromb Vasc Biol **39**(8): 1565–1573.

Stojanovic, O., J. Altirriba, D. Rigo, M. Spiljar, E. Evrard, B. Roska, S. Fabbiano, N. Zamboni, P. Maechler, F. Rohner-Jeanrenaud and M. Trajkovski (2021). "Dietary excess regulates absorption and surface of gut epithelium through intestinal PPARalpha." Nat Commun **12**(1): 7031.

Taylor, S. R., S. Ramsamooj, R. J. Liang, A. Katti, R. Pozovskiy, N. Vasan, S. K. Hwang, N. Nahiyaan, N. J. Francoeur, E. M. Schatoff, J. L. Johnson, M. A. Shah, A. J. Dannenberg, R. P. Sebra, L. E. Dow, L. C. Cantley, K. Y. Rhee and M. D. Goncalves (2021). "Dietary fructose improves intestinal cell survival and nutrient absorption." Nature **597**(7875): 263–267.

Uchida, A., M. C. Whitsitt, T. Eustaquio, M. N. Slipchenko, J. F. Leary, J. X. Cheng and K. K. Buhman (2012). "Reduced triglyceride secretion in response to an acute dietary fat challenge in obese compared to lean mice." Front Physiol **3**: 26.

Wang, H., W. Tang, P. Zhang, Z. Zhang, J. He, D. Zhu and Y. Bi (2020). "Modulation of gut microbiota contributes to effects of intensive insulin therapy on intestinal morphological alteration in high-fat-diet-treated mice." Acta Diabetol **57**(4): 455–467.

Watanabe, M., R. Tozzi, R. Risi, D. Tuccinardi, S. Mariani, S. Basciani, G. Spera, C. Lubrano and L. Gnessi (2020). "Beneficial effects of the ketogenic diet on nonalcoholic fatty liver disease: A comprehensive review of the literature." Obes Rev **21**(8): e13024.

Xiao, C., P. Stahel, A. L. Carreiro, Y. H. Hung, S. Dash, I. Bookman, K. K. Buhman and G. F. Lewis (2019). "Oral Glucose Mobilizes Triglyceride Stores From the Human Intestine." Cell Mol Gastroenterol Hepatol **7**(2): 313–337.

Yamauchi, K., H. Kamisoyama and Y. Isshiki (1996). "Effects of fasting and refeeding on structures of the intestinal villi and epithelial cells in White Leghorn hens." Br Poult Sci **37**(5): 909–921.

Yang, Z. and S. F. Liao (2019). "Physiological Effects of Dietary Amino Acids on Gut Health and Functions of Swine." Front Vet Sci **6**: 169.

Yen, C. E., D. W. Nelson and M. I. Yen (2015). "Intestinal triacylglycerol synthesis in fat absorption and systemic energy metabolism." J Lipid Res **56**(3): 489–501.

Zembroski, A. S., T. D'Aquila and K. K. Buhman (2021). "Characterization of cytoplasmic lipid droplets in each region of the small intestine of lean and diet-induced obese mice in response to dietary fat." Am J Physiol Gastrointest Liver Physiol **321**(1): G75–G86.

Zhang, H., M. Leveille, E. Courty, A. Gunes, N. N. B and J. L. Estall (2020). "Differences in metabolic and liver pathobiology induced by two dietary mouse models of nonalcoholic fatty liver disease." Am J Physiol Endocrinol Metab **319**(5): E863–E876.

Zhou, W., E. A. Davis and M. J. Dailey (2018). "Obesity, independent of diet, drives lasting effects on intestinal epithelial stem cell proliferation in mice." Exp Biol Med (Maywood) **243**(10): 826–835.

Zhu, J., B. Lee, K. K. Buhman and J. X. Cheng (2009). "A dynamic, cytoplasmic triacylglycerol pool in enterocytes revealed by ex vivo and in vivo coherent anti-Stokes Raman scattering imaging." J Lipid Res **50**(6): 1080–1089.

Chapter 4 GLP-1R and GLP-2R signalling control intestinal adaptations to the increased metabolic demand and food intake associated with cold stress

Publication in revision:

Morrow, N.M.*, Hanson, A.A.*, Fong-McMaster, C., Livingston, D.B.H., Osman, H., Hamilton, L., Trzaskalski, N.A., Locatelli, C.A.A., Bellefleur, M.N., Messika-Zeitoun, E., Cino, S.M., Pulente, S.M., Abramchuk, I., Zhao, X., Lorenzen-Schmidt, I., Morissette, A., Power, K.A., Harper, M.E., Mulvihill, E.E.

*co-first authors

4.1 Abstract

Chronic cold exposure in mice increases metabolic demand and food intake; the gut correspondingly expands its absorptive surface area. Gut enteroendocrine cells produce peptide hormones including glucagon-like peptide-1 (GLP-1), GLP-2, and glucose-dependent insulinotropic polypeptide (GIP) in response to a meal to facilitate nutrient absorption and post-prandial metabolism. We hypothesized that GLP-1, GLP-2, and GIP receptor signalling pathways were required for small intestinal adaptations to chronic cold stress. Male and female wild-type, double incretin receptor knockout (*Glp1r*$^{-/-}$*Gipr*$^{-/-}$; DIRKO), and glucagon-like peptide double receptor knockout (*Glp1r*$^{-/-}$*Glp2r*$^{-/-}$; GLPDRKO) mice were housed for five weeks in cold (6 ºC) or thermoneutral (27 ºC; TN) control conditions. Cold-stressed mice consumed significantly more food compared to TN controls, independent of genotype. Jejunal circumference, villi length, and crypt depth were significantly greater in cold-stressed WT and DIRKO mice, but not GLPDRKO mice, compared to TN controls. Experiments in *Glp2r*$^{-/-}$ mice revealed that GLP-2R was required for jejunal villi length expansion despite significantly elevated plasma active GLP-1 levels. In line with this, GLPDRKO, but not *Glp2r*$^{-/-}$mice, failed to gain body weight over the five-week experiment compared to WT controls. Therefore, while

GLP-2R action was required for cold stress-induced jejunal villi lengthening, this adaptation was dispensable for body weight gain in the presence of GLP-1R signalling.

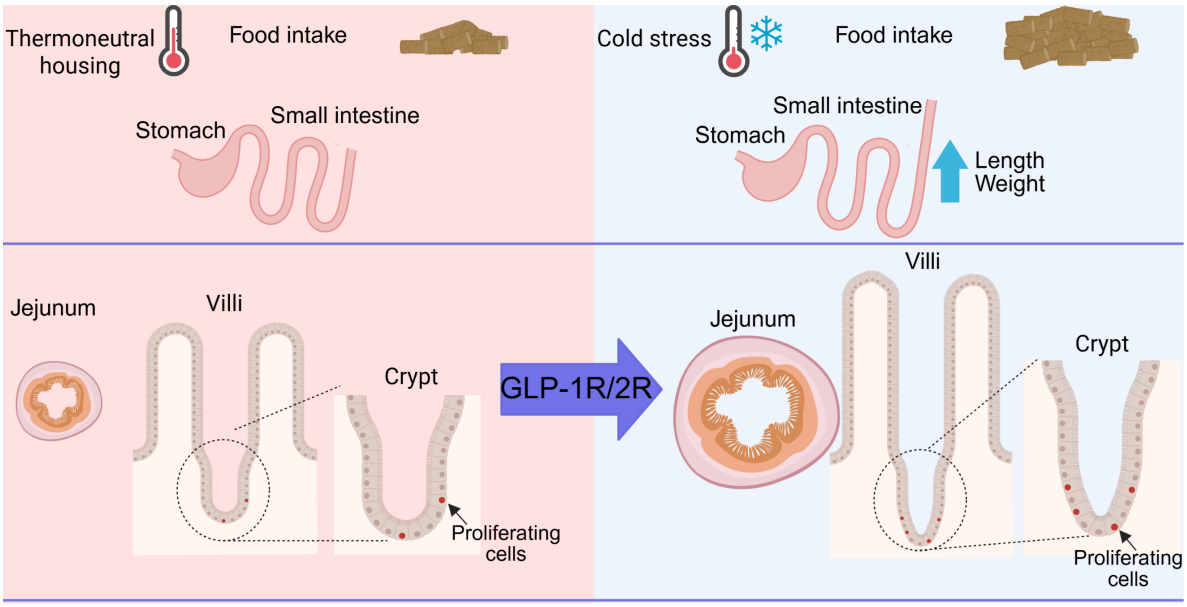

Graphical Abstract iii.

4.2 List of abbreviations

Actb: Beta-actin

BAT: Brown adipose tissue

DPP4: Dipeptidyl peptidase 4

DIRKO: Double incretin receptor knockout

GLP-1: Glucagon-like peptide-1

GLP-1R: GLP-1 receptor

GLP-2: Glucagon-like peptide-2

GLP-2R: GLP-2 receptor

GIP: Glucose-dependent insulinotropic polypeptide

GIPR: GIP receptor

GLPDRKO: Glucagon-like peptide double receptor knockout

IGF: Insulin-like growth factor-1

IGF-1R: Insulin-like growth factor-1 receptor

KGF: Keratinocyte growth factor

PC1/3: Prohormone convertase 1/3

PPARα: Peroxisome proliferator-activated receptor alpha

TN: Thermoneutral

UCP1: Uncoupling protein 1

Rps9: Ribosomal protein S9

SCFA: Short-chain fatty acid

4.3 Introduction

As temperatures fall below the thermal neutral zone, body temperature is initially maintained by shivering thermogenesis via skeletal muscle and chronically by non-shivering

thermogenesis in brown adipose tissue (BAT) (Foster and Frydman 1979, Beaudry and McClelland 2010, Blondin 2023). Specifically, animals chronically housed in the cold balance this heat loss by increasing their energy expenditure. The inner mitochondrial membrane of BAT contains a high density of uncoupling protein 1 (UCP1), which translocates protons to the mitochondrial matrix, uncoupling substrate oxidation from ATP production and generating heat. Chronic cold exposure in rodents increases BAT mass, mitochondria, and UCP1 content, leading to a browning of white adipose tissue (Cohen and Spiegelman 2015). To meet this increased energy demand, rodents housed in the cold increase food intake proportional to the temperature drop (Chevalier, Stojanovic et al. 2015, Zhao, Yang et al. 2022). Interestingly, small intestinal mass also increases proportionally to the temperature drop (Zhao, Yang et al. 2022). Intestinal circumference and villus length have also been shown to be greater with chronic cold stress, where markers of proliferation increase and markers of apoptosis at the villus tip decrease (Chevalier, Stojanovic et al. 2015); evidence of a directional role for the gut microbiota has been implicated in this form of gut plasticity (Chevalier, Stojanovic et al. 2015, Wang, Wu et al. 2024). However, the hormonal signals underlying induction of these circuits to mediate this plasticity are not fully elucidated.

Enteroendocrine cells in the gut epithelium sense meal ingestion and secrete gut hormones to maximize nutrient absorption (Paternoster and Falasca 2018, Gribble and Reimann 2019). These hormones include glucagon-like peptide 1 (GLP-1), GLP-2, and glucose-dependent insulinotropic polypeptide (GIP). GLP-1 and GLP-2 are sister peptides, produced through cleavage of the same preproglucagon polypeptide in intestinal L cells by prohormone convertase 1/3 (PC1/3) (Mojsov, Heinrich et al. 1986, Orskov, Holst et al. 1986). PC1/3 also cleaves the proGIP precursor in intestinal K cells yielding GIP (Ugleholdt, Poulsen et al. 2006). GLP-1 and GIP both amplify glucose-stimulated insulin secretion from pancreatic islets (Nauck and Meier 2016) whereas both GLP-1 and GLP-2 promote gut surface area expansion (Drucker and Yusta

2014, Koehler, Baggio et al. 2015). Drugs modelled to activate GLP-2 receptor (GLP-2R) signalling are used to manage short bowel disease and are effective at removing or decreasing parenteral nutrition dependence in ~65% of patients (Zhu and Li 2022). However, despite their significant quality of life improvements, they can be accompanied by significant gastrointestinal side effects, including nausea, vomiting, abdominal pain, diarrhea, fatigue, and weight loss (Zhu and Li 2022). GLP-2R signalling increases villus length by promoting intestinal cell proliferation and inhibiting apoptosis at the villus tip (Drucker, Shi et al. 1997). By contrast, pharmacological GLP-1 receptor (GLP-1R) signalling achieved through activation by exendin-4 treatment has been shown to increase crypt number in the proximal intestine and colon, leading to increased intestinal circumference and length (Simonsen, Pilgaard et al. 2007, Koehler, Baggio et al. 2015). Interestingly, in mice, genetic elimination of the glucagon receptor (*Gcgr*$^{-/-}$) leads to a ~3 to 30-fold increase in physiological circulating GLP-1 and GLP-2 levels (Gelling, Du et al. 2003, Ali, Lamont et al. 2011, Grigoryan, Kedees et al. 2012), as well as increased small and large intestinal length (Koehler, Baggio et al. 2015), indicating that increasing endogenous levels of GLP-1 and GLP-2 can also lead to an expansion of the gut surface area. Therefore, using extreme models of physiology to understand the role of these receptor signalling pathways may uncover important mediators in gut plasticity.

GLP-1R, GLP-2R, and GIPR signalling play clear roles in regulating metabolism, intestinal growth, and inflammation at pharmacological levels. Within minutes, however, the serine protease dipeptidyl peptidase 4 (DPP4) cleaves two amino acids from endogenous GLP-1, GLP-2, and GIP, rendering them inactive (Baggio and Drucker 2007, Drucker and Yusta 2014). Both GLP-2 and GIP have circulating half-lives of 7 min (Drucker, Shi et al. 1997, Hartmann, Harr et al. 2000, Meier, Nauck et al. 2004), whereas GLP-1 has a circulating half-life of 1-2 min (Deacon, Johnsen et al. 1995). Many cells within the gastrointestinal tract, and therefore in proximity to the enteroendocrine cells that produce them, express GLP-1R, GLP-2R, and GIPR. Specifically,

duodenal Brunner's glands, stomach gland parietal cells (Wismann, Barkholt et al. 2017), the myenteric nerve plexus, and crypt Paneth cells express *Glp1r* mRNA (Kedees, Guz et al. 2013, Pyke, Heller et al. 2014). *Glp1r* mRNA is also detected in both Tαβ and Tγδ subsets of intraepithelial lymphocytes (Yusta, Baggio et al. 2015, He, Kahles et al. 2019, Wong, Yusta et al. 2022), which have been shown to control T cell-induced inflammation (Wong, Yusta et al. 2022, Wong, McLean et al. 2024). Vagal afferents, enteric neurons, myenteric plexus nerve fibrils, enteroendocrine cells, and subepithelial myofibroblasts express *Glp2r* mRNA (Orskov, Hartmann et al. 2005, Nelson, Sharp et al. 2007). Gut CD146+ stromal cells express *Gipr* mRNA and play a role in attenuating gut inflammation (Hammoud, Kaur et al. 2024). Obesity (Trzaskalski, Vulesevic et al. 2023) and age (Varin, Mulvihill et al. 2019) are associated with enhanced expression and activity of the pro-inflammatory DPP4. The impact of chronic cold stress on DPP4, a gene containing a glucocorticoid response element in its promoter (Diaz-Jimenez, Petrillo et al. 2020), expression and activity levels has not been elucidated.

We hypothesized that GLP-1R, GLP-2R, and GIPR signalling mediate the gut surface area expansion in response to chronic cold stress. Moreover, we investigated the roles of these gut hormone receptor signalling pathways in the adaptations of post-prandial metabolism to chronic cold stress.

4.4 Materials and methods

Animal housing

Male and female wild-type C57BL/6J mice were purchased (The Jackson Laboratory, Bar Harbor, USA) and bred in-house. Double incretin receptor knockout (DIRKO) mice (Hansotia, Baggio et al. 2004), and glucagon-like peptide double receptor knockout (GLPRDKO) mice were generously provided by Dr. Daniel Drucker (University of Toronto Lunenfeld-Tanenbaum Research Institute, Toronto, Canada). *Glp1r*$^{-/-}$ mice (Scrocchi, Brown et al. 1996) were crossed with *Glp2r*$^{-/-}$ mice to

generate *Glp1r*$^{+/-}$*Glp2r*$^{+/-}$, then bred to generate *Glp1r*$^{-/-}$*Glp2r*$^{-/-}$ and wild-type controls. At 8-12 or 28-35 weeks of age, mice were individually housed with nesting materials in temperature-controlled chambers set to 6 ˚C (cold) or 27 ˚C (thermoneutral; TN), under a 12-hour light/dark cycle for 5 weeks at the University of Ottawa Heart Institute. Mice were fed a standard laboratory diet (22% kcal from fat, 55% kcal from carbohydrates, 23% kcal from protein; Envigo 2019). Six cohorts of mice were used for this study. An estimate of average food intake was measured in grams by the change in food mass from the week prior and divided by the number of days. Fat and lean mass were determined by EchoMRI (EchoMRI-100 machine, Echo Medical Systems, Houston, USA) scanning of individual awake mice. All experiments undertaken were approved by the University of Ottawa Animal Care Committee (AUP 2909 & 4379).

Metabolic Tests

Lipid tolerance test: Mice were fasted for five hours and gavaged with 200 µL of olive oil. Blood from the tail vein was collected from baseline (prior to gavage), 10 minutes, 1, 2, and 3 hours after gavage in ethylenediaminetetraacetic acid (EDTA) coated capillary tubes for total GLP-1 and GIP measurements at baseline and 15 minutes post-gavage. Plasma triglycerides were measured using the colorimetric assay with Infinity Triglyceride Liquid Stable Reagent. Intestinal transit test: Mice were fasted for 2 hours and administered a 300 µL oral gavage of 6% w/v carmine red solution in 0.5% w/v methyl cellulose and food was available *ad libitum* for the remainder of the experiment (Schonkeren, Seeldrayers et al. 2023). Intestinal transit time was defined as the interval from gavage to the first red fecal pellet.

Blood and tissue collection

Blood was taken at the start of the light cycle in the *ad libitum* state at weeks 1, 2 and 4 in the *Glp2r*$^{-/-}$ mice and WT controls, where 10% TED (5000 KIU/mL Trasylol, 1.2 mg/mL EDTA (ethylenediaminetetraacetic acid), 0.1 nmol/L Diprotin A) (vol/vol) was added for active plasma

GLP-1 (K1503OD-2, MSD) measurements. Mice were euthanized by CO_2 inhalation and cervical dislocation. Blood was taken at endpoint via cardiac puncture in EDTA coated syringes. Blood was centrifuged at 4 ºC and 12 000 rpm for 10 minutes. Plasma was stored at -80 ºC until analysis. Total plasma GLP-1 levels (K15171C-2, MSD, total plasma GIP levels (81527, Crystal Chem), and leptin levels (90030, Crystal Chem) were measured according to the manufacturer's instructions. Plasma DPP4 activity was measured as previously described (Trzaskalski, Vulesevic et al. 2023). Lipids were extracted from ~100 mg of liver using the Folch method with cholesteryl oleate [Cholesteryl-1,2 -^{3}H(N)] (Perkin Elmer) for recovery calculations, as described previously (Mulvihill, Varin et al. 2017, Burke, Telford et al. 2019). Liver triglyceride levels were quantified using the Infinity Triglyceride Liquid Stable Reagent and liver total cholesterol levels were quantified using the Infinity Cholesterol Liquid Stable Reagent. The small intestine was divided into duodenum, proximal jejunum, distal jejunum, and ileum (1:1:1:1 ratio) and flushed with cold phosphate-buffered saline (PBS). Tissue segments used for histology were fixed in 4% paraformaldehyde for 24 hours at room temperature prior to paraffin embedding. Tissues were flash frozen and stored at -80ºC until analysis. Fecal short-chain fatty acid (SCFA) analyses were performed as previously described and expressed as a percent of total SCFA (acetate, propionate, and butyrate) (Livingston, Sweet et al. 2023).

Histology and immunostaining

Five-micron sections of jejunal samples were stained with hematoxylin and eosin. Photomicrographs were obtained with a Leica Aperio Versa slide scanner. Circumference (2-3/mouse), villi length (15–30/mouse), and crypt depth (20-35/mouse) measurements were performed using ImageScope software. One sample did not have full villi lengths and was therefore excluded from the Figure 1 data set. Four samples did not have full villi lengths and were therefore excluded from the Supplemental Figure 2 data set. Five-micron sections of jejunal samples were used for immunostaining. Sections were deparaffinized with an autostainer and

antigen retrieval was performed with a Decloaking chamber (BioCare Medical) in 10 mM citric acid buffer (pH 6.0). Slides were cooled at room temperature for 10 minutes followed by five washes in distilled water. Sections were blocked with 10% donkey serum for 30 minutes at room temperature followed by incubation with primary antibody against Ki67 (Abcam ab16667; 1:200) or PBS as a negative control at 4ºC overnight. Sections were then washed twice with PBS for 5 minutes each on a shaker followed by incubation with a secondary antibody (donkey anti-rabbit, Invitrogen A32794, 1:500) for 30 minutes at room temperature. Sections were then washed twice with PBS for 5 minutes on a shaker and mounted for microscopy. Photomicrographs were obtained with a Leica Aperio Versa slide scanner and analyzed by a custom Cell Profiler pipeline where the number of Ki67+ nuclei were expressed as a percentage of the total nuclei number of the tissue section.

Jejunal mitochondrial DNA quantification

Jejunal DNA was isolated as previously described (Quiros, Goyal et al. 2017). Briefly, jejunum (10 mg) was homogenized in DNA lysis buffer (pH 8.0) [100 mM Tris-HCL (pH 8.0), 5 mM EDTA, 0.2% SDS, 200 mM NaCl] and incubated with proteinase K solution (Sigma) at 55 °C overnight. RNAse A was added, and samples were incubated at 37 °C for 30 min. DNA was pelleted using phenol/chloroform/isoamyl alcohol (25:24:1) (PCIAA) (Sigma) and isopropanol, and pellets were washed with 70% ethanol and dissolved in UltraPure Distilled Water (Invitrogen). Mitochondrial to nuclear DNA ratios were measured with quantitative real time PCR (CFX96, Bio-Rad) with mitochondrial cytochrome c oxidase (*mt-Co1*) and mitochondrial NADH dehydrogenase 1 (*mt-Nd1*) and nuclear DNA hexokinase 2 (*Hk2*) and beta-2 microglobulin (*B2m*) primers. Ratios were calculated using the $2^{-\Delta\Delta CT}$ method.

High resolution respirometry

Mitochondrial respiration was assessed in fresh jejunum tissue from 3-4 mice per group using an Oxygraph-2k system (OROBOROS Instruments, Innsbruck, Austria). Jejunal tissue was isolated, first cleaned with PBS then immediately flushed and stored in cold biopsy preservation buffer (BIOPS) (pH 7.1, (5.77 mM Na^{2+}ATP, 10 mM Ca-EGTA buffer, 0.1 µM free calcium, 6.56 mM $MgCl_2$·6H2O, 20 mM taurine, 20 mM imidazole, 60 mM K-lactobionate, 15 mM phosphocreatine, 0.5 mM DTT, 50 mM MES). Tissue was gently teased apart in BIOPS with forceps on ice, followed by permeabilization with saponin (50 µg/mL) for 30 min on a rocker at 4 °C. Samples were transferred to Miro5 buffer (pH 7.1, 110 mM sucrose, 60 mM potassium lactobionate, 20 mM taurine, 10 mM monobasic potassium phosphate, 3 mM magnesium chloride, 20 mM HEPES, 0.5 mM EGTA, 1 mg/mL BSA) and washed for 3 x 10 min on a rocker at 4 °C. Samples were quickly blotted on filter paper, weighed, and placed in 2 mL Miro5 in the chambers. All measurements were collected in duplicate at 37 °C with a constant stirring speed of 750 rpm. Oxygen concentration in the chambers was maintained at 400 µM throughout the experiment. The assay involved the sequential addition of 2 mM malate, 5 mM glutamate, and 10 mM pyruvate (complex I leak respiration), 5 mM ADP (complex I oxidative phosphorylation), 10 mM succinate (complex I + II oxidative phosphorylation), 2.5 µM oligomycin (complex I + II leak respiration), 0.5 µM FCCP (maximal respiration), and 2.5 µM antimycin A (non-mitochondrial respiration). All values were corrected for non-mitochondrial respiration. Data from one sample was removed due to mechanical over-permeabilization. DatLab 7.4 (OROBOROS Instruments, Innsbruck, Austria) was used for analysis.

RNA isolation and gene expression

Jejunal RNA was isolated with TRIzol Reagent (Ambion) as per manufacturer's protocol and reverse transcribed using a High-Capacity cDNA Reverse Transcription Kit (Fisher Scientific 43-688-14). Quantitative Real Time Polymerase chain reaction (qRT-PCR) was performed with Applied Biosystems TaqMan Gene Expression Master Mix (4369016) on the QuantStudio 5.

mRNA abundance was calculated using the standard curve qRT-PCR method and normalized to the housekeeping gene (Ribosomal protein S9; *Rps9*), denoted as absolute mRNA. Confirmation of genotype by qPCR was performed in all mice.

Statistical analysis

Statistical analysis was performed using GraphPad Prism (version 10.2.2). Data are shown as mean ± SEM. Two-way ANOVA with post-hoc Tukey's multiple comparisons correction was performed on analyses with multiple genotypes and housing temperature. Two-way ANOVA with repeated measures and post-hoc Tukey's multiple comparisons correction was performed on analyses with multiple genotypes and housing temperature over time.

4.5 Results

4.5.1 Small intestinal adaptations to increased food intake with cold stress require GLP-1R and GLP-2R signalling

To determine the impact of GLP-1R, GLP-2R, or GIPR on gut surface area expansion with cold stress, we used double receptor knockout mice for *Glp1r*$^{-/-}$*Gipr*$^{-/-}$ (DIRKO) and *Glp1r*$^{-/-}$ *Glp2r*$^{-/-}$ (GLPDRKO) to account for overlapping or compensatory roles in the intestinotrophic action of these gut hormones (Bahrami, Yusta et al. 2010, Koehler, Baggio et al. 2015, Hammoud, Kaur et al. 2024). Male and female DIRKO, GLPDRKO, and WT controls were housed for 5 weeks at TN or cold temperatures. Cold stress did not significantly impact body weight within any genotype for either sex (Figure 1a, b). GLPDRKO mice, however, weighed significantly less compared to WT and DIRKO mice (Figure 1a, b). Continuing previous reports (Irwin, Francis et al. 2011, Zhao, Yang et al. 2022), cold stress increased average daily food consumption in all genotypes and both sexes (Figure 1c, d). Jejunal *Glp1r* mRNA levels were significantly greater in cold-stressed male and female WT mice compared to TN controls (Figure

1e, f). Jejunal *Glp1r* mRNA levels were not detected in male or female DIRKO or GLPDRKO mice (Figure 1e, f). Jejunal *Glp2r* mRNA levels were significantly greater in cold-stressed male and female WT mice compared to TN controls, and ablated in GLPDRKO mice (Figure 1g, h). Jejunal *Gipr* mRNA levels were unchanged in cold-stressed male and female WT mice, and not detected in DIRKO mice (Figure 1i, j). Fasting plasma total GLP-1 levels were greater with cold stress in male (t test, *P*=0.0633*)* and female (t test, *P*=0.0320) WT mice and GLPDRKO mice (significant), but not in DIRKO mice (Supplemental Figure 1a, b), consistent with the engagement of adrenergic stimulation of GLP-1 secretion (Claustre, Brechet et al. 1999, Harada, Kitaguchi et al. 2015). Additionally, the greater mRNA expression of jejunal *Glp1r* and *Glp2r* that accompanied the greater food intake with chronic cold stress in WT mice underlined a biological response from one or both receptors.

Consistent with previous reports (Chevalier, Stojanovic et al. 2015, Stojanovic, Altirriba et al. 2021, Zhao, Yang et al. 2022), small intestinal length and weight expanded with the increased metabolic demand and food intake in response to cold stress in male and female WT mice (Figure 1k-n). Small intestinal length failed to increase in male DIRKO and GLPDRKO with cold stress (Figure 1k). In female mice, while small intestinal length was greater with cold stress in all genotypes, the extent of this increase was significantly blunted in GLPDRKO mice (Figure 1l). While small intestinal weight was significantly greater in both DIRKO and GLPDRKO mice with cold stress, this increase was significantly blunted in GLPDRKO mice, independent of sex (Figure 1m, n). Consistent with previous reports (Chevalier, Stojanovic et al. 2015, Stojanovic, Altirriba et al. 2021), jejunal circumference and villi length expanded with the increased metabolic demand and food intake in response to cold stress in male and female WT mice (Figure 1o-t). Unlike male DIRKO mice, GLPDRKO mice failed to increase jejunal circumference with cold stress, suggesting an impact from the loss of GLP-2R signalling (Figure 1o, q). In female mice, while jejunal circumference was significantly greater with cold stress in all

genotypes, the extent of this increase was significantly ablated in GLPDRKO mice (Figure 1p). Unlike DIRKO mice, both male and female GLPDRKO mice failed to increase jejunal villi length with cold stress, indicating an impact from the loss of GLP-2R signalling (Figure 1r, s, t). Additionally, the impact of the loss of GLP-2R signalling on the intestinal response to increased food intake with cold stress was maintained in the duodenum and jejunum of male mice aged to 25 weeks, demonstrating conservation of this response with age (Supplemental Figure 2a-d). Overall, these data point to a requirement of GLP-2R signalling to expand jejunal villi length and circumference, impacting small intestinal weight in response to the increased food intake upon chronic cold housing.

Figure 4.1 GLP-2R is required for cold-stress induced increases in intestinal surface area. Male wild-type (WT) (TN, n= 10; C, n= 11), *Glp1r*$^{-/-}$*Gipr*$^{-/-}$ (DIRKO) (TN, n= 4; C, n= 4), and *Glp1r*$^{-/-}$*Glp2r*$^{-/-}$ (GLPDRKO) (TN, n= 10; C, n= 8) and female WT (TN, n= 9; C, n= 8), DIRKO (TN, n= 5; C, n= 4), and GLPDRKO (TN, n= 9; C, n= 10) mice were housed at TN (27 °C) or cold (6 °C) temperatures for 5 weeks. Body weight gain over time in (a) male and (b) female mice, where stars indicate statistical differences for that time point; GLPDRKO vs WT controls (grey) and GLPDRKO vs DIRKO (blue). Average daily food intake estimates in (c) male and (d) female mice. Mice were fasted for 5 hours prior to endpoint. Jejunal RNA was isolated from male WT (TN, n= 7; C, n= 7), DIRKO (TN, n= 4; C, n= 4), and GLPDRKO (TN, n= 6; C, n= 5) and female WT (TN, n= 6; C, n= 5), DIRKO (TN, n= 5; C, n= 4), and GLPDRKO (TN, n= 5; C, n= 6). Jejunal *Glp1r* mRNA levels in (e) male and (f) female mice. Jejunal *Glp2r* mRNA levels in (g) male and (h) female mice. Jejunal *Gipr* mRNA levels in (i) male and (j) female mice. Small intestinal tissue was collected for morphological measurements in male wild-type (WT) (TN, n= 10; C, n= 10-11), DIRKO (TN, n= 4; C, n= 4), and GLPDRKO (TN, n= 10; C, n= 8) and female WT (TN, n= 9; C, n= 8), DIRKO (TN, n= 5; C, n= 4), and GLPDRKO (TN, n= 9; C, n= 10). Small intestinal length in (k) male and (l) female mice. Small intestinal weight in (m) male WT (TN, n= 7; C, n= 10), DIRKO (TN, n= 4; C, n= 4), and GLPDRKO (TN, n= 8; C, n= 6) and (n) female mice WT (TN, n= 6; C, n= 6), DIRKO (TN, n= 5; C, n= 4), and GLPDRKO (TN, n= 7; C, n= 7). Jejunal circumference in (o) male and (p) female mice with (q) representative images. Jejunal villi length in (r) male and (s) female mice. Representative images of villi (t) were cropped and rotated to align villi in the same orientation. Uncropped images are available in the Data Supplement. Two-way ANOVA with a Tukey test correction for multiple comparisons was used to determine statistical significance between housing temperature and genotype. For qPCR analyses, “n.d.” denotes not detected. **P*<0.05, ***P*<0.01, ****P*<0.001, *****P*<0.0001.

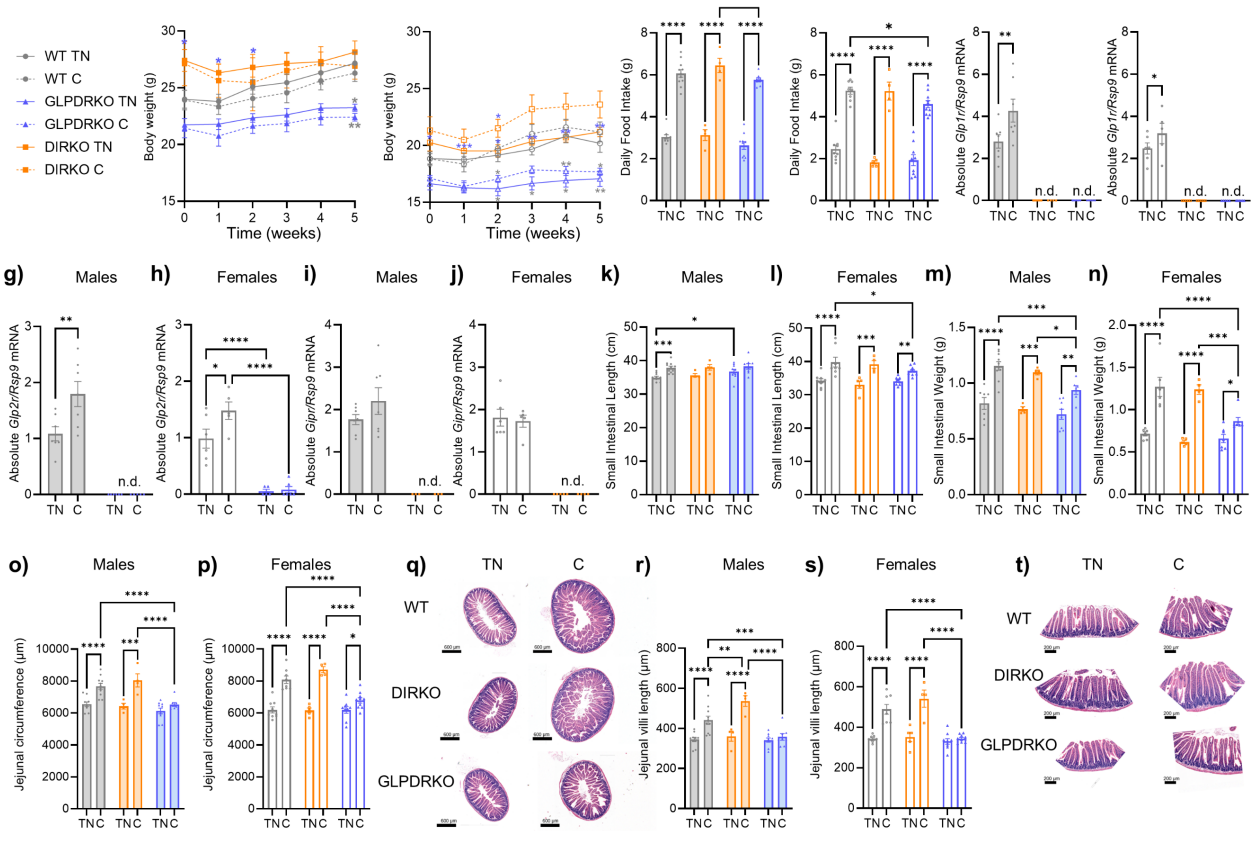
WT TN
WT C
GLPDRKO TN
GLPDRKO C
DIRKO TN
DIRKO C
Body weight (g)
Time (weeks)
Daily Food Intake (g)
Absolute Glp1r/Rsp9 mRNA
n.d.
TNC
g) Males
h) Females
i) Males
j) Females
k) Males
l) Females
m) Males
n) Females
Absolute Glp2r/Rsp9 mRNA
Absolute Gipr/Rsp9 mRNA
Small Intestinal Length (cm)
Small Intestinal Weight (g)
o) Males
p) Females
q) TN
C
r) Males
s) Females
t) TN
C
Jejunal circumference (µm)
Jejunal villi length (µm)
WT
DIRKO
GLPDRKO

4.5.2 Jejunal increases in proliferation with cold stress are lost in GLPDRKO mice.

Intestinal stem and progenitor cell proliferation within intestinal crypts drives cell migration along the villus (Parker, Maclaren et al. 2017). Consistent with the expansion of intestinal surface area observed with the increased food intake that accompanies chronic cold stress, crypt depth was significantly greater with cold stress in WT mice (Figure 2a, b). Unlike in DIRKO mice, jejunal crypt depth failed to expand in GLPDRKO mice, independent of sex (Figure 2a, b). Curiously, duodenal and jejunal crypt depths were not different with housing temperature in male mice aged to 25 weeks (Supplemental Figure 2e-f), suggesting that increased crypt depth did not necessitate greater intestinal circumference or villi length at this age. To determine if the increased jejunal surface area was mediated by increased proliferation, the percentage of Ki67-positive nuclei was quantified in jejunal sections. The percentage of Ki67-positive nuclei localized to crypt cells and was significantly greater in cold-stressed WT but not GLPDRKO mice, independent of sex (Figure 2c-e). Overall, these results are in line with enhanced GLP-2R action, previously shown to increase villus length by promoting intestinal cell proliferation and inhibiting apoptosis at the villus tip (Drucker, Shi et al. 1997).

We next investigated molecular signatures associated with the intestinal action of gut hormones that may accompany the changes in intestinal surface area observed with the increase in food intake that accompanied the chronic cold stress. Since the intestinotrophic effects of pharmacological GLP-1R and GLP-2R activation both require keratinocyte growth factor (KGF/*Fgf7)* (Orskov, Hartmann et al. 2005, Koehler, Baggio et al. 2015) and pharmacological GLP-2 also requires insulin-like growth factor-1 (IGF) action to increase villus length and small intestinal weight (Rowland, Trivedi et al. 2011), we measured the mRNA expression of these target genes in response to cold stress. Jejunal *Fgf7* mRNA levels were greater, but not significantly (P=0.0637), in cold-stressed male WT mice compared to TN

controls; however, this change was not conserved in female WT mice (Supplemental Figure 3a, b). Cold stress did not impact jejunal *Fgf7* mRNA levels in GLPDRKO mice, independent of sex (Supplemental Figure 3a, b). Cold stress did not significantly increase jejunal *Igf1* or *Igf1r* mRNA levels in WT mice in both sexes (Supplemental Figure 3c-f). Intestinal beta-actin (*Actb)* is required for the maintenance of the intestinal epithelial barrier (Lechuga, Naydenov et al. 2020). Consistent with small intestinal surface area expansion, jejunal *Actb* mRNA levels were significantly greater with cold stress in male WT, but not in GLPDRKO mice or in female mice of either genotype (Figure 2f, g). Gut DPP4 action includes the hydrolysis of dietary peptides (Tiruppathi, Miyamoto et al. 1993). Male WT mice displayed significantly greater jejunal *Dpp4* mRNA levels with cold stress compared to TN controls (Supplemental Figure 3g). However, this change was not conserved in female WT or GLPDRKO mice (Supplemental Figure 3g, h). Together, these data underscore the complexity of the molecular mechanisms driving intestinal surface area expansion in response to physiological increases in gut hormone action and food intake, where changes in mRNA signatures cannot be detected at the whole tissue level.

In intestinal organoids, mitochondrial copy number increases during differentiation, and mitochondrial electron transport chain activity is required for the initiation of crypt formation (Rodriguez-Colman, Schewe et al. 2017). In various species, cold stress can change mitochondrial gene expression, and increase BAT mitochondrial DNA content, shape, and membrane permeability (Cohen and Spiegelman 2015, Lubawy, Chowanski et al. 2022). Jejunal mitochondrial content, shown by the ratio of mitochondrial (*mt-Co1*) DNA levels to nuclear (*Hk2*) DNA levels, was not impacted by cold stress in WT mice (Figure 2h, i; Supplemental Figure 3i, j). In GLPDRKO mice, however, jejunal mitochondrial content was significantly lower with cold stress, independent of sex (Figure 2h, i; Supplemental Figure 3i, j). These data suggest that GLP-1R/2R signalling is required to maintain jejunal mitochondrial levels. To investigate the impact of this lower mitochondrial content, jejunal oxygen consumption rates per milligram of

tissue were determined by high-resolution respirometry. Jejunal oxygen consumption was not different in male cold-stressed mice, independent of genotype (Figure 2j). Therefore, the lower jejunal mitochondrial content in male GLPDRKO mice did not significantly impact jejunal oxidative capacity. In female mice, oxygen consumption was significantly greater in the tissues of cold-stressed GLPDRKO mice compared to TN controls in response to malate, pyruvate, and glutamate, indicating an increased complex I leak respiration (Figure 2k). Similarly, complex I-driven oxidative phosphorylation was significantly greater in the tissues of cold-stressed GLPDRKO mice compared to TN controls (Figure 2k). The tissue response to succinate and oligomycin, targeting complex I and II oxidative phosphorylation and leak, respectively, was not different in the tissues of cold-stressed mice compared to controls, independent of genotype (Figure 2k). These data suggest that a compensatory increase in jejunal oxidative capacity in female GLPDRKO mice is upstream to the proliferative response with cold stress.

Figure 4.2 Jejunal increases in proliferation and maintenance of jejunal mitochondrial content with cold stress require GLP-2R. Male and female WT and GLPDRKO mice were housed at TN (27 °C) or cold (6 °C) temperatures for 5 weeks. Small intestinal tissue was collected for morphological measurements in male wild-type (WT) (TN, n= 10; C, n= 11), DIRKO (TN, n= 4; C, n= 4), and GLPDRKO (TN, n= 10; C, n= 8) and female WT (TN, n= 9; C, n= 8), DIRKO (TN, n= 5; C, n= 4), and GLPDRKO (TN, n= 9; C, n= 10).Jejunal crypt depth in (a) male and (b) female mice. Jejunal sections from male WT (TN, n= 7; C, n= 7) and GLPDRKO (TN, n= 6; C, n= 5), and female WT (TN, n= 6; C, n= 5) and GLPDRKO (TN, n= 5; C, n= 6) were immunostained for (c) Ki67 and quantified as a positive percentage area, normalized to total nuclear area in (d) male and (e) female mice. Jejunal RNA and mitochondrial DNA were extracted from male WT (TN, n= 7; C, n= 7) and GLPDRKO (TN, n= 6; C, n= 5), and female WT (TN, n= 6; C, n= 5) and GLPDRKO (TN, n= 5; C, n= 6). Jejunal gene expression levels *Actb* in (f) male and (g) female mice. Jejunal mitochondrial DNA levels were measured in (h) male and (i) female mice. Jejunal high-resolution respirometry flux per mg tissue was measured in (j) male WT (TN, n= 3; C, n= 3) and GLPDRKO (TN, n= 4; C, n= 4), and (k) female WT (TN, n= 3; C, n= 3) and GLPDRKO (TN, n= 3; C, n= 4) mice. CI: Complex I. CII: Complex II. OXPHOS: oxidative phosphorylation. Two-way ANOVA with a Tukey test correction for multiple comparisons was used to determine statistical significance between housing temperature and genotype. **P*<0.05, ***P*<0.01, ****P*<0.001, *****P*<0.0001.

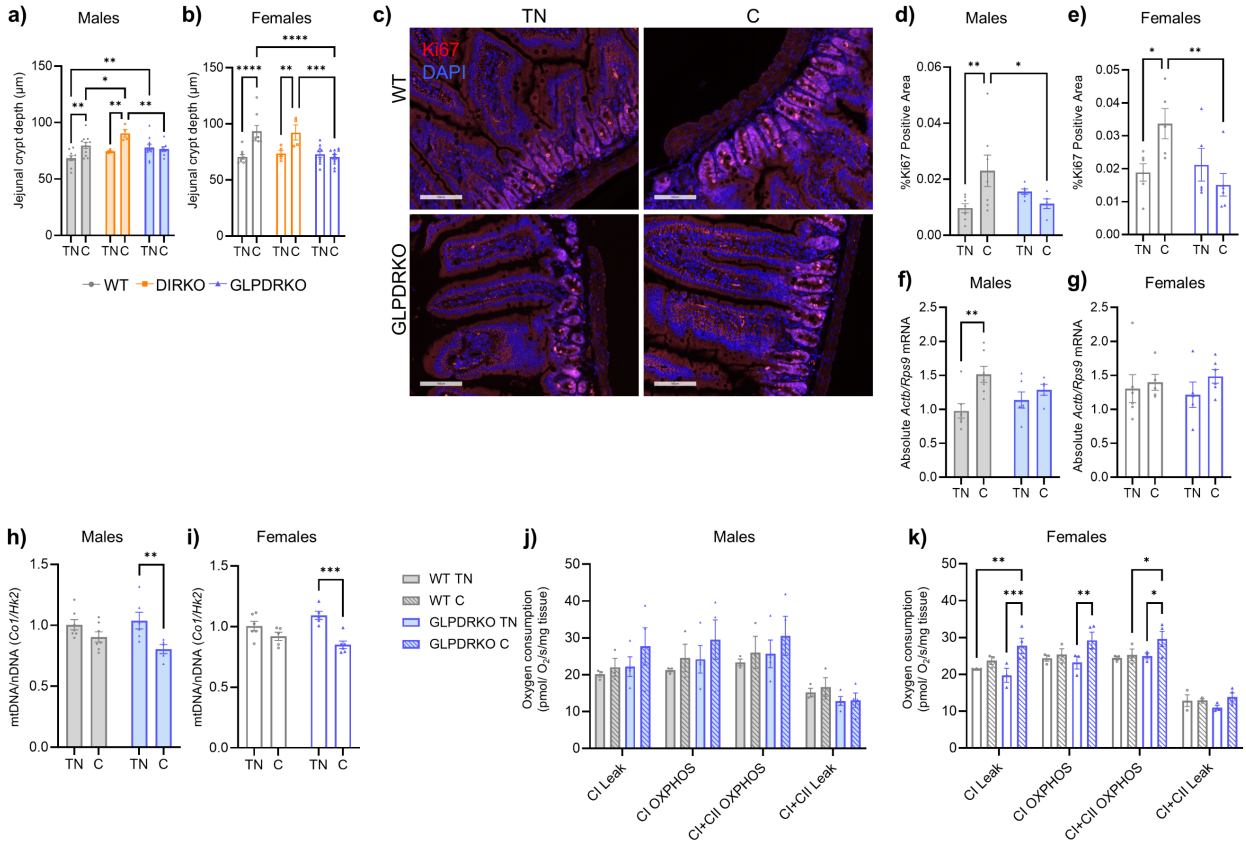
a)
Males
b)
Females
Jejunal crypt depth (µm)
TNC TNC TNC
WT DIRKO GLPDRKO
c)
TN
C
WT
GLPDRKO
Ki67
DAPI
d)
Males
e)
Females
%Ki67 Positive Area
TN C TN C
f)
Males
g)
Females
Absolute Actb/Rps9 mRNA
h)
Males
i)
Females
mtDNA/nDNA (Co1/Hk2)
WT TN
WT C
GLPDRKO TN
GLPDRKO C
j)
Males
k)
Females
Oxygen consumption (pmol/ O2/s/mg tissue)
CI Leak
CI OXPHOS
CI+CII OXPHOS
CI+CII Leak

4.5.3 Cold stress in GLPDRKO male mice does not significantly impact plasma leptin levels, body weight gain, or lipid tolerance but does significantly shorten intestinal transit time

Leptin deficient mice (*ob/ob*), a genetic model of overeating, have greater small intestinal length, jejunal perimeter, and jejunal villi length (Stojanovic, Altirriba et al. 2021). Consistent with the overeating phenotype and intestinal adaptations observed in cold-stressed mice, fasting plasma leptin levels were significantly lower with cold stress in WT mice compared to TN controls (Figure 3a). The impact of cold stress to lower plasma leptin levels in GLPDRKO mice, however, was minimal and not significant (Figure 3a). Chronic cold stress did not significantly impact body weight or lean mass gain from baseline to endpoint in WT mice, however, led to a significant decrease in fat mass consistent with lower plasma leptin levels (Figure 3b-d). Overall, male GLPDRKO mice were significantly lighter than WT controls, independent of housing temperature (Figure 3b). GLPDRKO mice experienced an increase in lean mass and maintained fat mass, leading to an overall neutral impact of cold stress on body weight gain (Figure 3b-d). Liver mass was not different with housing temperature, independent of genotype, but fasting liver triglyceride levels were significantly lower in male cold-stressed mice, independent of genotype, compared to TN controls (Figure 3e, f). Liver total cholesterol levels were not significantly impacted by housing temperature or genotype (Supplemental Figure 4a).

Dietary fat and fibre significantly impact intestinal surface area and lipid handling (Stojanovic, Altirriba et al. 2021, Morrow, Locatelli et al. 2022, Morrow, Trzaskalski et al. 2022). To assess the impact of the failed gut surface area expansion in male GLPDRKO mice on dietary fat handling, a lipid tolerance test was performed following a 5 hour fast. Additionally, both GLP-1R and GLP-2R signalling modulate the rate at which dietary triglycerides appear in plasma, however, in opposing manners (Hsieh, Longuet et al. 2009, Hsieh, Longuet et al. 2010, Hsieh, Trajcevski et al. 2015). Cold stress did not significantly impact fasting plasma triglyceride

levels or lipid tolerance upon an acute dietary fat challenge, independent of genotype (Figure 3g, h). However, TN-housed GLPDRKO mice displayed significantly worse lipid tolerance compared to WT controls, phenocopying the *Glp1r*$^{-/-}$ mouse (Hsieh, Longuet et al. 2010) (Figure 3h). Plasma total GLP-1 levels 10 minutes post-oil gavage increased significantly from baseline in cold-stressed WT mice (Figure 3i). Plasma total GIP levels significantly increased from baseline with the oil gavage in WT mice, independent of housing temperature, and cold-stressed male GLPDRKO mice (Figure 3j). Fasting plasma DPP4 activity levels were similar in cold-stressed male mice compared to TN controls (Figure 3k). Together these data indicate that while the loss of GLP-2R signalling was required for gut surface area expansion with cold stress, this did not significantly impact lipid tolerance.

To investigate the impact of the failed surface area expansion in GLPDRKO mice, an intestinal transit time test was performed. Cold stress significantly shortened intestinal transit time to less than 200 minutes, independent of genotype (Figure 3l). The magnitude of transit time shortening from TN controls, however, was significantly greater in cold-stressed GLPDRKO mice (Figure 3l). Consistent with greater food consumption, the percent abundance of fecal butyrate levels, primarily produced by gut bacteria (Singh, Lee et al. 2022), was significantly greater in cold-stressed male mice, independent of genotype (Figure 3m). Correspondingly, the percent abundance of fecal acetate levels was significantly lower with cold stress, independent of genotype (Supplemental Figure 4b). The percent abundance of fecal propionate levels was unchanged with housing temperature and genotype (Supplementary Figure 4c).

Figure 4.3 Cold stress in male GLPDRKO male mice does not significantly impact plasma leptin levels, body weight gain, or lipid tolerance. Male WT (TN, n= 10; C, n= 11) and GLPDRKO mice (TN, n= 10; C, n= 8) were housed at TN (27 °C) or cold (6 °C) temperatures for 5 weeks. Fasting plasma (a) leptin levels. Body (b) weight, (c) lean mass, and (d) fat mass were measured at baseline and endpoint. Liver (e) mass and (f) triglyceride levels in WT (TN, n= 7; C, n= 7) and GLPDRKO mice (TN, n= 6; C, n= 5). After 2 weeks of temperature housing, WT (TN, n= 7; C, n= 7) and GLPDRKO mice (TN, n= 6; C, n= 5) mice were fasted for 5 hours and administered a dietary fat challenge of 200 µL of olive oil. Fasting plasma (g) triglyceride levels. Plasma (h) triglyceride levels with AUC (inset). Black stars indicate statistical differences among genotypes. Plasma (i) GLP-1 and (j) GIP levels at baseline (0) and 10 minutes after the olive oil gavage (10). Fasting plasma (k) DPP4 activity. After 4 weeks of temperature housing, WT (TN, n= 7; C, n= 7) and GLPDRKO mice (TN, n= 6; C, n= 5) mice were fasted for 2 hours and administered an oral gavage of carmine red. Intestinal (l) transit time was measured from gavage to first red fecal pellet. Short chain fatty acids were extracted from the feces of male WT (TN, n= 10; C, n= 11) and GLPDRKO mice (TN, n= 10; C, n= 7) for (m) butyrate measurements expressed as a percentage of total short chain fatty acids. Two-way ANOVA with repeated measures and a Tukey test correction for multiple comparisons was used to determine statistical significance between housing temperature and genotype for both body weight and composition as well as plasma GIP levels. Two-way ANOVA with a Tukey test correction for multiple comparisons was used to determine statistical significance between housing temperature and genotype. *P<0.05, **P<0.01, ***P<0.001, ****P<0.0001.

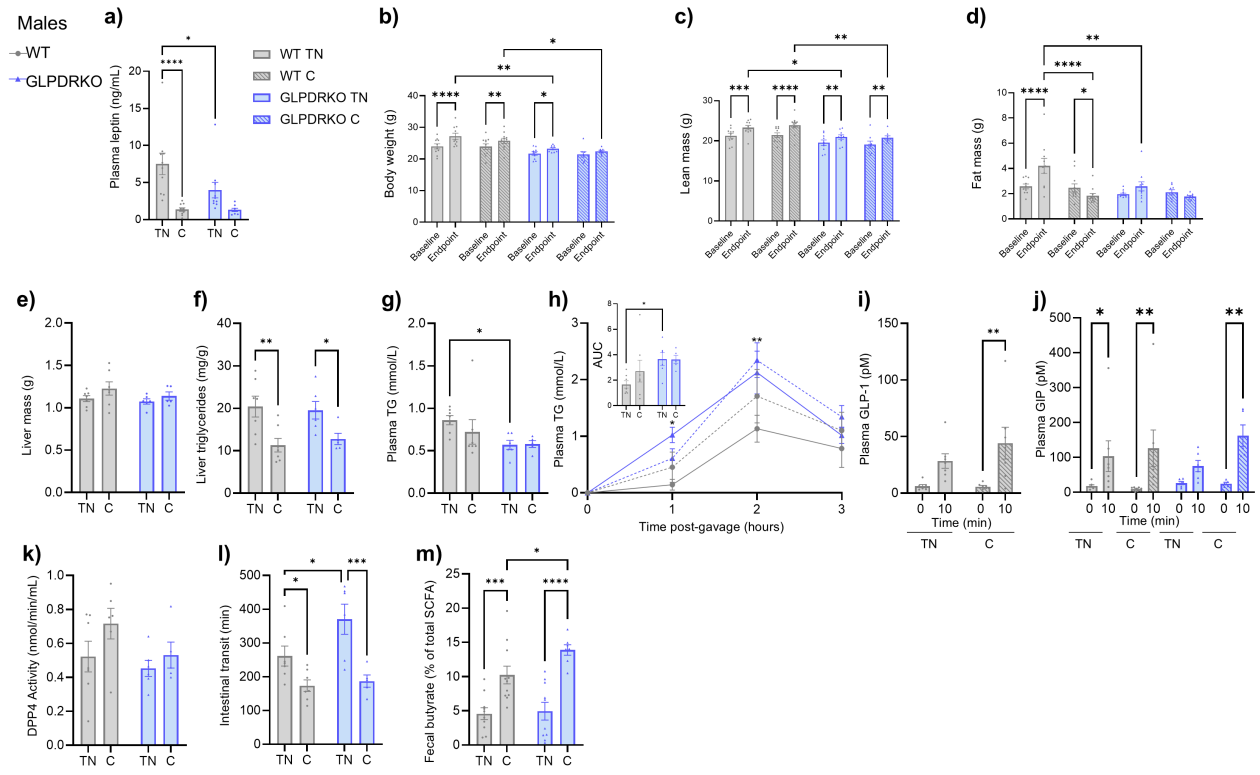
Males
WT
GLPDRKO
a)
b)
c)
d)
WT TN
WT C
GLPDRKO TN
GLPDRKO C
Plasma leptin (ng/mL)
Body weight (g)
Lean mass (g)
Fat mass (g)
Baseline
Endpoint
TN
C
e)
f)
g)
h)
i)
j)
Liver mass (g)
Liver triglycerides (mg/g)
Plasma TG (mmol/L)
AUC
Time post-gavage (hours)
Plasma GLP-1 (pM)
Plasma GIP (pM)
Time (min)
k)
l)
m)
DPP4 Activity (nmol/min/mL)
Intestinal transit (min)
Fecal butyrate (% of total SCFA)

4.5.4 Cold stress in GLPDRKO female mice does not significantly impact plasma leptin levels, body weight gain, or lipid tolerance but does significantly shorten intestinal transit time

In female mice, plasma leptin levels were significantly lower with cold stress independent of genotype (Figure 4a). Chronic cold stress did not significantly impact body weight or lean mass gain from baseline in female WT mice, however, led to a significant decrease in fat mass, consistent with lower plasma leptin levels (Figure 4b-d). Overall, female GLPDRKO mice were significantly lighter than WT controls, independent of housing temperature (Figure 4b). Female GLPDRKO mice experienced a significant increase in lean mass and maintained fat mass, leading to an overall neutral impact of cold stress on body weight gain, independent of housing temperature (Figure 3b-d). Liver mass was not different with housing temperature, independent of genotype, and liver triglyceride levels were only lower (trend; P=0.0683) in cold-stressed WT, but not in GLPDRKO mice, compared to TN controls (Figure 4e, f). Liver total cholesterol levels were not different in female mice, independent of genotype or housing temperature (Supplemental Figure 4d).

Fasting plasma triglyceride levels were significantly lower in female WT, but not GLPDRKO cold-stressed mice compared to TN controls (Figure 4g). Female WT mice displayed significantly greater plasma triglyceride levels during the lipid tolerance test with cold stress compared to TN controls (Figure 4h). In female GLPDRKO mice, however, this difference with cold stress was lost (Figure 4h). Plasma total GLP-1 levels in females were significantly greater in cold-stressed WT mice in response to the oil gavage compared to baseline (Figure 4i). Plasma total GIP levels increased significantly in response to the oil gavage in the female cold-stressed WT and GLPDRKO mice and to levels significantly greater than TN controls (Figure 4j). Plasma DPP4 activity levels were significantly greater in cold-stressed female mice compared to TN controls (Figure 4k), independent of genotype, suggesting that the stress

response element (Diaz-Jimenez, Petrillo et al. 2020) for *Dpp4* in female mice was more sensitive than in males to cold stress.

Cold stress significantly shortened intestinal transit time to less than 200 minutes in both WT and GLPDRKO female mice (Figure 4l). The magnitude of this shortened transit time from TN controls was significantly greater in cold-stressed GLPDRKO mice (Figure 4l). The percent abundance of fecal butyrate levels was significantly greater in both cold-stressed female WT and GLPDRKO mice compared to TN controls (Figure 4m). Correspondingly, the percent abundance of fecal acetate was significantly lower with cold stress, independent of genotype (Supplemental Figure 4e). The percent abundance of fecal propionate levels was unchanged by housing temperature and genotype (Supplementary Figure 4f). Together, these data highlight the impact of increased food intake on transit time and SCFA production.

Figure 4.4 Cold stress in female GLPDRKO female mice does not significantly impact plasma leptin levels, body weight gain, or lipid tolerance and intestinal transit time. Female WT (TN, n= 9; C, n= 8) and GLPDRKO (TN, n= 9; C, n= 10) mice were housed at TN (27 °C) or cold (6 °C) temperatures for 5 weeks. Fasting plasma (a) leptin levels. Body (b) weight, (c) lean mass, and (d) fat mass were measured at baseline and endpoint. Liver (e) mass and (f) triglyceride levels from female WT (TN, n= 6; C, n= 5) and GLPDRKO (TN, n= 5; C, n= 6). After 2 weeks of temperature housing, female WT (TN, n= 6; C, n= 5) and GLPDRKO (TN, n= 5; C, n= 6) mice were fasted for 5 hours and administered a dietary fat challenge of 200 µL of olive oil. Fasting plasma (g) triglyceride levels. Plasma (h) triglyceride levels with AUC (inset). Black stars indicate statistical differences among genotypes. Grey stars indicate statistical differences in WT mice among housing temperature. Plasma (i) GLP-1 and (j) GIP levels at baseline (0) and 10 minutes after the olive oil gavage (10). Fasting plasma (k) DPP4 activity. After 4 weeks of temperature housing, female WT (TN, n= 6; C, n= 5) and GLPDRKO (TN, n= 5; C, n= 6) mice were fasted for 2 hours and administered an oral gavage of carmine red. Intestinal (l) transit time was measured from gavage to first red fecal pellet. Short chain fatty acids were extracted from the feces of female WT (TN, n= 6; C, n= 5) and GLPDRKO (TN, n= 6; C, n= 6) for (m) butyrate measurements expressed as a percentage of total short chain fatty acids. Two-way ANOVA with a Tukey test correction for multiple comparisons was used to determine statistical significance between housing temperature, genotype, and time for both body weight and composition as well as plasma GIP levels. Two-way ANOVA with a Tukey test correction for multiple comparisons was used to determine statistical significance between housing temperature and genotype. *P<0.05, **P<0.01, ***P<0.001, ****P<0.0001.

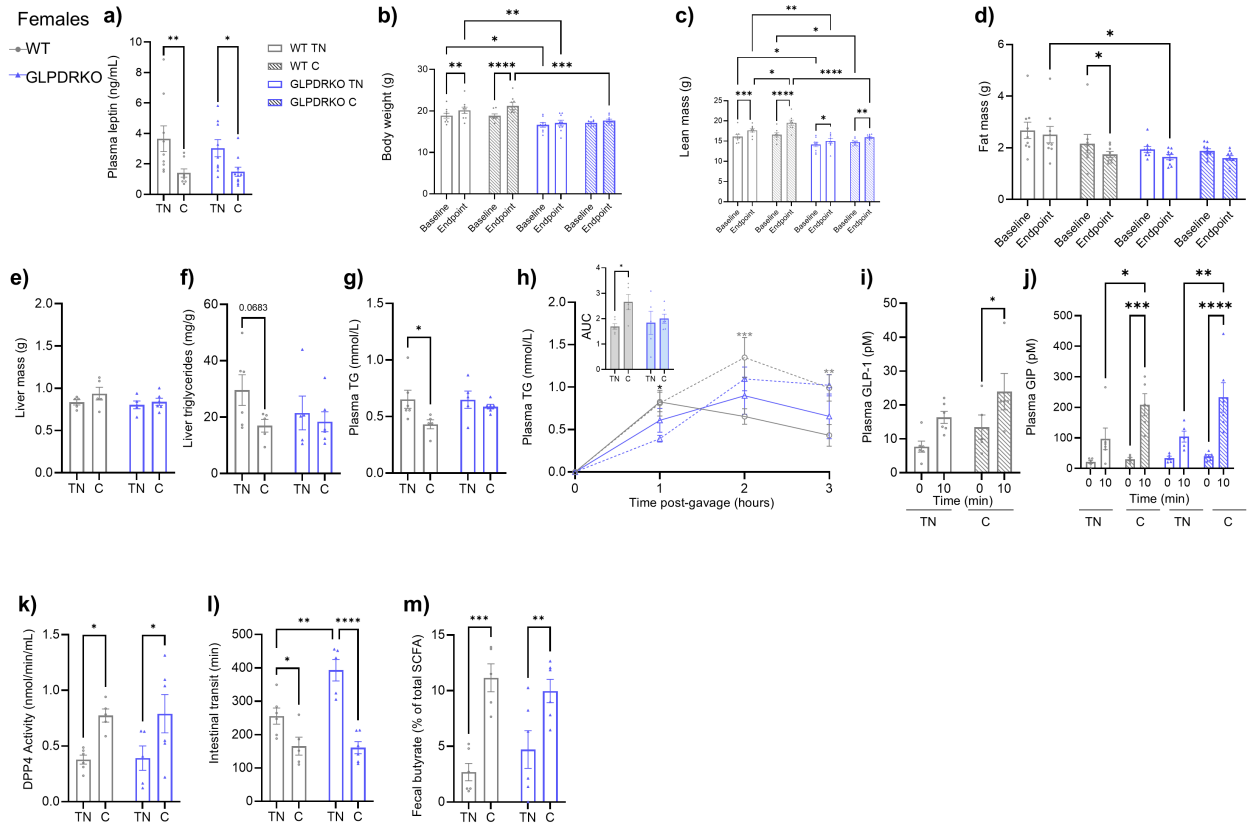
Females
WT
GLPDRKO
a)
Plasma leptin (ng/mL)
WT TN
WT C
GLPDRKO TN
GLPDRKO C
TN C TN C
b)
Body weight (g)
Baseline Endpoint
c)
Lean mass (g)
d)
Fat mass (g)
e)
Liver mass (g)
f)
Liver triglycerides (mg/g)
0.0683
g)
Plasma TG (mmol/L)
h)
Plasma TG (mmol/L)
AUC
Time post-gavage (hours)
i)
Plasma GLP-1 (pM)
Time (min)
j)
Plasma GIP (pM)
Time (min)
k)
DPP4 Activity (nmol/min/mL)
l)
Intestinal transit (min)
m)
Fecal butyrate (% of total SCFA)

4.5.5 GLP-2R signalling is indispensable for jejunal villi length expansion in response to the increased food intake that accompanies chronic cold temperature housing.

The requirement of GLP-2R signalling to expand jejunal villi length and circumference in response to increased food intake with chronic cold stress was observed when comparing morphological results in DIRKO and GLPDRKO mice compared to WT controls. As such, the impact of the loss of GLP-2R action was only assessed in the absence of GLP-1R signalling. To confirm the requirement of GLP-2R action and unveil the potential compensatory role of GLP-1R action in the expansion intestinal surface area, male *Glp2r*$^{-/-}$ mice were housed at TN (27 °C) or cold (6 °C) for 5 weeks. Daily body weight measurements revealed no significant impact of housing temperature, independent of genotype (Figure 5a). As expected, average daily food intake was significantly greater with cold stress, independent of genotype (Figure 5b). Jejunal *Glp2r* mRNA levels were undetectable in *Glp2r*$^{-/-}$ mice (Supplemental Figure 4g). Jejunal *Glp1r* mRNA levels were unchanged in *Glp2r*$^{-/-}$ mice compared to WT controls (Supplemental Figure 4h). Plasma active GLP-1 levels obtained in the *ad libitum* fed state were higher, but not significantly, in male WT mice (Figure 5c). Loss of GLP-2R signalling, however, led to significantly greater plasma active GLP-1 levels at week 1, 2, and 4 of cold temperature housing (Figure 5d). Loss of GLP-2R signalling did not impact the increase in small intestinal length or weight observed with cold stress (Figure 5e, f). Loss of GLP-2R action did not impact jejunal circumference or crypt depth (data not shown), however, significantly blunted the increase in jejunal villi length observed with cold stress compared to WT controls (Figure 5g, h). Loss of GLP-2R action did not significantly impact the effect of cold stress on body weight, lean mass, or fat mass (Figure 5k-m). Taken together, these data revealed that GLP-2R signalling alone was indispensable for jejunal villi length expansion in response to the increased metabolic demand and food intake that accompany chronic cold temperature housing. Moreover, compensation for the loss of GLP-2R action, including by GLP-1R signalling, maintained

expansion of intestinal length, weight, and preserves body weight gain in response to chronic cold stress.

Figure 4.5 GLP-2R signalling is indispensable for jejunal villi length expansion in response to the increased food intake that accompanies chronic cold temperature housing. Male WT (TN, n= 4; C, n= 5) and $Glp2r^{-/-}$ (TN, n= 6; C, n= 6) mice were housed at TN (27 °C) or cold (6 °C) for 5 weeks. (a) Daily body weight gain over time. (b) Average daily food intake estimates. Blood was taken at the start of the light cycle for ad libitum plasma active GLP-1 levels in (c) WT and (d) $Glp2r^{-/-}$ mice. Mice were fasted for 5 hours prior to endpoint. Small intestinal (e) length (f) weight. Jejunal (g) circumference (h) villi length, and (i) crypt depth. Representative images of villi (j) were cropped and rotated to align villi in the same orientation. Uncropped images are available in the Data Supplement. Body (k) weight, (l) lean mass, and (m) fat mass were measured at baseline and endpoint. Two-way ANOVA with a Tukey test correction for multiple comparisons was used to determine statistical significance between housing temperature and genotype. *P<0.05, **P<0.01, ***P<0.001, ****P<0.0001.

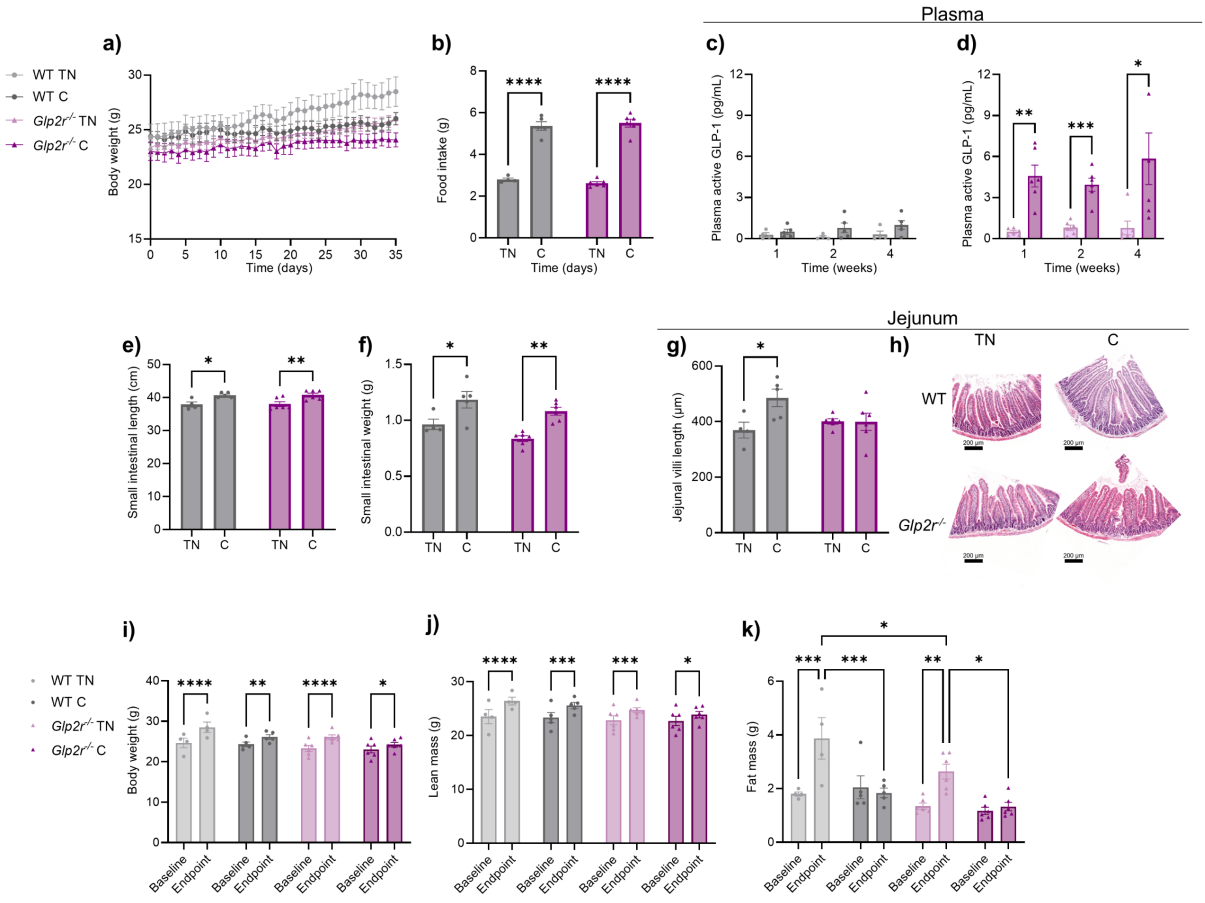
a)
WT TN
WT C
Glp2r-/- TN
Glp2r-/- C
Body weight (g)
Time (days)
b)
Food intake (g)
TN
C
Time (days)
Plasma
c)
Plasma active GLP-1 (pg/mL)
Time (weeks)
d)
Plasma active GLP-1 (pg/mL)
Time (weeks)
e)
Small intestinal length (cm)
f)
Small intestinal weight (g)
Jejunum
g)
Jejunal villi length (µm)
h)
TN
C
WT
Glp2r-/-
i)
WT TN
WT C
Glp2r-/- TN
Glp2r-/- C
Body weight (g)
Baseline
Endpoint
j)
Lean mass (g)
k)
Fat mass (g)

4.6 Discussion:

Previous studies have shown that housing mice at cold temperatures significantly increases food intake, intestinal length and mass as well as absorptive surface area (Chevalier, Stojanovic et al. 2015, Zhao, Yang et al. 2022, Wang, Wu et al. 2024). While food intake doubled and small intestinal length and weight were greater with cold stress in WT, DIRKO and GLPDRKO mice, gut surface area expansion only occurred in the WT and DIRKO mice, but not GLPDRKO mice, indicating that GLP-1R and GIPR signalling were dispensable for this phenotype. Specifically, cold exposure increased jejunal circumference, villi length, and crypt depth in a GLP-2R-dependent manner; these effects were associated with increased abundance of Ki67+ crypt cells. Despite this failed surface area expansion, body weight, composition, and lipid tolerance were not significantly impacted by cold stress in male and female GLPDRKO mice, highlighting the extreme adaptability of the small intestine.

Treatment of male mice with GLP-1R agonist liraglutide and female mice with exendin-4 increases small intestinal length and weight (Koehler, Baggio et al. 2015). In our study, the requirement of endogenous GLP-1R signalling to increase small intestinal length was only observed cold-stressed male and not female mice, suggesting that a sex difference in a compensatory intestinotrophic signalling molecule. Consistent with this, cold stressed female GLPDRKO mice displayed significantly greater jejunal *Fgf7* mRNA levels compared to WT controls and jejunal *Igf1r* mRNA levels compared to GLPDRKO TN controls. Indeed, adaptive increases in intestinal surface area and absorptive capacity in response to dietary changes or genetic models of overeating, require peroxisome proliferator-activated receptor alpha (PPARα), and intestinal-specific deletion of PPARα leads to differential expression of intestinal *Fgf7* (Stojanovic, Altirriba et al. 2021). Cold stress still led to a significant increase in small intestinal weight in both male and female GLPDRKO mice, which is consistent with findings in rats where

increasing endogenous gut hormone levels by DPP4 inhibition does not significantly impact intestinal weight (Simonsen, Pilgaard et al. 2007). Still, the impact of cold stress on intestinal mass was significantly smaller in GLPDRKO mice compared to that in cold-stressed WT and DIRKO mice, suggesting that the expansion in villi length via GLP-2R signalling contributed to this mass. The intestinotrophic effects of GLP-2 in the colon require KGF produced by gut GLP-2R+ myofibroblasts, as shown in *Fgf7*$^{-/-}$ mice, (Orskov, Hartmann et al. 2005). GLP-2 also increases expression and secretion of insulin-like growth factor-1 (IGF-1) from GLP-2R+ myofibroblasts (Markovic and Brubaker 2019), leading to proliferation in an epithelial-IGF-dependent manner (Rowland, Trivedi et al. 2011). In our study, despite the increased abundance of Ki67+ cells and intestinal surface area in cold-stressed WT mice, we only observed a small trend for increased *Fgf7* mRNA levels in male WT mice only, and no differences in *Igf1,* or *Igf1r* mRNA levels. Similarly, *Fgf7, Igf1*, and *Igf1r* mRNA levels were unchanged with housing temperature in male GLPDRKO mice. Therefore, while exogenous GLP-2 requires the expression of these key proteins to elicit its intestinotrophic effects, this mechanism does not appear to require increases at the gene expression level.

While we observed the expansion in gut surface area after 5 weeks of cold temperature housing, increases in intestinal mass with decreasing housing temperatures have also been reported to occur by 2 weeks (Zhao, Yang et al. 2022). Interestingly, body mass over 2 weeks remains constant across 11 different ambient temperatures between 5 and 35ºC in both male and female mice (Zhao, Yang et al. 2022), as increased energy expenditure is matched with increased energy intake. Specifically, the maintenance of body weight as ambient temperature decreases is driven by decreases in white adipose tissue and contributions from increased liver and small intestinal weight by the same magnitude (Zhao, Yang et al. 2022). In our study, body fat mass gain was blunted in our cold-stressed mice compared to TN controls, consistent with lower plasma leptin levels. Our 5-week study demonstrated significant increases in body weight in male and

female WT mice, however, this body weight increase was not observed in GLPDRKO male or female mice despite a doubling in food intake. The contributing factors to this lack of body weight gain are unclear, however, are consistent in the TN-housed GLPDRKO mice. Consistent with the increase in metabolic demand, cold stressed male WT and GLPDRKO mice had significantly lower hepatic lipid levels compared to TN controls. In female mice, no significant differences in hepatic triglycerides were observed with cold stress in WT or GLPDRKO mice, highlighting sex differences in hepatic lipid metabolism. Interestingly, hepatic triglyceride levels are reported to be significantly greater in mice housed for 60 days at -5ºC compared to mice housed at 25ºC (Wang, Wu et al. 2024), suggesting that hepatic fatty acid oxidation becomes impaired over time or at this extreme temperature.

The impact of cold stress on intestinal lipid metabolism in this study was sex dependent. In male mice, cold stress did not change intestinal lipid handling, indicating that despite the greater capacity to store lipids in the small intestine paired with the greater energy demand by peripheral tissues, plasma triglyceride levels remained consistent with those in TN-housed mice in an acute dietary fat challenge. Rather, the changes observed in this study were driven by genotype, where male GLPDRKO mice displayed greater post-oil plasma triglyceride levels. The phenotype of significantly worse lipid tolerance in male GLPDRKO mice resembles that of a *Glp1r*$^{-/-}$ mouse (Hsieh, Longuet et al. 2010), as *Glp2r*$^{-/-}$ mice display similar lipid tolerance compared to controls (Fuchs, Yusta et al. 2020). Together, this suggests that the role of endogenous GLP-1R signalling in the control of intestinal lipoprotein secretion in male mice dominates, consistent with results from hamsters with prolonged co-infusion of GLP-1 and GLP-2 (Hein, Baker et al. 2013). In female mice, by contrast, cold-stressed WT mice had greater post-oil triglyceride levels compared to TN controls. Cold stress, however, did not worsen lipid tolerance in female GLPDRKO mice, suggesting that cold-stress induced increases in intestinal-triglyceride secretion require either GLP-1R or GLP-2R. Moreover, female cold-stressed GLPDRKO mice displayed significantly

greater jejunal oxygen consumption, which may limit the availability of fatty acids for chylomicron production. Finally, while male GLPDRKO mice more similarly phenocopy the *Glp1r*$^{-/-}$ mouse (Hsieh, Longuet et al. 2010) in terms of lipid tolerance, this genotype impact was not observed in female mice, highlighting a sex difference in the balance of GLP-1 and GLP-2 control of intestinal lipid metabolism. The specific GLP-1R/GLP-2R+ cell types and mechanisms underlying this maintenance in body composition and lipid tolerance remain unsolved.

Cold stress in mice has also been shown to change the composition of the gut microbiota and that fecal transplants from cold-stressed donors to room temperature-housed mice elicits the same increases in intestinal morphology, independent of food intake (Chevalier, Stojanovic et al. 2015, Wang, Wu et al. 2024). These studies demonstrate an association of the fecal and cecal SCFA levels to the expansion of the gut surface area (Chevalier, Stojanovic et al. 2015). While our data reflect a shift in the proportion of SCFA with cold stress, these shifts persisted in our GLPDRKO mice, where the gut surface area adaptation to cold stress was blunted despite increased food intake. The increase in fecal butyrate levels observed likely rather reflects the increase in gross energy of feces observed as ambient temperature drops (Zhao, Yang et al. 2022). Certainly, microbial products beyond fecal SCFA levels, including bile acids, play important roles in host metabolism and several studies find impacts of GLP-1R and GLP-2R signalling on the gut microbiota composition (Everard, Lazarevic et al. 2011, Wu, Ren et al. 2018, Covasa, Stephens et al. 2019, Wong, Yusta et al. 2022). Taken together, these data suggest that the proliferative response to the increased fuel availability still requires GLP-2R signalling.

In our study, we found that cold stress significantly decreased intestinal transit time compared to TN controls, and to a greater extent in GLPDRKO mice. The decreased intestinal transit time could be driven by increased gut motility or increased food intake during the experiment. A doubling in the speed of intestinal transit has also been observed in both male and female C57BL/6NJ mice housed at 22ºC compared to 30ºC for 2 weeks, although food intake was

comparable among housing temperatures (Han, Hudson-Paz et al. 2024). Rather, increased intestinal transit at 22ºC was corticotropin-releasing hormone dependent (Han, Hudson-Paz et al. 2024). Daily food intake was similar among cold-stressed genotypes, suggesting that this magnitude of change from the TN to cold stressed GLPDRKO mice was driven by factors beyond the volume of food introduced to the system. Applying SCFA to colonic segments modulates gut motility; namely acetate and propionate have been shown to decrease the contraction rate whereas butyrate has been shown to increase it (Hurst, Kendig et al. 2014). While our fecal SCFA levels reflect a profile that would support greater gut motility, this would be confounded by the role gut hormones play in gastric emptying and gut motility. GLP-1 slows gastric emptying and gut motility while both GLP-1 and GLP-2 have been shown to act as ileal “brakes”, slowing nutrient transit in the small intestine to facilitate nutrient absorption (Idrizaj, Biagioni et al. 2024). Despite this, GLPDRKO mice housed at TN demonstrate significantly lower intestinal transit time compared to WT mice housed at TN, leading to a greater magnitude of change with cold stress. This suggests compensatory mechanisms manifest to slow nutrient transit for efficient nutrient absorption. Interestingly, in contrast to the inhibitory role GLP-1 plays in the stomach and the small intestine, central GLP-1 action has been shown to increase colonic transit time (Nakade, Tsukamoto et al. 2007), which may explain the longer intestinal transit time in TN GLPDRKO mice. Nevertheless, these data suggest that cold stress, where gut hormone receptor signalling is high, uncouples the feedback mechanisms that GLP-1R and GLP-2R govern for intestinal transit in the post-prandial state.

In conclusion, in the state of increased metabolic demand that accompanies cold stress, increased food intake drives intestinal surface area expansion by proliferation in a GLP-2R-dependent manner in male and female mice. Importantly, the data from the middle-aged mice reveal that the GLP-2R-dependent increase in intestinal surface area with cold stress was conserved. These findings also highlight sex differences in the effects of cold housing that are

independent of the increased intestinal surface area and the endogenous roles of GLP-1 and GLP-2 in post-prandial metabolism.

4.7 Sources of Funding

This work was supported by NSERC grants 551669-152199-2004 to E.E.M., 2018-06545 to K.A.P., and RGPIN/04468-2020 to M.E.H. N.M.M., C.F.M., and S.M.P. were supported by CIHR Canada Graduate Scholarship Frederick Banting and Charles Best Doctoral Award. D.B.H.L. was supported by the Nutrition and Mental Health Doctoral Scholarship. N.A.T. was supported by a UOHI Cardiac Endowment scholarship. C.A.A.L. was supported by a Queen Elizabeth II scholarship. I.A. was supported by an NSERC-USRA.

4.8 Disclosures

The Mulvihill lab has received funding from the Merck IISP program for pre-clinical studies unrelated to this work. The other authors have no disclosures.

Author Contributions:

Study concept and design: N.M.M., A.A.H., and E.E.M.; Acquisition of data: N.M.M., A.H., C.F.M., D.L., H.O., L.H., S.M.P., N.A.T., C.A.A.L., M.N.B., E.M.Z., S.M.C., I.A., X.Z., I.L.S., and E.E.M. Analysis of data: N.M.M., A.A.H., C.F.M., D.L., H.O., L.H., and E.E.M., Drafting of the manuscript: N.M.M., A.A.H., C.F.M., A.M., and E.E.M. Critical revision of the manuscript for important intellectual content: N.M.M., C.F.M., D.L., S.M.P., C.A.A.L., I.A., I.L.S., A.M., K.A.P., M.E.H., E.E.M. Obtained funding: E.E.M, M.E.H, and K.A.P.

Supplemental Figure 4-1 Male wild-type (WT) (TN, n= 10; C, n= 10), *Glp1r*$^{-/-}$*Gipr*$^{-/-}$ (DIRKO) (TN, n= 4; C, n= 4), and *Glp1r*$^{-/-}$*Glp2r*$^{-/-}$ (GLPDRKO) (TN, n= 10; C, n= 8) and female WT (TN, n= 9; C, n= 8), DIRKO (TN, n= 5; C, n= 4), and GLPDRKO (TN, n= 9; C, n= 10) mice were housed at TN (27 °C) or cold (6 °C) temperatures for 5 weeks. Fasting plasma GLP-1 in (a) male and (b) female mice. Two-way ANOVA with a Tukey test correction for multiple comparisons was used to determine statistical significance between housing temperature and genotype. **P*<0.05, ***P*<0.01, ****P*<0.001, *****P*<0.0001.

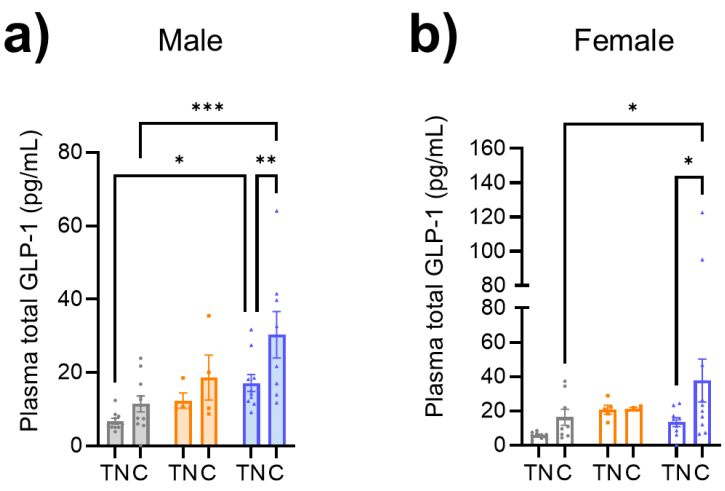
a)
Male
b)
Female
Plasma total GLP-1 (pg/mL)
0
20
40
60
80
160
140
120
100
TNC
TNC
TNC
*
**
***

Supplemental Figure 4-2 Male 25–30-week-old WT (TN, n= 6; C, n= 6), DIRKO (TN, n= 6; C, n= 6), and GLPDRKO (TN, n= 4; C, n= 5) mice were housed at TN (27 °C) or cold (6 °C) temperatures for 5 weeks. Mice were fasted for 5 hours prior to tissue collection. Duodenal (a) circumference WT (TN, n= 6; C, n= 6) DIRKO (TN, n= 6; C, n= 6), and GLPDRKO (TN, n= 4; C, n= 5) and (b) villi length WT (TN, n= 6; C, n= 5) DIRKO (TN, n= 6; C, n= 5), and GLPDRKO (TN, n= 4; C, n= 5). Jejunal (c) circumference WT (TN, n= 6; C, n= 6), DIRKO (TN, n= 6; C, n= 6), and GLPDRKO (TN, n= 4; C, n= 5), (d) villi length. Crypt depth in the (e) duodenum WT (TN, n= 6; C, n= 6), DIRKO (TN, n= 6; C, n= 5), and GLPDRKO (TN, n= 4; C, n= 5) and (f) jejunum WT (TN, n= 6; C, n= 6), DIRKO (TN, n= 6; C, n= 5), and GLPDRKO (TN, n= 4; C, n= 5). Two-way ANOVA with a Tukey test correction for multiple comparisons was used to determine statistical significance between housing temperature and genotype. *P<0.05, **P<0.01, ***P<0.001, ****P<0.0001.

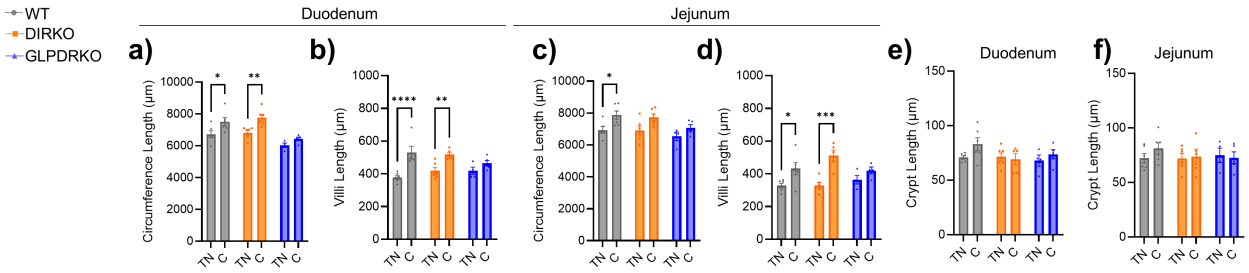
WT
DIRKO
GLPDRKO
Duodenum
Jejunum
a)
b)
c)
d)
e)
f)
Circumference Length (µm)
Villi Length (µm)
Crypt Length (µm)
TN
C

Supplemental Figure 4-3 Male WT (TN, n= 7; C, n= 7) and GLPDRKO (TN, n= 6; C, n= 5) as well as female WT (TN, n= 6; C, n= 5) and GLPDRKO (TN, n= 5; C, n= 6) mice were housed at TN (27 °C) or cold (6 °C) temperatures for 5 weeks. Jejunal gene expression levels of *Fgf7* in (a) male and (b) female mice. Jejunal gene expression levels of *Igf1* in (c) male and (d) female mice. Jejunal gene expression levels of *Igf1r* in (e) male and (f) female mice. Jejunal gene expression levels of *Dpp4* in (g) male and (h) female mice. Jejunal mitochondrial DNA levels in (i) male and (j) female mice. Two-way ANOVA with a Tukey test correction for multiple comparisons was used to determine statistical significance between housing temperature and genotype. **P*<0.05, ***P*<0.01, ****P*<0.001, *****P*<0.0001.

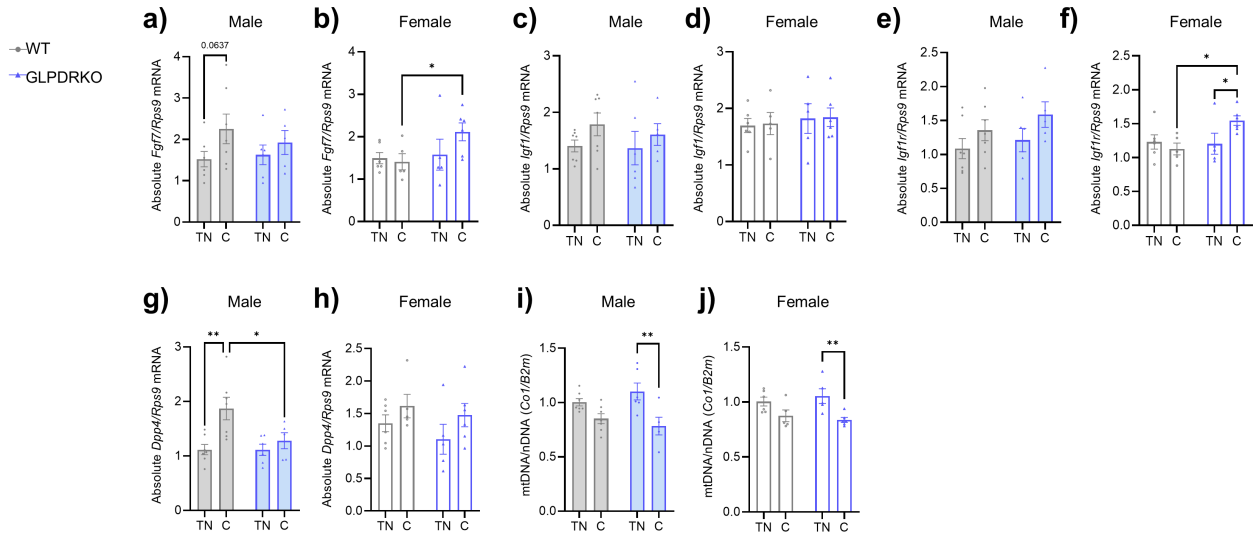
WT
GLPDRKO
a)
Male
Absolute Fgf7/Rps9 mRNA
0.0637
b)
Female
Absolute Fgf7/Rps9 mRNA
*
c)
Male
Absolute Igf1/Rps9 mRNA
d)
Female
Absolute Igf1/Rps9 mRNA
e)
Male
Absolute Igf1r/Rps9 mRNA
f)
Female
Absolute Igf1r/Rps9 mRNA
*
*
g)
Male
Absolute Dpp4/Rps9 mRNA
**
*
h)
Female
Absolute Dpp4/Rps9 mRNA
i)
Male
mtDNA/nDNA (Co1/B2m)
**
j)
Female
mtDNA/nDNA (Co1/B2m)
**
TN
C

Supplemental Figure 4-4. Male and female WT and GLPDRKO mice were housed at TN (27 °C) or cold (6 °C) temperatures for 5 weeks. Liver (a) total cholesterol levels in male WT (TN, n= 7; C, n= 7) and GLPDRKO (TN, n= 6; C, n= 5) mice. Short chain fatty acids were extracted from the feces of male WT (TN, n= 10; C, n= 11) and GLPDRKO mice (TN, n= 10; C, n= 7) for (b) acetate and (c) propionate levels expressed as a percentage of total SCFA in male mice. Liver (d) total cholesterol levels in female WT (TN, n= 6; C, n= 5) and GLPDRKO (TN, n= 5; C, n= 6) mice. Fecal (e) acetate and (f) propionate levels expressed as a percentage of total SCFA in female WT (TN, n= 6; C, n= 5) and GLPDRKO (TN, n= 6; C, n= 6) mice. Male WT and $Glp2r^{-/-}$ mice were housed at TN (27 °C) or cold (6 °C) for 5 weeks. Jejunal gene expression levels of (g) Glp2r and (h) Glp1r in WT and $Glp2r^{-/-}$ mice. For qPCR analyses, “n.d.” denotes not detected. Two-way ANOVA with a Tukey test correction for multiple comparisons was used to determine statistical significance between housing temperature and genotype. *P<0.05, **P<0.01, ***P<0.001, ****P<0.0001.

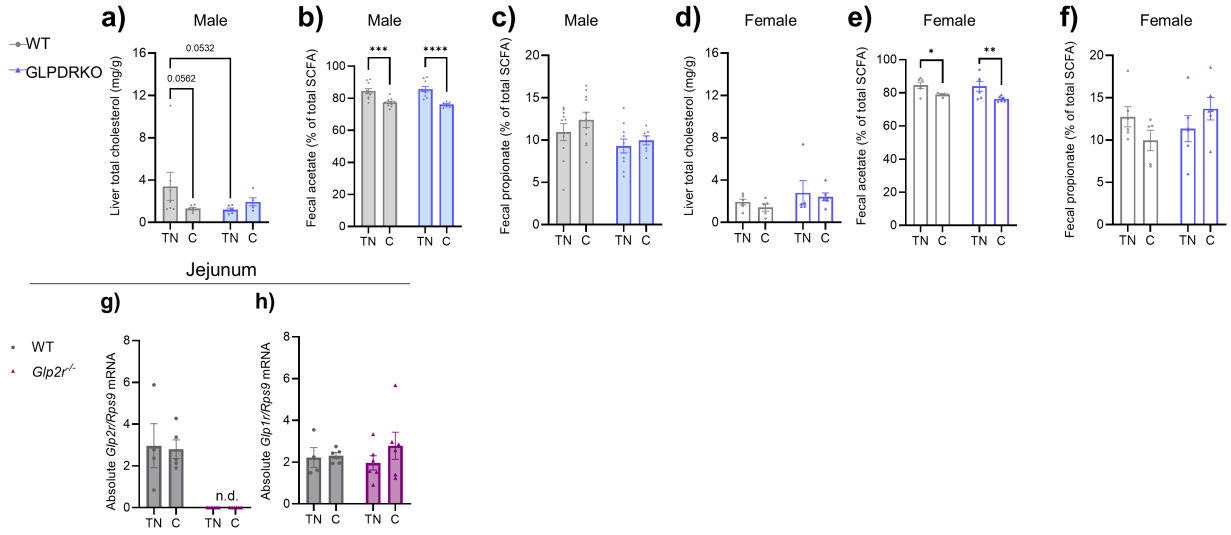
a)
Male
WT
GLPDRKO
Liver total cholesterol (mg/g)
0.0532
0.0562
TN C TN C
b)
Male
Fecal acetate (% of total SCFA)
***
****
c)
Male
Fecal propionate (% of total SCFA)
d)
Female
Liver total cholesterol (mg/g)
e)
Female
Fecal acetate (% of total SCFA)
*
**
f)
Female
Fecal propionate (% of total SCFA)
Jejunum
g)
h)
WT
Glp2r-/-
Absolute Glp2r/Rps9 mRNA
n.d.
Absolute Glp1r/Rps9 mRNA

4.9 References

Ali, S., B. J. Lamont, M. J. Charron and D. J. Drucker (2011). "Dual elimination of the glucagon and GLP-1 receptors in mice reveals plasticity in the incretin axis." J Clin Invest **121**(5): 1917–1929.

Baggio, L. L. and D. J. Drucker (2007). "Biology of incretins: GLP-1 and GIP." Gastroenterology **132**(6): 2131–2157.

Bahrami, J., B. Yusta and D. J. Drucker (2010). "ErbB activity links the glucagon-like peptide-2 receptor to refeeding-induced adaptation in the murine small bowel." Gastroenterology **138**(7): 2447–2456.

Beaudry, J. L. and G. B. McClelland (2010). "Thermogenesis in CD-1 mice after combined chronic hypoxia and cold acclimation." Comp Biochem Physiol B Biochem Mol Biol **157**(3): 301–309.

Blondin, D. P. (2023). "Human thermogenic adipose tissue." Curr Opin Genet Dev **80**: 102054.

Brubaker, P. L. (2018). "Glucagon-like Peptide-2 and the Regulation of Intestinal Growth and Function." Compr Physiol **8**(3): 1185–1210.

Burke, A. C., D. E. Telford, J. Y. Edwards, B. G. Sutherland, C. G. Sawyez and M. W. Huff (2019). "Naringenin Supplementation to a Chow Diet Enhances Energy Expenditure and Fatty Acid Oxidation, and Reduces Adiposity in Lean, Pair-Fed Ldlr(-/-) Mice." Mol Nutr Food Res **63**(6): e1800833.

Cani, P. D., S. Possemiers, T. Van de Wiele, Y. Guiot, A. Everard, O. Rottier, L. Geurts, D. Naslain, A. Neyrinck, D. M. Lambert, G. G. Muccioli and N. M. Delzenne (2009). "Changes in gut microbiota control inflammation in obese mice through a mechanism involving GLP-2-driven improvement of gut permeability." Gut **58**(8): 1091–1103.

Chevalier, C., O. Stojanovic, D. J. Colin, N. Suarez-Zamorano, V. Tarallo, C. Veyrat-Durebex, D. Rigo, S. Fabbiano, A. Stevanovic, S. Hagemann, X. Montet, Y. Seimbille, N. Zamboni, S. Hapfelmeier and M. Trajkovski (2015). "Gut Microbiota Orchestrates Energy Homeostasis during Cold." Cell **163**(6): 1360–1374.

Claustre, J., S. Brechet, P. Plaisancie, J. A. Chayvialle and J. C. Cuber (1999). "Stimulatory effect of beta-adrenergic agonists on ileal L cell secretion and modulation by alpha-adrenergic activation." J Endocrinol **162**(2): 271–278.

Cohen, P. and B. M. Spiegelman (2015). "Brown and Beige Fat: Molecular Parts of a Thermogenic Machine." Diabetes **64**(7): 2346–2351.

Dalby, M. J., A. W. Ross, A. W. Walker and P. J. Morgan (2017). "Dietary Uncoupling of Gut Microbiota and Energy Harvesting from Obesity and Glucose Tolerance in Mice." Cell Rep **21**(6): 1521–1533.

de Vos, W. M., H. Tilg, M. Van Hul and P. D. Cani (2022). "Gut microbiome and health: mechanistic insights." Gut **71**(5): 1020–1032.

Deacon, C. F., A. H. Johnsen and J. J. Holst (1995). "Human colon produces fully processed glucagon-like peptide-1 (7-36) amide." FEBS Lett **372**(2-3): 269–272.

Diaz-Jimenez, D., M. G. Petrillo, J. T. Busada, M. A. Hermoso and J. A. Cidlowski (2020). "Glucocorticoids mobilize macrophages by transcriptionally up-regulating the exopeptidase DPP4." J Biol Chem **295**(10): 3213–3227.

Drucker, D. J., Q. Shi, A. Crivici, M. Sumner-Smith, W. Tavares, M. Hill, L. DeForest, S. Cooper and P. L. Brubaker (1997). "Regulation of the biological activity of glucagon-like peptide 2 in vivo by dipeptidyl peptidase IV." Nat Biotechnol **15**(7): 673–677.

Drucker, D. J. and B. Yusta (2014). "Physiology and pharmacology of the enteroendocrine hormone glucagon-like peptide-2." Annu Rev Physiol **76**: 561–583.

Everard, A., V. Lazarevic, M. Derrien, M. Girard, G. G. Muccioli, A. M. Neyrinck, S. Possemiers, A. Van Holle, P. Francois, W. M. de Vos, N. M. Delzenne, J. Schrenzel and P. D. Cani (2011). "Responses of gut microbiota and glucose and lipid metabolism to prebiotics in genetic obese and diet-induced leptin-resistant mice." Diabetes **60**(11): 2775–2786.

Foster, D. O. and M. L. Frydman (1979). "Tissue distribution of cold-induced thermogenesis in conscious warm- or cold-acclimated rats reevaluated from changes in tissue blood flow: the dominant role of brown adipose tissue in the replacement of shivering by nonshivering thermogenesis." Can J Physiol Pharmacol **57**(3): 257–270.

Fuchs, S., B. Yusta, L. L. Baggio, E. M. Varin, D. Matthews and D. J. Drucker (2020). "Loss of Glp2r signaling activates hepatic stellate cells and exacerbates diet-induced steatohepatitis in mice." JCI Insight **5**(8).

Gelling, R. W., X. Q. Du, D. S. Dichmann, J. Romer, H. Huang, L. Cui, S. Obici, B. Tang, J. J. Holst, C. Fledelius, P. B. Johansen, L. Rossetti, L. A. Jelicks, P. Serup, E. Nishimura and M. J. Charron (2003). "Lower blood glucose, hyperglucagonemia, and pancreatic alpha cell hyperplasia in glucagon receptor knockout mice." Proc Natl Acad Sci U S A **100**(3): 1438–1443.

Grasset, E., A. Puel, J. Charpentier, X. Collet, J. E. Christensen, F. Terce and R. Burcelin (2017). "A Specific Gut Microbiota Dysbiosis of Type 2 Diabetic Mice Induces GLP-1 Resistance through an Enteric NO-Dependent and Gut-Brain Axis Mechanism." Cell Metab **25**(5): 1075–1090 e1075.

Gribble, F. M. and F. Reimann (2019). "Function and mechanisms of enteroendocrine cells and gut hormones in metabolism." Nat Rev Endocrinol **15**(4): 226–237.

Grigoryan, M., M. H. Kedees, M. J. Charron, Y. Guz and G. Teitelman (2012). "Regulation of mouse intestinal L cell progenitors proliferation by the glucagon family of peptides." Endocrinology **153**(7): 3076–3088.

Guan, X., H. E. Karpen, J. Stephens, J. T. Bukowski, S. Niu, G. Zhang, B. Stoll, M. J. Finegold, J. J. Holst, D. Hadsell, B. L. Nichols and D. G. Burrin (2006). "GLP-2 receptor localizes to enteric neurons and endocrine cells expressing vasoactive peptides and mediates increased blood flow." Gastroenterology **130**(1): 150–164.

Hammoud, R., K. D. Kaur, J. A. Koehler, L. L. Baggio, C. K. Wong, K. E. Advani, B. Yusta, I. Efimova, F. M. Gribble, F. Reimann, S. Fishman, C. Varol and D. J. Drucker (2024). "Glucose-dependent insulinotropic polypeptide receptor signaling alleviates gut inflammation in mice." JCI Insight **10**(3).

Han, A., C. Hudson-Paz, B. G. Robinson, L. Becker, A. Jacobson, J. A. Kaltschmidt, J. L. Garrison, A. S. Bhatt and D. M. Monack (2024). "Temperature-dependent differences in mouse gut motility are mediated by stress." Lab Anim (NY) **53**(6): 148–159.

Hansotia, T., L. L. Baggio, D. Delmeire, S. A. Hinke, Y. Yamada, K. Tsukiyama, Y. Seino, J. J. Holst, F. Schuit and D. J. Drucker (2004). "Double incretin receptor knockout (DIRKO) mice reveal an essential role for the enteroinsular axis in transducing the glucoregulatory actions of DPP-IV inhibitors." Diabetes **53**(5): 1326–1335.

Harada, K., T. Kitaguchi and T. Tsuboi (2015). "Integrative function of adrenaline receptors for glucagon-like peptide-1 exocytosis in enteroendocrine L cell line GLUTag." Biochem Biophys Res Commun **460**(4): 1053–1058.

Hartmann, B., M. B. Harr, P. B. Jeppesen, M. Wojdemann, C. F. Deacon, P. B. Mortensen and J. J. Holst (2000). "In vivo and in vitro degradation of glucagon-like peptide-2 in humans." J Clin Endocrinol Metab **85**(8): 2884–2888.

He, S., F. Kahles, S. Rattik, M. Nairz, C. S. McAlpine, A. Anzai, D. Selgrade, A. M. Fenn, C. T. Chan, J. E. Mindur, C. Valet, W. C. Poller, L. Halle, N. Rotllan, Y. Iwamoto, G. R. Wojtkiewicz, R. Weissleder, P. Libby, C. Fernandez-Hernando, D. J. Drucker, M. Nahrendorf and F. K. Swirski (2019). "Gut intraepithelial T cells calibrate metabolism and accelerate cardiovascular disease." Nature **566**(7742): 115–119.

Hein, G. J., C. Baker, J. Hsieh, S. Farr and K. Adeli (2013). "GLP-1 and GLP-2 as yin and yang of intestinal lipoprotein production: evidence for predominance of GLP-2-stimulated postprandial lipemia in normal and insulin-resistant states." Diabetes **62**(2): 373–381.

Hsieh, J., C. Longuet, C. L. Baker, B. Qin, L. M. Federico, D. J. Drucker and K. Adeli (2010). "The glucagon-like peptide 1 receptor is essential for postprandial lipoprotein synthesis and secretion in hamsters and mice." Diabetologia **53**(3): 552–561.

Hsieh, J., C. Longuet, A. Maida, J. Bahrami, E. Xu, C. L. Baker, P. L. Brubaker, D. J. Drucker and K. Adeli (2009). "Glucagon-like peptide-2 increases intestinal lipid absorption and chylomicron production via CD36." Gastroenterology **137**(3): 997–1005, 1005 e1001–1004.

Hsieh, J., K. E. Trajcevski, S. L. Farr, C. L. Baker, E. J. Lake, J. Taher, J. Iqbal, M. M. Hussain and K. Adeli (2015). "Glucagon-Like Peptide 2 (GLP-2) Stimulates Postprandial Chylomicron Production and Postabsorptive Release of Intestinal Triglyceride Storage Pools via Induction of Nitric Oxide Signaling in Male Hamsters and Mice." Endocrinology **156**(10): 3538–3547.

Idrizaj, E., C. Biagioni, C. Traini, M. G. Vannucchi and M. C. Baccari (2024). "Glucagon-like Peptide-2 Depresses Ileal Contractility in Preparations from Mice through Opposite Modulatory Effects on Nitrergic and Cholinergic Neurotransmission." Int J Mol Sci **25**(3).

Irwin, N., J. M. Francis and P. R. Flatt (2011). "Alterations of glucose-dependent insulinotropic polypeptide (GIP) during cold acclimation." Regul Pept **167**(1): 91–96.

Kedees, M. H., Y. Guz, M. Grigoryan and G. Teitelman (2013). "Functional activity of murine intestinal mucosal cells is regulated by the glucagon-like peptide-1 receptor." Peptides **48**: 36–44.

Koehler, J. A., L. L. Baggio, B. Yusta, C. Longuet, K. J. Rowland, X. Cao, D. Holland, P. L. Brubaker and D. J. Drucker (2015). "GLP-1R agonists promote normal and neoplastic intestinal growth through mechanisms requiring Fgf7." Cell Metab **21**(3): 379–391.

Lechuga, S., N. G. Naydenov, A. Feygin, M. Cruise, J. M. Ervasti and A. I. Ivanov (2020). "Loss of beta-Cytoplasmic Actin in the Intestinal Epithelium Increases Gut Barrier Permeability in vivo and Exaggerates the Severity of Experimental Colitis." Front Cell Dev Biol **8**: 588836.

Livingston, D. B. H., A. Sweet, A. Rodrigue, L. Kishore, J. Loftus, F. Ghali, S. Mahmoodianfard, C. Celton, F. Hosseinian and K. A. Power (2023). "Dietary Flaxseed and Flaxseed Oil Differentially Modulate Aspects of the Microbiota Gut-Brain Axis Following an Acute Lipopolysaccharide Challenge in Male C57Bl/6 Mice." Nutrients **15**(16).

Lubawy, J., S. Chowanski, Z. Adamski and M. Slocinska (2022). "Mitochondria as a target and central hub of energy division during cold stress in insects." Front Zool **19**(1): 1.

Markovic, M. A. and P. L. Brubaker (2019). "The roles of glucagon-like peptide-2 and the intestinal epithelial insulin-like growth factor-1 receptor in regulating microvillus length." Sci Rep **9**(1): 13010.

Meier, J. J., M. A. Nauck, D. Kranz, J. J. Holst, C. F. Deacon, D. Gaeckler, W. E. Schmidt and B. Gallwitz (2004). "Secretion, degradation, and elimination of glucagon-like peptide 1 and gastric inhibitory polypeptide in patients with chronic renal insufficiency and healthy control subjects." Diabetes **53**(3): 654–662.

Mojsov, S., G. Heinrich, I. B. Wilson, M. Ravazzola, L. Orci and J. F. Habener (1986). "Preproglucagon gene expression in pancreas and intestine diversifies at the level of post-translational processing." J Biol Chem **261**(25): 11880–11889.

Morrow, N. M., C. A. A. Locatelli, N. A. Trzaskalski, C. T. Klein, A. A. Hanson, H. Alhadi, I. Tripathi, A. C. Clement, S. Imran, I. Lorenzen-Schmidt and E. E. Mulvihill (2022). "Adaptation to short-term extreme fat consumption alters intestinal lipid handling in male and female mice." Biochim Biophys Acta Mol Cell Biol Lipids **1867**(11): 159208.

Morrow, N. M., N. A. Trzaskalski, A. A. Hanson, E. Fadzeyeva, D. E. Telford, S. S. Chhoker, B. G. Sutherland, J. Y. Edwards, M. W. Huff and E. E. Mulvihill (2022). "Nobiletin Prevents High-Fat Diet-Induced Dysregulation of Intestinal Lipid Metabolism and Attenuates Postprandial Lipemia." Arterioscler Thromb Vasc Biol **42**(2): 127–144.

Mulvihill, E. E., E. M. Varin, B. Gladanac, J. E. Campbell, J. R. Ussher, L. L. Baggio, B. Yusta, J. Ayala, M. A. Burmeister, D. Matthews, K. W. A. Bang, J. E. Ayala and D. J. Drucker (2017). "Cellular Sites and Mechanisms Linking Reduction of Dipeptidyl Peptidase-4 Activity to Control of Incretin Hormone Action and Glucose Homeostasis." Cell Metab **25**(1): 152–165.

Nauck, M. A. and J. J. Meier (2016). "The incretin effect in healthy individuals and those with type 2 diabetes: physiology, pathophysiology, and response to therapeutic interventions." Lancet Diabetes Endocrinol **4**(6): 525–536.

Nelson, D. W., J. W. Sharp, M. S. Brownfield, H. E. Raybould and D. M. Ney (2007). "Localization and activation of glucagon-like peptide-2 receptors on vagal afferents in the rat." Endocrinology **148**(5): 1954–1962.

Orskov, C., B. Hartmann, S. S. Poulsen, J. Thulesen, K. J. Hare and J. J. Holst (2005). "GLP-2 stimulates colonic growth via KGF, released by subepithelial myofibroblasts with GLP-2 receptors." Regul Pept **124**(1-3): 105–112.

Orskov, C., J. J. Holst, S. Knuhtsen, F. G. Baldissera, S. S. Poulsen and O. V. Nielsen (1986). "Glucagon-like peptides GLP-1 and GLP-2, predicted products of the glucagon gene, are secreted separately from pig small intestine but not pancreas." Endocrinology **119**(4): 1467–1475.

Parker, A., O. J. Maclaren, A. G. Fletcher, D. Muraro, P. A. Kreuzaler, H. M. Byrne, P. K. Maini, A. J. Watson and C. Pin (2017). "Cell proliferation within small intestinal crypts is the principal driving force for cell migration on villi." FASEB J **31**(2): 636–649.

Paternoster, S. and M. Falasca (2018). "Dissecting the Physiology and Pathophysiology of Glucagon-Like Peptide-1." Front Endocrinol (Lausanne) **9**: 584.

Pyke, C., R. S. Heller, R. K. Kirk, C. Orskov, S. Reedtz-Runge, P. Kaastrup, A. Hvelplund, L. Bardram, D. Calatayud and L. B. Knudsen (2014). "GLP-1 receptor localization in monkey and human tissue: novel distribution revealed with extensively validated monoclonal antibody." Endocrinology **155**(4): 1280–1290.

Quiros, P. M., A. Goyal, P. Jha and J. Auwerx (2017). "Analysis of mtDNA/nDNA Ratio in Mice." Curr Protoc Mouse Biol **7**(1): 47–54.

Reiner, J., P. Berlin, J. Held, J. Thiery, J. Skarbaliene, J. Griffin, W. Russell, P. O. Eriksson, M. Berner-Hansen, L. Ehlers, B. Vollmar, R. Jaster, M. Witte and G. Lamprecht (2022). "Dapiglutide, a novel dual GLP-1 and GLP-2 receptor agonist, attenuates intestinal insufficiency in a murine model of short bowel." JPEN J Parenter Enteral Nutr **46**(5): 1107–1118.

Rodriguez-Colman, M. J., M. Schewe, M. Meerlo, E. Stigter, J. Gerrits, M. Pras-Raves, A. Sacchetti, M. Hornsveld, K. C. Oost, H. J. Snippert, N. Verhoeven-Duif, R. Fodde and B. M. Burgering (2017). "Interplay between metabolic identities in the intestinal crypt supports stem cell function." Nature **543**(7645): 424–427.

Rowland, K. J., S. Trivedi, D. Lee, K. Wan, R. N. Kulkarni, M. Holzenberger and P. L. Brubaker (2011). "Loss of glucagon-like peptide-2-induced proliferation following intestinal epithelial insulin-like growth factor-1-receptor deletion." Gastroenterology **141**(6): 2166–2175 e2167.

Schonkeren, S. L., S. Seeldrayers, M. S. Thijssen, W. Boesmans, R. C. J. Langen and V. Melotte (2023). "An optimization and refinement of the whole-gut transit assay in mice." Neurogastroenterol Motil **35**(8): e14586.

Scrocchi, L. A., T. J. Brown, N. MaClusky, P. L. Brubaker, A. B. Auerbach, A. L. Joyner and D. J. Drucker (1996). "Glucose intolerance but normal satiety in mice with a null mutation in the glucagon-like peptide 1 receptor gene." Nat Med **2**(11): 1254–1258.

Simonsen, L., S. Pilgaard, C. Orskov, M. M. Rosenkilde, B. Hartmann, J. J. Holst and C. F. Deacon (2007). "Exendin-4, but not dipeptidyl peptidase IV inhibition, increases small intestinal mass in GK rats." Am J Physiol Gastrointest Liver Physiol **293**(1): G288–295.

Singh, V., G. Lee, H. Son, H. Koh, E. S. Kim, T. Unno and J. H. Shin (2022). "Butyrate producers, "The Sentinel of Gut": Their intestinal significance with and beyond butyrate, and prospective use as microbial therapeutics." Front Microbiol **13**: 1103836.

Stojanovic, O., J. Altirriba, D. Rigo, M. Spiljar, E. Evrard, B. Roska, S. Fabbiano, N. Zamboni, P. Maechler, F. Rohner-Jeanrenaud and M. Trajkovski (2021). "Dietary excess regulates absorption and surface of gut epithelium through intestinal PPARalpha." Nat Commun **12**(1): 7031.

Tiruppathi, C., Y. Miyamoto, V. Ganapathy and F. H. Leibach (1993). "Genetic evidence for role of DPP IV in intestinal hydrolysis and assimilation of prolyl peptides." Am J Physiol **265**(1 Pt 1): G81–89.

Trzaskalski, N. A., B. Vulesevic, M. A. Nguyen, N. Jeraj, E. Fadzeyeva, N. M. Morrow, C. A. Locatelli, N. Travis, A. A. Hanson, J. R. Nunes, C. O'Dwyer, J. N. van der Veen, I. Lorenzen-

Schmidt, R. Seymour, S. M. Pulente, A. C. Clement, A. M. Crawley, R. L. Jacobs, M. A. Doyle, C. L. Cooper, K. H. Kim, M. D. Fullerton and E. E. Mulvihill (2023). "Hepatocyte-derived DPP4 regulates portal GLP-1 bioactivity, modulates glucose production, and when absent influences NAFLD progression." JCI Insight **8**(2).

Ugleholdt, R., M. L. Poulsen, P. J. Holst, J. C. Irminger, C. Orskov, J. Pedersen, M. M. Rosenkilde, X. Zhu, D. F. Steiner and J. J. Holst (2006). "Prohormone convertase 1/3 is essential for processing of the glucose-dependent insulinotropic polypeptide precursor." J Biol Chem **281**(16): 11050–11057.

Varin, E. M., A. A. Hanson, J. L. Beaudry, M. A. Nguyen, X. Cao, L. L. Baggio, E. E. Mulvihill and D. J. Drucker (2020). "Hematopoietic cell- versus enterocyte-derived dipeptidyl peptidase-4 differentially regulates triglyceride excursion in mice." JCI Insight **5**(16).

Varin, E. M., E. E. Mulvihill, J. L. Beaudry, G. Pujadas, S. Fuchs, J. F. Tanti, S. Fazio, K. Kaur, X. Cao, L. L. Baggio, D. Matthews, J. E. Campbell and D. J. Drucker (2019). "Circulating Levels of Soluble Dipeptidyl Peptidase-4 Are Dissociated from Inflammation and Induced by Enzymatic DPP4 Inhibition." Cell Metab **29**(2): 320–334 e325.

Wang, Z., Y. Wu, X. Li, X. Ji and W. Liu (2024). "The gut microbiota facilitate their host tolerance to extreme temperatures." BMC Microbiol **24**(1): 131.

Wismann, P., P. Barkholt, T. Secher, N. Vrang, H. B. Hansen, P. B. Jeppesen, L. L. Baggio, J. A. Koehler, D. J. Drucker, D. A. Sandoval and J. Jelsing (2017). "The endogenous preproglucagon system is not essential for gut growth homeostasis in mice." Mol Metab **6**(7): 681–692.

Wong, C. K., B. A. McLean, L. L. Baggio, J. A. Koehler, R. Hammoud, N. Rittig, J. M. Yabut, R. J. Seeley, T. J. Brown and D. J. Drucker (2024). "Central glucagon-like peptide 1 receptor activation inhibits Toll-like receptor agonist-induced inflammation." Cell Metab **36**(1): 130–143 e135.

Wong, C. K., B. Yusta, J. A. Koehler, L. L. Baggio, B. A. McLean, D. Matthews, R. J. Seeley and D. J. Drucker (2022). "Divergent roles for the gut intraepithelial lymphocyte GLP-1R in control of metabolism, microbiota, and T cell-induced inflammation." Cell Metab **34**(10): 1514–1531 e1517.

Yusta, B., L. L. Baggio, J. Koehler, D. Holland, X. Cao, L. J. Pinnell, K. C. Johnson-Henry, W. Yeung, M. G. Surette, K. W. Bang, P. M. Sherman and D. J. Drucker (2015). "GLP-1R Agonists Modulate Enteric Immune Responses Through the Intestinal Intraepithelial Lymphocyte GLP-1R." Diabetes **64**(7): 2537–2549.

Yusta, B., L. Huang, D. Munroe, G. Wolff, R. Fantaske, S. Sharma, L. Demchyshyn, S. L. Asa and D. J. Drucker (2000). "Enteroendocrine localization of GLP-2 receptor expression in humans and rodents." Gastroenterology **119**(3): 744–755.

Zhao, Z., R. Yang, M. Li, M. Bao, D. Huo, J. Cao and J. R. Speakman (2022). "Effects of ambient temperatures between 5 and 35 degrees C on energy balance, body mass and body composition in mice." Mol Metab **64**: 101551.

Zhu, C. and Y. Li (2022). "An updated overview of glucagon-like peptide-2 analog trophic therapy for short bowel syndrome in adults." J Int Med Res **50**(3): 3000605221086145.

Chapter 5 Discussion

Cardiovascular disease (CVD) is a leading cause of death in patients with T2DM and accounts for one-third of all deaths in Canada (Wu and Parhofer 2014, Scherer and Hill 2016). The increasing prevalence of T2DM, now affecting over 2 million Canadians, underscores the urgent need to develop effective therapeutics and uncover fundamental biology underlying this disease. Diabetic dyslipidemia, driven by elevated fasting and post-prandial triglyceride levels and LDL-cholesterol levels (Wu and Parhofer 2014) is a key driver of CVD in T2DM. Statins are first line therapies for dyslipidemia as they are effective at LDL-cholesterol lowering and reducing major adverse cardiovascular outcomes, yet significant CVD risk remains in T2DM patients (Wu and Parhofer 2014). This highlights the need for a deeper understanding of the mechanisms underlying dysregulated triglyceride metabolism and atherosclerotic plaque progression. Critical to systemic lipid and lipoprotein metabolism lies the small intestine. Although the atherogenicity of intestinally derived lipoproteins is increasingly appreciated, the complex interplay of the mechanisms underlying nutrient absorption, storage, the production of triglyceride-rich lipoproteins, and peptide hormone production are not well understood. The overarching goal of this thesis was to uncover and characterize the adaptability of the gut to nutritional and environmental stresses and their impacts on lipid handling, surface area expansion, and systemic metabolic responses.

5.1 Nobiletin confers cardiometabolic protection and provides opportunities to uncover important metabolic changes in diet-induced obesity

Hepatic insulin resistance significantly contributes to the hyperglycemia, hyperinsulinemia, and hypertriglyceridemia observed in individuals living with metabolic disease, and as such, many studies have focused on elucidating pathways in the liver that contribute to metabolic disease. The contribution of the small intestine, however, can often be overlooked as simply a conduit for

nutrients. Post-prandial but not fasting triglycerides exhibit a strong association with coronary artery disease, shown to be statistically independent and stronger than that of HDL-cholesterol (Patsch, Miesenbock et al. 1992). Individuals with coronary artery disease display significantly higher plasma triglyceride levels in response to an oral lipid tolerance test than healthy controls (Patsch, Miesenbock et al. 1992). Nobiletin is a citrus flavonoid that has previously been shown to prevent obesity and attenuate dyslipidemia in HFHC-fed male WT (Lee, Cha et al. 2013, He, Nohara et al. 2016, Kim, Choi et al. 2017, Morrow, Burke et al. 2020) and *Ldlr*$^{-/-}$ mice (Mulvihill, Assini et al. 2011, Burke, Sutherland et al. 2018). Nobiletin administered as either prevention (Mulvihill, Assini et al. 2011) or intervention (Burke, Sutherland et al. 2018) treatment in *Ldlr*$^{-/-}$ mice reduces atherosclerosis, VLDL-triglyceride secretion, and hepatic triglyceride accumulation. Nobiletin reduces hepatic-FA synthesis and enhances hepatic-FA oxidation (Mulvihill, Assini et al. 2011, Burke, Sutherland et al. 2018). The observation that nobiletin also attenuates fasting intestinal triglyceride accumulation in *Ldlr*$^{-/-}$ mice fed a HFHC diet (Mulvihill, Assini et al. 2011) was the starting point of this project. In Chapter 2, we evaluated the impact of adding nobiletin, a citrus flavonoid, to a HFHC diet on intestinal insulin sensitivity and intestinal lipid metabolism in mice.

Impaired lipid tolerance in obesity and insulin resistance is well characterized, with both human and animal studies showing overproduction of apoB48-containing particles and delayed triglyceride clearance (Haidari, Leung et al. 2002, Duez, Lamarche et al. 2006, Federico, Naples et al. 2006, Adeli and Lewis 2008, Douglass, Malik et al. 2012, Uchida, Whitsitt et al. 2012). In Chapter 2, while HFHC-fed *Ldlr*$^{-/-}$ mice displayed significantly higher baseline and post-prandial triglyceride levels in both the chylomicron fraction and the VLDL fraction of plasma, poloxamer experiments revealed that HFHC-fed *Ldlr*$^{-/-}$ mice displayed significantly lower post-prandial plasma triglyceride levels compared to SLD-fed controls. Delayed intestinal-triglyceride secretion rates in diet-induced obese mice have been previously observed (Douglass, Malik et

al. 2012, Uchida, Whitsitt et al. 2012) and elevated fasting triglycerides have been shown to predict delayed post-prandial triglyceride clearance in humans with obesity and insulin resistance (Larsen, Goll et al. 2015). In Chapter 2, we found that this slower intestinal-triglyceride secretion rate was driven by significantly smaller triglyceride:apoB48 ratio observed in HFHC-fed mice compared to SLD-fed controls. Examining the results from the non-poloxamer and poloxamer studies together, as well as clearance assays, we concluded that the post-prandial lipemia in HFHC-fed mice was driven by both the prolonged excursion of intestinal-triglycerides and the delayed clearance of these particles.

In Chapter 2, we found that nobiletin did not significantly impact overall lipid tolerance in non-poloxamer experiments performed in *Ldlr*$^{-/-}$ mice. However, nobiletin reduced the triglyceride content of the VLDL-sized particles of plasma post-acute dietary fat challenge, likely due to the preserved clearance capacity as previously shown for hepatic-derived VLDL particles (Mulvihill, Assini et al. 2011). Poloxamer experiments revealed that nobiletin treatment in both WT and *Ldlr*$^{-/-}$ mice, enhanced the rate of dietary lipid excursion. This increased intestinal-triglyceride secretion rate was independent of any changes in plasma apoB48 levels compared to HFHC alone. Mice treated with nobiletin displayed significantly greater changes in plasma apoB48 levels compared to SLD-fed mice in poloxamer experiments. Altogether, this data suggested that HFHC-diet-fed *Ldlr*$^{-/-}$ mice, independent of nobiletin treatment, secreted more chylomicron particles than the SLD-fed controls. Our triglyceride:apoB48 ratio analyses, however, revealed that nobiletin treatment led to a greater amount of triglyceride per intestinal lipoprotein particle compared to HFHC-fed mice, although chylomicrons from chow-fed mice remained the most enriched. An important limitation in this conclusion is the hepatic contribution of apoB48 in mice, which is not observed in humans (Higuchi, Hospattankar et al. 1988, D'Aquila, Hung et al. 2016). Future experiments measuring the size of chylomicrons sampled from the lymph versus the plasma by electron microscopy (Kohan, Wang et al. 2012) are

required, and detection of the abundance of their associated apolipoproteins by immunogold labelling or proteomics analyses by mass spectrometry may unveil important players in the respective circulatory compartments.

While intestinal insulin resistance promotes chylomicron production via enhanced microsomal triglyceride transfer protein activity (Bozzetto, Della Pepa et al. 2020), in Chapter 2, we found that HFHC-fed mice also accumulated jejunal triglycerides in the fed state, which eventually cleared after 9h of fasting. We found that HFHC-feeding in male *Ldlr*$^{-/-}$ mice reduced intestinal insulin sensitivity leading to enhanced jejunal *de novo* lipogenesis, which, together with dietary lipids, led to greater intestinal triglyceride storage in the fed and fasted states, contributing prolonged post-prandial lipemia. Indeed, enhanced *de novo* lipogenesis rates as shown by radiolabelled acetate incorporation into lipids have been observed in duodenal specimens obtained from individuals undergoing bariatric surgery (Veilleux, Grenier et al. 2014). Nobiletin-treated mice did not accumulate jejunal triglyceride more than SLD-fed mice, even in the fed state. The addition of nobiletin to the HFHC diet in male *Ldlr*$^{-/-}$ mice improved the sensitivity of the insulin signalling pathway downstream of mTORC1, leading to lower jejunal *Srebf1c* mRNA expression in the refed and post-olive oil states compared to HFHC-fed mice. The impact of the increased jejunal *Srebf1c* mRNA expression on the rate of *de novo* lipogenesis was confirmed *in vivo* by administering radiolabelled acetate, which was significantly lower with nobiletin treatment compared to mice fed the HFHC diet alone. Therefore, we concluded that nobiletin prevented intestinal insulin resistance induced by chronic HFHC-diet feeding, leading to intestinal triglyceride storage at similar levels to chow-fed mice in the fed and fasted state. Overall, we concluded that the ability of nobiletin to shorten the post-prandial window was two-fold. First, we found that nobiletin increased the triglyceride content per chylomicron, resulting in lower residual intestinal triglycerides after a dietary fat challenge. Second, we found that nobiletin enhanced post-prandial

triglyceride-lipoprotein clearance. Altogether, these results underscore relationship between intestinal insulin resistance, enhanced intestinal lipid storage, and post-prandial lipemia.

Our contributions in Chapter 2 demonstrated a greater pool of fatty acids from *de novo* lipogenesis, which was associated with an inefficient excursion of dietary fatty acids following an acute challenge compared to a chow-fed mouse. To begin to unravel this mechanism, an oral glucose and fat tolerance test should be performed in chow versus HFD-fed mice across the progression of diet-induced obesity. Specifically, 5 hour fasted mice would receive an oral gavage of an equal parts glucose-lipid emulsion containing ^{14}C-glucose and ^{3}H-triolein, similar to what has been done previously (Fischer, Behrens et al. 2020). In poloxamer experiments, experimental endpoints would be 2 hours or 4 hours post-gavage, whereby blood would be collected every 30 minutes prior. In plasma, the ^{14}C -labelled fatty acids would be contributed by *de novo* lipogenesis, the dietary fatty acids would be contributed by ^{3}H -triolein, and the remaining fatty acids would be from the previous meal or circulating fatty acids. Lipid extractions from the intestine would reveal the contribution of *de novo* lipogenesis and dietary fats to the total lipid pool. Complementary experiments could place the ^{3}H on palmitate for intraperitoneal injections to mimic circulating free fatty acids prior to the glucose-lipid emulsion, maintaining the ^{14}C-glucose. These experiments would significantly enhance our understanding of how delayed intestinal-triglyceride secretion rate manifests and if this is protective or maladaptive. In non-poloxamer experiments, plasma, intestine, liver, heart as well as white and brown adipose tissue would be collected 2- and 4-hours post-gavage for radioactivity measurements. This experiment would allow us to evaluate tissue fuel preference and measure their contributions to chylomicron composition. This approach is physiologically relevant and would address the significant gap in knowledge regarding the fate of fatty acids from difference sources in response to a meal during health and metabolic disease in both sexes. Probing the rate of use of fatty acids pools would help delineate the enhanced substrates for chylomicron synthesis

observed in our studies and may reveal novel targets to limit the number of these particles into blood circulation for cardiovascular protection without causing malabsorption. Additionally, capturing the contribution of the liver overshadowing the clearance of these particles with the use of tracers on dietary fatty acids and measure the amount that enters the liver over time would significantly enhance our understanding of the dynamics of the lipid tolerance test.

Evidence for the metabolic benefits of nobiletin in female mice are limited to a study in a mouse model of Alzheimer's disease (amyloid precursor protein/presenilin; APP/PS1 double transgenic mouse) (Kim, Nohara et al. 2021), post-menopause osteoporosis (Wang, Xie et al. 2019), diet-induced obesity (Morrow, Burke et al. 2020). In Chapter 2, we tested the ability of nobiletin to confer metabolic protection in female *Ldlr*$^{-/-}$ mice. The addition of nobiletin to the HFHC prevented body weight gain and attenuated liver triglyceride levels in female *Ldlr*$^{-/-}$ mice, as previously shown in female C57BL/6J mice (Morrow, Burke et al. 2020). Similar to male *Ldlr*$^{-/-}$ mice, nobiletin lowered fasting jejunal triglyceride levels, preserved small intestinal weight, and attenuated small intestinal shortening in female *Ldlr*$^{-/-}$ mice. Unlike in male mice, nobiletin treatment in female *Ldlr*$^{-/-}$ mice did not lead to an enrichment of triglycerides on chylomicrons, did not enhance intestinal-triglyceride secretion rates compared to mice fed the HFHC diet alone, nor did it lower post-oil jejunal triglycerides. Therefore, the prevention of obesity by nobiletin treatment does not appear to normalize intestinal triglyceride secretion rates in female mice as it does in male mice. Indeed, while acute elevations of plasma free fatty acids stimulate intestinal triglyceride rich lipoprotein production in men and in male hamsters (Lewis, Naples et al. 2004, Duez, Lamarche et al. 2008), the improvements of intestinal lipid handling conferred by nobiletin appears to be independent of preventing this supply of fatty acids to the enterocyte. Also unlike in male mice, nobiletin treatment did not attenuate jejunal *Srebf1c* mRNA levels or jejunal triglyceride storage post-acute dietary fat challenge. Female mice are more insulin sensitive and do not develop hyperinsulinemia with high-fat diet feeding to the same extent as males

(Pettersson, Walden et al. 2012). The enhanced insulin sensitivity in females favours energy storage in adipose tissue (Varlamov, Bethea et al. 2014). Therefore, since HFHC-diet fed males progress to a more insulin-resistant state than females, the window for improvement conferred by nobiletin is greater in males than in females. Altogether, this may explain why nobiletin does not further lower jejunal *Srebf1c* mRNA expression. Moreover, the metabolic profile favouring energy storage over mobilization appears to extend to the intestine, which may override nobiletin's ability to enhance the excursion of dietary fatty acids. Whether this effect in intestinal lipid metabolism is biologically distinct prior to puberty is unclear. Puberty in mice begins on average around 4 weeks of age, where a transient insulin resistance manifests at puberty onset (Teixeira, Tavares et al. 2021). Therefore, performing acute dietary fat challenges in mice prior to puberty, at puberty onset, and post-puberty could discern the relationship between favoured energy storage and insulin resistance in female mice. Similarly, a mouse model of menopause treated with 4-vinylcyclohexene diepoxide to cause ovarian failure and fed a HFD to induce obesity display a doubling of fasting insulin levels compared to HFD-fed controls (Romero-Aleshire, Diamond-Stanic et al. 2009). Performing acute dietary fat challenges in this model of menopause compared to HFD controls would significantly enhance our understanding of the biological influences versus hormonal influences on intestinal lipid metabolism. Moreover, understanding the impact of favoured storage over oxidation on long term cardiovascular outcomes may uncover if these pathways are important to target to prevent disease or to maintain cardiometabolic health.

Small intestinal length was significantly shorter in HFHC-fed mice compared to chow-fed controls. Both high-fat diets (60% of calories from fat) and high-fat, high-sucrose diets (60% calories from fat, 25% from sucrose) shorten the small intestine (Stojanovic, Altirriba et al. 2021). By contrast, diets of low caloric density per gram by 40% compared to the chow diet led to overeating and lengthening of the gut (Stojanovic, Altirriba et al. 2021). This suggests that, since high-fat diets are more energy-rich than standard chow, mice consume less food by mass, leading

to gut atrophy. Alternatively, one study demonstrated with a low-fat diet control that it is the low fibre content, and not the fat content, that drives the reduction of colon and small intestinal during chronic high-fat diet feeding (Dalby, Ross et al. 2017). The intestinotrophic effect of fibre is supported by another study comparing purified diets and fibre-free diets to chow-diets (Hunt, Hartmann et al. 2021, Glenny, Liu et al. 2024). In Chapter 2, we found that chronic HFHC-diet feeding significantly shortened small intestinal length in both male and female *Ldlr*$^{-/-}$ mice. The addition of nobiletin to the same HFHC diet, which was therefore matched for fibre content and calories consumed, significantly attenuated the shortening of the small intestine in both male and female mice. We observed significantly higher plasma GLP-1 levels post-oil with nobiletin treatment. GLP-1 is co-secreted with GLP-2 in equimolar ratios, and both GLP-1R and GLP-2R action exert intestinotrophic effects. Chronic GLP-1R agonist treatment with exendin-4 increases intestinal circumference and length (Koehler, Baggio et al. 2015) whereas GLP-2 increases villus height (Drucker, Shi et al. 1997). To block endogenous GLP-2R action, we treated mice with a GLP-2R antagonist, GLP-2 3-33 (30 ng/day) for 2 weeks after a 10-week induction on the HFHC diet. GLP-2 3-33 treatment led to shorter jejunal villi length in HFHC-diet fed *Ldlr*$^{-/-}$ mice, as previously shown in diet-induced obese mice (Baldassano, Amato et al. 2013) but had no impact with nobiletin co-treatment. Despite higher plasma GLP-1, and presumably GLP-2, in nobiletin-treated mice, signaling through GLP-1R or GLP-2R did not significantly impact the prevention of HFHC diet-induced shortening of the small intestine. The intestinotrophic effects of nobiletin have been tested in both diet-induced obesity and antibiotic-induced intestinal barrier dysfunction. Fourteen days of nobiletin treatment in diet-induced obese male mice led to longer intestinal crypts and higher expression levels of intestinal tight junction proteins zonula occluden protein-1 (ZO-1) and Occludin (Yang, Pang et al. 2025). In a model of antibiotic-induced intestinal injury, the addition of nobiletin (0.5% weight/weight) to a standard diet for twenty days prevented the loss of goblet cells, increased the protein levels of ZO-1 and Occludin, and lowered the mRNA expression of colonic *Tnfα* (Zhan, Yang et al. 2024). The addition of nobiletin (0.01%

weight/weight) to a chow diet in a mouse model of experimental colitis induced by dextran sodium sulphate in drinking water for 7 days attenuates weight loss, prevents colon length shortening, and maintains epithelial barrier integrity as determined by FITC-dextran experiments (Wen, Zhao et al. 2020). Altogether, this suggest that nobiletin impacts the intestinal barrier independent of its anti-obesity effects, which may be one of the ways nobiletin lowers systemic inflammation during atherosclerosis (Burke, Sutherland et al. 2018).

In Chapter 2, we also found that nobiletin significantly increased plasma GLP-1 levels post-oil gavage. Nobiletin has also been shown to restore the rhythmicity of GLP-1 secretion that is lost with chronic HFD feeding (Martchenko, Biancolin et al. 2022). The GLP-1R agonist exendin-4 significantly decreases the triglyceride content in the triglyceride-rich fraction of plasma as well as apoB48 levels following an acute dietary fat challenge in mice (Hsieh, Longuet et al. 2010), which is the opposite of the phenotype observed with nobiletin treatment. In hamsters, acute GLP-2 analogue, hGly^{2}-GLP-2, treatment significantly increases the triglyceride content of triglyceride-rich lipoproteins and increases the ^{3}H-triolein radiolabel incorporation specifically into plasma triglycerides post-acute dietary fat challenge compared to controls (Hsieh, Longuet et al. 2009), which was similar to the phenotype we were observing with nobiletin treatment. GLP-1 has a circulating half-life of 1-2 min (Deacon, Johnsen et al. 1995), and GLP-2 has a circulating half-life of 7 min (Drucker, Shi et al. 1997, Hartmann, Harr et al. 2000), therefore we hypothesized that nobiletin required GLP-2R signalling to enhance intestinal-triglyceride secretion. To block GLP-2R action, we treated mice with a GLP-2R antagonist, GLP-2 3-33 (30 ng/day) for 2 weeks after a 10-week induction on the HFHC diet. GLP-2 3-33 treatment led to shorter jejunal villi length in HFHC-diet fed *Ldlr*$^{-/-}$ mice, as previously shown in diet-induced obese mice (Baldassano, Amato et al. 2013). However, GLP-2 3-33 treatment did not significantly impact nobiletin's ability to lower post-prandial jejunal triglyceride levels and did not significantly decrease intestinal-triglyceride secretion compared to controls.

To further confirm the involvement of gut hormone action in nobiletin's ability to confer metabolic protection and improve intestinal lipid handling, we employed the use of *Glp1r*$^{-/-}$*Glp2r*$^{-/-}$ mice. *Glp1r*$^{-/-}$ mice display significantly increased accumulation of triglycerides in plasma and the triglyceride-rich lipoproteins fraction as well as triglyceride-rich lipoprotein apoB48 levels post-oil gavage (Hsieh, Longuet et al. 2010). *Glp2r*$^{-/-}$ mice display similar plasma-triglyceride excursion following an olive oil gavage compared to wild-type controls, although trends for decreased secretion are observed (Fuchs, Yusta et al. 2020). Prior to induction of the HFHC diet, *Glp1r*$^{-/-}$ *Glp2r*$^{-/-}$ mice displayed a trend for impaired lipid tolerance compared to wild-type controls, phenocopying the *Glp1r*$^{-/-}$ mouse. Nobiletin treatment did not significantly impact intestinal triglyceride secretion rates, gastric emptying, or intestinal absorptive surface area in *Glp1r*$^{-/-}$*Glp2r*$^{-/-}$ mice. In Chapter 2, diet-induced obese *Glp1r*$^{-/-}$*Glp2r*$^{-/-}$ mice displayed significantly impaired glucose tolerance compared to wild-type controls. Nevertheless, nobiletin was also able to prevent obesity and significantly improve glucose tolerance in *Glp1r*$^{-/-}$*Glp2r*$^{-/-}$ mice. Altogether, this study highlighted the association of intestinal insulin sensitivity with efficient dietary fat handling. However, the increase in circulating GLP-1 levels observed with nobiletin treatment are not mediating the anti-obesity effects. Although not directly measured, this suggests that nobiletin's prevention of obesity in these mice also maintains the sensitivity of GIPR signalling, the other incretin hormone (Dupre, Ross et al. 1973), despite the chronic HFHC-diet feeding. Indeed, diet-induced obesity induces GIPR resistance, making it a difficult target for diabetes management on its own. Future studies evaluating the requirement of GIPR signalling for nobiletin to improve glucose tolerance in diet-induced obese mice should be explored using *Gipr*$^{-/-}$ mice or the *Glp1r*$^{-/-}$*Gipr*$^{-/-}$ mice. While *Glp1r*$^{-/-}$*Gipr*$^{-/-}$ mice are resistant to diet-induced obesity, they do display glucose intolerance. Therefore, this model would allow us to determine if nobiletin's ability to improve glucose tolerance and post-prandial lipemia are secondary to its anti-obesity effects. If nobiletin still confers these metabolic benefits, this would merit performing an unbiased screen for candidate circulating hormones, cytokines, metabolites, or peptides. While it is very likely that

the mechanisms underlying nobiletin's ability to confer metabolic protection are pleiotropic, overlapping, and compensatory, capturing the metabolic milieu induced by nobiletin treatment may lead to the identification of strong therapeutic targets for anti-obesity medications.

Nobiletin promoted efficient dietary triglyceride excursion from the intestine into plasma, resulting in a shorter period of post-prandial lipemia, which may contribute to nobiletin's protection from atherosclerosis. To determine the impact of improved intestinal lipid metabolism in nobiletin's protection from atherosclerosis, studies using models of dysregulated TRL metabolism must be employed. Nobiletin amplifies of circadian rhythms (He, Nohara et al. 2016), where the CLOCK proteins (*Clock*$^{\Delta/\Delta}$ mice) are required for nobiletin treatment to prevent obesity and metabolic dysregulation (He, Nohara et al. 2016). Interestingly, *Clk*$^{\Delta19/\Delta19}$*Apoe*$^{-/-}$ mice display enhanced atherosclerosis progression due to enhanced intestinal cholesterol absorption and reduced efflux capacity of macrophages (Pan, Jiang et al. 2013). Evaluating nobiletin's ability to prevent atherosclerosis in *Clk*$^{\Delta19/\Delta19}$*Apoe*$^{-/-}$ mice and intestinal specific deletion of CLOCK, would further unravel the mechanisms and impact underlying nobiletin's ability to improve intestinal lipid metabolism. Moreover, due to the relationship between hypertriglyceridemia and lower HDL-cholesterol in humans, studies employing mouse models with human CETP to further assess nobiletin's impact of atherosclerosis progression are required. Finally, while prevention studies are critical for the understanding of disease progression and nobiletin's impact on attenuating this process, studies using nobiletin treatment as an intervention are more translationally impactful. Performing lipid tolerance tests across an intervention study with nobiletin would also provide an opportunity evaluate the impact of restored intestinal insulin sensitivity on intestinal lipid handling as well as restored systemic insulin sensitivity for the clearance of triglyceride-rich lipoproteins on atherosclerosis regression.

5.2 Investigating the adaptability of the gut to extreme carbohydrate restriction

Nutrition is a critical component to the management of T2DM. Since 2017, Diabetes Canada, Diabetes UK, Diabetes Australia, and the American Diabetes Association have established statements of support for the use of low-carbohydrate diets and ketogenic diets with adequate protein intake for the management of T2DM under the supervision of their physician (Evert, Dennison et al. 2019, 2020). Compared to a moderate carbohydrate diet of 26-45% of a 2000 kcal daily energy intake, the ketogenic diet is less than 10% of this energy intake (Feinman, Pogozelski et al. 2019). The near absence of dietary carbohydrate from the diet reduces blood glucose levels and relieves the drive for insulin production (Ruppert and Kersten 2024, Dynka, Rodzen et al. 2025). While macronutrient proportions are not strictly prescribed, protein accounts for 10-30%, making fat the major energy source of the ketogenic diet (Dynka, Rodzen et al. 2025). As a result, most energy is derived from fatty acid oxidation. Acetyl-CoA products from fatty acid oxidation serve as the building blocks for ketone body formation, predominantly in the liver. Tissues peripheral to the liver such as the brain, heart, and skeletal muscle oxidize ketone bodies back to acetyl-CoA for entry into the tricarboxylic acid cycle or are diverted to lipogenesis or sterol synthesis pathways. Consumption of ketogenic diets often leads lowers glycemia, improves insulin sensitivity, and weight loss (Firman, Mellor et al. 2024), although the exact mechanisms are still poorly understood. While there is evidence for improved LDL-cholesterol levels, concerns remain on the chronic consumption of diets high in saturated fats and cardiovascular risk, including the impact on post-prandial triglyceride metabolism (Patsch, Miesenbock et al. 1992, Firman, Mellor et al. 2024). In Chapter 3, we characterized the impact of short-term ketogenic diet feeding on intestinal lipid handling and intestinal morphology compared to HFHC diet and chow diet control in male and female mice.

In Chapter 3, both male and female mice fed the ketogenic diet displayed significantly greater plasma triglyceride levels following an acute dietary fat challenge compared to mice fed the HFHC- or chow-diets after three weeks of feeding. To determine if short term ketogenic diet feeding changed the rate at which intestinal-triglycerides were secreted, we used poloxamer-407 to block the clearance of lipoproteins. While male mice previously fed the ketogenic diet displayed significantly accelerated intestinal-triglyceride secretion compared to chow-controls, intestinal triglyceride secretion was unchanged among diet groups in female mice. In line with this, the plasma triglyceride responses in poloxamer and non-poloxamer experiments were 1.5-2-fold greater in male ketogenic diet-fed mice compared to that in females. Indeed, sex hormone estrogen (E2 estradiol) treatment suppresses lymphatic triglyceride transport in ovariectomized rats (Liu, Shen et al. 2021), which may explain the slower rate in female mice compared to males. Since all mice received the same volume of oil for the dietary fat challenge, we further explored the impact of the background diet on the substrate volume for chylomicron production.

Jejunal triglyceride levels were unchanged among diet groups in both male and female mice post-acute dietary fat challenge. Since we did not observe a difference in jejunal *Srebf1* mRNA levels, we concluded that the contribution of fatty acids from *de novo* lipogenesis was minimal to this lipid pool. Since we fasted the mice for 5 hours prior to the acute dietary fat challenges, we measured the triglyceride stores at this timepoint throughout the small intestine. We found that 5-hour fasted male mice previously fed the ketogenic diet stored more triglycerides in the jejunum than chow-controls. We found that 5-hour fasted female mice fed the ketogenic diet stored significantly more triglycerides throughout the first three quarters of the small intestine (duodenum to distal jejunum) compared to controls. Therefore, we concluded that dietary fatty acids from the previous meal were stored, providing a greater substrate pool for chylomicron production. Several studies have demonstrated that the preferred substrate for chylomicron formation is dietary TG from the previous meal (Fielding, Callow et al. 1996, Evans,

Kuusela et al. 1998, Jackson, Robertson et al. 2002, Silva, Wright et al. 2005, Jacome-Sosa, Hu et al. 2021). Future experiments, however, will be required to confirm this contribution and explore the impact of the ketogenic diet on the dynamics of producing chylomicrons with fatty acids from the previous meal prior to the incoming dietary fatty acids and *de novo* fatty acids induced by insulin. Experiments employing an overnight fast followed by an oral gavage to mimic the respective diets with ^{14}C-glucose and ^{3}H-triolein as tracers. For the ketogenic diet, a 0.6% ^{14}C-glucose and 67.3% ^{3}H -triolein in a 15.3% casein solution compared to the chow-diet mimic of 64.6% ^{3}H-deoxyglucose, 9% ^{3}H -triolein, and 19% casein solution. Following the meal mimic gavage, mice should be fasted for 5 hours, where intestinal segments should be collected in half of the mice for baseline measurements whereas the other half of the mice should receive the acute dietary fat challenge of 200 µL of olive oil. Plasma should be collected for total triglyceride levels and detection of ^{3}H- and ^{14}C-labelled fatty acids from the meal mimic gavage. Intestinal segments and liver lobes should be collected 4 hours post-oil gavage for lipid extractions and total triglyceride levels and ^{3}H- and ^{14}C-labelled fatty acids. These experiments will delineate the contribution of the first meal and *de novo* lipogenesis to the fasting and post-acute dietary fat challenge triglyceride mass in the intestine and blood compartments over time, and how the mice on the ketogenic diet partition these lipids according to their energy needs compared to chow-fed controls. Additionally, capturing the contribution of the liver to clear these particles would add significant clarity to the dynamics of the lipid tolerance across the diet groups.

Another consideration is the contribution of circulating free fatty acids, which remain high in the fasted and fed state of ketogenic diet fed mice, to the intestinal storage pool. Under chow-fed conditions, enterocytes use amino acids such as glutamine, glutamate, and aspartate as a primary fuel source (Alpers 2000). With ketogenic diet feeding, enterocytes engage in enhanced fatty acid oxidation and ketogenesis, as shown by enhanced HMGCS2, which localizes to the

villus tips (Wang, Zhou et al. 2017). Therefore, in addition to the meal mimic experiments outlined above, experiments employing intraperitoneal injections of radiolabelled palmitate and measuring their uptake into the intestine, liver, and plasma would add clarity to their contribution to the postprandial intestinal lipid pools. Specifically, experiments should be performed in fasted and fed mice chronically fed the chow or ketogenic diet. These experiments would help delineate the enhanced substrates for chylomicron synthesis observed in our studies and may reveal novel targets to limit the number of these particles into blood circulation for cardiovascular protection without causing malabsorption.

As previously discussed and demonstrated in Chapter 2, a delay in intestinal triglyceride secretion rate has been observed in diet-induced obesity mice even after three weeks of diet feeding (Douglass, Malik et al. 2012). In Chapter 3, we found that three weeks of HFHC-diet feeding did not significantly impact lipid tolerance and five weeks of HFHC-diet feeding intestinal-triglyceride secretion rates with poloxamer relative to chow-fed controls. This suggests that despite significant adiposity at this time point, control of intestinal lipoprotein remained intact. The lack of difference in our GBD and WD-fed mice could also be driven by differences in carbohydrate sources. Additionally, our GBD may be obesogenic and induce some liver steatosis particularly in male mice as previously seen (Zhang, Leveille et al. 2020).

In contrast to a similar absolute level of triglycerides stored in the jejunum among male and female mice post-acute dietary fat challenge observed in Chapter 2, female mice in Chapter 3, displayed 2-fold higher intestinal triglyceride levels at fasting and post-oil compared to males independent of diet. These results contrast what we observed in the same experiments in *Ldlr*$^{-/-}$ mice (Chapter 2), highlighting a potential role for the LDLR to mediate this sex difference. Indeed, LDLR plays a critical role in regulating triglyceride clearance and production. Female *Ldlr*$^{-/-}$ mice have been shown to display more severe atherosclerosis than males after 14 weeks of HFHC-diet feeding (Mansukhani, Wang et al. 2017). Female wild-type mice are more insulin

sensitive and do not develop hyperinsulinemia with high-fat diet feeding to the same extent as males (Pettersson, Walden et al. 2012). The enhanced insulin sensitivity in females favours energy storage in adipose tissue (Varlamov, Bethea et al. 2014), however, our findings from Chapter 2 and 3 suggest that this energy storage phenotype extends to the small intestine. Interestingly the sex differences were less pronounced or absent in HFHC-diet fed mice. While overall lipid tolerance in the non-poloxamer study demonstrated a ~2-fold increase in the change in plasma triglyceride levels in male versus female HFHC-diet fed mice, the intestinal-triglyceride secretion rates were similar in male and female HFHC-diet fed mice. This suggested that the capacity to clear post-prandial triglycerides was greater in female than male mice, consistent with the sex difference in insulin sensitivity (Pettersson, Walden et al. 2012, Varlamov, Bethea et al. 2014). Fasting-refeeding experiments with the respective chow, HFHC, or ketogenic diets revealed that similar to the acute dietary fat challenge, refed plasma triglyceride levels were significantly greater in male ketogenic diet fed mice compared to mice fed the chow diet. Surprisingly, no differences in jejunal triglycerides were observed in the refed state among diet groups. In female mice, refeeding did not impact plasma triglyceride levels, but female mice fed the ketogenic diet stored significantly more triglycerides in the refed state compared to both the chow- and Western-diet fed mice. This highlighted greater capacity to store triglycerides in the intestine to control post-prandial lipemia.

In Chapter 2, we found that chronic HFHC-diet feeding significantly shortened small intestinal length in both male and female *Ldlr*$^{-/-}$ mice. In Chapter 3, male mice fed the ketogenic diet displayed significantly longer small intestines with no differences in villi length. Unlike the male mice, small intestinal length was not impacted by short term ketogenic diet feeding in female mice. Instead, villi length in the proximal jejunum was significantly greater in female mice fed the ketogenic diet. Despite the high caloric density of the ketogenic diet whereby a smaller mass is required to obtain the same number of calories as the chow diet, lengthening of the

small intestine still occurred. While in our study KD-fed male and female mice displayed significantly higher mRNA expression levels of *Pparα,* which plays a direct role in intestinal villi length elongation (Stojanovic, Altirriba et al. 2021), additional evidence for intestinotrophic effects of the ketogenic have been put forth. Indeed, self-renewing *Lgr5*$^{+}$ stem cells express *Hmgcs2* and ketogenic diet feeding significantly enhances their self-renewal in an HMGCS2-dependent manner (Cheng, Biton et al. 2019). Additionally, ketogenic diet feeding has been previously shown to increase differentiation leading to more enterocytes, goblet cells, and Paneth cells (Wang, Zhou et al. 2017). Therefore, while we conclude the greater absorptive surface area may be in response to the increase in dietary fat absorption required by the ketogenic diet, this effect may be mediated by ketone bodies. Studies evaluating the intestinotrophic effects of the ketogenic diet or ketone bodies themselves in a model of short bowel syndrome may provide new therapeutic strategies for individuals living with this condition.

The role of fasting intestinal lipids at the baseline of an acute dietary fat challenge raises a few questions regarding extent to which the gut can adapt. First, on the “breaking point” of the intestine to store dietary lipids to control the post-prandial window. If we compared lipid tolerance at week 1, versus week 2 versus week 4 of ketogenic diet feeding in the same mice, would we see an improvement in the control of post-prandial lipids as the gut surface area expands? Second, if we increased the fasting time from 5 hours to 16 hours, where intestinal lipids significantly decrease (Korbelius, Vujic et al. 2019), or to a point where intestinal lipid stores are similar in the mice previously fed the ketogenic diet versus control diet, would these mice still display impaired lipid tolerance? Third, ketone bodies not only act as fuel sources but also serve as signalling molecules and epigenetic modifications (Dabek, Wojtala et al. 2020) do they target gene expression in the small intestine? Finally, evaluating the impact of different ketogenic diet compositions on intestinal lipid handling, such as plant-based diets, would help understand the contribution of saturated versus unsaturated dietary fatty acids to the post-

prandial lipemia observed in our ketogenic diet study and may also address the cardiovascular risk associated with ketogenic diets rich in saturated fatty acids (Gardner, Vadiveloo et al. 2023).

Short term ketogenic diet feeding enhanced fasting intestinal lipid stores and worsened lipid tolerance in our study. Whether this phenotype is maintained long term is to be determined. Additionally, future experiments investigating the intestinal adaptations to the ketogenic diet as an intervention and using mouse models of type two diabetes could provide insights more relevant to human physiology. However, there are several differences in the adaptation to the ketogenic diet between mice and humans. Nutritional ketosis in mice can be observed within hours of ketogenic diet feeding in mice (Kalafut, Mitchell et al. 2022), whereas in humans this has been observed within three to five days (Hirschberger, Effinger et al. 2024). Mice lose weight within two weeks with ketogenic diet intervention (Kennedy, Pissios et al. 2007) whereas in humans, the magnitude and rate of weight loss is slower (Ting, Dugre et al. 2018, Hirschberger, Effinger et al. 2024). While many one or two year follow up studies evaluating the impact of ketogenic diet feeding in individuals with T2DM and obesity have shown improvements in glucose control and insulin requirement (Athinarayanan, Adams et al. 2019, Athinarayanan, Hallberg et al. 2020), long-term outcomes on major adverse cardiovascular events are lacking. Importantly while a shift from a greater proportion of small LDL particles at baseline to larger LDL particles at 2 years of ketogenic diet feeding was found in individuals living with T2DM, suggesting an improvement of the atherogenic lipoprotein profile, total LDL cholesterol levels significantly increased and carotid intima-media thickness was unchanged from baseline (Athinarayanan, Hallberg et al. 2020). Several studies have demonstrated attenuated atherosclerosis progression with ketogenic diet feeding compared to high-fat diet feeding in *Apoe*$^{-/-}$ mice (Castro, Kalecky et al. 2024) although atherosclerotic burden is still greater than chow-fed controls (Castro, Whalen et al. 2021). Given the role of non-fasting

hypertriglyceridemia on pro-atherogenic dyslipidemia (Hokanson and Austin 1996, Langsted, Freiberg et al. 2008), future preclinical experiments with ketogenic diet feeding should employ the use of mice with transgenic expression CETP on a Apoe$^{-/-}$, *Ldlr*$^{-/-}$, or human apoCIII overexpression background to generate an atherogenic lipid profile that more closely resembles that in humans (Hayek, Masucci-Magoulas et al. 1995). Additionally, future preclinical experiments in an atherosclerosis model employing a ketogenic diet intervention in combination with ezetimibe to inhibit intestinal cholesterol absorption may provide the weight loss benefits, glycemic control, and reduced insulin requirement from the ketogenic diet and potentiate atherosclerosis regression through the reduction of dietary cholesterol absorption.

5.3 Intestinal adaptations to low ambient temperature

The intestine is fundamental to overall metabolic health, serving as the primary site of absorption of carbohydrates, proteins, and fats, providing essential fuel to the body. The small intestine is in a continual state of growth and renewal. Intestinal crypts house stem cells that give rise to progenitor cells, which in turn proliferate to become mature epithelial cells that replace the previous lining of cells every three to five days (Gehart and Clevers 2019). As previously discussed, diet composition can significantly impact intestinal surface area. Evidence for a proportional relationship between intestinal absorptive area and food intake stems from observations in models of genetic overeating (*ob/ob* mice) who display longer and heavier guts as well as greater villi length compared to controls (Stojanovic, Altirriba et al. 2021). By contrast, caloric restriction (Chappell, Thompson et al. 2003, Stojanovic, Altirriba et al. 2021), parenteral and total parenteral nutrition (Buchman, Moukarzel et al. 1995, Ekelund, Kristensson et al. 2007), and prolonged fasting (Bahrami, Yusta et al. 2010) significantly atrophy the gut. Together, these findings add to our fundamental understanding of gut biology and have important implications for energy balance. Even when parenteral nutrition meets caloric needs, significant gut atrophy is still

observed (Sun, Spencer et al. 2006), underscoring the importance of nutrient absorption from the gut lumen as a mechanical stimulus for intestinal growth.

To balance the heat loss during chronic exposure to low ambient temperatures, non-shivering thermogenesis in brown adipose tissue increases energy expenditure to maintain body temperature (Foster and Frydman 1979, Beaudry and McClelland 2010, Blondin 2023). To meet this increased energy demand, food intake proportionally increases as temperature drops (Chevalier, Stojanovic et al. 2015, Zhao, Yang et al. 2022). Small intestinal surface area expansion is associated with the greater food consumption observed upon housing at lower ambient temperatures in mice (Chevalier, Stojanovic et al. 2015, Stojanovic, Altirriba et al. 2021, Zhao, Yang et al. 2022, Wang, Wu et al. 2024). Chevalier *et al*. found a directional role for the changes in the gut microbiota that manifest upon chronic cold stress, whereby germ free mice housed at room temperature receiving fecal transplants from cold-stressed donors also display this gut surface area expansion (Chevalier, Stojanovic et al. 2015). Stojanovic *et al*. found that intestinal PPARα action is essential for villi length expansion observed upon chronic cold stress (Stojanovic, Altirriba et al. 2021). Despite the well characterized integration of intestinotrophic gut hormone release with food intake (Paternoster and Falasca 2018, Gribble and Reimann 2019), the hormonal signals underlying induction of these circuits to mediate this plasticity have not been explored. In the final chapter of this thesis, we tested the requirement of gut hormone receptor signalling for the gut morphological changes that accompany the increased energy demand and food intake observed upon chronic cold temperature housing.

In Chapter 4, we used mice with systemic deletions of GLP-2R and GIPR actions in combination with a systemic deletion of GLP-1R action, namely *Glp1r*$^{-/-}$*Gipr*$^{-/-}$ and *Glp1r*$^{-/-}$*Glp2r*$^{-/-}$ mice. Double receptor knockout mice were used given the potential compensatory roles of these receptors related to intestinal growth. We found that food intake doubled with chronic cold stress, independent of sex and genotype. This increase in food intake with cold stress was accompanied

by significant increases in small intestinal weight in all genotypes, independent of sex. Similarly, the increase in food intake with cold stress was accompanied by a significant increase in small intestinal length in control mice, but not in male *Glp1r*$^{-/-}$*Gipr*$^{-/-}$ mice and *Glp1r*$^{-/-}$*Glp2r*$^{-/-}$ mice, consistent with the role for GLP-1R action to lengthen the small intestine (Koehler, Baggio et al. 2015). The increase in food intake with cold stress was associated with greater jejunal circumference, villi length, and crypt depth in WT and *Glp1r*$^{-/-}$*Gipr*$^{-/-}$ mice, but not *Glp1r*$^{-/-}$*Glp2r*$^{-/-}$ mice, indicating a role for GLP-2R action to expand the mucosal layer. Consistent with the failed surface area expansion and the known role of GLP-2R action to promote proliferation (Dube, Forse et al. 2006, Rowland, Trivedi et al. 2011), jejunal Ki67 percent area was unchanged with housing temperature in *Glp1r*$^{-/-}$*Glp2r*$^{-/-}$ mice, independent of sex, compared to WT controls. All together, we concluded that GLP-2R action, although on a background of systemic loss of GLP-1R action, was required for the increased villi length, crypt depth, and circumference observed with chronic cold stress.

Male mice housed at 4°C for 24 hours display significantly lower plasma triglyceride levels post-oil gavage compared to controls housed at 22°C whereby organ distribution of radiolabelled dietary fatty acids revealed significantly greater uptake in brown adipose tissue of cold-exposed mice (Bartelt, Bruns et al. 2011). Similarly, one week of housing at 6°C compared to 30°C in male mice led to significantly lower plasma triglyceride levels in response to an acute dietary fat challenge, driven by significant increases in fatty acid uptake by brown adipose tissue (Evangelakos, Kuhl et al. 2022). Overall, these findings are consistent with the enhanced capacity of brown adipose tissue to catabolize lipids to produce heat. In Chapter 4, we performed a lipid tolerance test after two weeks of cold temperature housing. In male mice, plasma triglyceride levels following an acute dietary fat challenge were similar in mice previously housed at 6°C compared to 27°C, suggesting that the enhanced capacity to clear plasma triglycerides following an acute dietary fat challenge observed at 24 hours (Bartelt, Bruns et al.

2011) and 1 week (Evangelakos, Kuhl et al. 2022) of cold exposure was attenuated by two weeks. Experiments testing lipid tolerance over time would be required to definitively conclude this, however, would significantly enhance our understanding of the systemic metabolic adaptations to chronic cold exposure. Additionally, unlike the males, female cold-stressed WT mice had greater post-oil triglyceride levels compared to TN controls. Experiments administering an oral gavage of employing positron emission tomography (PET) tracers such as ^{18}F-BODIPY-labelled fatty acids to assess the distribution of tracer uptake over time, as shown previously with intravenous administration (Wang, Wang et al. 2020), would add significant resolution to this metabolic adaptation and unveil sex differences potentially driven by body fat distribution. A direct comparison of dietary fatty acid BAT uptake between males versus females has not been performed, although molecular characterizations within 90 minutes of cold exposure demonstrate a sex difference in the machinery engaged in response to acute cold exposure, including the rapid induction of UCP-1 levels in males compared to females (Cheung, Yiu et al. 2024). Additionally, female, but not male mice exposed to the cold displayed significantly greater plasma DPP4 activity compared to thermoneutral controls. Plasma DPP4 activity increases during metabolic disease, but also in response to the stress hormones glucocorticoids due to its glucocorticoid-responsive promoter elements (Diaz-Jimenez, Petrillo et al. 2020). Indeed, DPP4 inhibitors have been shown to enhance BAT UCP1 mRNA and protein levels in response to diet-induced obesity, which was associated with increases in energy expenditure (Takeda, Sawazaki et al. 2018). Moreover, while soluble DPP4 treatment of cultured adipocytes inhibits the increase in *Ucp1* mRNA with β-adrenoreceptor agonism, the addition of a DPP4 inhibitor restores *Ucp1* mRNA levels. Therefore, exploring the impact of DPP4 activity using DPP4 inhibitors or genetic deletions in male versus female BAT function and lipid tolerance warrants further investigation.

The impaired lipid tolerance observed in female WT mice with cold stress was lost in the female GLPDRKO mice despite similarly elevated fasting plasma DPP4 levels. Unlike the male GLPDRKO mice, which phenocopy the *Glp1r*$^{-/-}$ mouse (Hsieh, Longuet et al. 2010) in terms of lipid tolerance, this genotype impact was not observed in female mice, indicating a sex difference on the impact of GLP-1R and GLP2R signalling in intestinal lipid metabolism. In our study, we found that female GLPDRKO mice displayed significantly elevated jejunal capacity for mitochondrial respiration suggesting enhanced fatty acid oxidation may explain the lower plasma triglyceride levels during the dietary fat challenge. The enhanced mitochondrial respiration observed in these mice would fit with the findings from Li et al, where enhanced mitochondrial respiration was associated with reduced chylomicron secretion (Li, Rodia et al. 2019), however, additional experiments are required. First, delineating if the phenotype we are observing is due to enhanced intestinal triglyceride secretion or impaired clearance with poloxamer experiments must be performed. Additionally, the role of GIPR action in GLPDRKO mice may be heightened. High fat diet-fed male mice with a BAT-specific deletion of *Gipr* display significantly impaired lipid tolerance when housed at room temperature, but not when housed at 30°C (Beaudry, Kaur et al. 2019), indicating a temperature dependence on BAT GIPR action in the clearance of plasma triglycerides. Experiments employing this BAT specific deletion of *Gipr* in male and female mice housed at 6°C compared to 30°C would further define this intestinal-BAT-axis in the control of circulating post-prandial triglycerides.

Overall, our results in Chapter 4 are consistent with the requirement of endogenous GLP-2R action to restore small intestinal weight, villus height, and crypt cell proliferation upon refeeding after a prolonged fast (Bahrami, Yusta et al. 2010). While GLP-2 promotes crypt cell proliferation, these cells do not express the GLP-2R. Therefore, the intestinotrophic actions of GLP-2 are indirect. Within the gut, GLP-2R+ cells gut include vagal afferents, subepithelial myofibroblasts, enteric neurons, enteroendocrine cells, and myenteric plexus nerve fibrils (Walsh, Yusta et al.

2003, Orskov, Hartmann et al. 2005, Guan, Karpen et al. 2006, Nelson, Sharp et al. 2007). At pharmacological levels, GLP-2R action increases in IGF-1 secretion from subepithelial myofibroblasts, which activates the IGF-1 receptor on intestinal epithelial cells to stimulate proliferation (Dube, Forse et al. 2006, Rowland, Trivedi et al. 2011). In our study, we observed an increase in the abundance of the Ki67 marker for proliferation in crypts, but we did not observe any differences in the mRNA expression of jejunal *Igf1* or *Igf1r*. Interestingly, treatment of mice with epidermal growth factor (EGF), but not IGF1, during the refeeding period restores small intestinal weight in *Glp2r*$^{-/-}$ mice (Bahrami, Yusta et al. 2010). Therefore, physiological increases in GLP-2 with refeeding appear to exert intestinotrophic effects upstream of EGF receptor signalling. Future experiments should explore the ability of EGF treatment to expand the absorptive surface area in cold-stressed *Glp1r*$^{-/-}$*Glp2r*$^{-/-}$ or in mice with an intestinal-specific deletion of *Glp2r.* Additionally, experiments employing EGF inhibitor CI-1003 to prevent the expansion of absorptive surface area in wild-type mice and the impact this would have on cold tolerance would provide mechanistic clarity and further underscore the importance of this expansion on energy harvest during increased metabolic demand. Finally, future experiments should challenge mice with selective deletion of *Glp2r* from intestinal myofibroblasts versus enteroendocrine cells versus enteric neurons to chronic cold stress and measuring not only the mucosal responses, but also the impact on nutrient absorption using radiolabelled or heavy isotope labelled nutrients. These experiments would significantly enhance the resolution of the pathways engaged during the physiological increases in GLP-2 and the impact on whole-body metabolism. Specifically, a myofibroblast-specific deletion of GLP-2R would confirm the IGF-1 or EGF signalling axis for intestinal surface area expansion during chronic cold stress. The enteroendocrine-cell specific deletion may reveal a paracrine loop of complementary or regulatory hormones affecting nutrient absorption. The enteric neuron-specific deletion of GLP-2R may reveal a role for gut-brain axis communication affecting satiety and feeding behaviour. Moreover, treating mice with the cell-specific deletions of GLP-2 action with GLP-2 analogues would

complement these findings and expand our understanding of GLP-2's fundamental biology and the cell-specific requirement of GLP-2R action in gut plasticity. GLP-2 analogues are already approved therapies for the management of short bowel syndrome and are effective at removing or decreasing the dependence on parenteral nutrition in ~65% of individuals (Zhu and Li 2022). Therefore, the findings from experiments with cell-specific deletions of GLP-2R action should be complemented in studies using a mouse model of parenteral nutrition to investigate the impact of these deletions on the mucosal layer and nutrient absorption. All together, understanding the exact pathways engaged during the intestinotrophic effects of GLP-2R in the presence and absence of luminal nutrients may explain the heterogeneity of the GLP-2 analogue response and may lead to more therapeutic options with less side effects for individuals living with bowel diseases and malnutrition.

5.4 Final conclusions

Collectively, these studies add to our understanding of the molecular mechanisms underlying both early and long-term intestinal adaptations to increased dietary fat, Western-style diets, and caloric intake. These studies also uncovered contributions of endogenous gut hormone receptor signalling to intestinal lipid metabolism, intestinal growth, and sex-specific changes to the intestinal response to metabolic challenges. Recent clinical studies have discovered greater weight loss with dual agonists combining GLP-1R-GIPR action compared to that seen with GLP-1RAs alone (Frias, Nauck et al. 2018, Baggio and Drucker 2021), and dual agonists for GLP-1R/GLP-2R dapiglutide is being investigated in the DREAM Trial (NCT05788601) as a target for obesity and low-grade inflammation. The recent reporting of GIPR+ pericytes in the gut and their role in inflammation has unlocked a new line of probing the post-prandial control of GIPR signalling within the gut (Hammoud, Kaur et al. 2024), where endogenous GIP production is stimulated by chylomicrons (Psichas, Larraufie et al. 2017), and GIPR agonism enhances intestinal-triglyceride secretion in mice (Hsieh, Longuet et al. 2010)

and rats (Wang, Khan et al. 2025). This tight interconnection between dietary fat absorption and GIPR signalling also provides a new avenue for biological questions and therapeutic targets for dyslipidemia. Moreover, recent studies have demonstrated a functional role of GLP-1 9-36, the metabolite of DPP4 activity, in inhibiting glucagon secretion (Gandasi, Gao et al. 2023). Given the abundant expression and activity of gut enterocyte and endothelial DPP4 (Mulvihill, Varin et al. 2017), surely, this metabolite accumulates in the lamina propria, where its local impact remains to be solved.

Figure 5.1 Summary of major findings and potential impact. This thesis evaluated the impact of modulating dietary intake across all three chapters, where two key themes emerged: jejunal lipid accumulation and absorptive surface area expansion. In Chapter 2, high-fat, high-cholesterol diet feeding increased jejunal lipid accumulation and insulin resistance. Additionally, insulin resistance contributed to jejunal lipid accumulation, which together exacerbated post-prandial lipemia. The addition of nobiletin to the high-fat, high-cholesterol diet significantly improved insulin sensitivity and lowered jejunal lipid accumulation, contributing to the impact of nobiletin to improve dyslipidemia. In Chapter 3, ketogenic diet feeding significantly increased fasting jejunal lipid accumulation and expanded small intestinal absorptive surface area. Both male and female mice displayed impaired lipid tolerance, however, this was more severe in male mice previously fed the ketogenic diet compared to females. In Chapter 4, GLP-1R and GLP-2R signalling contribute to the expansion of small intestinal absorptive surface area that is required to maintain normal body weight gain when metabolic demand is increased with temperature stress. Dyslipidemia is a significant driver of atherosclerosis progression. Understanding the target pathway of nobiletin to confer metabolic protection may reveal important therapeutic targets for cardiometabolic disease. Evaluating the long-term impact of post-prandial lipemia on atherosclerosis progression upon chronic ketogenic diet feeding in males and females is required. Teduglutide is an approved therapy for the management of short bowel syndrome. GLP-1R and GLP-2R agonists may provide alternative therapy options for these individuals. GLP-1R agonists not only improve glycemic control, but also induce weight loss and lower inflammation, which are significant drivers of cardiometabolic disease. Dual and triple agonists for these receptors are being evaluated for their therapeutic potential. Overall, expanding our understanding of fundamental gut hormone biology has and will continue to improve human health and quality of life.

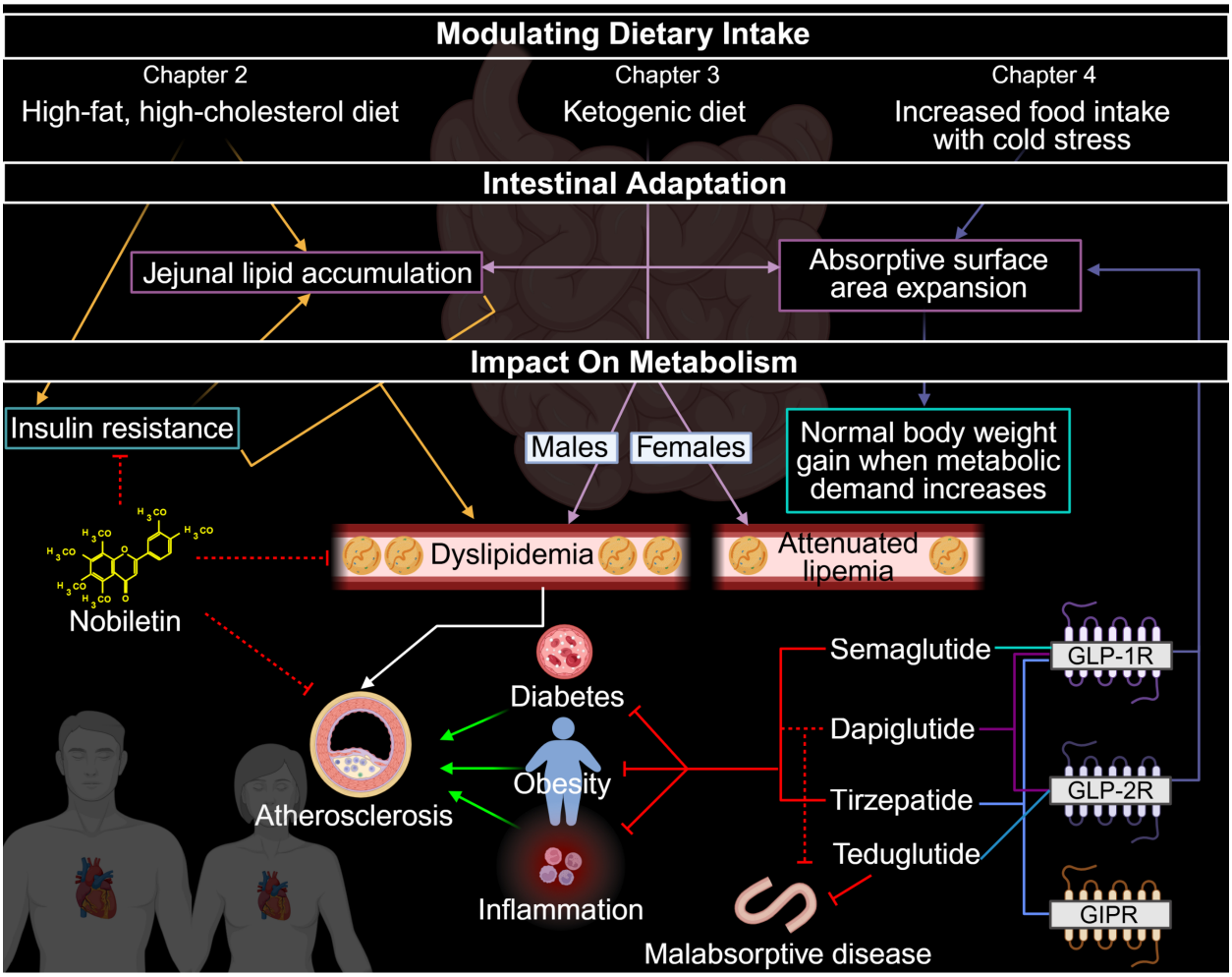
Modulating Dietary Intake
Chapter 2
High-fat, high-cholesterol diet
Chapter 3
Ketogenic diet
Chapter 4
Increased food intake with cold stress
Intestinal Adaptation
Jejunal lipid accumulation
Absorptive surface area expansion
Impact On Metabolism
Insulin resistance
Males
Females
Normal body weight gain when metabolic demand increases
Dyslipidemia
Attenuated lipemia
Nobiletin
Diabetes
Obesity
Atherosclerosis
Inflammation
Malabsorptive disease
Semaglutide
Dapiglutide
Tirzepatide
Teduglutide
GLP-1R
GLP-2R
GIPR

5.5 References

(2020). "Diabetes Canada Position Statement on Low-Carbohydrate Diets for Adults With Diabetes: A Rapid Review." Can J Diabetes 44(4): 295–299.

Adeli, K. and G. F. Lewis (2008). "Intestinal lipoprotein overproduction in insulin-resistant states." Curr Opin Lipidol 19(3): 221–228.

Alpers, D. H. (2000). "Is glutamine a unique fuel for small intestinal cells?" Curr Opin Gastroenterol 16(2): 155.

Athinarayanan, S. J., R. N. Adams, S. J. Hallberg, A. L. McKenzie, N. H. Bhanpuri, W. W. Campbell, J. S. Volek, S. D. Phinney and J. P. McCarter (2019). "Long-Term Effects of a Novel Continuous Remote Care Intervention Including Nutritional Ketosis for the Management of Type 2 Diabetes: A 2-Year Non-randomized Clinical Trial." Front Endocrinol (Lausanne) 10: 348.

Athinarayanan, S. J., S. J. Hallberg, A. L. McKenzie, K. Lechner, S. King, J. P. McCarter, J. S. Volek, S. D. Phinney and R. M. Krauss (2020). "Impact of a 2-year trial of nutritional ketosis on indices of cardiovascular disease risk in patients with type 2 diabetes." Cardiovasc Diabetol 19(1): 208.

Baggio, L. L. and D. J. Drucker (2021). "Glucagon-like peptide-1 receptor co-agonists for treating metabolic disease." Mol Metab 46: 101090.

Bahrami, J., B. Yusta and D. J. Drucker (2010). "ErbB activity links the glucagon-like peptide-2 receptor to refeeding-induced adaptation in the murine small bowel." Gastroenterology 138(7): 2447–2456.

Baldassano, S., A. Amato, F. Cappello, F. Rappa and F. Mule (2013). "Glucagon-like peptide-2 and mouse intestinal adaptation to a high-fat diet." J Endocrinol 217(1): 11–20.

Bartelt, A., O. T. Bruns, R. Reimer, H. Hohenberg, H. Ittrich, K. Peldschus, M. G. Kaul, U. I. Tromsdorf, H. Weller, C. Waurisch, A. Eychmuller, P. L. Gordts, F. Rinninger, K. Bruegelmann, B. Freund, P. Nielsen, M. Merkel and J. Heeren (2011). "Brown adipose tissue activity controls triglyceride clearance." Nat Med 17(2): 200–205.

Beaudry, J. L., K. D. Kaur, E. M. Varin, L. L. Baggio, X. Cao, E. E. Mulvihill, H. E. Bates, J. E. Campbell and D. J. Drucker (2019). "Physiological roles of the GIP receptor in murine brown adipose tissue." Mol Metab 28: 14–25.

Beaudry, J. L. and G. B. McClelland (2010). "Thermogenesis in CD-1 mice after combined chronic hypoxia and cold acclimation." Comp Biochem Physiol B Biochem Mol Biol 157(3): 301–309.

Blondin, D. P. (2023). "Human thermogenic adipose tissue." Curr Opin Genet Dev 80: 102054.

Bozzetto, L., G. Della Pepa, C. Vetrani and A. A. Rivellese (2020). "Dietary Impact on Postprandial Lipemia." Front Endocrinol (Lausanne) 11: 337.

Buchman, A. L., A. A. Moukarzel, S. Bhuta, M. Belle, M. E. Ament, C. D. Eckhert, D. Hollander, J. Gornbein, J. D. Kopple and S. R. Vijayaroghavan (1995). "Parenteral nutrition is associated with intestinal morphologic and functional changes in humans." JPEN J Parenter Enteral Nutr 19(6): 453–460.

Burke, A. C., B. G. Sutherland, D. E. Telford, M. R. Morrow, C. G. Sawyez, J. Y. Edwards, M. Drangova and M. W. Huff (2018). "Intervention with citrus flavonoids reverses obesity and improves metabolic syndrome and atherosclerosis in obese Ldlr(-/-) mice." J Lipid Res 59(9): 1714–1728.

Castro, R., K. Kalecky, N. K. Huang, K. Petersen, V. Singh, A. C. Ross, T. Neuberger and T. Bottiglieri (2024). "A very-low carbohydrate content in a high-fat diet modifies the plasma metabolome and impacts systemic inflammation and experimental atherosclerosis." J Nutr Biochem 126: 109562.

Castro, R., C. A. Whalen, S. Gullette, F. J. Mattie, C. Florindo, S. G. Heil, N. K. Huang, T. Neuberger and A. C. Ross (2021). "A Hypomethylating Ketogenic Diet in Apolipoprotein E-Deficient Mice: A Pilot Study on Vascular Effects and Specific Epigenetic Changes." Nutrients 13(10).

Chappell, V. L., M. D. Thompson, M. G. Jeschke, D. H. Chung, J. C. Thompson and S. E. Wolf (2003). "Effects of incremental starvation on gut mucosa." Dig Dis Sci 48(4): 765–769.

Cheng, C. W., M. Biton, A. L. Haber, N. Gunduz, G. Eng, L. T. Gaynor, S. Tripathi, G. Calibasi-Kocal, S. Rickelt, V. L. Butty, M. Moreno-Serrano, A. M. Iqbal, K. E. Bauer-Rowe, S. Imada, M. S. Ulutas, C. Mylonas, M. T. Whary, S. S. Levine, Y. Basbinar, R. O. Hynes, M. Mino-Kenudson, V. Deshpande, L. A. Boyer, J. G. Fox, C. Terranova, K. Rai, H. Piwnica-Worms, M. M. Mihaylova, A. Regev and O. H. Yilmaz (2019). "Ketone Body Signaling Mediates Intestinal Stem Cell Homeostasis and Adaptation to Diet." Cell 178(5): 1115–1131 e1115.

Cheung, S. W. M., J. H. C. Yiu, K. T. C. Chin, J. Cai, A. Xu, C. M. Wong and C. W. Woo (2024). "Content of stress granules reveals a sex difference at the early phase of cold exposure in mice." Am J Physiol Endocrinol Metab 326(1): E29–E37.

Chevalier, C., O. Stojanovic, D. J. Colin, N. Suarez-Zamorano, V. Tarallo, C. Veyrat-Durebex, D. Rigo, S. Fabbiano, A. Stevanovic, S. Hagemann, X. Montet, Y. Seimbille, N. Zamboni, S. Hapfelmeier and M. Trajkovski (2015). "Gut Microbiota Orchestrates Energy Homeostasis during Cold." Cell 163(6): 1360–1374.

D'Aquila, T., Y. H. Hung, A. Carreiro and K. K. Buhman (2016). "Recent discoveries on absorption of dietary fat: Presence, synthesis, and metabolism of cytoplasmic lipid droplets within enterocytes." Biochim Biophys Acta 1861(8 Pt A): 730–747.

Dabek, A., M. Wojtala, L. Pirola and A. Balcerczyk (2020). "Modulation of Cellular Biochemistry, Epigenetics and Metabolomics by Ketone Bodies. Implications of the Ketogenic Diet in the Physiology of the Organism and Pathological States." Nutrients 12(3).

Dalby, M. J., A. W. Ross, A. W. Walker and P. J. Morgan (2017). "Dietary Uncoupling of Gut Microbiota and Energy Harvesting from Obesity and Glucose Tolerance in Mice." Cell Rep 21(6): 1521–1533.

Deacon, C. F., A. H. Johnsen and J. J. Holst (1995). "Human colon produces fully processed glucagon-like peptide-1 (7-36) amide." FEBS Lett 372(2-3): 269–272.

Diaz-Jimenez, D., M. G. Petrillo, J. T. Busada, M. A. Hermoso and J. A. Cidlowski (2020). "Glucocorticoids mobilize macrophages by transcriptionally up-regulating the exopeptidase DPP4." J Biol Chem 295(10): 3213–3227.

Douglass, J. D., N. Malik, S. H. Chon, K. Wells, Y. X. Zhou, A. S. Choi, L. B. Joseph and J. Storch (2012). "Intestinal mucosal triacylglycerol accumulation secondary to decreased lipid secretion in obese and high fat fed mice." Front Physiol 3: 25.

Drucker, D. J., Q. Shi, A. Crivici, M. Sumner-Smith, W. Tavares, M. Hill, L. DeForest, S. Cooper and P. L. Brubaker (1997). "Regulation of the biological activity of glucagon-like peptide 2 in vivo by dipeptidyl peptidase IV." Nat Biotechnol 15(7): 673–677.

Dube, P. E., C. L. Forse, J. Bahrami and P. L. Brubaker (2006). "The essential role of insulin-like growth factor-1 in the intestinal tropic effects of glucagon-like peptide-2 in mice." Gastroenterology 131(2): 589–605.

Duez, H., B. Lamarche, K. D. Uffelman, R. Valero, J. S. Cohn and G. F. Lewis (2006). "Hyperinsulinemia is associated with increased production rate of intestinal apolipoprotein B-48-containing lipoproteins in humans." Arterioscler Thromb Vasc Biol 26(6): 1357–1363.

Duez, H., B. Lamarche, R. Valero, M. Pavlic, S. Proctor, C. Xiao, L. Szeto, B. W. Patterson and G. F. Lewis (2008). "Both intestinal and hepatic lipoprotein production are stimulated by an acute elevation of plasma free fatty acids in humans." Circulation 117(18): 2369–2376.

Dupre, J., S. A. Ross, D. Watson and J. C. Brown (1973). "Stimulation of insulin secretion by gastric inhibitory polypeptide in man." J Clin Endocrinol Metab 37(5): 826–828.

Dynka, D., L. Rodzen, M. Rodzen, A. Pacholak-Klimas, G. Ede, S. Sethi, D. Lojko, K. Barton, K. Berry, A. Deptula, Z. Grzywacz, P. Martin, J. Unwin and D. Unwin (2025). "Ketogenic Diets for Body Weight Loss: A Comparison with Other Diets." Nutrients 17(6).

Ekelund, M., E. Kristensson, M. Ekelund and E. Ekblad (2007). "Total parenteral nutrition causes circumferential intestinal atrophy, remodeling of the intestinal wall, and redistribution of eosinophils in the rat gastrointestinal tract." Dig Dis Sci 52(8): 1833–1839.

Evangelakos, I., A. Kuhl, M. Baguhl, C. Schlein, C. John, J. K. Rohde, M. Heine, J. Heeren and A. Worthmann (2022). "Cold-Induced Lipoprotein Clearance in Cyp7b1-Deficient Mice." Front Cell Dev Biol 10: 836741.

Evans, K., P. J. Kuusela, M. L. Cruz, I. Wilhelmova, B. A. Fielding and K. N. Frayn (1998). "Rapid chylomicron appearance following sequential meals: effects of second meal composition." Br J Nutr 79(5): 425–429.

Evert, A. B., M. Dennison, C. D. Gardner, W. T. Garvey, K. H. K. Lau, J. MacLeod, J. Mitri, R. F. Pereira, K. Rawlings, S. Robinson, L. Saslow, S. Uelmen, P. B. Urbanski and W. S. Yancy, Jr. (2019). "Nutrition Therapy for Adults With Diabetes or Prediabetes: A Consensus Report." Diabetes Care 42(5): 731–754.

Federico, L. M., M. Naples, D. Taylor and K. Adeli (2006). "Intestinal insulin resistance and aberrant production of apolipoprotein B48 lipoproteins in an animal model of insulin resistance and metabolic dyslipidemia: evidence for activation of protein tyrosine phosphatase-1B, extracellular signal-related kinase, and sterol regulatory element-binding protein-1c in the fructose-fed hamster intestine." Diabetes 55(5): 1316–1326.

Feinman, R. D., W. K. Pogozelski, A. Astrup, R. K. Bernstein, E. J. Fine, E. C. Westman, A. Accurso, L. Frassetto, B. A. Gower, S. I. McFarlane, J. V. Nielsen, T. Krarup, L. Saslow, K. S.

Roth, M. C. Vernon, J. S. Volek, G. B. Wilshire, A. Dahlqvist, R. Sundberg, A. Childers, K. Morrison, A. H. Manninen, H. M. Dashti, R. J. Wood, J. Wortman and N. Worm (2019). "Corrigendum to "Dietary carbohydrate restriction as the first approach in diabetes management: Critical review and evidence base" [Nutrition 31 (2015) 1-13]." Nutrition 62: 213.

Fielding, B. A., J. Callow, R. M. Owen, J. S. Samra, D. R. Matthews and K. N. Frayn (1996). "Postprandial lipemia: the origin of an early peak studied by specific dietary fatty acid intake during sequential meals." Am J Clin Nutr 63(1): 36–41.

Firman, C. H., D. D. Mellor, D. Unwin and A. Brown (2024). "Does a Ketogenic Diet Have a Place Within Diabetes Clinical Practice? Review of Current Evidence and Controversies." Diabetes Ther 15(1): 77–97.

Fischer, A. W., J. Behrens, F. Sass, C. Schlein, M. Heine, P. Pertzborn, L. Scheja and J. Heeren (2020). "Brown adipose tissue lipoprotein and glucose disposal is not determined by thermogenesis in uncoupling protein 1-deficient mice." J Lipid Res 61(11): 1377–1389.

Foster, D. O. and M. L. Frydman (1979). "Tissue distribution of cold-induced thermogenesis in conscious warm- or cold-acclimated rats reevaluated from changes in tissue blood flow: the dominant role of brown adipose tissue in the replacement of shivering by nonshivering thermogenesis." Can J Physiol Pharmacol 57(3): 257–270.

Frias, J. P., M. A. Nauck, J. Van, M. E. Kutner, X. Cui, C. Benson, S. Urva, R. E. Gimeno, Z. Milicevic, D. Robins and A. Haupt (2018). "Efficacy and safety of LY3298176, a novel dual GIP and GLP-1 receptor agonist, in patients with type 2 diabetes: a randomised, placebo-controlled and active comparator-controlled phase 2 trial." Lancet 392(10160): 2180–2193.

Fuchs, S., B. Yusta, L. L. Baggio, E. M. Varin, D. Matthews and D. J. Drucker (2020). "Loss of Glp2r signaling activates hepatic stellate cells and exacerbates diet-induced steatohepatitis in mice." JCI Insight 5(8).

Gandasi, N. R., R. Gao, L. Kothegala, A. Pearce, C. Santos, S. Acreman, D. Basco, A. Benrick, M. V. Chibalina, A. Clark, C. Guida, M. Harris, P. R. V. Johnson, J. G. Knudsen, J. Ma, C. Miranda, M. Shigeto, A. I. Tarasov, H. Y. Yeung, B. Thorens, I. W. Asterholm, Q. Zhang, R. Ramracheya, G. Ladds and P. Rorsman (2023). "GLP-1 metabolite GLP-1(9-36) is a systemic inhibitor of mouse and human pancreatic islet glucagon secretion." Diabetologia.

Gardner, C. D., M. K. Vadiveloo, K. S. Petersen, C. A. M. Anderson, S. Springfield, L. Van Horn, A. Khera, C. Lamendola, S. M. Mayo, J. J. Joseph, L. American Heart Association Council on and H. Cardiometabolic (2023). "Popular Dietary Patterns: Alignment With American Heart Association 2021 Dietary Guidance: A Scientific Statement From the American Heart Association." Circulation 147(22): 1715–1730.

Gehart, H. and H. Clevers (2019). "Tales from the crypt: new insights into intestinal stem cells." Nat Rev Gastroenterol Hepatol 16(1): 19–34.

Glenny, E. M., J. Liu, H. G. Skinner, T. L. McFarlane, K. K. Reed, A. Weninger, Z. Djukic, M. A. Pellizzon and I. M. Carroll (2024). "Purified diets containing high levels of soluble fiber and grain-based diets promote similar gastrointestinal morphometry yet distinct microbial communities." Appl Environ Microbiol 90(11): e0155224.

Gribble, F. M. and F. Reimann (2019). "Function and mechanisms of enteroendocrine cells and gut hormones in metabolism." Nat Rev Endocrinol 15(4): 226–237.

Guan, X., H. E. Karpen, J. Stephens, J. T. Bukowski, S. Niu, G. Zhang, B. Stoll, M. J. Finegold, J. J. Holst, D. Hadsell, B. L. Nichols and D. G. Burrin (2006). "GLP-2 receptor localizes to enteric neurons and endocrine cells expressing vasoactive peptides and mediates increased blood flow." Gastroenterology 130(1): 150–164.

Haidari, M., N. Leung, F. Mahbub, K. D. Uffelman, R. Kohen-Avramoglu, G. F. Lewis and K. Adeli (2002). "Fasting and postprandial overproduction of intestinally derived lipoproteins in an animal model of insulin resistance. Evidence that chronic fructose feeding in the hamster is accompanied by enhanced intestinal de novo lipogenesis and ApoB48-containing lipoprotein overproduction." J Biol Chem 277(35): 31646–31655.

Hammoud, R., K. D. Kaur, J. A. Koehler, L. L. Baggio, C. K. Wong, K. E. Advani, B. Yusta, I. Efimova, F. M. Gribble, F. Reimann, S. Fishman, C. Varol and D. J. Drucker (2024). "Glucose-dependent insulinotropic polypeptide receptor signaling alleviates gut inflammation in mice." JCI Insight 10(3).

Hartmann, B., M. B. Harr, P. B. Jeppesen, M. Wojdemann, C. F. Deacon, P. B. Mortensen and J. J. Holst (2000). "In vivo and in vitro degradation of glucagon-like peptide-2 in humans." J Clin Endocrinol Metab 85(8): 2884–2888.

Hayek, T., L. Masucci-Magoulas, X. Jiang, A. Walsh, E. Rubin, J. L. Breslow and A. R. Tall (1995). "Decreased early atherosclerotic lesions in hypertriglyceridemic mice expressing cholesteryl ester transfer protein transgene." J Clin Invest 96(4): 2071–2074.

He, B., K. Nohara, N. Park, Y. S. Park, B. Guillory, Z. Zhao, J. M. Garcia, N. Koike, C. C. Lee, J. S. Takahashi, S. H. Yoo and Z. Chen (2016). "The Small Molecule Nobiletin Targets the Molecular Oscillator to Enhance Circadian Rhythms and Protect against Metabolic Syndrome." Cell Metab 23(4): 610–621.

Higuchi, K., A. V. Hospattankar, S. W. Law, N. Meglin, J. Cortright and H. B. Brewer, Jr. (1988). "Human apolipoprotein B (apoB) mRNA: identification of two distinct apoB mRNAs, an mRNA with the apoB-100 sequence and an apoB mRNA containing a premature in-frame translational stop codon, in both liver and intestine." Proc Natl Acad Sci U S A 85(6): 1772–1776.

Hirschberger, S., D. Effinger, P. Yoncheva, A. Schmid, M. N. Weis, L. M. Holdt, D. Teupser and S. Kreth (2024). "The impact of a ketogenic diet on weight loss, metabolism, body composition and quality of life." iScience 27(12): 111291.

Hokanson, J. E. and M. A. Austin (1996). "Plasma triglyceride level is a risk factor for cardiovascular disease independent of high-density lipoprotein cholesterol level: a meta-analysis of population-based prospective studies." J Cardiovasc Risk 3(2): 213–219.

Hsieh, J., C. Longuet, C. L. Baker, B. Qin, L. M. Federico, D. J. Drucker and K. Adeli (2010). "The glucagon-like peptide 1 receptor is essential for postprandial lipoprotein synthesis and secretion in hamsters and mice." Diabetologia 53(3): 552–561.

Hsieh, J., C. Longuet, A. Maida, J. Bahrami, E. Xu, C. L. Baker, P. L. Brubaker, D. J. Drucker and K. Adeli (2009). "Glucagon-like peptide-2 increases intestinal lipid absorption and chylomicron production via CD36." Gastroenterology 137(3): 997–1005, 1005 e1001–1004.

Hunt, J. E., B. Hartmann, K. Schoonjans, J. J. Holst and H. Kissow (2021). "Dietary Fiber Is Essential to Maintain Intestinal Size, L-Cell Secretion, and Intestinal Integrity in Mice." Front Endocrinol (Lausanne) 12: 640602.

Jackson, K. G., M. D. Robertson, B. A. Fielding, K. N. Frayn and C. M. Williams (2002). "Olive oil increases the number of triacylglycerol-rich chylomicron particles compared with other oils: an effect retained when a second standard meal is fed." Am J Clin Nutr 76(5): 942–949.

Jacome-Sosa, M., Q. Hu, C. M. Manrique-Acevedo, R. D. Phair and E. J. Parks (2021). "Human intestinal lipid storage through sequential meals reveals faster dinner appearance is associated with hyperlipidemia." JCI Insight 6(15).

Kalafut, K. C., S. J. Mitchell, M. R. MacArthur and J. R. Mitchell (2022). "Short-Term Ketogenic Diet Induces a Molecular Response That Is Distinct From Dietary Protein Restriction." Front Nutr 9: 839341.

Kennedy, A. R., P. Pissios, H. Otu, R. Roberson, B. Xue, K. Asakura, N. Furukawa, F. E. Marino, F. F. Liu, B. B. Kahn, T. A. Libermann and E. Maratos-Flier (2007). "A high-fat, ketogenic diet induces a unique metabolic state in mice." Am J Physiol Endocrinol Metab 292(6): E1724–1739.

Kim, E., K. Nohara, M. Wirianto, G. Escobedo, Jr., J. Y. Lim, R. Morales, S. H. Yoo and Z. Chen (2021). "Effects of the Clock Modulator Nobiletin on Circadian Rhythms and Pathophysiology in Female Mice of an Alzheimer's Disease Model." Biomolecules 11(7).

Kim, Y. J., M. S. Choi, J. T. Woo, M. J. Jeong, S. R. Kim and U. J. Jung (2017). "Long-term dietary supplementation with low-dose nobiletin ameliorates hepatic steatosis, insulin resistance, and inflammation without altering fat mass in diet-induced obesity." Mol Nutr Food Res 61(8).

Koehler, J. A., L. L. Baggio, B. Yusta, C. Longuet, K. J. Rowland, X. Cao, D. Holland, P. L. Brubaker and D. J. Drucker (2015). "GLP-1R agonists promote normal and neoplastic intestinal growth through mechanisms requiring Fgf7." Cell Metab 21(3): 379–391.

Kohan, A. B., F. Wang, X. Li, S. Bradshaw, Q. Yang, J. L. Caldwell, T. M. Bullock and P. Tso (2012). "Apolipoprotein A-IV regulates chylomicron metabolism-mechanism and function." Am J Physiol Gastrointest Liver Physiol 302(6): G628–636.

Korbelius, M., N. Vujic, V. Sachdev, S. Obrowsky, S. Rainer, B. Gottschalk, W. F. Graier and D. Kratky (2019). "ATGL/CGI-58-Dependent Hydrolysis of a Lipid Storage Pool in Murine Enterocytes." Cell Rep 28(7): 1923–1934 e1924.

Langsted, A., J. J. Freiberg and B. G. Nordestgaard (2008). "Fasting and nonfasting lipid levels: influence of normal food intake on lipids, lipoproteins, apolipoproteins, and cardiovascular risk prediction." Circulation 118(20): 2047–2056.

Larsen, M. A., R. Goll, S. Lekahl, O. S. Moen and J. Florholmen (2015). "Delayed clearance of triglyceride-rich lipoproteins in young, healthy obese subjects." Clin Obes 5(6): 349–357.

Lee, Y. S., B. Y. Cha, S. S. Choi, B. K. Choi, T. Yonezawa, T. Teruya, K. Nagai and J. T. Woo (2013). "Nobiletin improves obesity and insulin resistance in high-fat diet-induced obese mice." J Nutr Biochem 24(1): 156–162.

Lewis, G. F., M. Naples, K. Uffelman, N. Leung, L. Szeto and K. Adeli (2004). "Intestinal lipoprotein production is stimulated by an acute elevation of plasma free fatty acids in the fasting state: studies in insulin-resistant and insulin-sensitized Syrian golden hamsters." Endocrinology 145(11): 5006–5012.

Li, D., C. N. Rodia, Z. K. Johnson, M. Bae, A. Muter, A. E. Heussinger, N. Tambini, A. M. Longo, H. Dong, J. Y. Lee and A. B. Kohan (2019). "Intestinal basolateral lipid substrate transport is linked to chylomicron secretion and is regulated by apoC-III." J Lipid Res 60(9): 1503–1515.

Liu, M., L. Shen, Q. Yang, A. M. Nauli, M. Bingamon, D. Q. Wang, Y. M. Ulrich-Lai and P. Tso (2021). "Sexual dimorphism in intestinal absorption and lymphatic transport of dietary lipids." J Physiol 599(22): 5015–5030.

Mansukhani, N. A., Z. Wang, V. P. Shively, M. E. Kelly, J. M. Vercammen and M. R. Kibbe (2017). "Sex Differences in the LDL Receptor Knockout Mouse Model of Atherosclerosis." Artery Res 20: 8–11.

Martchenko, A., A. D. Biancolin, S. E. Martchenko and P. L. Brubaker (2022). "Nobiletin ameliorates high fat-induced disruptions in rhythmic glucagon-like peptide-1 secretion." Sci Rep 12(1): 7271.

Morrow, N. M., A. C. Burke, J. P. Samsoondar, K. E. Seigel, A. Wang, D. E. Telford, B. G. Sutherland, C. O'Dwyer, G. R. Steinberg, M. D. Fullerton and M. W. Huff (2020). "The citrus flavonoid nobiletin confers protection from metabolic dysregulation in high-fat-fed mice independent of AMPK." J Lipid Res 61(3): 387–402.

Mulvihill, E. E., J. M. Assini, J. K. Lee, E. M. Allister, B. G. Sutherland, J. B. Koppes, C. G. Sawyez, J. Y. Edwards, D. E. Telford, A. Charbonneau, P. St-Pierre, A. Marette and M. W. Huff (2011). "Nobiletin attenuates VLDL overproduction, dyslipidemia, and atherosclerosis in mice with diet-induced insulin resistance." Diabetes 60(5): 1446–1457.

Mulvihill, E. E., E. M. Varin, B. Gladanac, J. E. Campbell, J. R. Ussher, L. L. Baggio, B. Yusta, J. Ayala, M. A. Burmeister, D. Matthews, K. W. A. Bang, J. E. Ayala and D. J. Drucker (2017). "Cellular Sites and Mechanisms Linking Reduction of Dipeptidyl Peptidase-4 Activity to Control of Incretin Hormone Action and Glucose Homeostasis." Cell Metab 25(1): 152–165.

Nelson, D. W., J. W. Sharp, M. S. Brownfield, H. E. Raybould and D. M. Ney (2007). "Localization and activation of glucagon-like peptide-2 receptors on vagal afferents in the rat." Endocrinology 148(5): 1954–1962.

Orskov, C., B. Hartmann, S. S. Poulsen, J. Thulesen, K. J. Hare and J. J. Holst (2005). "GLP-2 stimulates colonic growth via KGF, released by subepithelial myofibroblasts with GLP-2 receptors." Regul Pept 124(1-3): 105–112.

Palmisano, B. T., S. Yu, J. C. Neuman, L. Zhu, T. Luu and J. M. Stafford (2021). "Low-density lipoprotein receptor is required for cholesteryl ester transfer protein to regulate triglyceride metabolism in both male and female mice." Physiol Rep 9(4): e14732.

Pan, X., X. C. Jiang and M. M. Hussain (2013). "Impaired cholesterol metabolism and enhanced atherosclerosis in clock mutant mice." Circulation 128(16): 1758–1769.

Paternoster, S. and M. Falasca (2018). "Dissecting the Physiology and Pathophysiology of Glucagon-Like Peptide-1." Front Endocrinol (Lausanne) 9: 584.

Patsch, J. R., G. Miesenbock, T. Hopferwieser, V. Muhlberger, E. Knapp, J. K. Dunn, A. M. Gotto, Jr. and W. Patsch (1992). "Relation of triglyceride metabolism and coronary artery disease. Studies in the postprandial state." Arterioscler Thromb 12(11): 1336–1345.

Pettersson, U. S., T. B. Walden, P. O. Carlsson, L. Jansson and M. Phillipson (2012). "Female mice are protected against high-fat diet induced metabolic syndrome and increase the regulatory T cell population in adipose tissue." PLoS One 7(9): e46057.

Psichas, A., P. F. Larraufie, D. A. Goldspink, F. M. Gribble and F. Reimann (2017). "Chylomicrons stimulate incretin secretion in mouse and human cells." Diabetologia 60(12): 2475–2485.

Romero-Aleshire, M. J., M. K. Diamond-Stanic, A. H. Hasty, P. B. Hoyer and H. L. Brooks (2009). "Loss of ovarian function in the VCD mouse-model of menopause leads to insulin resistance and a rapid progression into the metabolic syndrome." Am J Physiol Regul Integr Comp Physiol 297(3): R587–592.

Rowland, K. J., S. Trivedi, D. Lee, K. Wan, R. N. Kulkarni, M. Holzenberger and P. L. Brubaker (2011). "Loss of glucagon-like peptide-2-induced proliferation following intestinal epithelial insulin-like growth factor-1-receptor deletion." Gastroenterology 141(6): 2166–2175 e2167.

Ruppert, P. M. M. and S. Kersten (2024). "Mechanisms of hepatic fatty acid oxidation and ketogenesis during fasting." Trends Endocrinol Metab 35(2): 107–124.

Scherer, P. E. and J. A. Hill (2016). "Obesity, Diabetes, and Cardiovascular Diseases: A Compendium." Circ Res 118(11): 1703–1705.

Silva, K. D., J. W. Wright, C. M. Williams and J. A. Lovegrove (2005). "Meal ingestion provokes entry of lipoproteins containing fat from the previous meal: possible metabolic implications." Eur J Nutr 44(6): 377–383.

Stojanovic, O., J. Altirriba, D. Rigo, M. Spiljar, E. Evrard, B. Roska, S. Fabbiano, N. Zamboni, P. Maechler, F. Rohner-Jeanrenaud and M. Trajkovski (2021). "Dietary excess regulates absorption and surface of gut epithelium through intestinal PPARalpha." Nat Commun 12(1): 7031.

Sun, X., A. U. Spencer, H. Yang, E. Q. Haxhija and D. H. Teitelbaum (2006). "Impact of caloric intake on parenteral nutrition-associated intestinal morphology and mucosal barrier function." JPEN J Parenter Enteral Nutr 30(6): 474–479.

Takeda, K., H. Sawazaki, H. Takahashi, Y. S. Yeh, H. F. Jheng, W. Nomura, T. Ara, N. Takahashi, S. Seno, N. Osato, H. Matsuda, T. Kawada and T. Goto (2018). "The dipeptidyl peptidase-4 (DPP-4) inhibitor teneligliptin enhances brown adipose tissue function, thereby preventing obesity in mice." FEBS Open Bio 8(11): 1782–1793.

Teixeira, P. D. S., M. R. Tavares and D. Jose (2021). "Temporal characterization of the insulin resistance during puberty in mice." Endocr Regul 55(1): 1–4.

Ting, R., N. Dugre, G. M. Allan and A. J. Lindblad (2018). "Ketogenic diet for weight loss." Can Fam Physician 64(12): 906.

Uchida, A., M. C. Whitsitt, T. Eustaquio, M. N. Slipchenko, J. F. Leary, J. X. Cheng and K. K. Buhman (2012). "Reduced triglyceride secretion in response to an acute dietary fat challenge in obese compared to lean mice." Front Physiol 3: 26.

Varlamov, O., C. L. Bethea and C. T. Roberts, Jr. (2014). "Sex-specific differences in lipid and glucose metabolism." Front Endocrinol (Lausanne) 5: 241.

Veilleux, A., E. Grenier, P. Marceau, A. C. Carpentier, D. Richard and E. Levy (2014). "Intestinal lipid handling: evidence and implication of insulin signaling abnormalities in human obese subjects." Arterioscler Thromb Vasc Biol 34(3): 644–653.

Walsh, N. A., B. Yusta, M. P. DaCambra, Y. Anini, D. J. Drucker and P. L. Brubaker (2003). "Glucagon-like peptide-2 receptor activation in the rat intestinal mucosa." Endocrinology 144(10): 4385–4392.

Wang, H., M. Wang, K. Chansaenpak, Y. Liu, H. Yuan, J. Xie, H. Yin, R. T. Branca, Z. Li and Z. Wu (2020). "A Novel PET Probe for Brown Adipose Tissue Imaging in Rodents." Mol Imaging Biol 22(3): 675–684.

Wang, Q., Y. Zhou, P. Rychahou, T. W. Fan, A. N. Lane, H. L. Weiss and B. M. Evers (2017). "Ketogenesis contributes to intestinal cell differentiation." Cell Death Differ 24(3): 458–468.

Wang, R., M. S. A. Khan, K. Mukherjee, M. Ghanem and C. Xiao (2025). "Glucose-dependent insulinotropic polypeptide stimulates post-absorptive lipid secretion in the intestine." Front Physiol 16: 1549392.

Wang, Y., J. Xie, Z. Ai and J. Su (2019). "Nobiletin-loaded micelles reduce ovariectomy-induced bone loss by suppressing osteoclastogenesis." Int J Nanomedicine 14: 7839–7849.

Wang, Z., Y. Wu, X. Li, X. Ji and W. Liu (2024). "The gut microbiota facilitate their host tolerance to extreme temperatures." BMC Microbiol 24(1): 131.

Wen, X., H. Zhao, L. Wang, L. Wang, G. Du, W. Guan, J. Liu, X. Cao, X. Jiang, J. Tian, M. Wang, C. T. Ho and S. Li (2020). "Nobiletin Attenuates DSS-Induced Intestinal Barrier Damage through the HNF4alpha-Claudin-7 Signaling Pathway." J Agric Food Chem 68(16): 4641–4649.

Wu, L. and K. G. Parhofer (2014). "Diabetic dyslipidemia." Metabolism 63(12): 1469–1479.

Yang, N., Y. S. Pang, Y. Zheng, Y. J. Gong and W. J. Ding (2025). "Nobiletin restores the intestinal barrier of HFD-induced obese mice by promoting MHC-II expression and lipid metabolism." Mol Med 31(1): 26.

Zhan, M., X. Yang, C. Zhao, Y. Han, P. Xie, Z. Mo, J. Xiao, Y. Cao, H. Xiao and M. Song (2024). "Dietary nobiletin regulated cefuroxime- and levofloxacin-associated "gut microbiota-metabolism" imbalance and intestinal barrier dysfunction in mice." Food Funct 15(3): 1265–1278.

Zhang, H., M. Leveille, E. Courty, A. Gunes, N. N. B and J. L. Estall (2020). "Differences in metabolic and liver pathobiology induced by two dietary mouse models of nonalcoholic fatty liver disease." Am J Physiol Endocrinol Metab 319(5): E863–E876.

Zhao, Z., R. Yang, M. Li, M. Bao, D. Huo, J. Cao and J. R. Speakman (2022). "Effects of ambient temperatures between 5 and 35 degrees C on energy balance, body mass and body composition in mice." Mol Metab 64: 101551.

Appendix A

Chapter 1:

Chapter 1

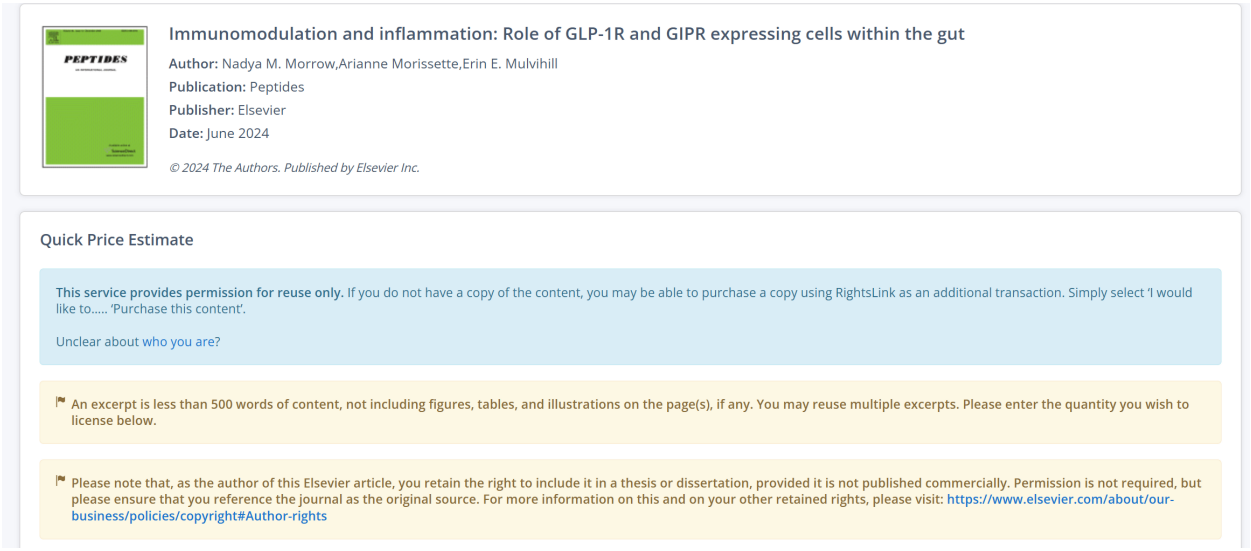

Immunomodulation and inflammation: Role of GLP-1R and GIPR expressing cells within the gut

Author: Nadya M. Morrow,Arianne Morissette,Erin E. Mulvihill
Publication: Peptides
Publisher: Elsevier
Date: June 2024

© 2024 The Authors. Published by Elsevier Inc.

Quick Price Estimate

This service provides permission for reuse only. If you do not have a copy of the content, you may be able to purchase a copy using RightsLink as an additional transaction. Simply select 'I would like to..... 'Purchase this content'.

Unclear about who you are?

An excerpt is less than 500 words of content, not including figures, tables, and illustrations on the page(s), if any. You may reuse multiple excerpts. Please enter the quantity you wish to license below.

Please note that, as the author of this Elsevier article, you retain the right to include it in a thesis or dissertation, provided it is not published commercially. Permission is not required, but please ensure that you reference the journal as the original source. For more information on this and on your other retained rights, please visit: https://www.elsevier.com/about/our-business/policies/copyright#Author-rights

Chapter 1

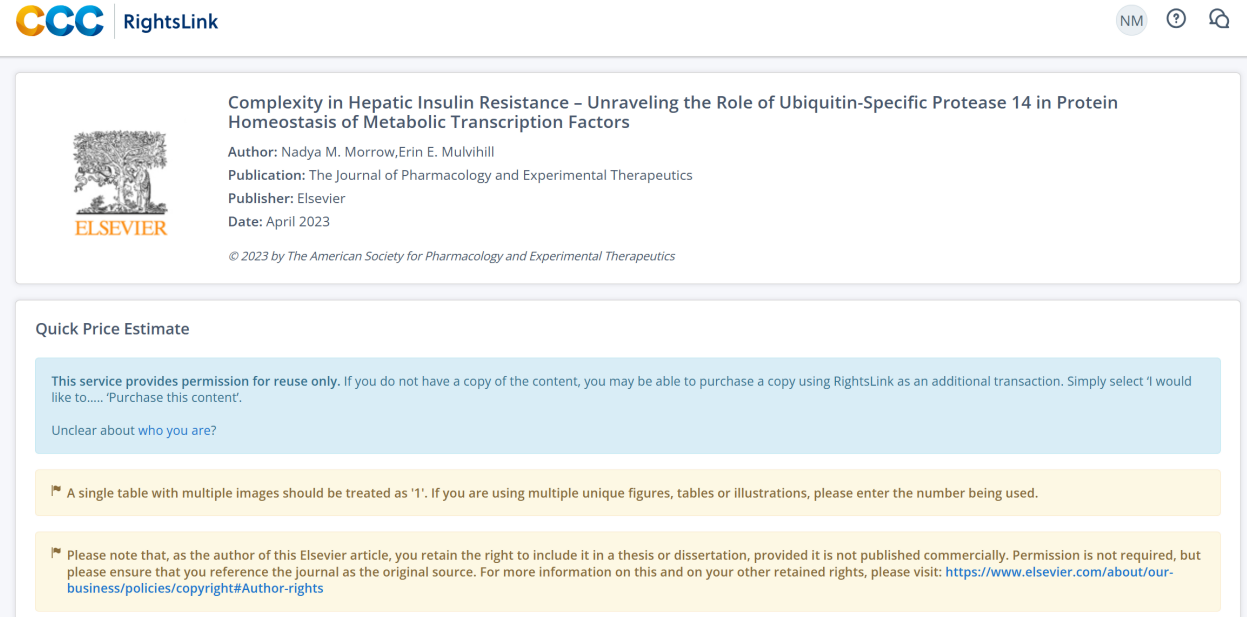

Manuscripts

Chapter 2

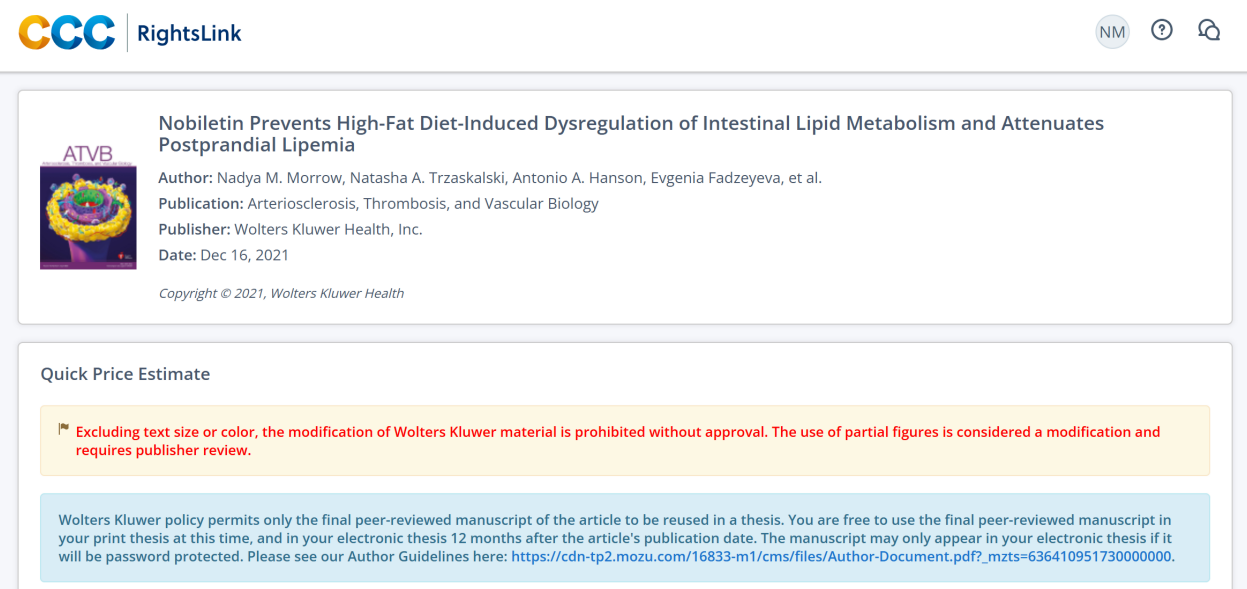

Chapter 3

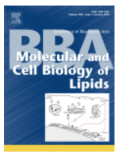

Adaptation to short-term extreme fat consumption alters intestinal lipid handling in male and female mice

Author:
Nadya M. Morrow,Cassandra A.A. Locatelli,Natasha A. Trzaskalski,Chelsea T. Klein,Antonio A. Hanson,Hadeel Alhadi,Ishika Tripathi,Andrew C. Clément,Sara Imran,Ilka Lorenzen-Schmidt,Erin E. Mulvihill

Publication: Biochimica et Biophysica Acta (BBA) - Molecular and Cell Biology of Lipids

Publisher: Elsevier

Date: November 2022

Appendix B

Animal Use and ethics approval

AUP Number: 2909 and 4379

Curriculum Vitae

Nadya M. Morrow, MSc

PhD Candidate

University of Ottawa Heart Institute

POST-SECONDARY EDUCATION

University	Degree	Program	Dates
University of Ottawa	PhD	Biochemistry	09/2019 to present
University of Western Ontario	MSc	Biochemistry	09/2017 to 09/2019
University of Windsor	BSc	Honours Biochemistry Minor in French Studies	09/2013 to 04/2017

GRADUATE SCHOLARSHIPS

Title	Source	Duration	Amount
Banting & Best Canada Graduate Scholarship – Doctoral Program	Canadian Institute of Health Research	2021 – 2024	$35,000 per year
Ontario Graduate Scholarship	The Government of Ontario & the University of Ottawa	2021 (declined)	$15,000
Queen Elizabeth II Graduate Scholarship in Science and Technology	The Government of Ontario & the University of Ottawa	2020 – 2021	$15,000
University of Ottawa Cardiac Endowment Fund at the Heart Institute	University of Ottawa Heart Institute	2020-2022	$20,000 per year

Title of PhD Thesis: *Molecular insights into the adaptability of the gut*

Title of MSc Thesis: *Nobiletin corrects intestinal insulin resistance and lipid metabolism in Ldlr$^{-/-}$ mice fed a high-fat diet.*

AWARDS AND DISTINCTIONS

2024 Outstanding Poster Award – $1095. Gordon Research Conference, Lipoprotein Metabolism, Waterville Valley, USA.

2024 Best Poster Award - $150. University of Ottawa Department of Biochemistry, Microbiology and Immunology, Ottawa, Canada.

2024 Dr. Yves Marcel Award for the Best Basic Science Oral Presentation – $200

36th Annual Ottawa Cardiovascular Research Day, Ottawa, Canada.

2023 Maximize your Research on Obesity and Diabetes (MyRoad) Travel Award – $500
12th Annual Diabetes Research Envisioned and Accomplished in Manitoba (DREAM) Symposium Trainee Day. Winnipeg, Manitoba.

2023 CIHR-ICRH Fall Travel Award - $1500. Canadian Vascular and Lipid Summit, Prince Edward County, Canada.

2023 Ottawa Region Cardiovascular Research Trainee of the Year – $1000. University of Ottawa Heart Institute. Ottawa, Ontario.

2023 Syed Sattar PhD Student Award - $500 and Departmental Seminar. University of Ottawa Department of Biochemistry, Microbiology and Immunology, Ottawa, Canada.

2023 Frans Leenen Trainee Publication of the Year 2021 (Basic Sciences) - $100 University of Ottawa Heart Institute.

2022 CSATVB Trainee Travel Subsidy Award - $450. Canadian Society of Atherosclerosis, Thrombosis and Vascular Biology (CSATVB), Canadian Vascular and Lipid Summit, Whistler, Canada.

2021 Coralie Lalonde UOHI Innovation Award – Finalist. 33rd Annual Ottawa Cardiovascular Research Day, Canada.

2020 Best Poster Presentation Award - $400. Montréal Diabetes Research Conference, Montréal, Canada.

2018 CSATVB Trainee Travel Subsidy Award - $660. Canadian Society of Atherosclerosis, Thrombosis and Vascular Biology (CSATVB), International Symposium on Atherosclerosis, Toronto, Canada.

2018 First Place Poster Presentation. Department of Biochemistry Research Showcase Day, University of Western Ontario, Canada.

2017 Dr. Michael and Ann Kane Science Scholarship - $1,000. Awarded to an outstanding graduating Chemistry and Biochemistry student. Department of Chemistry and Biochemistry, University of Windsor.

	Summary of academic activities per year						
Year	**Research articles**	**Review Articles**	**Commentary Articles**	**Award Lectures**	**Abstracts (oral presentation)**	**Abstracts (poster presentation)**	**Total**
2025						1	1
2024		2			1	3	6
2023	2		1	2	1	3	9
2022	1				1	5	7
2021	1	1	1			3	6
2020	1	1				3	5
2019					1	4	5
2018			1		2	2	5
Total	**5**	**4**	**3**	**2**	**6**	**24**	**44**

REFEREED PUBLICATIONS

a) Research articles

1. Fadzeyeva, E., Locatelli, C.A.A., Trzaskalski, N.A., Nguyen, M., Capozzi, M.E., Vulesevic, B., **Morrow, N.M.**, Ghorbani, P., Hanson, A.A., Lorenzen-Schmidt, I., Doyle, M., Seymour, R., Varin, E.M., Fullerton, M.D., Campbel, J.E., Mulvihill, E.E. *Pancreas-derived DPP4 is not essential for glucose homeostasis under metabolic stress*. iScience. (2023) PMID: 37216093
2. Trzaskalski, N.A., Vulesevic, B., Nguyen, M., Jeraj, N., Fadzeyeva, E., **Morrow, N.M.,** Locatelli, C. A.A., Travis, N., Hanson, A.A., Nunes., J.R.C., O-Dwyer, C., van der Veen J.N., Lorenzen-Schmidt, I., Seymour, R., Pulente, S., Clement, A.C., Crawley, A., Jacobs, R.L., Doyle, M.A., Cooper, C.L., Kim, K., Fullerton, M.D., Mulvihill, E.E. *Hepatocyte-derived DPP4 regulates portal GLP-1 bioactivity, modulates glucose production, and when absent influences NAFLD progression*. JCI Insight. (2023) PMID: 36472923
3. **Morrow, N.M.**, Locatelli, C.A., Trzaskalski, N.A., Klein, C.T.*****, Hanson, A.A., Alhadi, H.*****, Tripathi, I.*****, Clément, A.C., Imran, S.*, Lorenzen-Schmidt, I., Mulvihill, E.E. *Adaptation to short-term extreme fat consumption alters intestinal lipid handling in male and female mice*. Biochimica et Biophysica Acta Mol Cell Biol Lipids. (2022) PMID: 35926775 *****Undergraduate students under my supervision.
4. **Morrow, N.M.**, Trzaskalski, N.A., Hanson, A.A., Fadzeyeva, E., Telford, D.E., Chhoker, S., Sutherland, B.G., Edwards, J.Y., Huff, M.W., Mulvihill, E.E. *Nobiletin prevents high-fat diet-induced dysregulation of intestinal lipid metabolism and attenuates post-prandial lipemia*. Arterioscler Thromb Vasc Biol. (2021) PMID: 34911361

5. **Morrow, N.M.**, Burke, A.C., Samsoondar, J.P., Seigle, K. E., Wang, A., Telford, D.E., Sutherland, B.G., O'Dwyer, C., Steinberg, G.R., Fullerton, M.D., Huff, M.W. *The citrus flavonoid nobiletin confers protection from metabolic dysregulation in high-fat-fed mice independent of AMPK*. J Lipid Res. 2020. PMDI: 31964763

b) Review articles

1. Morissette, A, Mullur, N. **Morrow, N.M.,** Mulvihill, E.E. *GLP-1 Receptor Agonist-Based therapies and Cardiovascular Risk in Diabetes and Obesity: A Review of Mechanisms*. Journal of Endocrinology. (2024).
2. **Morrow, N.M.**, Morissette, A., Mulvihill, E.E. *Immunomodulation and inflammation: Role of GLP-1R and GIPR expressing cells within the gut.* Peptides. (2024) PMID: 38555054
3. **Morrow, N.M.**, Hanson, A.A., Mulvihill, E.E. *Distinct Identity of GLP-1R, GLP-2R, and GIPR Expressing Cells and Signaling Circuits Within the Gastrointestinal Tract.* Front Cell Dev Biol. (2021) PMID: 34660576
4. Asif, S., **Morrow, N.M.**, Mulvihill, E.E., Kim, K. *Understanding dietary intervention-mediated epigenetic modifications in metabolic diseases.* Front Genet. (2020) PMID: 33193730

c) Commentary articles

1. **Morrow, N.M.** and Mulvihill E.E. *Complexity in Hepatic Insulin Resistance – Unraveling the Role of Ubiquitin-Specific Protease 14 in Protein Homeostasis of Metabolic Transcription Factors.* Journal of Pharmacology and Experimental Therapeutics. (2023) PMID: 36927510 *Graphical abstract selected as April 2023 issue cover.
2. **Morrow, N.M.** and Mulvihill E.E. *Open chromatin state of Dpp4 with glucocorticoid treatment -setting up shop for metasteroid diabetes?* Endocrinology. (2021) PMID: 34694370
3. **Morrow, N.M.** and M.W. Huff. *Knockdown of Delta-5 Fatty Acid Desaturase Is More Than Just a Fad*. Arterioscler Thromb Vasc Biol, 2018. PMID: 29282245

d) Award Lectures

1. Syed Sattar PhD Student Award Lecture: Targeting Gut Lipid Storage With Dietary Interventions. University of Ottawa Department of Biochemistry, Microbiology and Immunology, Ottawa, Canada. February 2023.

2. Frans Leenen Trainee Publication of the Year 2021 (Basic Sciences). Nobiletin Prevents High-Fat Died-Induced Dysregulation of Intestinal Lipid Metabolism and Attenuates Post-prandial Lipemia. University of Ottawa Heart Institute. Ottawa, ON. January 2023.

e) Abstracts selected for oral presentation:

1. Investigating the roles of GLP-1R+, GLP-2R+, and GIPR+ cells within the gut in the fasting refeeding response. Ottawa Cardiovascular Research Day. Ottawa, Ontario. May 2024. ***Yves Marcel Award for Best Basic Science Oral Presentation**

2. Glucagon-like peptide 1 and 2 double receptor knockout (GLPDRKO) mice have higher post-prandial lipids and glucose in a sex- and meal-dependent manner. Canadian Vascular and Lipid Summit (CLC & CSATVB). Prince Edward Country, ON. September

2023. ***CIHR-ICRH Fall Travel Award**

3. Control of Post-prandial Intestinal Metabolism by Gut Hormone Receptor Signalling. Canadian Islet Research and Training Network (CIRTN) Conference. Calgary, AB. November 2022.

4. Nobiletin Prevents High-fat Diet-Induced Intestinal Dysregulation to Prevent Post-prandial Lipemia. Canadian Vascular and Lipid Summit (CLC & CSATVB). Banff, AB, October 2019.

5. Nobiletin corrects intestinal insulin resistance and lipid metabolism in *Ldlr*$^{-/-}$ mice fed a high-fat diet. International Symposium on Atherosclerosis, Toronto, ON. June 2018. ***CSATVB Trainee Travel Subsidy Award**

6. Nobiletin prevents obesity, hepatic steatosis, dyslipidemia, and insulin resistance independent of adipocyte AMP-activated protein kinase. Canadian Lipoprotein Conference, Toronto, ON. June 2018.

f) Abstracts selected for Poster Presentation:

1. Investigating the roles of GLP-1R+, GLP-2R+, and GIPR+ cells within the gut in the fasting refeeding response. International Conference on Mucosal Immunology. Copenhagen, Denmark. July 2024.

2. Investigating the roles of GLP-1R+, GLP-2R+, and GIPR+ cells within the gut during cold stress. Gordon Research Conference – Lipoprotein Metabolism. Waterville Valley, New Hampshire. June 2024. ***Outstanding Poster Presentation Award**

3. Investigating the roles of GLP-1R+, GLP-2R+, and GIPR+ cells within the gut in the fasting refeeding response. Ottawa Institute of Systems Biology National Research Council Trainee Day. Ottawa, Ontario. April 2024.

4. Glucagon-like peptide 1 and 2 double receptor knockout (GLPDRKO) mice have higher post-prandial lipids and glucose in a sex- and meal-dependent manner. 12th Annual Diabetes Research Envisioned and Accomplished in Manitoba (DREAM) Symposium Trainee Day. Winnipeg, Manitoba. November 2023. ***MyRoad Travel Award**

5. Endogenous Incretin Hormone Signalling Is Required for Obesity Progression In Male And Female Mice. Ottawa Cardiovascular Research Day. Ottawa, Ontario. May 2023.
6. Control of Post-prandial Intestinal Metabolism by Gut Hormone Receptor Signalling. MetPhys. Hilton Head, South Carolina. May 2023.

7. Characterizing gut metabolic pathways and GLP-1 action during fasting and refeeding in healthy and diet-induced obese female mice. Canadian Vascular and Lipid Summit (CLVS). Whistler, BC. October, 2022. ***CSATVB Trainee Travel Subsidy Award**

8. Control of Post-prandial Intestinal Metabolism by Gut Hormone Receptor Signalling. University of Ottawa Faculty of Medicine Research Day. Ottawa, Ontario. September 2022.

9. Intestinal adaptation to short-term, extreme fat consumption alters intestinal lipid handling in male and female mice. Biochemistry, Microbiology and Immunology Research Symposium. Montebello, Québec. May 2022.
10. Glucagon-like peptides 1 and 2 receptor signalling regulate the intestinal metabolic switch from fasting to refeeding in a sex-dependent manner. Ottawa Cardiovascular Research Day. Ottawa, Ontario. May 2022.

11. Sex Differences in the Metabolic Switch from Fasting to Refeeding in the Murine Jejunum. Vascular Discover: From Genes to Medicine (ATVB). Seattle, Washington. May 2022.

12. Post-prandial regulation of intestinal triglyceride secretion by gut hormone receptor signalling. Canadian Student Health Research Forum. Online. June 2021.
13. Uncovering the physiological roles of gut hormone receptor signalling in dysregulated triglyceride-rich lipoprotein secretion during diet-induced obesity. Ottawa Cardiovascular Research Day. Online. May 2021.

14. Physiological roles of gut hormone receptor signalling in dysregulated intestinal lipid metabolism during diet-induced obesity. Insulin 100. Online. March 2021.

15. Post-prandial Regulation of Intestinal Triglyceride Secretion by Gut Hormone Receptor Signalling. University of Ottawa Faculty of Medicine Research Day. Online. September 2020.

16. Post-prandial regulation of intestinal triglyceride secretion by gut hormone receptor signalling. Canadian Vascular and Lipid Summit (CLC & CSATVB). Online. October 2020.

17. Huff, M.W. Nobiletin Prevents High-fat Diet-Induced Intestinal Dysregulation to Prevent Post-prandial Lipemia. Montreal Diabetes Research Conference. Montreal, QC, January 2020. ***Best Poster Presentation Award**

18. Nobiletin corrects intestinal lipid metabolism in *Ldlr*$^{-/-}$ mice fed a high-fat diet. Robarts Research Retreat, London, ON. June 2019.

19. Nobiletin corrects intestinal lipid metabolism in *Ldlr*$^{-/-}$ mice fed a high-fat diet. Arteriosclerosis, Thrombosis, and Vascular Biology, Scientific Sessions meeting, Boston, MA. May 2019.

20. Nobiletin corrects intestinal lipid metabolism in *Ldlr*$^{-/-}$ mice fed a high-fat diet. Department of Medicine Research Day, London, ON. May 2019.

21. Nobiletin corrects intestinal lipid metabolism in *Ldlr*$^{-/-}$ mice fed a high-fat diet. London Health Research Day, London, ON. April 2019.

22. Nobiletin corrects intestinal lipid metabolism in *Ldlr*$^{-/-}$ mice fed a high-fat diet. Robarts Research Retreat, London, ON. June 2018. }

23. Nobiletin corrects intestinal lipid metabolism in *Ldlr*$^{-/-}$ mice fed a high-fat diet. London Health Research Day, London, ON. April 2018.

TEACHING EXPERIENCE

a) Courses

University	Title	Supervisor	Dates	Description of Duties
University of Ottawa	Teaching Assistant	Dr. Keith Wheaton	01/2025 to 04/2025	*Metabolic Pathways of Human Diseases TMM3103* Held 4 pre-quiz office hours, quiz viewings, and graded oral presentations.
University of Western Ontario	Teaching Assistant	Dr. Derek McLachlin	01/2018 to 04/2018 & 01/2019 to 04/2019	*Biochemistry Laboratory* 3380G Supervised the weekly experiments of 8-10 students, held office hours, and marked laboratory reports.
University of Western Ontario	Teaching Assistant	Dr. Chris Brandl	01/2018 to 04/2018	*Biochemistry and Molecular Biology* 2280A Administrative assistant to the course responsible for proofreading exams, proctoring, and marking.
University of Western Ontario	Teaching Assistant	Dr. David Litchfield	09/2017 to 12/2017	*Biological Macromolecules* 3381A Delivered an exam review lecture, held office hours, answered student questions by online forums, and marked final exam.

b) Undergraduates Supervised

Semesters (s)	Name	Level	Program	Project for course	Direct Supervisor	Co-Supervisor
Summer 2025	Sebastian Cino	BSc	University of British Columbia	Co-Op		X
Summer 2025	Ethel Messika-Zeitoun	BSc	uOttawa	Summer rotation	X	
Winter 2025 & Summer 2025	Mélodie Bellefleur	BSc	uOttawa Translational Molecular Medicine	Winter rotation and summer NSERC	X	
Fall 2023 & Winter 2024	Hoda Osman	BSc	uOttawa Translational Molecular Medicine	Honours' Project	X	
Fall 2023 & Winter 2024	Mariam Mahran	BSc	uOttawa Translational Molecular Medicine	Honours' Project		X

Winter 2022, Summer 2022, Fall 2022, Winter 2023	Chelsea Klein	BSc	uOttawa Translational Molecular Medicine	Winter rotation (2022), NSERC (2022), Honours' Project (2022-2023)	X	
Winter 2022	Ishika Tripathi	BSc	uOttawa Translational Molecular Medicine	Winter rotation (2022)	X	
Summer 2022	Hadeel Al Hadi	BSc	uOttawa Translational Molecular Medicine	NSERC	X	
Winter 2022	Sara Iman	BSc	uOttawa Health Sciences	Winter rotation	X	

c) Mentorship and training

Name of mentorship program	Dates	Position
BMIGSA Mentor-Mentee Mentorship Program	02/2023 – 08/2024	Mentor
Hong Kong National Grant Funding Agency (RGC) | Dr. Kyoung-Han Kim	01/2022 & 01/2023	Reviewer in Training
Diabetes Action Canada Training and Mentoring Program, Diabetes Canada: ULTRA Scientist day	11/2022	Delegate
Stem Cell Network and Ottawa Bioinformatics Core Facility. RNA-seq Analysis Workshop	06/2022	Participant

SERVICE TO THE UNIVERSITY

a) Memberships on University committees

Name of committee	Dates	Role
UOHI Trainee Committee	06/2023 to 08/2024	Social Coordinator
Inaugural Regenerative Medicine Research Day	03/2023	Co-Organizer
UOHI Targeting Scholarship Applications Strategically: Helpful Tips for Graduate Students".	08/2022 & 08/2023	Panelist –
UOHI Trainee Committee	09/2021 to 04/2022 and 09/2022 to 04/2023	UOHI Work in Progress Rounds Coordinator

Biochemistry, Microbiology, and Immunology Graduate Student Association (BMIGSA)	09/2021 to 04/2022	VP Professional Development
Targeting Scholarship Applications Strategically: Helpful Tips for Graduate Students | UOHI Trainee Committee	September 2020 & September 2021	Co-Organizer and Moderator
UOHI Trainee Committee	05/2020 to 04/2021	Communications Officer
Biochemistry, Microbiology, and Immunology Graduate Student Association (BMIGSA)	09/2020 to 04/2021	VP Outreach
Robarts Association of Trainees	06/2018 to 06/2019	Communications Executive
Robarts Research Institute Vascular Discovery Night, University of Western Ontario	2019	Laboratory demonstration

SERVICE TO THE COMMUNITY

a) Memberships of conference organizing committees (last 5 years)

Name of committee	Conference Date	Role
Ottawa Cardiovascular Research Day Planning Committee	May 2025	Co-organizer
Canadian Lipid and Vascular Summit Trainee Planning Committee	September 2023	Lead organizer
Ottawa Cardiovascular Research Day Planning Committee	May 2022 and May 2023	Co-organizer
Canadian Lipid and Vascular Summit Trainee Planning Committee	October 2022	Co-organizer
Canadian Lipid and Vascular Summit	October 2020	Moderator
Robarts Research Retreat	June 2019	Co-organizer

b) Community and volunteer involvement

Name of organization/event	Dates	Role
Ottawa High School Science Innovation Challenge	February 2023	Career Panelist
Canadian Lipids Journal Club	06/2020 to 06/2021	Founder and Organizer
500 Women in Science – London Pod	06/2019	Member
London Ramblers Basketball Association	01/2018 to 004/2018	Assistant Coach